PETROFACIES AND PALEOTECTONIC EVOLUTION OF GONDWANAN AND

POST-GONDWANAN SEQUENCES OF NEPAL

Except where reference is made to the work of others, the work described in this thesis is my own or was done in collaboration with my advisory committee.
This thesis does notinclude proprietary
or classified information.

_____

Raju Prasad Sitaula

Certificate of Approval:

_____	_____
Charles E. Savrda Professor Geology and Geography	Ashraf Uddin, Chair Associate Professor Geology and Geography
_____	_____
Willis E. Hames Professor Geology and Geography	George T. Flowers Dean Graduate School

PETROFACIES AND PALEOTECTONIC EVOLUTION OFGONDWANAN AND POST-GONDWANAN SEQUENCES OF NEPAL

Raju Prasad Sitaula

A Thesis

Submitted to

the Graduate Faculty of

Auburn University

in Partial Fulfillment of the

Requirement for the

Degree of

Master of Science

Auburn, Alabama

Auburn, Alabama
December 18, 2009

PETROFACIES AND PALEOTECTONIC EVOLUTION OF GONDWANAN AND

POST-GONDWANAN SEQUENCES OF NEPAL

Raju Prasad Sitaula

_____

Raju Prasad Sitaula

_____

Date of Graduation

VITA

Raju Prasad Sitaula, son of Mr. Murari Prasad Sitaula and Mrs. Renuka Devi Sharma Sitaula, was born in 1979 in Bhadrutar, Nuwakot. He passed his school Leaving Certificate Examination in 1996 from Adarsha Yog Hari Madhyamik Vidhyalaya. He passed the Proficiency Certificate Level Examination in 1998 from Amrit Science College. He received his Bachelor of Science and Master of Science degrees in Geology in 2002 and 2005, respectively, from Tri-Chandra Multiple Campus and Tribhuvan University in Nepal. He entered the graduate school at Auburn University to pursue his second Masters degree from the Department of Geology and Geography in Fall 2007.

THESIS ABSTRACT

PETROFACIES AND PALEOTECTONIC EVOLUTION OF GONDWANAN AND POST-GONDWANAN SEQUENCES OF NEPAL

Raju Prasad Sitaula

Master of Science, December 18, 2009
(Bachelor of Science, Trichandra College, Nepal, 2004)
(Master of Science, Tribhuvan University, Nepal, 2005)

206 Typed Pages

Directed by Ashraf Uddin

The Gondwanan sequences are widely distributed in several intracratonic basins of peninsular India and also as discontinuous patches along the Himalayan orogenic belt. The Tansen Group (2400 m) in western Nepal is thicker and more complete than the Katari (380 m) and the Barahachettra (350 m) groups located in eastern Nepal.

In the Tansen Group, modal compositions of sandstone change from arkosic (Permo-Carboniferous unit) to quartz arenitic and then to litharenitic (Eocene-Early Miocene). Similar modal compositions are also present only in alleged Permo-Carboniferous units Katari and Barahachettra groups of eastern Nepal. The quartzofeldspathic sandstones of the Permo-Carboniferous Sisne (western Nepal) and Saptakoshi (eastern Nepal) formations show high Eu values. The Quartzite unit of the Saptakoshi Formation seems similar to the Amile Formation of western Nepal as both contain higher percentages of mature quartz and stable heavy minerals, and show similar

REE patterns. High contents of lithic fragments with relatively rare feldspars indicate that the Tamrang sandstones were deposited in the juvenile foreland basin between India and Tibet like the Eocene Bhainskati Formation of western Nepal.

Garnet chemistry suggests sediment supply from variously graded metamorphic rocks. Tourmaline chemistry indicates sediments derivation from both lithium-high and lithium-low igneous rocks. Chrome-spinels with low TiO_2 contents in the Taltung Formation show evidence of provenance from alkaline basalts.

Cooling ages of detrital muscovites from the Permo-Carboniferous units of all three study sections show some older ages (300 Ma to 1700 Ma) and few younger (17 Ma to 25 Ma) ages. The older ages could be related to the magmatism in the Indian craton (e.g., Malani Rhyolite, Erinpura Granite, Chotanagpur Gneissic Terrain). Ages ~ 40 Ma muscovites from the Bhainskati Formation suggest a Himalayan orogenic source. Relatively younger ages, however, could indicate about the possible argon loss from the muscovite or misinterpretation of the stratigraphy.

This study suggests that the stratigraphy of the Gondwana sequences in eastern Nepal needs to be re-evaluated. The existing quartzite unit of supposedly Permo-Carboniferous Saptakoshi Formation (eastern Nepal) should belong to Late Cretaceous, equivalent to the Amile Formation of western Nepal. The Tamrang Formation (eastern Nepal), which is currently considered as Permo-Carboniferous to Cretaceous, could be an equivalent unit of the Eocene Bhainskati Formation of western Nepal.

ACKNOWLEDGEMENTS

I would like to express my thanks and gratitude to my dear teacher Dr. Ashraf Uddin for bringing me to Auburn University and giving me the chance to get a Master's degree in Geology. Dr. Uddin helped me not only as the principal advisor but also as a real guardian to get the best outcome of this research.

I would like to express my sincere thanks to Dr. Charles Savrda, who helped with significant editing in this thesis. It would have been difficult to get this research work done without Dr. Savrda. I also would like to thank Dr. Willis Hames for help with the geochronology part of this research.

I also acknowledge Mr. Chris Fleisher of University of Georgia for help during microprobe analysis. I thank Dr. Bishal Nath Upreti and Dr. Megh Raj Dhital for continuously guiding me through my research, supporting my fieldwork, and reviewing my thesis work. I want to thank my colleagues Pawan Budhathoki, Ashok Sigdel, and Biraj Gautam for their immense help in my fieldwork. I also want to pay my sincere thanks to Mr. Suryalal Shrestha who provided lodging support at Masyam, Palpa, during my fieldwork at the Tansen section. I am truly grateful to my colleagues at Auburn University, Subhadip Mandal and Shahadat Hossain, for their significant support throughout the development of thesis work, for literature review, lab work, data analysis

and computer work. I am thankful for Subhadip not only for his support but also for the support I got from him while sharing an apartment.

I am very grateful to Eva Lilly and Sheila Arington for their kind support throughout my study with all administrative work. John Simms always helped to solve the computer hardware problems I got during my work in the department. I also like to thank Dr. Zeki Billor for his moral support and proper guidance for muscovite separation.

I also want to pay my sincere thanks to my seniors Prakash Dhakal and Mohammad Wahidur Rahman for their guidance. Prakash was the one who helped me to adjust with educational system and social life in United States. I am also grateful to Bibek Upreti for his support in my thesis work as well as in my daily life. It was Bibek who broke most of my sandstones samples which were very hard.

This research was funded by the U.S National Science Foundation (NSF-EAR-0310306), Geological Society of America, and the Department of Geology and Geography of Auburn University.

I want to thank my parents who gave me the opportunity to see this wonderful world and supported me in every step of my life. I would like to thank my brother and sisters for their love and support.

Style manual or journal used

Geological Society of America Bulletin

Computer software used

Adobe Acrobat 6 Professional

Adobe Illustrator 8.0

Adobe Photoshop CS 2

Macromedia FreeHand 11.0

Golden Software Grapher 3.0

Golden Software Surfer 8.0

Microsoft Excel 2007

Microsoft Word 2007

Microsoft Office Picture Manager 2007

TABLE OF CONTENTS

LIST OF FIGURES

LIST OF TABLES

CHAPTER 1: INTRODUCTION

1.1 INTRODUCTION

Studies of petrofacies evolution are based on the assumption that the composition of detrital sediments records the composition of the source rocks from which those sediments were derived (Dickinson and Suczek, 1979). This theoretical relationship enables interpretation of paleogeography, paleoclimate, ancient plate tectonic settings (Graham et al., 1976; Dickinson and Suczek, 1979), and rock-uplift and exhumation histories (Graham et al., 1976) from the sedimentary record. Sometimes sedimentary rocks may provide the only source of this information particularly in cases of deeply denuded source terranes. The validity of this assumption has been demonstrated for numerous samples detrital sediments and sedimentary rocks (Dickinson, 1970; Dickinson and Suczek, 1979). However, interpretation of provenance from sediment compositional data also requires consideration of other controlling factors such as transport distance, time, energy, and climate (Suttner, 1974; Johnsson, 1993).

Sandstone compositional studies are very important in tracing sediment provenance (Dickinson and Suczek, 1979). Sandstone compositional analyses, in which proportions of detrital framework grains within a sand (stone) sample are plotted on various ternary plots (QtFL, QmFLt, etc.), can distinguish various tectonic settings of source areas (Ingersoll et al., 1995). Composition of detrital sediments is controlled by

various factors, including source rocks, modes of transportation, depositional environments, climate, and diagenesis (Suttner, 1974). Provenance studies that focus on key attributes of detrital mineralogy provide important constraints on basin evolution and unroofing history of orogenic belts.

The term "Gondwanaland' was coined by Eduard Suess, referring to India as the land of 'Gond', which was the name of a local Indian tribe. However, Gondwanaland is now defined as southern supercontinent that existed from 550 Ma to 167 Ma (Fig. 1.1).

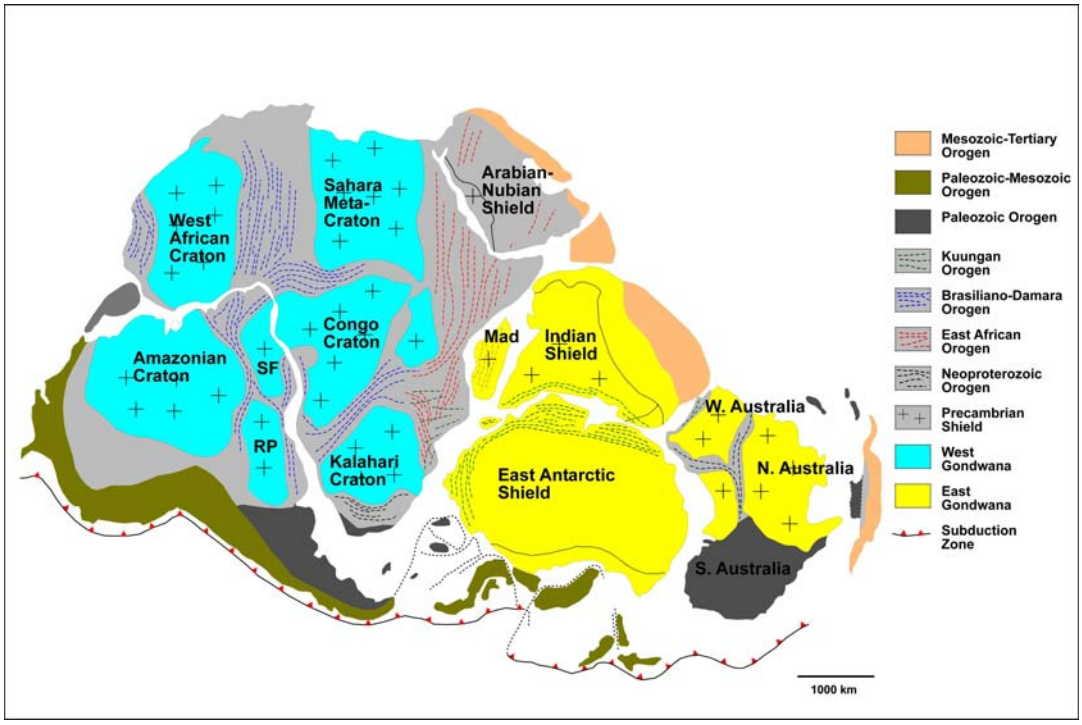

Figure 1.1 Configuration of continental masses in Gondwanaland (after Gray et al., in press)

Sedimentary sequences deposited from early Carboniferous to Late Jurassic in peninsular India (Gondwanaland) are known as Gondwanan sequences (Wadia, 1919). Most of these sequences were deposited in continental depositional environment with few marine invasions. The name is also applied to the sequences deposited in other parts of

Gondwanaland during that period, including there now in Australia, Africa, South America and Antarctica.

The Gondwanan system in the Indian subcontinent is not confined to peninsular India. Outliers of Gondwanan sequences have been found in northern India across the Indo-Gangetic plain in the western Himalayas (Punjab Salt Range, Afghanistan, Kashmir) and the eastern Himalayas (Nepal, Sikkim, Bhutan, Assam, etc.). These are known as extra-peninsular Gondwanan sequences. Gondwanan strata of peninsular India are thick and relatively undisturbed, whereas the extra-peninsular occurrences are incomplete and have been folded, compressed, and, in many cases, metamorphosed.

The provenance history of the Gondwanan sequences in the Nepal Himalaya (Lesser Himalaya) has not been studied as thoroughly as the Gondwanan sequences of peninsular India. Although parts of this sequence have been studied (Bashyal, 1980, Sakai, 1983; Dhital, 1992; DeCelles et al., 2004; Najman et al., 2005) at different localities along the Nepal Himalaya, a complete and comparative study has not been done. The Tansen Group in western Nepal consists of relatively complete and thick Gondwanan and post-Gondwanan sequences documenting sedimentation for an extended period ranging from late Carboniferous to early Miocene (DeCelles et al., 2004). However, the sequences in the eastern part (Katari and Barahchettra groups) are thinner and incomplete and stratigraphy has received little attention. As the Gondwanan sequences of the eastern part of Nepal are close to the Main Central and Main Boundary thrust (MCT and MBT) zones, they are intensely deformed by numerous imbricate faults (Dhital, *unpublished*). A thorough study comparing and contrasting Gondwanan

sequences from the Nepal Himalaya and India has not been done. Sakai (1983) made an effort to correlate the Gondwanan sequences of the Tansen Group of Nepal with Indian units. However, this correlation was based solely on lithology.

1.2 LOCATION OF THE STUDY AREA

The present study is focused on Gondwanan sequences preserved in three sections within the Nepal Himalaya (Fig. 1.2).

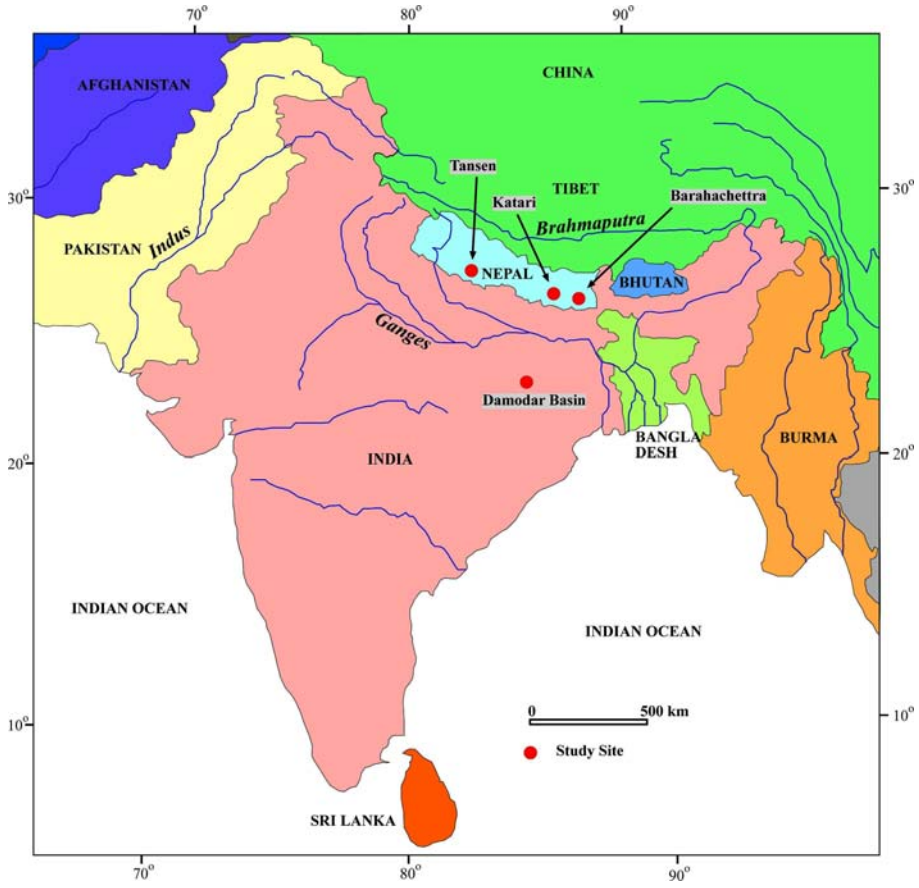

Figure 1.2 Location map of study sites in Nepal. Map also shows the Damodar Basin of Peninsular India.

These selected sections are distributed from western part of Nepal to eastern part. The Tansen Group is approximately 400 km west of Kathmandu valley in the Palpa District and is easily accessible with motor vehicles. The Barahachettra and Katari groups are exposed approximately 650 km and 500 km, respectively, to the east of Kathmandu valley and are also easily accessible.

Damodar basin, type locality of peninsular Indian Gondwanan sequences, is approximately 100 km southeast of New Delhi and only 300 km south of the Barahachettra Group in eastern Nepal.

1.3 PREVIOUS WORK

Medlicott (1864) documented a tillitic horizon,--the Blaini Formation-- in the Lesser Himalaya of the Simla area (India). Pilgrim and West (1928) carried out further detailed lithostratigraphic studies of this and correlated it with the Lower Gondwanan tillitic sequences of peninsular India. However, when Early Cambrian and late Precambrian fossils were discovered from the Krol and Tal formations above the Blaini Formation (Azmi and Pancholi, 1983), these tillitic beds were interpreted as a Proterozoic sequences. Auden (1935) was the first to record Gondwanan sequences in eastern Nepal based on mapping along the Lesser Himalaya.

In contrast with the tillitic beds in the western Himalaya, most of tillitic beds in the eastern Himalaya are considered to be part of the Lower Gondwanan system based on occurrence of plant fossils. However, Gansser (1983) introduced the Diuri Formation, a

boulder bed sequence lacking coal from the Bhutan Lesser Himalaya and correlated it with the late Precambrian tilloids.

Sakai (1983) developed a detailed stratigraphy of the Tansen Group. He identified five stratigraphic units in the group including the Sisne, Taltung, Amile, and Bhainskati formations. Earlier, the distribution of this group was thought to be confined to the Tansen-Sallyan-Jajarkot area of western Nepal. However, later works show that it is distributed over a much wider area (Upreti, 1999) and may be present beneath the recent Gangetic sediments of the Terai plain overlain by the Siwalik sediments (Friedenreich et al., 1994). Bashyal (1980) divided Gondwanan sequences in eastern Nepal into 5 units and grouped them together as the Barahachettra Formation. Dhital and Kizaki (1987) recognized another diamictite horizon in the Dang-Sallyan area within low-grade metamorphic rocks constituting a thrust sheet covering the sedimentary rocks of the Lesser Himalaya. Dhital (1992) worked on the diamictitic unit within Gondwanan sequences at three different locations in Nepal and mapped the Gondwanan sequences in the Barahachettra area.

DeCelles et al. (1998) studied the fluvial history of the Dumri Formation and, based on detrital zircon dates, assigned an early Miocene age. Zircon and Nd-isotopic dates generated by Decelles et al. (2004) indicate an Archean to Early Proterozoic Indian cratonic provenance for the Amile Formation. DeCelles et al. (2004) determined the provenance of the Eocene Bhainskati Formation to be Tethyan and Lesser Himalayan rocks. The increased proportion of late Proterozoic zircons in fluvial litharenites of the lower Miocene Dumri Formation reflects a Greater Himalayan provenance (DeCelles et

al., 2004). The time lag between Eocene deposition in the western and eastern parts of Nepal was determined to be 2 m.y. (Najman et al., 2005) suggesting that early exhumation of the Himalayas was diachronous.

1.4 OBJECTIVES

This study focuses on evaluating the petrofacies evolution and paleotectonic settings of Gondwanan sequences of Nepal, in order to reconstruct the paleogeographic scenario of Gondwanaland, the late Paleozoic supercontinent of the southern hemisphere. Several approaches were taken to carry out this study.

Petrographic studies of representative Gondwanan sandstone samples from three different sections of Nepal were performed to picture characteristic modes of occurrence and environments of deposition. Traditional heavy mineral studies and mineral chemistry of representative heavy minerals of Gondwanan sandstones collected from the three study sections were completed to evaluate the provenance and weathering history of the sediments. Bulk whole-rock chemistry of major, trace, and rare-earth elements of selected Gondwanan samples were performed to decipher their probable source rocks, paleogeographic positions, and weathering history. Laser $^{40}Ar/^{39}Ar$ geochronology of detrital muscovite grains from allegedly similar stratigraphic levels of Gondwanan sequences at three localities was used to uncover temporal relationships and probable tectonic histories of source terranes. Ultimately, this research sought to evaluate the long-disputed along-strike stratigraphy of Gondwanan sequences of Nepal.

CHAPTER 2: GONDWANAN SEQUENCES OF NEPAL HIMALAYA

2.1 GENERAL GEOLOGICAL SETTING OF NEPAL HIMALAYA

Nepal occupies the central segment of the 2400-km-long Himalayan arc. Similar to other parts of the Himalayas, from south to north, Nepal can be subdivided into the following five major tectonic zones: (1) the Gangetic Plain, consisting of recent alluvial deposits of Ganga river system; (2) the Siwaliks or sub-Himalayas are typically Miocene deposits, deposited in the foreland depression developed after collision of the Indian plate with the Tibetian block; (3) the Lesser Himalayas consist of a thick succession of Precambrian to early Paleozoic low-grade and high-grade metamorphic rocks; (4) the Higher Himalayas consist of high-grade metamorphic gneiss, schists, marble and quartzite; and (5) the Tibetan or Tethys Himalayas are thick successions of fossiliferous rocks deposited during Paleozoic and Mesozoic eras (Fig. 2.1).

These tectonic zones are separated from each other by thrust and fault boundaries. The thrust system in the Nepal Himalaya includes the Main Frontal Thrust (MFT) between Siwaliks and Gangetic Plain, the Main Boundary Thrust (MBT) between the Lesser Himalaya and the Siwaliks, the Main Central Thrust (MCT) between the Higher Himalaya and the Lesser Himalaya, and the South Tibetian Detachment System (STDS), which is a gravity driven normal fault.

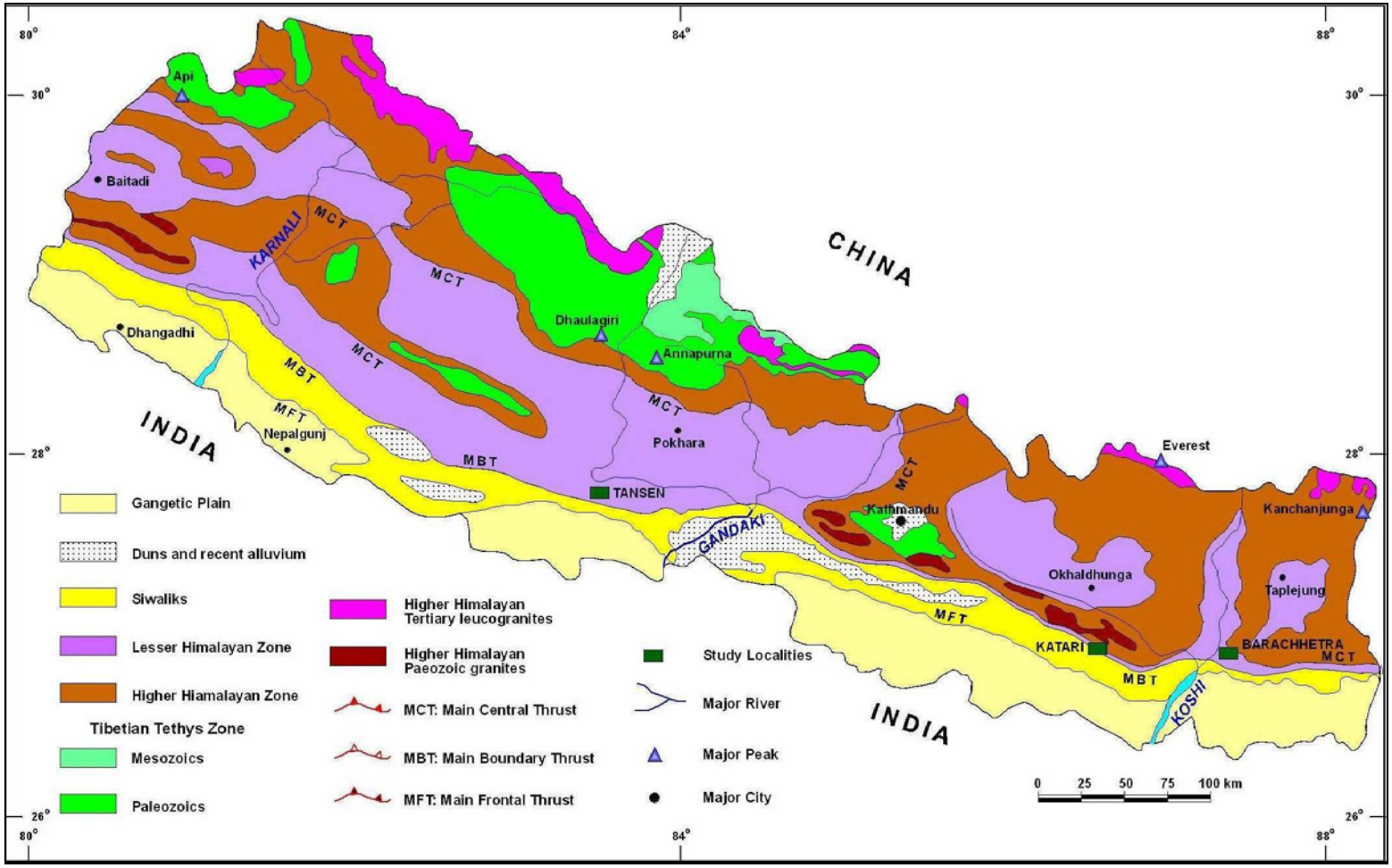

Figure 2.1 Geological map of Nepal showing locations of Gondwanan sequences investigated in this study (after Amatya and Jnawali, 1994)

2.2 GONDWANAN STRATRIGRAPHY OF NEPAL

The Lesser Himalayas contain three units: (1) The lowermost Precambrian to early Paleozoic low-grade metamorphic unit, (2) a late Paleozoic to early Cenozoic Gondwanan sequence, and (3) a late Precambrian high-grade metamorphic unit. The Gondwanan rocks occur in patches in the Lesser Himalayas. The lowermost unit is considered as the equivalent of the Vindhyan Group of peninsular India, which is unconformably underlain by Gondwanan sequences. The unconformity between these two groups is known as the Great Lesser Himalayan Unconformity (Upreti, 1999) or Pan-African Unconformity (Valdiya, 1997) and is contemporary with Late Pan-African diastrophism. The late Precambrian high-grade metamorphic unit is actually an allocthonus unit thrusted over other Lesser Himalayan rocks and likely has a root zone within the Higher Himalaya.

2.2.1 TANSEN GROUP

The Tansen Group (type locality of Gondwanan sequences in Nepal) is a largely continental deposit, with some periodic marine incursions. The lithological succession and fossil content of Gondwanan sequences in the Tansen area have been very well studied. The Tansen Group consists of the Sisne Formation (Lower Gondwana), the Taltung and Amile formations (Upper Gondwana), and the Bhainskati and Dumri formations (post-Gondwana) (Figs. 2.2, 2.3A, B).

Sisne Formation: The Sisne Formation unconformably overlies the Kerabari Dolomite of the Kaligandaki Supergroup. This disconformity is the same as the Pan-

African disconformity. However, the base of the Sisne Formation cannot be defined in Tansen area due to its fault relation with the Kerabari Dolomite. The reported maximum thickness of this formation is 1020 m (Sakai, 1983). The Sisne Formation mostly consists of diamictite and mudstone with some beds of sandstone and conglomerate. Diamictite with both clayey matrix and sandy matrix are present in the area. The majority of the clasts are granites, gneissic rocks, limestone, sandstone, and dolomite ranging in size from sand to boulder. Though there is no direct evidence of a glacial origin for the diamictite (e.g., striations), the deposit is considered as glacial based on poor sediment sorting, and presence of dropstone in interbedded clay layers.

Sandstone beds are more prominent in the middle part of Sisne section, which is about 80 m thick at the type section (Sakai, 1983). Beds are massive in the middle part but gradually show climbing ripples and parallel lamination in the upper part. Sandstone beds are highly fractured as a result of various tectonic stresses (Fig. 2.4). The uppermost part of the Sisne Formation consists of bioturbated mudstone. Some shale floats resembling the Ritung Bioturbated Member of the upper part of the Sisne Formation contain bryozoan remains (*Fenestella, Polypora* and *Acanthocladia)*, which is consistent with Carboniferous *Fenestella* shales in the Lower Gondwana of Salt Range (Sakai, 1983).

Taltung Formation: The Taltung Formation unconformably overlies the Sisne Formation; angular boulders of the Sisne diamictite and shale occur in the basal conglomerate of the Taltung Formation (Figs. 2.2, 2.3A, B). The basal member of the

Taltung Formation, the Charchare Conglomerate, is ~13 m thick at the type locality area (Sakai, 1983).

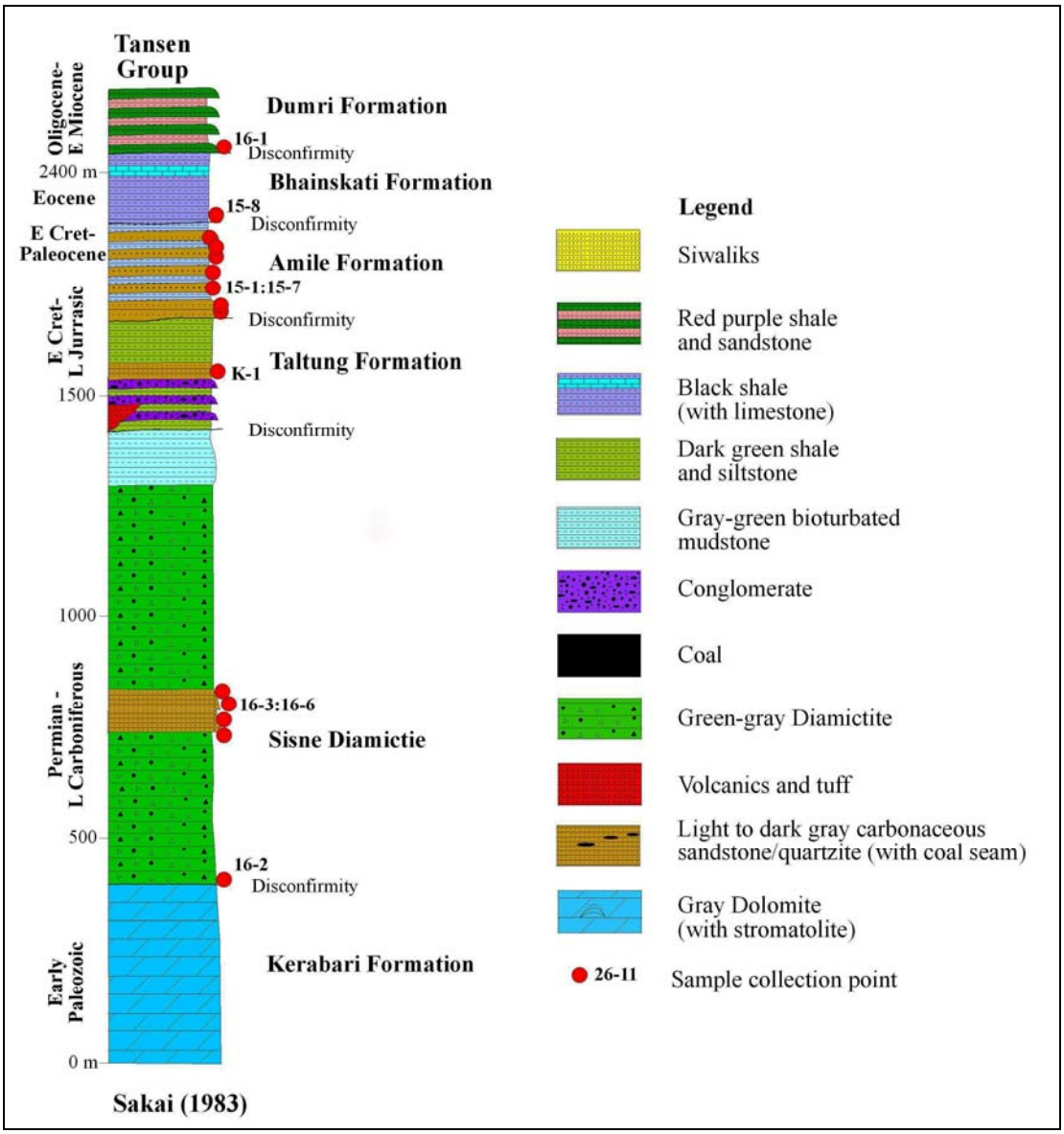

Figure 2.2 Stratigraphic column of the Tansen Group, eastern Nepal (after Sakai, 1983), showing position of samples used in the current study.

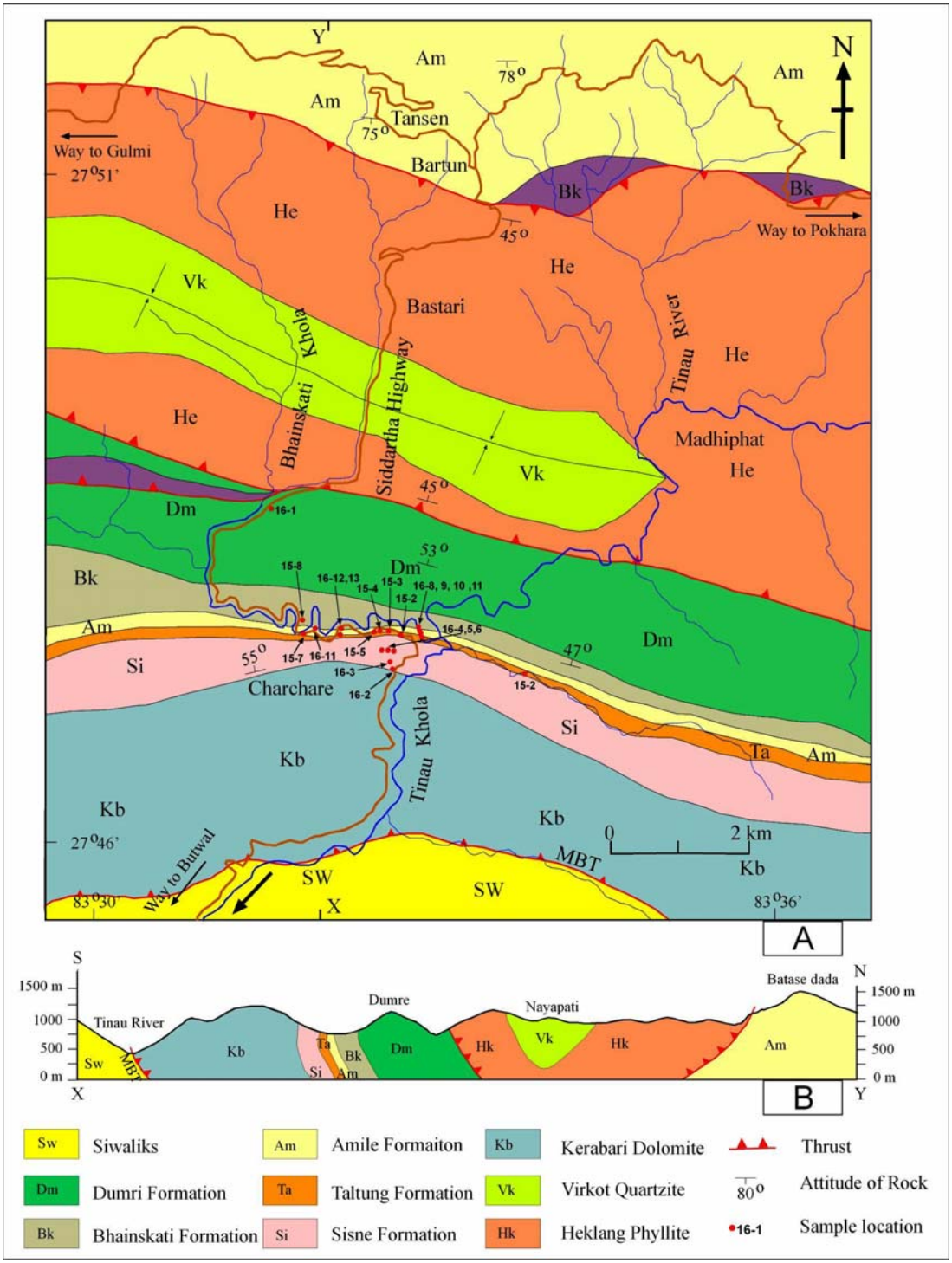

Figure 2.3 Geological map (A) of Tansen area (after Sakai, 1983) and geological cross section (B) of Tansen area.

The conglomerate beds fine upward and are capped by sandstone beds. Pebbles of conglomerate are composed mostly of quartzite and volcanic rocks. Locally, the pebbles are imbricated. Imbrications suggest that the flow direction during the deposition of conglomerate was from SE to NW. Associated with the lower part of the Taltung Formation and Charchare Conglomerate is the Aulis Basalt, which is present in the southern part of Tansen area (Sakai, 1983). The basalt is porphyritic with plagioclase phenocrysts and dark-green to gray.

Figure 2.4 Roadside outcrop of the Sisne Sandstone near Charchare area.

The lower member of the Taltung Formation consists of several upward fining sequences, each of which consists of conglomerate, sandstone, and silty shale. Plant

fossils referable to Upper Gondwana are found in siltstone beds (Sakai, 1983). This member is interpreted as meandering fluvial deposit.

Rhythmic sequences of sand and shale characterize the upper member of the Taltung Formation. The thickness of each rhythm ranges from 8 – 20 m. The light green sandstone beds are mostly massive but some are cross bedded and contain scour-and-fill structures. Shales are characterized by hematite speckles and calcareous concretions. The lower part of the Taltung Formation contains the fossil plant genera *Ptillophyllum*, *Pterophyllum*, *Cladophrebis* and *Elatocladus*, which indicates a Jurassic-Cretaceous age (Sakai, 1983).

Amile Formation: The total thickness of the Amile Formation is 230 m at the type locality. The basal unit of the formation consists of conglomeratic quartz arenite followed by white quartz arenite (Fig. 2.4) with interbedded shale.

The middle member of the Amile Formation is characterized by the presence of fossiliferous argillaceous limestones, siltstones, and hematitic quartz arenite. Limestone beds yield several types of marine fossils including bivalves, gastropods, echinoids, and corals (Sakai, 1983).

Figure 2.5 Steeply dipping Amile Quartzite along Bhainskati Khola near the Charchare area, western Nepal.

The upper Member of the formation is characterized by an increase in mud content in quartzose beds and the presence of calcareous muddy sandstones and carbonaceous shales. The uppermost part of the formation consists of bioturbated carbonaceous muddy sandstone containing coalified wood fragments. The Amile Formation is considered as Cretaceous to Paleocene in age based on its stratigraphic position and presence of scleractinian corals, which are also present in the Jurassic-Cretaceous Tal Formation of the Kumaon Himalaya (Sakai, 1983) However, that part of the Tal Formation is no longer considered as the Tal Formation (Valdiya, 1997).

Bhainskati Formation: The Bhainskati Formation is not considered as Gondwanan deposits as it was deposited after the break up of Gondwanaland. However, it was deposited in the same basin where Gondwanan sequences were deposited. The contact between the Bhainskati Formation and the underlying Gondwanan sediments is unconformable. The total thickness of the formation at the type locality is about 160 m. The Bhainskati Formation consists of largely black shale, interbedded with calcareous, fossiliferous, and greenish-reddish shale. The hematite beds are present at top part.

The fossiliferous beds of the Bhainskati Formation contain abundant bivalves, gastropods, and larger foraminifera (Sakai, 1983). Black shale beds contain pyritized wood fragments. The presence of *Nummulites sp* in the Bhainskati Formation indicates an Eocene age for this formation and suggests correlation with the Subathu Formation of the Kumaon Himalaya.

Dumri Formation: The Dumri Formation disconformably overlies the Bhainskati Formation (Figs. 2.2 and 2.3). The formation consists of a thick succession of medium-grained, bluish-gray quartzose sandstones interbedded with red and green shales. The proportion of shale decreases towards the upper part of the formation. Sandstones are quartzose wackes with little carbonaceous material. There are also several intraformational shale-pebble conglomerates and conglomeratic sandstones. The age of the Dumri Formation is not known. However, based on relationships with the underlying Bhainskati Formation and correlation with the Murree Group of Pakistan and the Dagshai Formation of Simla Himalaya, it is assigned an Early Miocene age.

2.2.2 BARAHACHETTRA AND KATARI GROUPS

Barahachettra Group: Bashyal (1980) identified Gondwanan sequences in the eastern part of Nepal and referred to that that tectono-stratigraphic package as the Barahachettra Formation. He divided the whole formation into five members and defined the Main Boundary Thrust (MBT) as the southern boundary of the formation. The latter was based on the consideration that the dolomite unit just north of the MBT is the youngest unit of the package. Dhital (1992), however, did not include the Dolomite Unit in that formation. He revised the stratigraphy and divided the sequences into the Saptakoshi Formation, the Kokaha Diamictite and the Tamrang Formation. He assigned the rank of 'Group' to the Barahachettra Formation of Bashyal (1979, 1980) (Figs. 2.6 and 2.7).

Quartzite unit of the Saptakoshi Formation unconformably overlies the dolomite beds of the Precambrian Lukuwa Formation. Notably, quartzites are absent on top of Precambrian basement in peninsular and in other extra-peninsular Gondwanan basins (Bashyal, 1979, 1980). The formation consists of medium to thick bedded, gray and dark gray, carbonaceous quartzite, carbonaceous shale, and conglomerate with lenses of coal. Bashyal (1980) reported the occurrence of plant species *Shizonera gondwanensis* at Takure Khola, which belongs to the Damuda flora of Permian age.

The Kokaha Diamictite consists of diamictite beds with clasts of quartzite, dolomite, schist, granite, shale and sandstone. The formation sharply overlies the Saptakoshi Formation. Some interbedded sandstones are also present in the formation

(Fig. 2.9). The Kokaha diamictite is overlain by calcareous sandstones of the Tamrang Formation. These sandstones are composed of quartz, calcite, and plagioclase in an argillo-calcareous matrix (Bashyal, 1980)

Katari Group: A small patch of Gondwanan sequence rocks is observed in the Katari area, eastern Nepal. Along the Maruwa Khola section, Gondwanan sequences are observed resting unconformably over stromatolitic dolomite (Figs. 2.7 and 2.8). In the basal part, thin beds of diamictite with dolomite clasts embedded in a dark gray matrix are overlain by a trachy-basalt (Dhital, *unpublished*). The latter rock consists of alkali feldspar and potassium-rich laths of sanidine. The volcanic unit is overlain by carbonaceous quartz arenite (Fig. 2.10) containing abundant coalified wood. The quartz arenites are followed by 1-m-thick interval of volcanic tuff and thick-bedded conglomerate. Greenish to bluish gray calcareous sandstones and dark gray shales are present in the upper section.

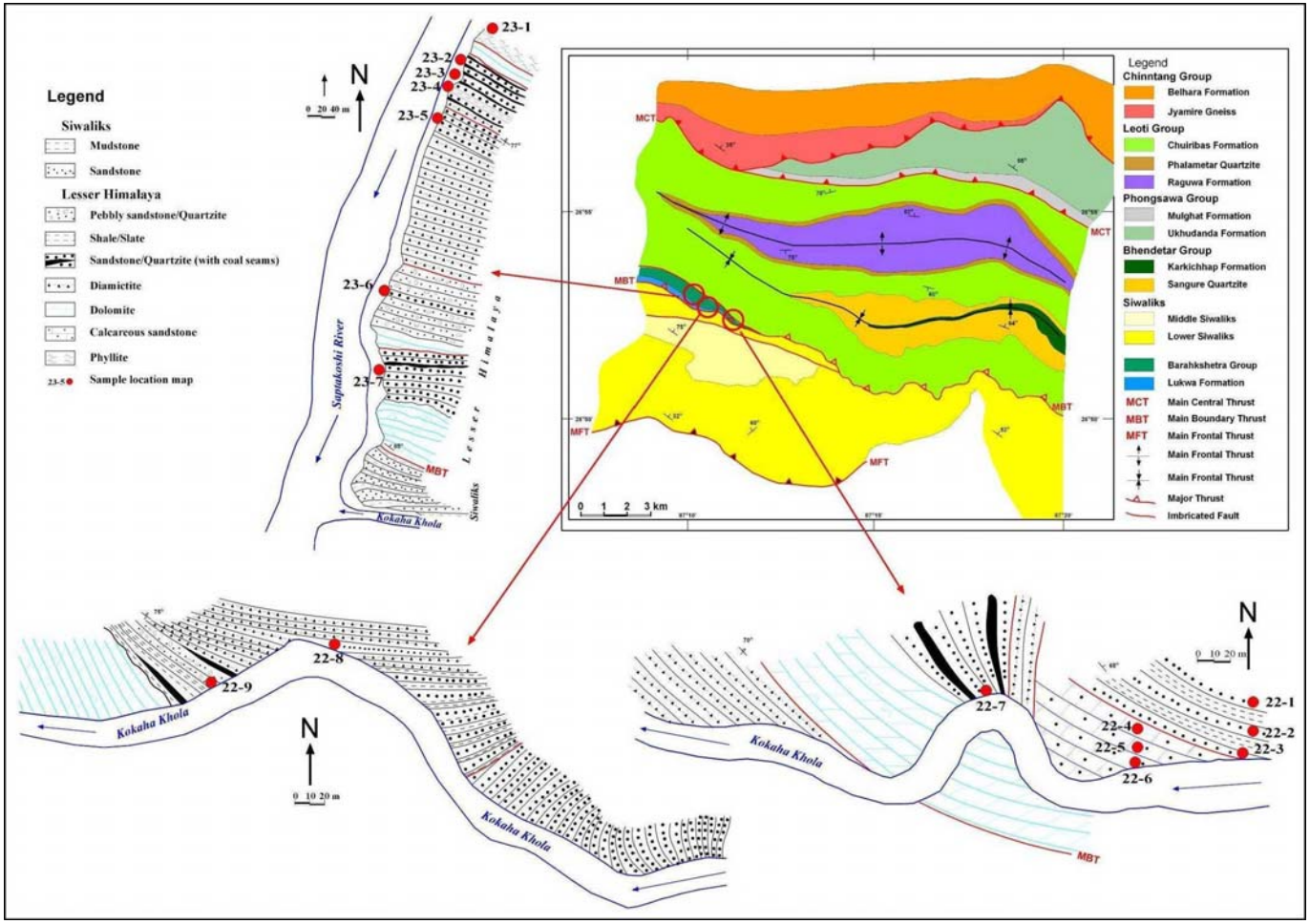

Figure 2.6 Geological map of the Barahachettra area (after Dhital, 1992 and 2006) and sample collection locations.

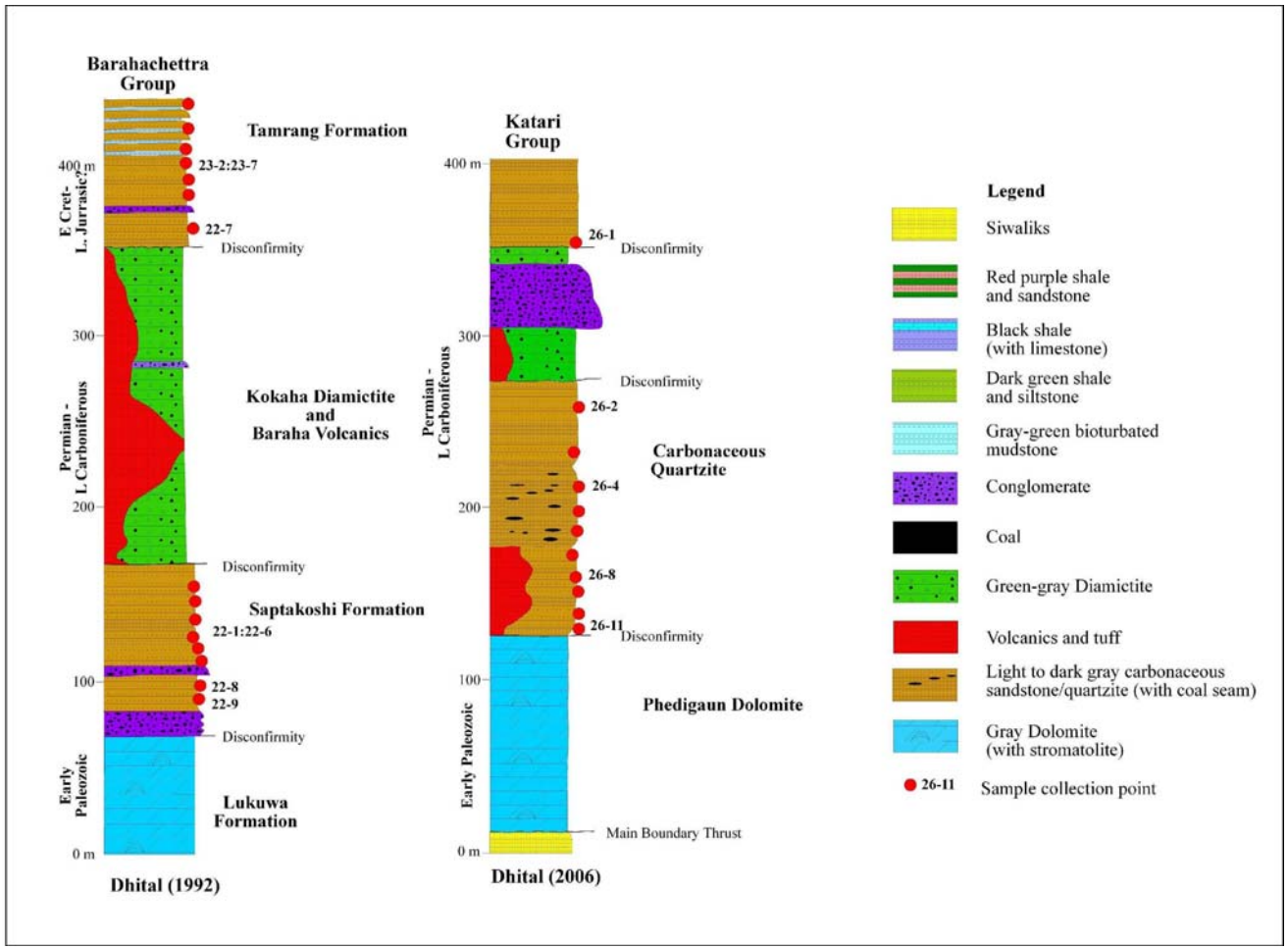

Figure 2.7 Stratigraphic Column of the Barahachettra (Dhital, 1992) and Katari groups (Dhital 2006), eastern Nepal.

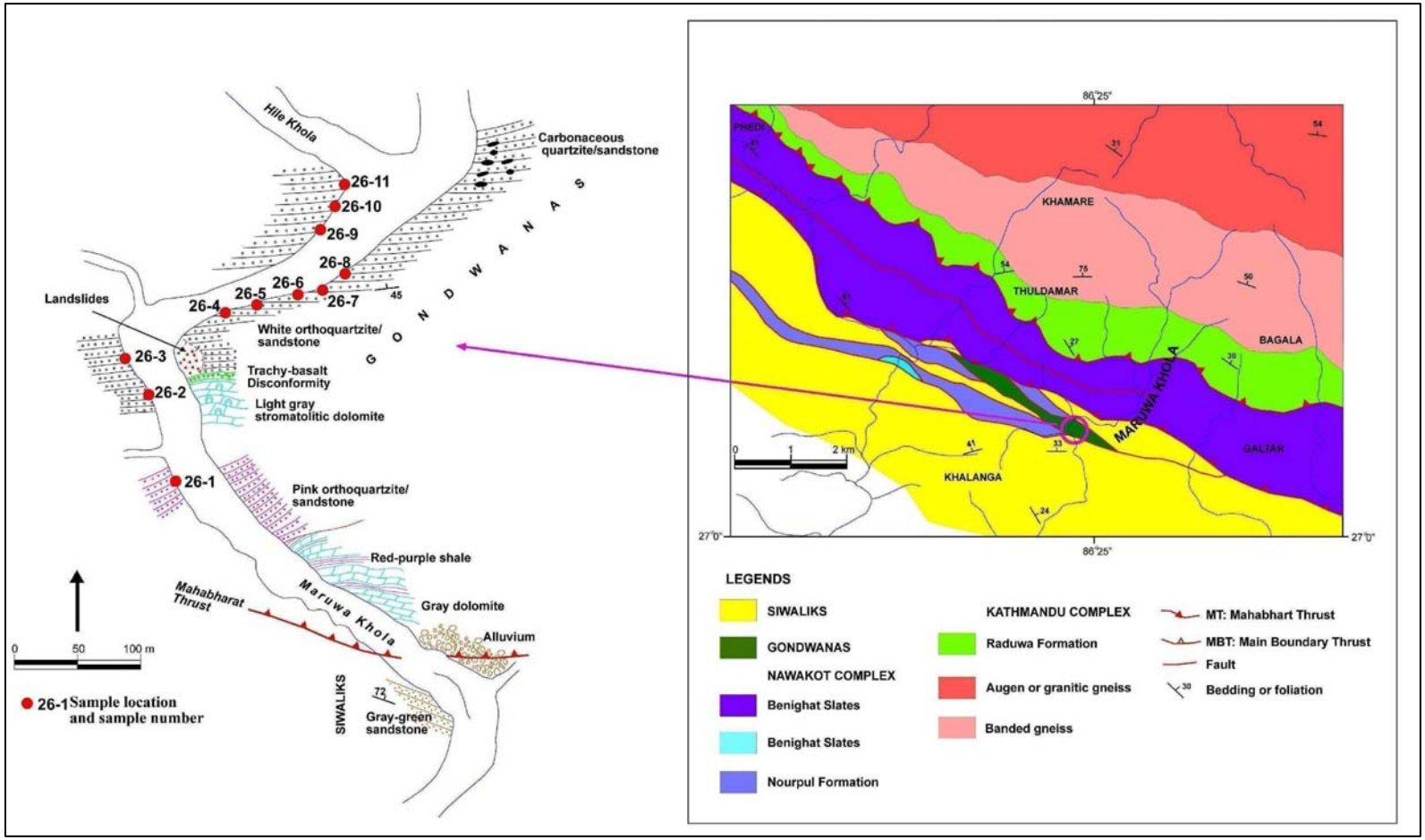

Figure 2.8 Geological map of the Katari area (Dhital, *unpublished*) and sample-collection locations.

Figure 2.9 Outcrop of Kokaha Diamictite along Kokaha Khola, eastern Nepal.

Figure 2.10 Outcrop of sandstone along Maruwa Khola in Katari area, eastern Nepal.

2.3 GONDWANAN SEQUENCES IN OTHER PARTS OF NEPAL

Sharma et al. (1984) worked on the Daban Group of Jajarkot-Piuthan-Sallyan area of western Nepal, which is equivalent to Gondwanan sequences. The lower unit (Kochhap Formation) of the Daban Group is equivalent to the Sisne Group, whereas the upper unit (Goyaltham Formation) is equivalent to the Taltung Formation.

Dhital and Kizaki (1987) worked on the Gondwanan section of the Dang area of western Nepal. They described the Sallyan Formation as consisting of phyllitic conglomerate and diamictite and the Phalabang Formation as consisting of phyllitic slates. These formations are considered to be Lower Gondwanan sequences. The Sattim Formation, characterized by alternating beds of quartzose sandstone and shale, is considered to be Upper Gondwana. The overlying Durbing Formation is considered to be a post-Gondwanan sequence.

In Surkhet area (Western Nepal), Shrestha et al. (1987) worked on the Surkhet Group and divided it into three formations: Melpani, Swat, and Suntar. However, only the Melpani Formation is considered to be part of an Upper Gondwanan sequence. The Swat and Suntar formations are considered to be post-Gondwanan sequences.

The ages and stratigraphic positions of some of the Gondwanan sequences of Nepal are doubtful due to the absence of fossils and tectonic complexities. However, correlation is been done between these sequences primarily based on lithology (Table 2.1).

Table 2.1 Generalized correlation of Gondwanan sequences of Nepal Himalaya

Age		**Surkhet Group (Kayastha, 1989)**	**Sallyan-Jajarkot Group (Shrestha, 1987)**	**Sharda Group (Dhital and Kizaki, 1987)**	**Tansen Group (Sakai, 1983**	**Katari Group (Dhital, 2006)**	**Barahachettra Group (Bashyal, 1980)**
Mid. Mioene	**Post Gondwana**	Suntar Formation	Dumri Formaiton	Durbing Formation	Dumri Formaiton		
Eocene		Swat Formation	Bhainskati Formation		Bhainskati Formation		
Late Cret-Paleocene	**Upper Gondwana**	Melpani Formation	Amile Formation	Sattim Formation	Amile Formation		
L. Jurassic-Early Cretaceous			Goyaltham Formation		Taltung Formation		
Permo-Carboniferous	**Lower Gondwana**		Kochhap Formation	Phalabang Formation Sallyan Formation	Sisne Formation	Katari Group	Barahachettra Group

2.3 DISTRIBUTION OF GONDWANAN BASINS IN PENINSULAR INDIA

The Carboniferous-Permian Gondwanan system occurs in a number of isolated basins of peninsular India. Three large tracts have been identified (Wadia, 1919): (1) a large linear tract in Bengal along the valley of the Damodar River, with sizeable exposures in the Rajmahal Hills; (2) an extensive outcrop in Madhya Pradesh, which follows the Mahanadi Valley; and (3) a series of more or less connected troughs forming an elongated band along the Godavari River (Fig. 2.11).

The major Gondwanan basins in peninsular India are the Pranita Godavari Basin (PGB), Mahanadi Basin (MB), Damodar Basin (DB), Son Basin (SB), Satpura Basin (SPB), and Rajmahal Basin (RB). All these basins are aligned with three linear tracts of India (Fig. 2.11).

The evolution of these basins is related to mountain building and other crustal movements. Earlier crustal movements include the rejuvenation of the Aravalli and the Eastern Ghat ranges, which caused the subsidence of large blocks between vertical or slightly inclined normal faults (Wadia, 1919). However, normal faulting in extensional lineaments between the cratonic blocks of India is also considered as the mechanism of Gondwanan basin development in India (Dutta, 2002). Most of the Gondwanan basins are half-graben basins bounded by a fault on one side. However, this mechanism does not apply to all Gondwanan basins.

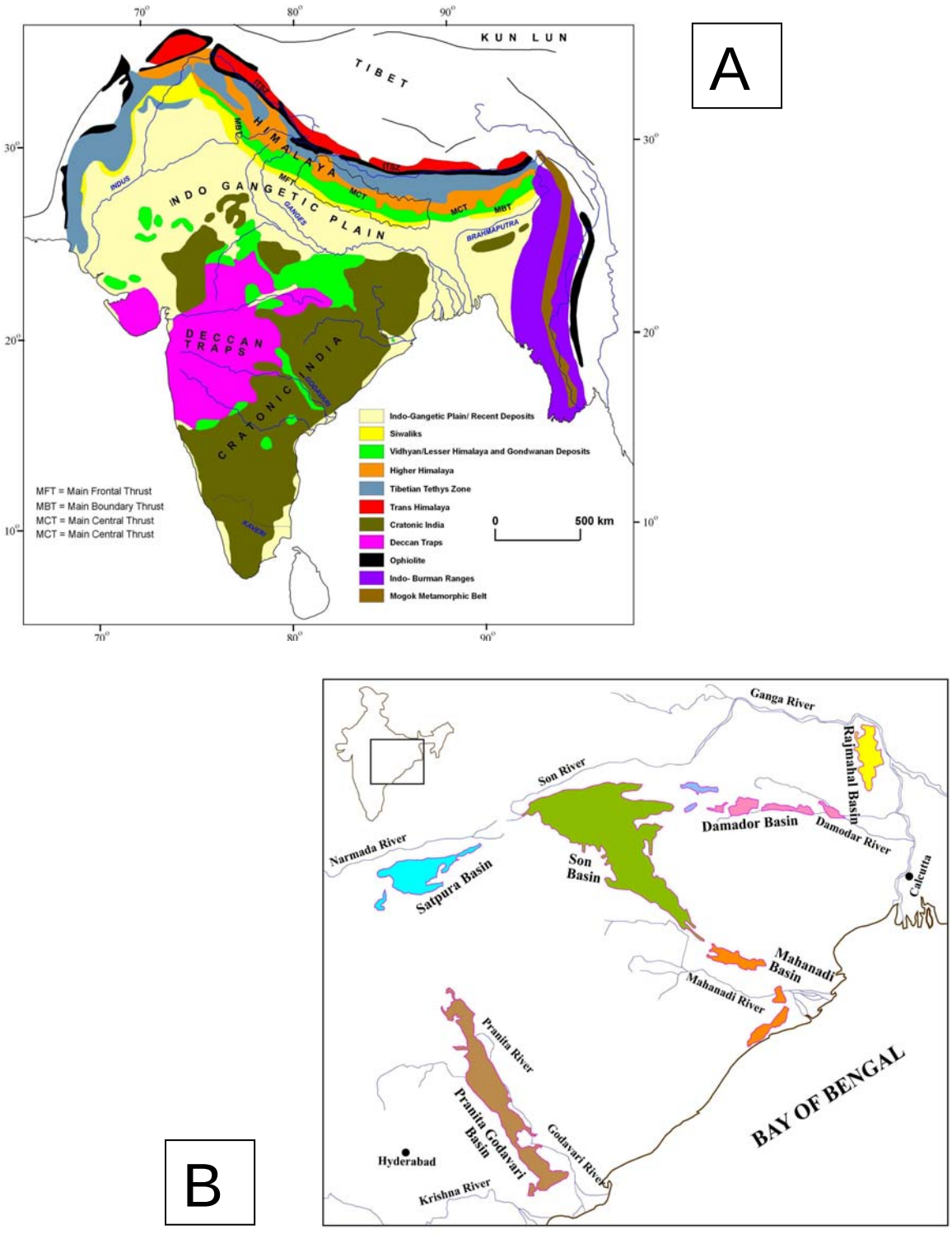

Figure 2.11 (A) Geological map of peninsular India (after Najman, 2005) and (B) distribution of Gondwanan basins in peninsular India (after Dutta, 2002)

The Gondwanan system of India is divided into three classic divisions-- the Lower, Middle and Upper--corresponding in a general way to the Permian, Triassic, and Jurassic of Europe, respectively (Wadia, 1919). These units have been further divided into different formations. Lithological associations of the Gondwanan sequences that are distinct are designated as facies. Veevers (1995) has provided a composite startigraphic column for the Damodar Basin (DB) (Fig. 2.12)

Talchir Formation: The Talchir Formation refers to of the lowermost beds of Gondwanan sequences that were first recognized in the Talchir district of Orissa, southeast India. This series is quite homogenous and uniform in composition over different basins and thus is considered as a valuable stratigraphic horizon. Boulder beds characteristically contain glaciated, striated, and faceted blocks embedded in a fine matrix, and, thus, suggest glacial action during the deposition. The formation is approximately 300 m thick in the Damodar basin and is considered to have been derived from a granitic source (Dutta, 2002)

Damuda Group: The Damuda Group is further divided into three formations: the Raniganj, the Barren Measures, and Barkar formations.

Barakar Formation: The Barakar Formation rests conformably upon the Talchir Formation and consists mostly of coarse-grained, white, massive sandstones and shales with coal seams. The Barakar Formation contains a large quantity of coal in thick seams. Sandstones of the Barakar Formation are more mature compared to the Talchir Formation; sandstones are subarkosic, occasionally grading to quartz arenite (Dutta, 2002).

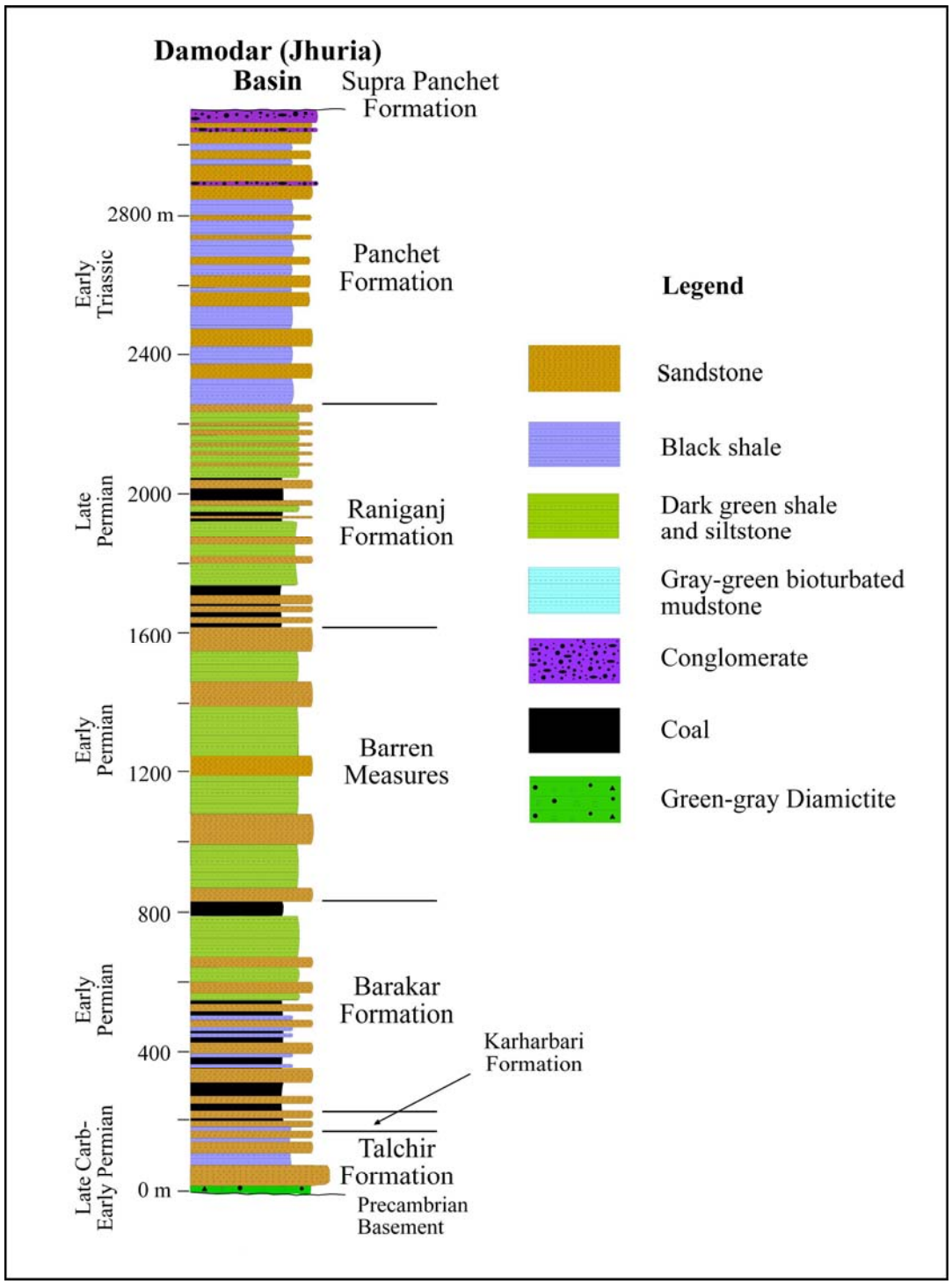

Figure 2.12 Stratigraphic column of Gondwanan sequences in the Damodar Basin (after Veveers and Tiwari, 1995).

Barren Measures: The Barren Measures is a thick sequence of carbonaceous shales with concretions of impure iron carbonates and oxides. This unit varies in thickness and composition among basins (Wadia, 1919). Towards the eastern part (in the DB), shale is more predominant, while in the west sandstone is more common, particularly in the PGB (Dutta, 2002).

Raniganj Formation: The Raniganj Formation consists of coal, carbonaceous shale, siltstone, and sandstone. Coal seams of the Raniganj Formation are thinner than those of the Barakar Fomation; sandstones, mostly arkosic and sub-arkosic, are finer than the Barakar sandstones (Dutta, 2002). The thickness of this formation ranges from 700 m to 900 m.

Panchet Formation: The Panchet Formation lies unconformably on the Raniganj Formation, but in some places it directly overlies the Barakar Formation. The formation contains alternations of red clay and coarse sandstone. However, greenish shale and sandstone are abundant in the lower part of the formation, near the boundary with the underlying Raniganj Formation (Dutta, 2002).

Mahadev Formation (Supra Panchet): The Mahadev Formation is well developed in Madhya Pradesh where a section of approximately 1,300 m is exposed near Nagpur. This formation contains of variegated, massive, coarse- to medium-grained sandstones with ferruginous and micaceous clay. Sandstones are super-mature quartz arenites with very little or no feldspar (Dutta, 2002). In the Damodar Basin, thick-bedded, massive sandstones and shale beds of the Mahadev Formation are exposed. The thickness of this formation is about 800 m at SB, but in some basins it just appears as a thin cover.

2.4 GONDWANAN STRATIGRAPHY OF OTHER PARTS OF EXTRA-PENINSULAR INDIA AND PARTS OF GONDWANALANDS

The Gondwanan sequences on the Indian subcontinent are not confined to peninsular India. Outliers of Gondwanan units have been found in northern India across the Indo-Gangetic plain in the western Himalayas (Punjab Salt Range, Hazara, Afghanistan, Kashmir) and the eastern Himalayas (Nepal, Sikkim, Bhutan, Assam, etc.). These units developed along the northern boundary of India during the Permo-Carboniferous (Fig. 2.13) and are known as extra-peninsular Gondwanan sequences. Gondwanan sequences of peninsular India are usually relatively undisturbed. The extra-peninsular occurrences have been folded, compressed, and, in many cases, metamorphosed. Basic problems related with Gondwanan sequences in extra-peninsular India along the Himalayan range include the identification and age evaluation of the sequences.

In Kumaon Himalaya, the Blaini Formation of the Krol Belt has been correlated with the Sisne Formation of Nepal (Sakai, 1983; Bashyal, 1979). However, later works disputed the late Paleozoic position of the Blaini Formation. *Nummulite*-bearing shales of the Subathu Formation of the Garhwal Himalaya are, however, easily correlated with the post-Gondwanan Bhainskati Formation of the Nepal Himalaya. Only Eocene and Upper Cretaceous units are present in Jammu and Simla area of the western Himalaya. In contrast, only Permian units are found in Bhutan and Arunachal areas of the eastern Himalaya.

Permian Gondwanan units have been reported from the Khalaspur Basin. Here, these are overlain by Miocene and younger deposits (Hossain et al., 2002). Gondwanan sequences have been divided into six facies including coal lithofacies. However, unlike in Nepal and India, marine successions have not been reported from this Bangladesh Gondwanan basin in Bangladesh.

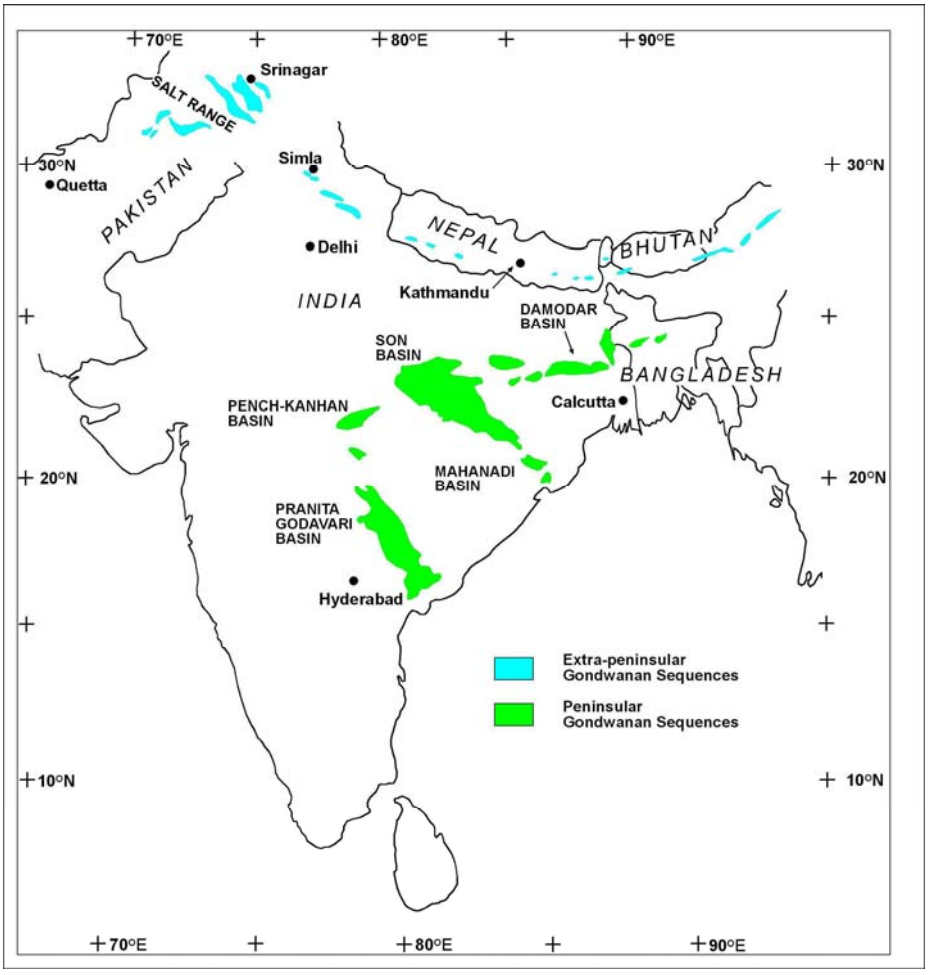

Figure 2.13 Distribution of Gondwanan basins on the Indian subcontinent (Frakes, 1975)

Fluvial conglomerates have been reported from this basin (Hossain et al., 2002). However, Gondwanan sequences of this basin belongs to peninsular Indian Gondwanan sequences based on paleo-tectonic reconstructions (Khan, 1994).

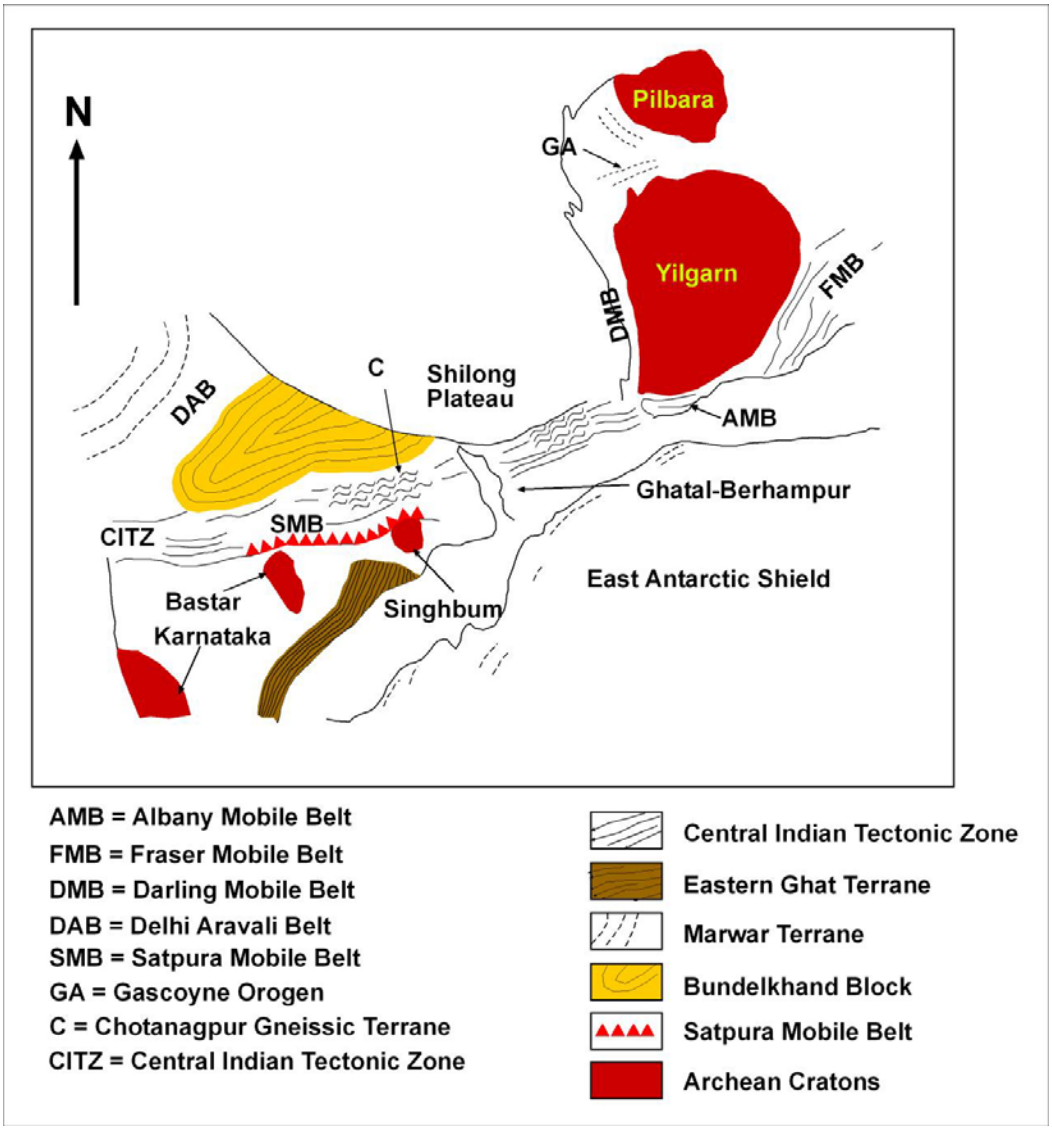

Figure 2.14 Main tectonic subdivision and relation of Indian Precambrian shield (after Khan, 1994).

Based on gravity data, the eastward extension of Gondwanan basins extends up to the Yilgarn craton of Western Australia (Fig. 2.14; Khan et al., 1994). This east-west stretched basin is the northernmost Gondwanan sub-basin that was separated from southern Gondwanan sub-basin by a northeast-southwest intra-cratonic high connecting the Shillong Massif and the Chhotanagpur gneissic terrane. The southern Gondwanan sub-basin was extended from Eastern Ghat palaeo-shelf to the western periphery of the Shillong plateau through Ghatal- Behrampur.

Gondwanan basins were distributed on all continental blocks of Gondwanaland including India, Australia, Antarctica, Africa, and South America. However, the distributions of basins and facies were controlled by paleolatitude and topographic highs (Fig. 2.15). Gondwanan sequences of peninsular India are usually correlated with the Collie Basin of Australia and Karoo Basin of South Africa (Veevers, 2006)).

The Collie Basin lies within the Yilgarn craton and contains Permian coal-bearing sequences (Veveers, 2006). The oldest unit of Collie Basin is the Stockton Formation, which consists of sandstone, shale, and diamictite confirming a glaciogenic origin of sediments. Three coal measures with varying thickness (Ewington, Premier, and Muja Coal measures) overly the Stockton Formation (Veveers, 2006). These coal measures are underlain by sandstones of the Cretaceous Nakina Formation.

The Karoo Basin of South Africa consists of several connected or isolated basins that developed between the Carboniferous and Jurassic. The Karoo system in the south, also known main Karoo system, includes the signature of a subduction environment. To the west, the system reflects deposition associated with an extensional environment

(Catuneanu et al., 2005). The lowermost part of the Dwyka Formation consists of glacial till. The overlying Volksrust Formation consists mostly of shale with sandstone. The Estcourt, Belmont, Otterburn, Mol Teno, and Elliot formations contain varying amount of sandstone and shale. The Estcourt Formation also contains several coal horizons. The total thickness of the Karoo system at the Main Karoo Basin (South Africa) is 1100 m.

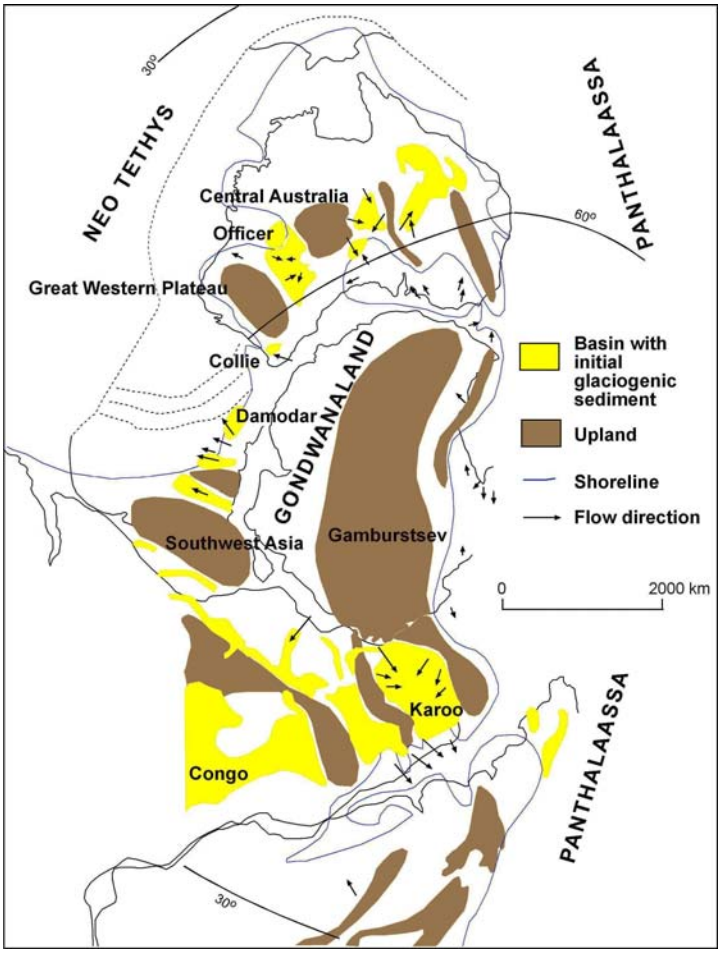

Figure 2.15 Distribution of Gondwanan basins in Gondwanaland in Early Permian (Veveers and Tiwari, 1995).

CHAPTER 3: EVOLUTION OF GONDWANAN BASINS

3.1 CONTINENTAL BREAK UP OF GONDWANALAND

The sedimentation cycle in the Purana Basin of peninsular India and its equivalents, in the Lesser Himalaya was ended by early Cambrian time contemporaneously with Pan-African mountain-building (Valdiya, 1997). However, due to localized uplift, narrow fluvial depositional system developed in the Zanskar and Hazara areas.

The break up of the Gondwanaland has been related with continental flood volcanism that occurred since early Mesozoic (Segev, 2002). Several models have been proposed to explain the mechanisms for the break up, but none of these are free from controversy. However, the popular model involves lower mantle upwelling. The Carboniferous Variscan (Hercynian) orogen has been related with the collision of several Gondwanan plates and Laurasia during the final assembly of Pangaean supercontinent and to post-convergent extension by crustal thinning, lowering of crustal viscosity, formation of numerous sedimentary basins and widespread alkaline magmatism between 320- 240 ma (Segev, 2002). The load of accumulated sediments in these rifted basin caused normal faulting that resulted in the famous half-graben Gondwanan basins.

The Gondwana supercontinent was bounded on its southern side until Early Jurassic by an active subduction zone responsible for the fold belts of South Africa,

South America, and southwest Antarctica. During the Jurassic, the Karoo area was uplifted and subsequent Karoo plume activity resulted in proto oceanic rifting between East Gondwana (India, Antarctica, and Australia) and West Gondwana (Africa and South America) (Segev, 2002).

Extensional movement between East Antarctica, India, and the western Australian margin was reactivated during the Early Cretaceous. The break up between India and Western Australia along the Cuvier and Gascyone Abyssal Plains started between 132-130 Ma (Segev, 2002). During that period, a variety of igneous rocks were emplaced in the northeast Indian graben along with seaward dipping flows forming the Rajmahal, Bengal and Sylhet traps (Fig. 3.1 A). After break up and initial drifting, the space between India and Antarctica was filled by Kerguelen plateau basalts. During the Upper Cretaceous, the rifting between Madagascar and Seychelles-India occurred, along with basaltic volcanism in Madagascar and Seychelles, and gabbroic intrusions in India.

The breakup between Seychelles and India was followed by rifting along the Goa, Narmada-Son, which resulted in the extrusion of the Deccan Trap basalts between 70-61 Ma (Segev, 2002) (Fig. 3.1B).

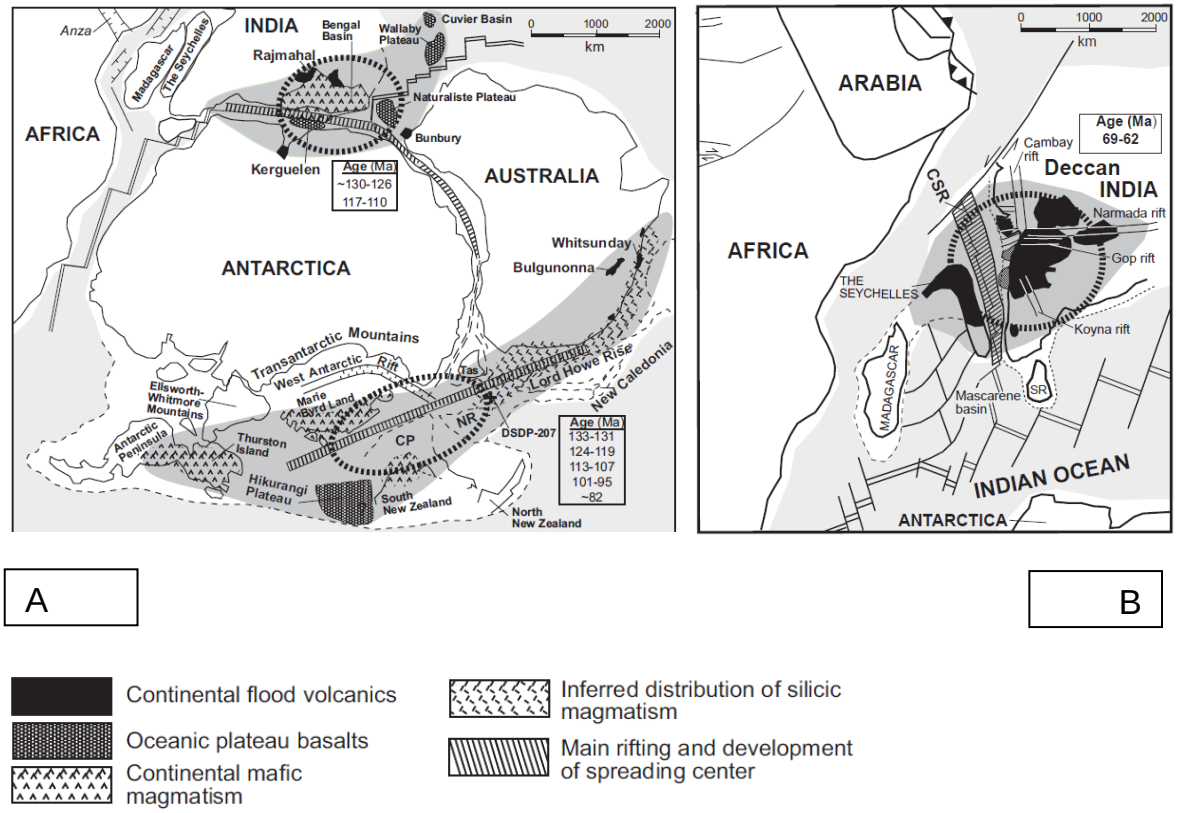

Figure 3.1 Generalized reconstructions of (A) Early Cretaceous and (B) Tertiary Gondwanaland (from Segev, 2002)

3.2 EVOLUTION OF PASSIVE MARGIN ALONG THE NORTHERN BOUNDARY OF PENINSULAR INDIA

The character of the northern margin of peninsular India prior to collision with Tibet remains controversial. What was the total length of India subducted beneath Tibet? In the various models and mechanism proposed, the length has been estimated to be as little as a few kilometers and as high as 2800 km. The latter estimate involves the concept of a 'Greater India'. India was a part of Gondwanaland from the Precambrian to Jurassic,

before it became isolated from Africa, Australia, and Antarctica. India remained a passive margin during its northeast-directed movement from the Cretaceous to the Eocene when it collided with Asia (Brookfield, 1993).

The Tibetian block was separated from India during the Permian, which resulted in subsidence of the High Himalaya and deposition of a very thick sedimentary succession on oceanic crust in the North Himalaya (Brookfield, 1993). Some still believe that a proto-Himalayan range and Himalayan micro-continent existed between the Lesser Himalaya and Tethys Himalayan zones between the Cambrian and late Paleozoic. Such a high would have an important role as a sedimentary and faunal barrier between the basins of both zones (Sakai, 1989) (Fig. 3.2). However, this hypothesis cannot be proved with existing stratigraphic, sedimentological, and paleomagnetic field data. Rather, spatial and environmental differentiation between the Lesser Himalayan and the Tethys Himalayan basins with separation of about 5,000 km is proposed as the probable cause of different sedimentary facies development in these two domains (Jain and Kunwar, 1970).

Generally, the classification of ‘extra-peninsular Gondwanan sequence’ is given only to the sequences developed in the Lesser Himalayan terrains that have more or less similar depositional environment and source rocks as peninsular Indian Gondwanan sequences.

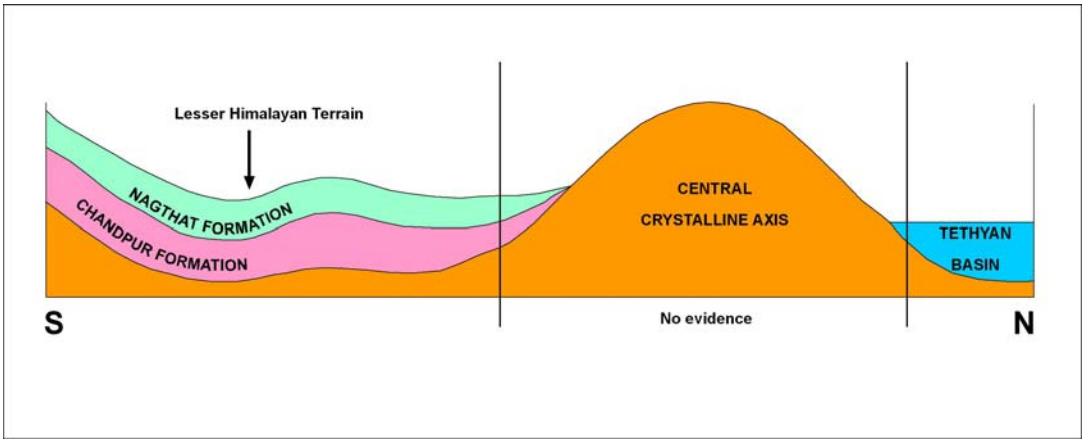

Figure 3.2 Schematic reconstruction of micro continent barrier supposed to have existed between the Lesser Himalayan and the Higher Himalayan terrains.

3.3 EVOLUTION OF FACIES AND CLIMATIC CONTROL DURING DEPOSITION OF GONDWANAN SEQUENCES

Variation of paleoclimate was an important factor controlling sedimentation in Gondwanan basins. The separations of eastern Gondwanaland from western Gondwanaland, then separation of India from Australia and later from Madagascar were accompanied by the northward movement of India. Hence, the distributions of lithologies on these basins are related with paleolatitudes (Fig. 3.3) of the basins and ongoing tectonic activity.

The composition of sand and clay minerals in shale, and the presence of coal in these different facies was controlled by climatic conditions during deposition (Dutta, 2002).

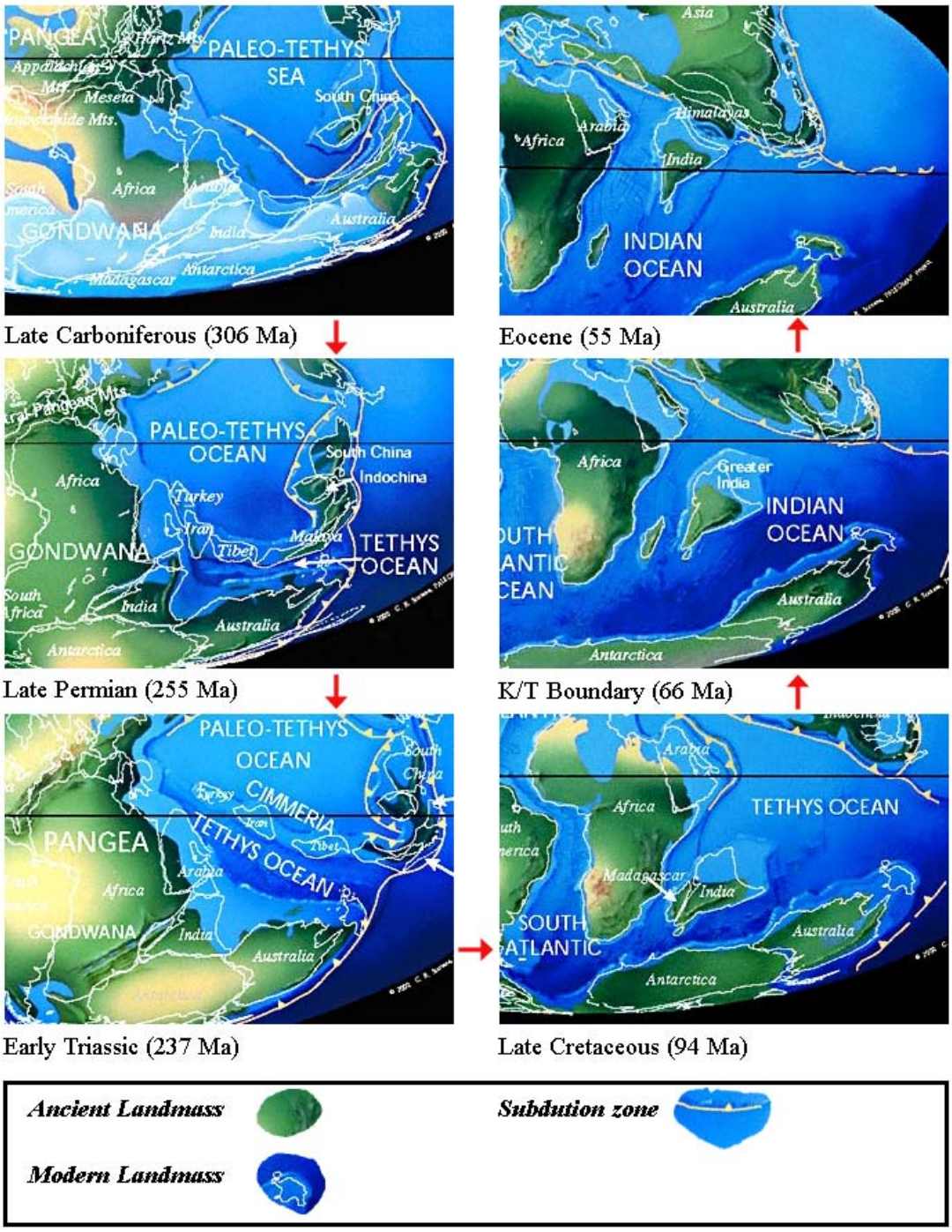

Figure 3.3 Paleogeography of Gondwanaland (www.paleoportal.com, 2009).

Dutta (2002) inferred that initial embryonic basins started to receive glacial deposits, when the Gondwanan basins were situated along southern high latitudes. Afterwards, glacial outwash plains and glacial lakes gave rise to a meandering fluvial system with well-defined channels and broad flood plains. The latter were filled with coal, carbonaceous shale, gray shale and siltstone (Dutta, 2002) during the Permian when the climate was humid. After sometime, climate became less humid and deposition of coal was reduced; sand, carbonaceous shale, and gray shale-siltstone became more abundant. However, coal-forming environments returned during the Late Permian, but were not as extensive as earlier (Dutta, 2002). Although this facies formed mainly in meandering fluvial systems, some marine signatures have been identified by some workers, reflecting, periodic incursion of the sea (Valdiya, 1997) (Fig 3.4). During the Triassic, coal-bearing facies were replaced by red-bed sequences (Dutta, 2002). Alternating sequences of bright colored red shale and feldspar-rich sandstones beds comprise the major thickness during this period. However, Triassic deposits are not present in extra-peninsular Gondwanan sequences.

Subsequently, a major tectonic event caused the entire source area throughout India to uplift due to rifting. This tectonic uplift was coupled with a change of climate from arid to warm humid conditions. Climatic change resulted in deposition of super-mature sediments, while tectonic uplift caused river systems to change from meandering to braided (Dutta, 2002). The overall change caused deposition of coarse-grained conglomerates, pebbly sandstones, and sandstones. These sediments covered the entire landscape and overlapped on to older sediments and basement rocks (Dutta, 2002).

Extra-peninsular Gondwanan sequences were being deposited in meandering-braided fluvial systems but also reflect periodic marine incursion. Few extra-peninsular Gondwanan successions consist of volcanic clasts and volcanic flows that show the proof of syn- or pre-depositional volcanic activities (Fig 21 B). During deposition of the Amile Formation, which is dominated by sandstones, the environment was shallow marine. The Eocene Bhanskati Formation not only shows the change in depositional environment from marine to continental but also a change in provenance from cratonic India to the Himalayan orogenic belt. Deposition of Gondwanan sequences in eastern and western parts of Nepal was not synchronous; sequences are older towards the west (Bashyal, 1980).

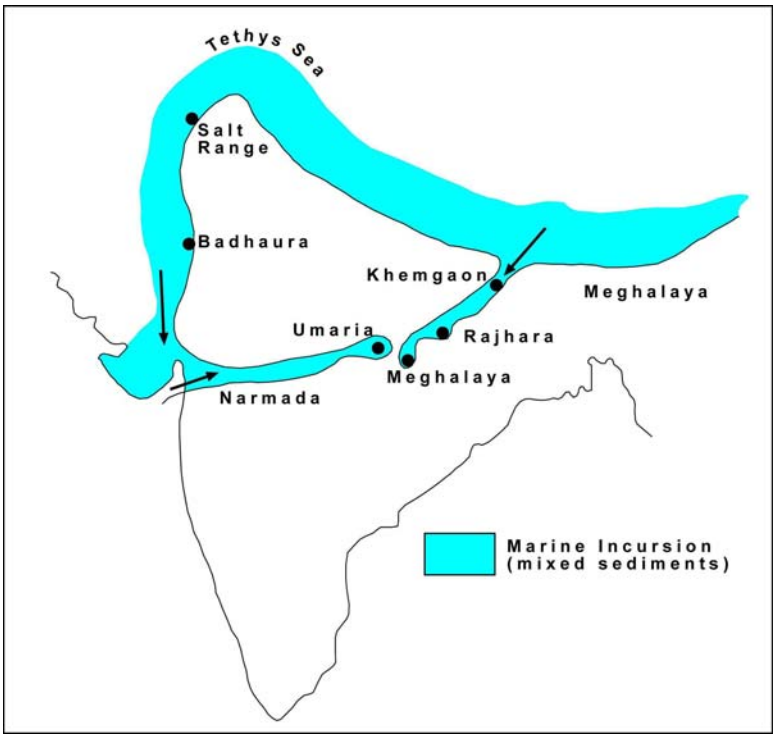

Figure 3.4 Marine incursion in Gondwanaland during the Permian (Valdiya, 1998).

CHAPTER 4: SANDSTONE PETROGRAPHY

4.1 INTRODUCTION

Sandstone petrography is a classical method of provenance study. Sandstone petrology is based on the assumption that sandstones from similar tectonic settings will have similar composition. The ratios of major clastic components (e.g., quartz, feldspar, and lithic fragments) from known tectonic settings have been plotted by several workers to discrminate various provenance fields (Dickinson and Suczek, 1979; Ingersoll and Suczek, 1979; Dickinson, 1985). Besides rock types in source areas, sediments are also influenced by climate, relief, transporting agent, weathering and diagenesis. Hence, sandstone composition can help to reconstruct paleogeography, paleotectonics, and paleoclimate (Suttner, 1977; Ingersoll et al., 1984; Johnson, 1993).

Provenance studies based on mineralogical abundance are based on the assumption that detrital composition has not been altered significantly by sedimentary processes including, transportation, weathering, and diagenesis. However, tectonic discrimination based on mineralogical analysis will not be that effective to trace provenance if there is mixing detritus derived from different source areas (Velbel, 1985). Multiple basin analytical techniques, including mineral chemistry, bulk-rock chemistry, detrital thermochornology, and traditional modal analysis, are generally required to identify the influence of multiple provenances or source terranes (Morton and Hallsworth, 1999).

4.2 METHODS

A total of twenty-three sandstone samples were collected from three different Gondwanan sequences of Nepal; the Tansen (western Nepal), Katari (eastern Nepal), and Barahachettra (eastern Nepal) groups. After preparation in the rock cutting lab of Department of Geology and Geography at Auburn University, samples were sent to Spectrum Laboratories in Vancouver, WA for preparation of petrographic thin sections. Half of each thin section was stained to assist in the identification of various feldspar grains. Mineralogical compositions of the samples were determined by compositional modal analysis following the Gazzi-Dickinson point-count convention which minimizes the control of grain size on sand composition (Dickinson, 1970; Ingersoll et al., 1984). A minimum of 300 framework grains were counted from each sample. Different end-members were recalculated from the point-count data to plot different ternary diagrams for the discrimination of tectonic setting (Dickinson, 1970; Dorsey, 1988; Uddin and Lundberg, 1998). The following compositional parameters (Table 4.1) were calculated: Qt = total quartz; Qm = monocrystalline quartzose grains; Qp = polycrystalline quartz grains, including chert grains; F = total feldspar grains; P = plagioclase feldspar grains; K = potassium feldspar grains; L = lithic fragments; Lt = total lithic fragments; Ls = sedimentary lithic fragments; Lv = volcanic lithic fragments; Lm =metamorphic lithic fragments.

Polycrystalline quartz is included at the Qt end member for QtFL plot to keep plutonic polycrystalline quartz grains distinct from the metaquartzite fragments. All quartzose grains are plotted at Qt end member for QtFL plots. This is intended to provide

emphasis to the stability of grains during various processes of sedimentary cycles including weathering, transport, etc. In contrast, chert and polycrystalline quartz are included in the Lt end-member on QmFLt plots. Details of the normalized modal compositional calculations are given in Table 4.2 .

Table 4.1 Recalculated modal parameters of sand and sandstone.

Primary parameters (after Graham et al., 1976; Dickinson and Suczek, 1979; Dorsey, 1988; Uddin and Lundberg, 1998)

Qt = Qm + Qp, where
- Qt = total quartzose grains
- Qm = monocrystalline quartz (> 0.625 mm)
- Qp = polycrystalline quartz (or chalcedony)

Feldspar Grains (F = P + K), where
- F = total feldspar grains
- P = plagioclase feldspar grains
- K = potassium feldspar grains

Unstable Lithic Fragments (Lt = Ls + Lv +Lm), where
- Lt = total unstable lithic fragments
- Lv = volcanic/metavolcanic lithic fragments
- Ls = sedimentary/metasedimentary lithic fragments
- Lm_1= very low- to low grade metamorphic lithic fragments
- Lm_2= low-to intermediate grade metamorphic lithic fragments

4.2 PETROGRAPHY

The Gondwanan and post-Gondwanan sequences of the Lesser Himalaya in Nepal are mostly continental and shallow marine deposits. The Gondwanan sequence was deposited on an eroded surface of Precambrian basement of the Lesser Himalaya. Like in all other peninsular and extra-peninsular Gondwanan sequences, Gondwanan stratigraphy of Nepal begins with a diamictite bed except for the Barahachettra Group.

4.2.1 TANSEN GROUP

4.2.1.1 Sisne Formation

The Sisne Formation is composed of a thick pile of diamictite and rthymite beds. However, there are few sandstone beds between the diamictites. Pale-green, medium-grained Sisne sandstones are highly fractured and consist of numerous quartz veins. Four sandstone samples were collected from the Sisne Formation: 16-3, 16-4, 16-5, and 16-6.

Sandstones of the Sisne Formation are composed mostly of quartz and feldspar. The average modal composition of the Sisne sandstone is $Qt_{56}F_{42}L_2$. Quartz grains are rounded to angular. Plagioclase, K- feldspar, and perthite are abundant and variably altered to clay minerals. A few low-medium grade metamorphic rock fragments are observed in the samples. Mica flakes are also abundant. The Sisne sandstone also contains common garnets (Fig. 4.1A), some of which are very well preserved.

The Sisne sandstones contain approximately 20% matrix, which consists of organic-rich and calcareous clay. Clay matrix resulted from alteration of feldspars. The

distribution of the matrix is not uniform in the formation. Sutured framework grain contacts are observed where matrix contents are low.

4.2.1.2 Taltung Formation

The Taltung Formation, which has been divided into two members, consists of cyclic deposits of conglomerate, sandstone, and shale in the lower member and rhythmic beds of sandstone and shale in the upper member (Sakai, 1983). The Aulis Basalt is also included in the Taltung Formation. In the absence of good outcrop during fieldwork for this study, only one sample (K-1) of sandstone from the lower member was collected from this formation.

The Taltung Formation sandstone sample consists mostly of quartz, feldspars, and volcanic fragments. The modal composition of the Taltung Formation is $Qt_{32}F_{36}L_{32}$. Monocrystalline quartz grains are subrounded to angular. A few grains of polycrystalline quartz are also present. Feldspar grains are highly altered and replaced by calcite. Volcanic fragments contain euhedral plagioclase crystals (Fig. 4.1B). Numerous irregular grains of organic material are also present in the sample. Rare metamorphic rock fragments variably altered to sericite are present in the thin section. The framework grains have been cemented and locally replaced by sparry calcite.

The Aulis Basalt is associated with lower member of the Taltung Formation in the Aulis area of Tansen. Sample 15-2 collected from that area shows the interstitial groundmass of lath-shaped plagioclase microlites (Fig. 4-5B).

4.2.1.3 Amile Formation

The Amile Formation consists of alternating layers of shale and quartzose sandstone. The middle part of the Amile Formation consists of calcareous beds, which according to Sakai (1983), yield several types of marine fossils. Five samples 16-12, 16-8, 16-9, 15-5 and 15-6 were collected from quartzose sandstone beds of the Amile Formation. The modal composition of the Amile Formation is $Qt_{100}F_0L_0$. Quartz grains are mostly monocrystalline.

The matrix content of the samples is very low. Some of the samples with very low matrix contents exhibit concavo-convex contacts between quartz grains (4.2 A), although interstitial space is locally filled with clay minerals. Samples from the lower part of the formation are cemented by hematite. Samples from the upper part of the formation contain common carbonaceous materials. Some heavy minerals like zircon, tourmalines are observed in all samples.

4.2.1.3 Bhainskati Formation

The Bhainskati Formation is dominated by black shale in the lower part with red purple shales and hematite bands in the upper part. Few sandstones beds are present within the upper part. One sample, 15-8 was collected from the Bhainskati Formation. The Bhainskati sandstone is dark gray. The modal composition of the sandstone is $Qt_{63}F_{13}L_{24}$. Quartz grains are very angular to angular. Feldspar grains are highly altered to clay minerals. Lithic fragments include high-grade metamorphic, low-grade metamorphic and sedimentary lithic grains.

The sample is characterized by fair amount of clay minerals. However, concavo-convex sutures between grains are also present locally (Fig. 4.2 B). Alteration of feldspars grains to sericite was observed which is more prominent along grain boundaries.

4.2.1.3 Dumri Formation

The Dumri Formation, the top most unit of the Tansen Group, is a thick series of medium-grained, bluish gray quartzose sandstones interbedded with red and green shales. As the objective of this work was initially focused on the Gondwanan sequences only one sample (sample 16-1) was collected from the Dumri Formation from the Makhlo Dumri area.

The Dumri sandstone (sample 16-1) is pale green. The modal composition of the sample is $Qt_{73}F_5L_{22}$. The sample consists of immature and various sized quartz grains. Most of the polycrystalline quartz grains are angular and irregular, whereas most of the monocrystalline grains are moderately- to well-rounded. The percentage of feldspar is very low. The few feldspar grains observed are plagioclase grains that show various degrees of alteration. Lithic fragments include low- to medium-grade metamorphic, chert, and volcanic clasts (Fig. 4.3 A).

Clay matrix makes up more than 25% of the total composition of this sample. The framework grains contacts vary from floating to sutured. Most of the framework grains show alteration along the grain boundaries.

4.2.2 KATARI GROUP

The entire Katari Group is considered to be a Permo-Carboniferous unit. It consists of diamictites, volcanic rocks, and quartzites. In the Katari Group, three types of quartzites are found in outcrops; white, carbonaceous, and calcareous. White quartzites are dominant in the lower part of the section, while carbonaceous and calcareous quartzites are dominant in the upper part. White quartzites are highly fractured, weathered and altered. As such, fresh sample collection was not possible from this unit. Two samples, 26-6 and 26-8, of carbonaceous-calcareous quartzites were collected from the Maruwa Khola section.

The average composition of the Katari Group sandstones is $Qt_{100}F_0L_0$, Samples contain ~ 65% monocrystalline grains. The sample consists of various sized quartz grains. Some of the grains are deformed following particular direction of deformation indicating post depositional deformation into polycrystalline quartz. However, some of them are not significantly distorted and preserve their rounded shapes (Fig. 4.3 B). Some of the quartz grains are altered along boundaries and fractures.

Matrix materials consist of mica and calcite in roughly equal abundance (~15%). Calcite is also present as the cement.

4.2.2 BARAHACHETTRA GROUP

The Barahachettra Group consists of diamictites, quartzites, calcareous sandstones, and volcanic tuffs. All these units were previously considered to have been deposited during the same geological age (Permo-Carboniferous). However, Dhital (1992) has proposed that the Group includes two temporally distinct formations; the Permo-Carboniferous Saptakoshi Formation and the Cretaceous Tamrang Formation.

4.2.2.1 Saptakoshi Formation

The Saptakoshi Formation consists of quartzites, diamictites, and volcanic materials. Four samples were collected from the Saptakoshi Formation; samples 22-7 (volcanic tuff) and 22-9 were collected along the Kokaha Khola, and samples 23-5 and 23-7 were taken along the Saptakoshi River. Sample 23-5 collected from sandstone interbed between diamictites, differs significantly from samples 23-7 and 22-9 which are mostly quartzites.

Sample 23-5 has the modal composition of $Qt_{60}F_{37}L_2$, with abundant various sized quartz clasts. Quartz grains are rounded to angular in shape. Plagioclase and potassium feldspars are abundant and are variably altered to clay minerals (4.4 A). A few chert grains were observed in the sample. Micas are also common. This sandstone is similar in composition to the Sisne sandstone of the Tansen Group of the western Nepal. Not only are feldspar contents high, but sample also contains common garnets as seen in the Sisne Formation.

Samples 22-9 and 22-7 have an average modal composition of $Qt_{100}F_{00}L_{00}$. Sixty five percentage of the quartz is monocrystalline. The quartz grains are deformed along particular direction indicating post depositional deformation (4.4 B). Matrix present in the samples is composed of micritic calcite and mica.

4.2.2.1 Tamrang Formation

The Tamrang Formation consists mostly of calcareous sandstones. Seven samples were collected from the Tamrang Formation along the Saptakoshi River (23-2, 23-3, 23-4) and along the Kokaha Khola (22-4, 22-5, 22-6). The modal composition of the Tamrang Sandstone is $Qt_{61}F_{29}L_{19}$. Tamrang sandstone consists of various sized and immature quartz grains. Feldspars are slightly smaller than quartz and are highly altered. The samples consist of various types of lithic fragments, including metamorphic (various grades) and sedimentary (chert and dolomite).

The matrix observed present in the samples are of two types; calcite and mica. The percentage of mica is higher in samples 22-4, 22-5, 23-2, and 23-3. However, in the samples 22-6 and 23-4, the proportion of micritic calcite matrix is higher. The framework grain contacts vary from concavo-convex to floating (4.5 A).

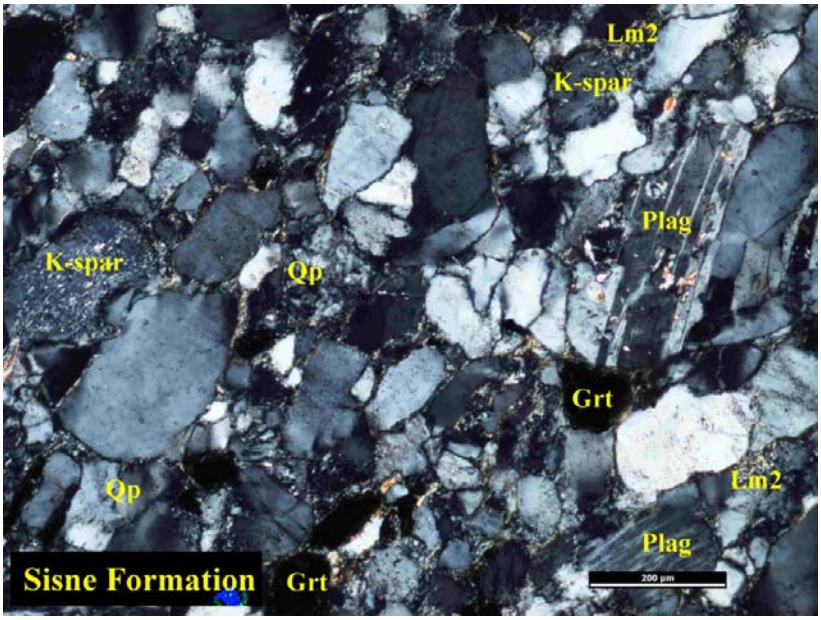

(A)

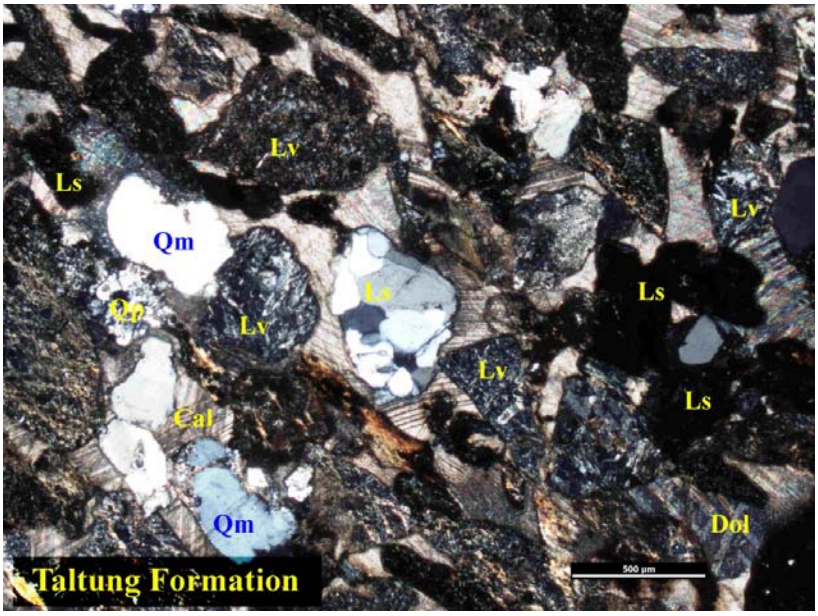

(B)

Figure 4.1 Representative photomicrographs of Gondwanan sandstones, western Nepal. (A) Sisne Formation; (B)Taltung Formation (Qp = polycrystalline quartz, Qm = monocrystalline quartz, Plag = plagioclase, K-spar = potassium feldspar, Grt= garnet, Lm_1= low-grade metamorphic lithics, Lm_2= low- to intermediate-grade metamorphic lithics, Ls = sedimentary lithic fragments, Lv = volcanic fragments, Cal = Calcite).

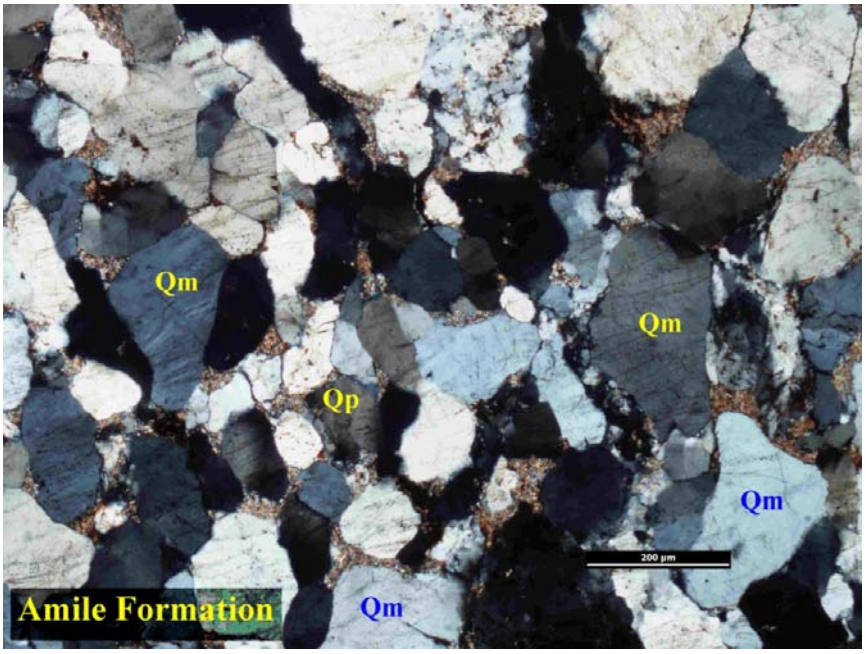

(A)

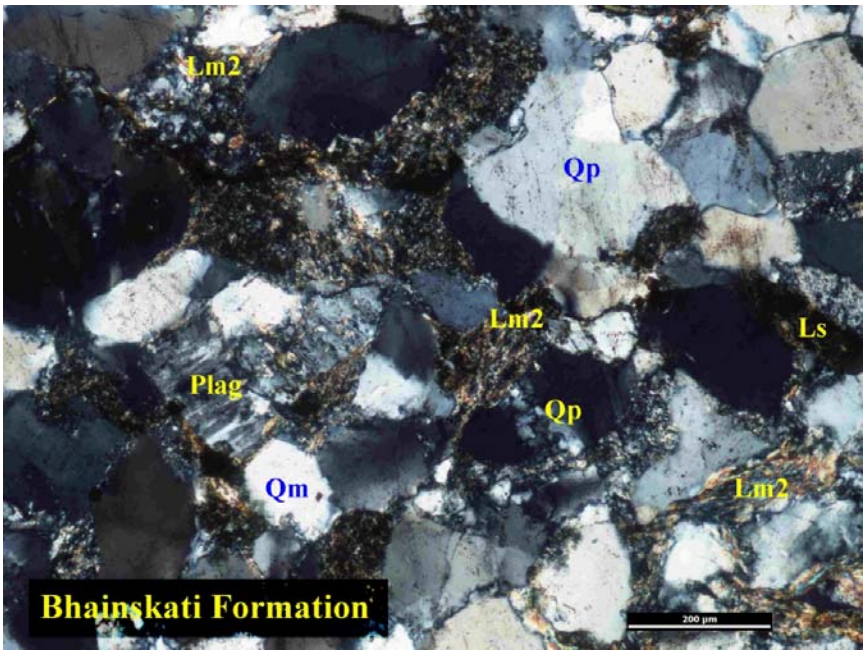

(B)

Figure 4.2 Representative photomicrographs of Gondwanan sandstones, western Nepal. (A) Amile Formation; (B) Bhainskati Formation (Qp = polycrystalline quartz, Qm = monocrystalline quartz, Plag = plagioclase, K-spar = potassium feldspar, Ls = sedimentary lithic fragments, Lm_2 = high-grade metamorphic fragments, Lm_1= low-grade metamorphic fragments).

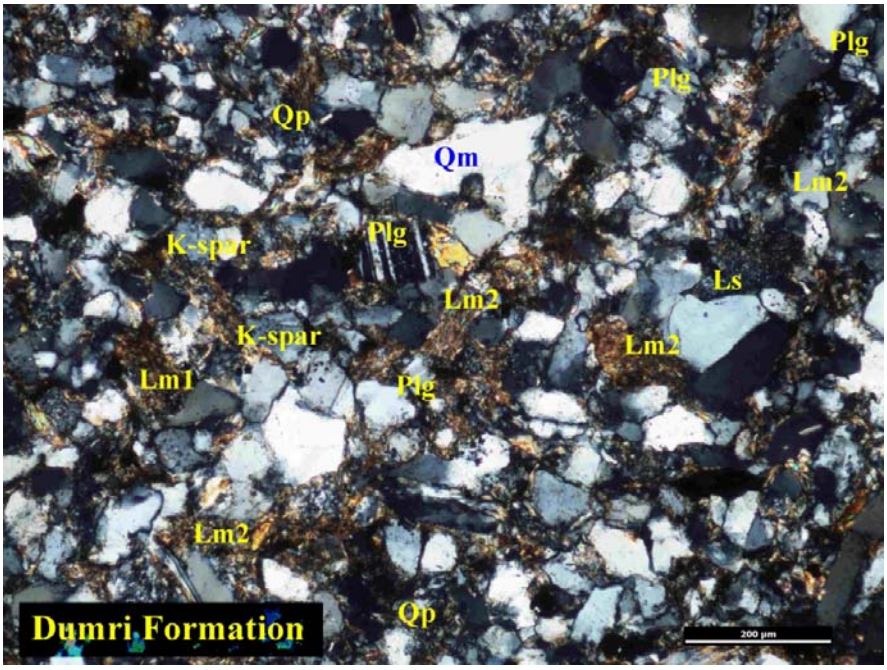

(A)

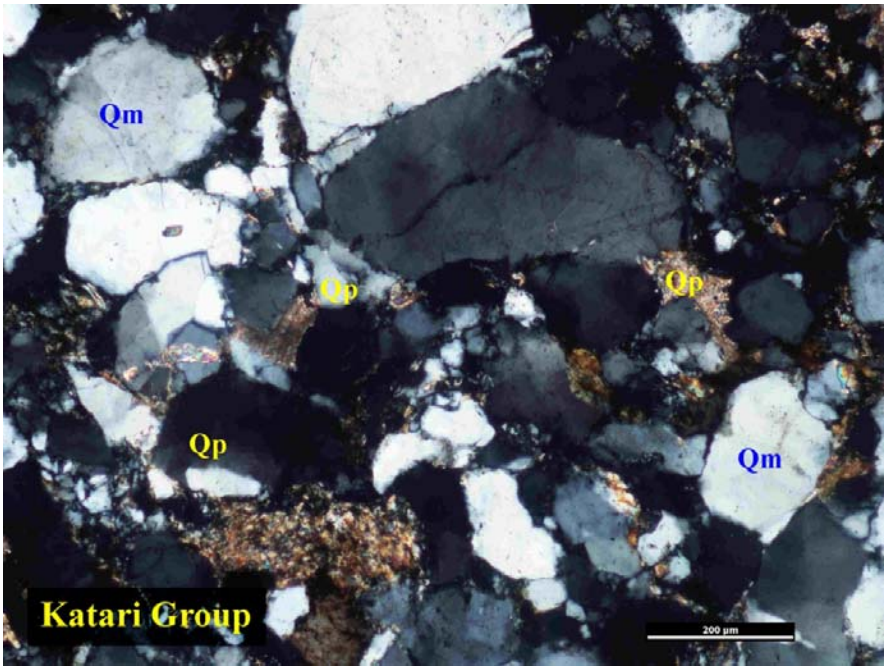

(B)

Figure 4.3 Representative photomicrographs of Gondwanan sandstones, (A) Dumri Formation, western Nepal. (B) Katari Group, eastern Nepal (Qp = polycrystalline quartz, Qm = monocrystalline quartz, Plag = plagioclase, K-spar = potassium feldspar, Ls = sedimentary lithic fragments, Lm_2 = low- to intermediate-grade metamorphic fragments, Lm_1= very low- to low-grade metamorphic fragments).

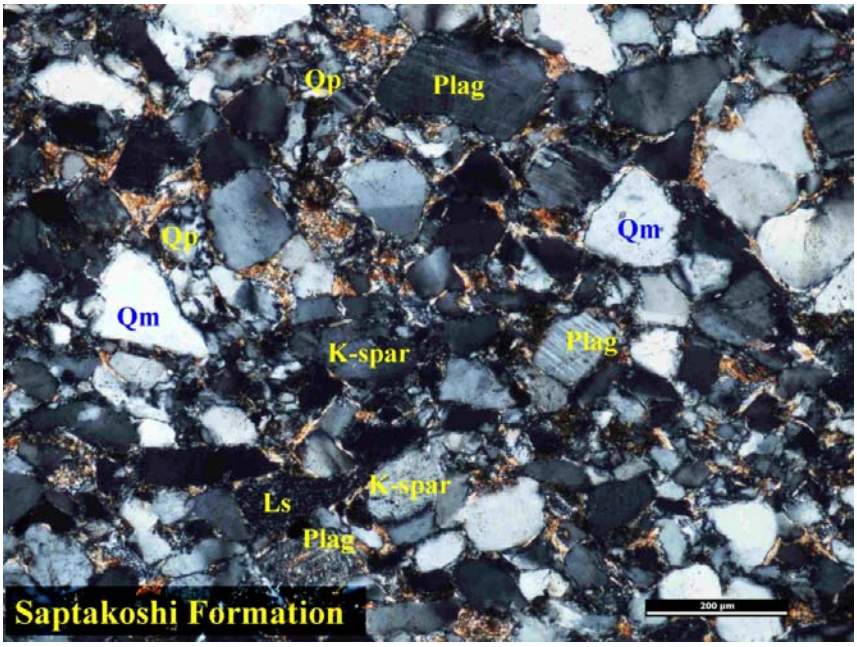

(A)

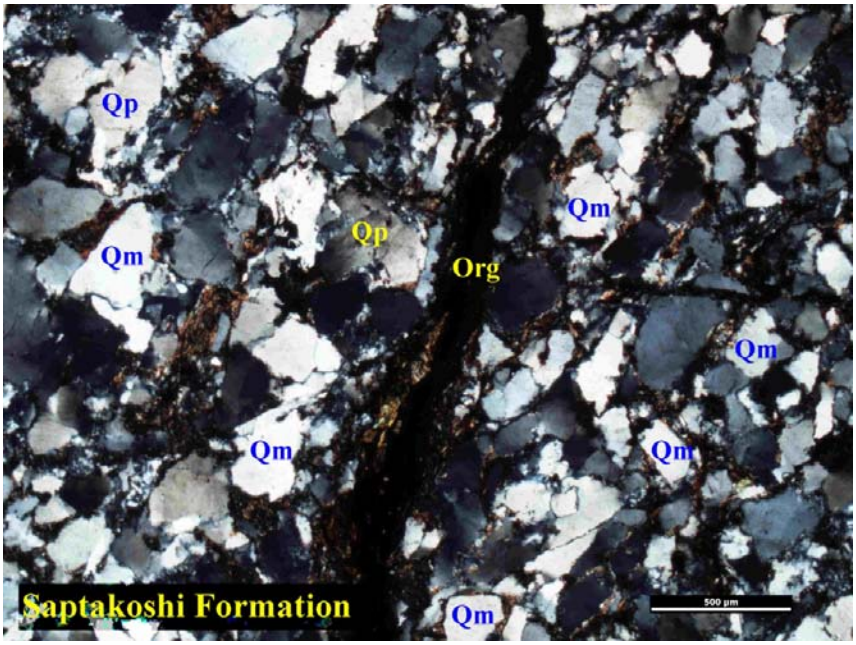

(B)

Figure 4.4 Representative photomicrographs of the Gondwanan sandstones, (A) Saptakoshi Formation, eastern Nepal, sample 23-5; (B) Saptakoshi Formation, eastern Nepal, sample 22-7 (Qp = polycrystalline quartz, Qm = monocrystalline quartz, Plag = plagioclase, K-spar = potassium feldspar, Ls = sedimentary lithic fragments, Lm_2 = low- to intermediate-grade metamorphic fragments, Lm_1= very low- to low-grade metamorphic fragments).

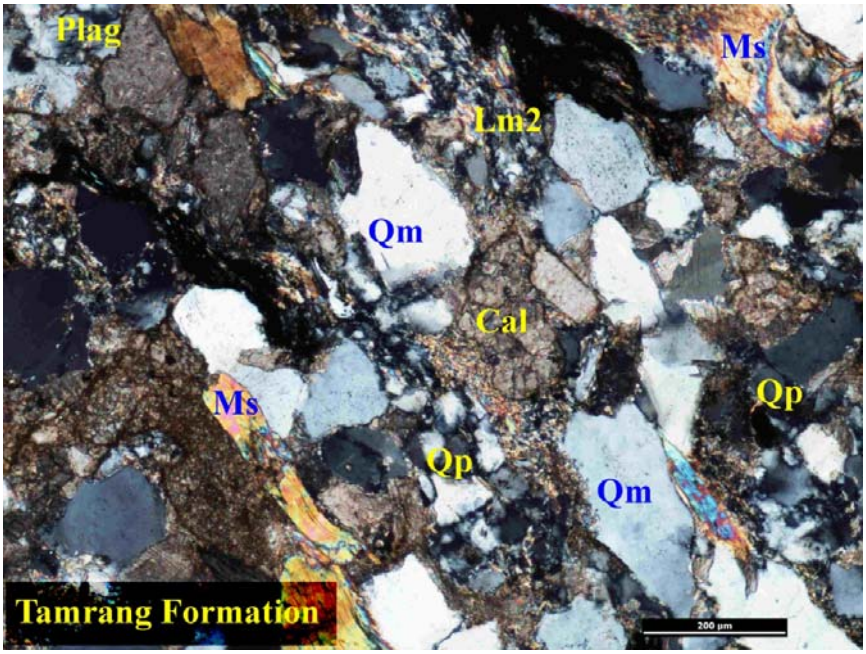

(A)

(B)

Figure 4.5 (A) Representative photomicrograph of the Tamrang sandstone, eastern Nepal (Qp = polycrystalline quartz, Qm = monocrystalline quartz, Plag = plagioclase, K-spar = potassium feldspar, Ms = muscovites, Lm_2 = low- to intermediate grade metamorphic fragments, Lm_1= very low- to low-grade metamorphic fragments); (B) Photomicrograph of Aulis Basalt (Tansen, western Nepal) with abundant plagioclase laths.

Table 4.2 Normalized modal compositions of Gondwanan sandstones in Nepal

	Qt	F	L	Qm	F	Lt	Qm	P	K	Ls	Lv	Lm
Rock Unit/Sample No.												
Dumri Fm												
16-1	73	5	22	65	5	30	92	6	2	27	0	73
Bhainskati Formation												
15-8	63	13	24	38	13	49	74	21	5	15	7	78
Amile Quartzite												
16-12	100	0	0	76	0	24	100	0	0	0	0	0
16-8	100	0	0	58	0	42	100	0	0	0	0	0
16-9	100	0	0	70	0	30	100	0	0	0	0	0
15-5	100	0	0	40	0	60	100	0	0	0	0	0
15-6	100	0	0	48	0	52	100	0	0	0	0	0
Mean	100	0	0	58	0	42	100	0	0	0	0	0
Standard Deviation	0	0	0	15	0	15	0	0	0	0	0	0
Taltung Fm												
K-1	32	36	32	15	26	59	15	37	48	43	40	17
Sisne Fm												
16-3	57	43	0	27	43	30	39	30	31	0	0	0
16-4	52	45	3	33	45	22	42	27	31	0	0	100
16-5	56	41	3	30	41	29	42	27	31	0	0	100
16-6	60	40	0	27	40	33	40	28	22	0	0	0
Mean	56	42	2	29	42	29	41	28	29	0	0	50
Standard Deviation	3	2	2	3	2	5	2	1	5	0	0	58
Katari Group												
26-6	100	0	0	68	0	32	100	0	0	0	0	0
26-8	100	0	0	62	0	38	100	0	0	0	0	0
Mean	100	0	0	65	0	35	100	0	0	0	0	0
Standard Deviation	0	0	0	4	0	4	0	0	0	0	0	0
Tamrang Formation												
22-4	57	16	27	27	16	57	63	9	28	0	0	100
22-5	58	20	22	27	20	53	57	17	26	13	0	87
22-6	66	18	18	31	18	51	53	10	37	0	0	100
23-2	63	27	8	29	27	42	51	5	46	0	0	100
23-4	59	19	22	33	19	48	64	13	23	0	0	100
22-10	60	19	21	22	19	59	46	15	39	14	0	86
22-6	66	18	18	31	18	51	53	10	37	0	0	100
Mean	61	20	19	29	20	52	55	11	34	4	0	96
Standard Deviation	4	4	6	4	4	6	6	4	8	7	0	7
Saptakoshi Formation												
23-5	60	37	3	22	37	41	37	32	31	0	0	3
Saptakoshi Formation (Quartzite)												
23-7	100	0	0	63	0	37	100	0	0	0	0	0
22-9	100	0	0	67	0	33	100	0	0	0	0	0
Mean	100	0	0	65	0	35	100	0	0	0	0	0
Standard Deviation	0	0	0	2.8	0	2.8	0	0	0	0	0	0

4.2 SANDSTONE MODES

A vertical profile is constructed to show the distribution of major framework grains used for modal analysis (Fig. 4.6). The Tansen Group (western Nepal) shows that the percentage of feldspar is relatively higher in the Permo-Carboniferous Sisne Formation than the younger units. The percentage of lithic fragments is higher in the Jurassic-Cretaceous Taltung Formation, Eocene Bhainskati Formation and early Miocene Dumri Formation. In the Cretaceous-Paleocene Amile Formation Quartz percentages are higher than other units.

The percentage of quartz in the Permo-Carboniferous Katari Group is higher than the Tansen Group of western Nepal. Further east, in the Barahachettra area, the quartz dominated during the initial phases of Permo-Carboniferous deposition. However, lithic fragments became more significant in the upper sections. The percentage of lithic fragments increases in the Tamrang Formation than in the underlying Barahachettra Formation.

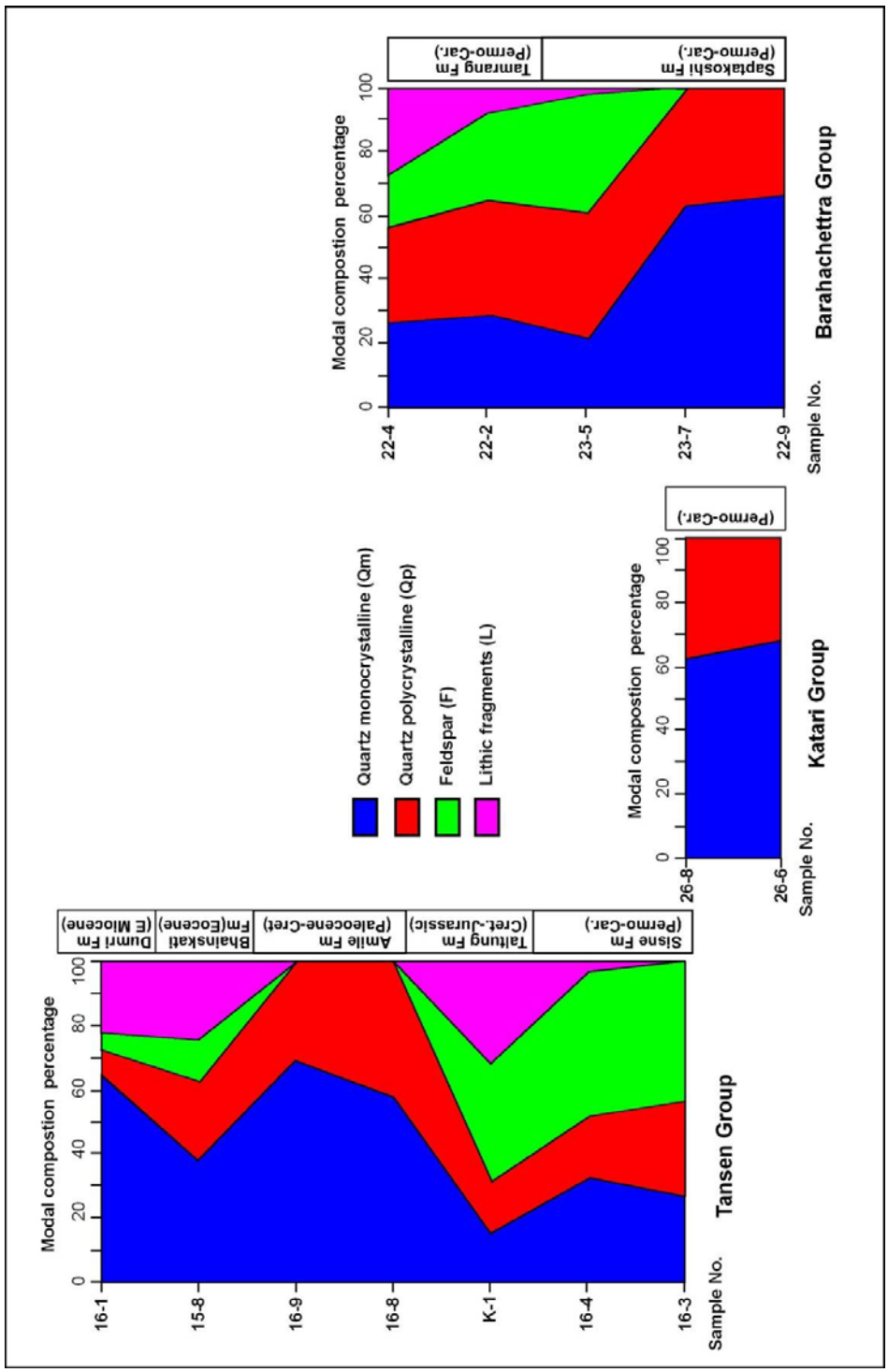

Figure 4.6 Variation of modal mineralogical composition of the Gondwanan sandstones of Nepal.

4.2 PETROFACIES EVOLUTION

Tectonic discrimination plots of Gondwanan sandstone from the three different sections of Nepal were prepared on the basis of modal compositional analyses of sandstone framework grains. Tectonic discrimination plots of Gondwanan sandstones from three different sections of Nepal were prepared based on modal compositional analysis of sandstone framework grains. The QtFL plot (Fig. 4.7) shows that the Sisne Formation sandstones are intermediate between "basement uplift" and "transitional continental" deposits. All diamictites of the Permo-Carboniferous in peninsular India were deposited in half-graben basins along major lineaments (Veevers and Tiwari, 1995). The high percentage of feldspars and low amount of lithic fragments ($Qt_{56}F_{42}L_2$) reflect that tectonic setting. Moreover, another controlling factor during the Permo-Carboniferous was climate; the area was situated at high southern latitude which inhibited intensive weathering. As the central part of the India was blocked by the Satpura-Bundhelkhand-Aravali mountain series (Naqvi, 2005), the northern part of peninsular India, which could have changed gradually from continental to shallow marine environments, was receiving sediments from the orogenic belts. However, in the QmFLt diagram, the Sisne Formation plots in the "dissected arc" due to concentration of monocrystalline quartz (Fig. 4.8). Plagioclase contents are almost equal to potassic feldspars (Fig. 4.9). Most point-count data plots at the Lm end of Ls-Lm-Lv triangular diagram (Fig. 4.10).

The Taltung Formation, with a modal composition of $Qt_{32}F_{36}L_{32}$, plots in "dissected arc" field (Fig. 4.7). The Taltung Formation consists mostly of continental

deposits and contains common volcanic fragments associated with the rifting of Australia from India and associated volcanic eruption (Sakai, 1989). The Taltung sandstones are dominated by volcanic and sedimentary fragments. They contain very few metamorphic lithic fragments. On the QmFLt plot, these sandstones fall in "transitional arc" field.

During deposition of the Amile Formation (Late Cretaceous to Paleocene), the sea level was falling globally (Vail, 1977) probably resulting in land barriers for sediment transport from source areas to the basins. Moreover, at that time India was characterized by humid and tropical climate in which intensive chemical weathering may have produced mature sands. The Amile Formation with modal composition of $Qt_{100}F_0L_0$ is a "craton interior" deposit (Fig. 4.7). However, presence of polycrystalline quartz pulls the Amile Formation down to the "Quartzose recycled" provenance field at the QmFLt plot (Fig. 4.8).

The Bhainskati Formation has higher lithic fragments than the underlying Amile Formation. The QtFL modal composition of the formation is $Qt_{63}F_{13}L_{24}$. Bhainskati deposition took place during the Eocene when India began colliding with Tibet (Sakai, 1983). DeCelles et al. (1998) suggested a back bulge setting for deposition of the Bhainskati Formation. The source rock for the sediment could be the Indian craton and also the Higher Himalaya and Tibetan Tethys sediments. The Bhainskati Formation has very low feldspar contents and plots in the "recycled orogenic" provenance field in the QtFL diagram (Fig. 4.7). But it falls in "transitional recycled" field on the QmFLt plot (Fig. 4.8).

The Dumri Formation, which has even higher lithic fragment contents than the Bhainskati Formation falls, in the "recycled orogenic" provenance field on the QtFL plot and in "the quartzose recycled" field on the QmFLt plot (Fig. 4.8). The modal composition of the Dumri Sandstone is $Qt_{73}F_5L_{22}$. As the Indian continent already had collided with Tibet before deposition of the Dumri Formation, the source terranes shifted from cratonic India to the Himalayan orogenic belt. The Higher Himalaya could have provided high-grade metamorphic fragments, while the Lesser Himalaya could be the source areas for the low-grade metamorphic and sedimentary grains.

The modal composition of the Permo-Carboniferous unit of the Katari Group is $Qt_{100}F_0L_0$, which fall in the "cratonic interior" provenance field on the QtFL plot (Fig. 4.8) and "quartzose recycled" field in the QmFLt plot (Fig. 4.9). However, it is unlikely to get major change in climatic conditions during same geological time interval between the depositional basins of the Tansen Group and the Katari groups, as both were part of the northern passive margin of the Indian peninsula aligned almost in the same latitude.

Further east, the Barahachettra section shows more problems to validate the present stratigraphy based on paleogeographic position of the Indian peninsula and stratigraphy of other contemporaneous Gondwanan units deposited in similar tectono-climatic domain (Tansen Group). The change in composition from $Qt_{60}F_{37}L_2$ for sandstone of the Saptakoshi Formation to $Qt_{100}F_{00}L_{00}$ of Saptakoshi quartzite and $Qt_{61}F_{29}L_{19}$ of the Tamrang Formation is unlikely to have occurred within Permo-Carboniferous when Gondwanaland was situated in southern high latitudes. The QtFl plot of the Tamrang Formation indicates a similarity to the Eocene Bhainskati Formation (Fig.

4.8). The Saptakoshi quartz arenite shows affinity to the late Cretaceous-early Paleocene Amile Formation and the Saptakoshi arkosic sandstone shows alikeness to the Permo-Carboniferous Sisne sandstone.

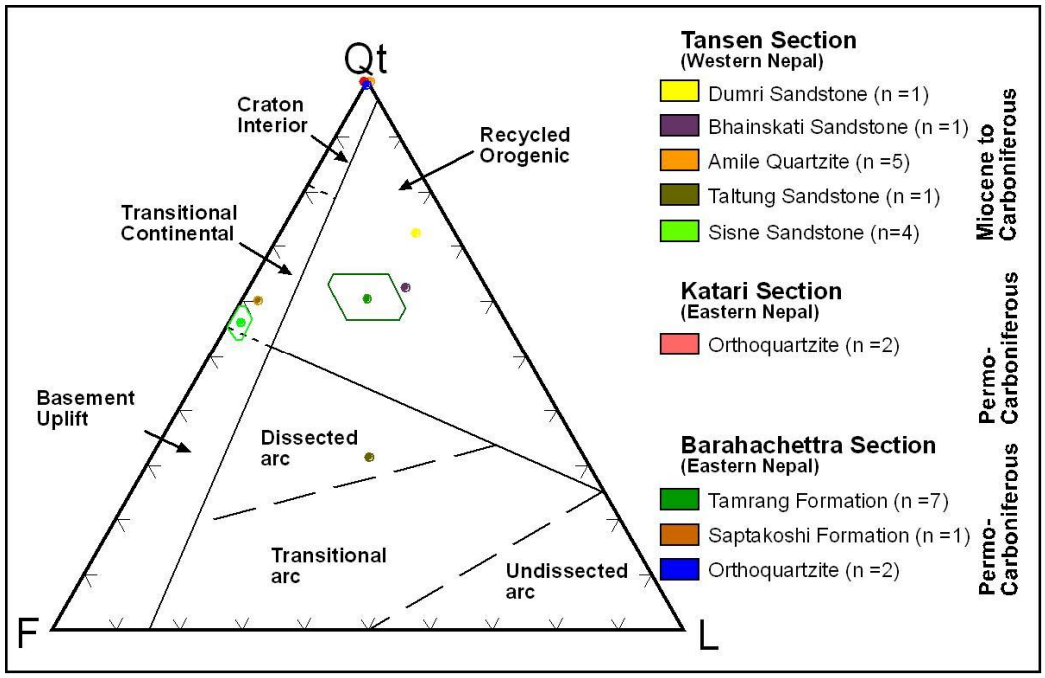

Figure 4.7 QtFL plot of Gondwanan sandstones of Nepal showing mean and standard deviation polygons (provenance fields are taken from Dickinson, 1985).

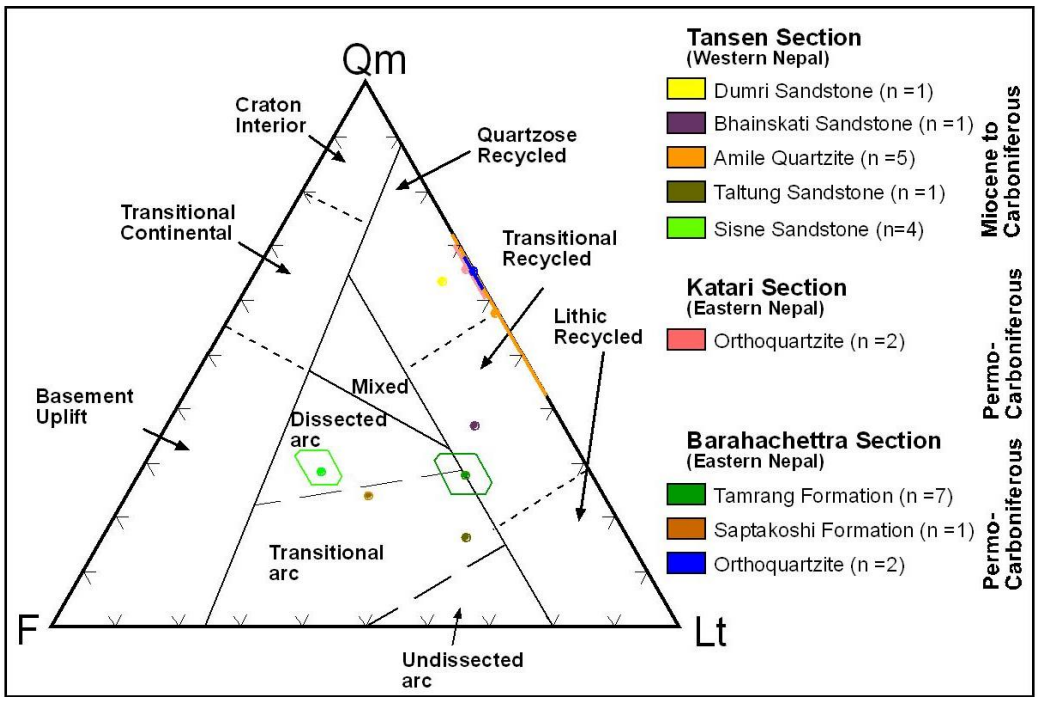

Figure 4.8 QmFLt plot of Gondwanan sandstone of Nepal showing mean and standard deviation polygons (provenance fields are taken from Dickinson, 1985).

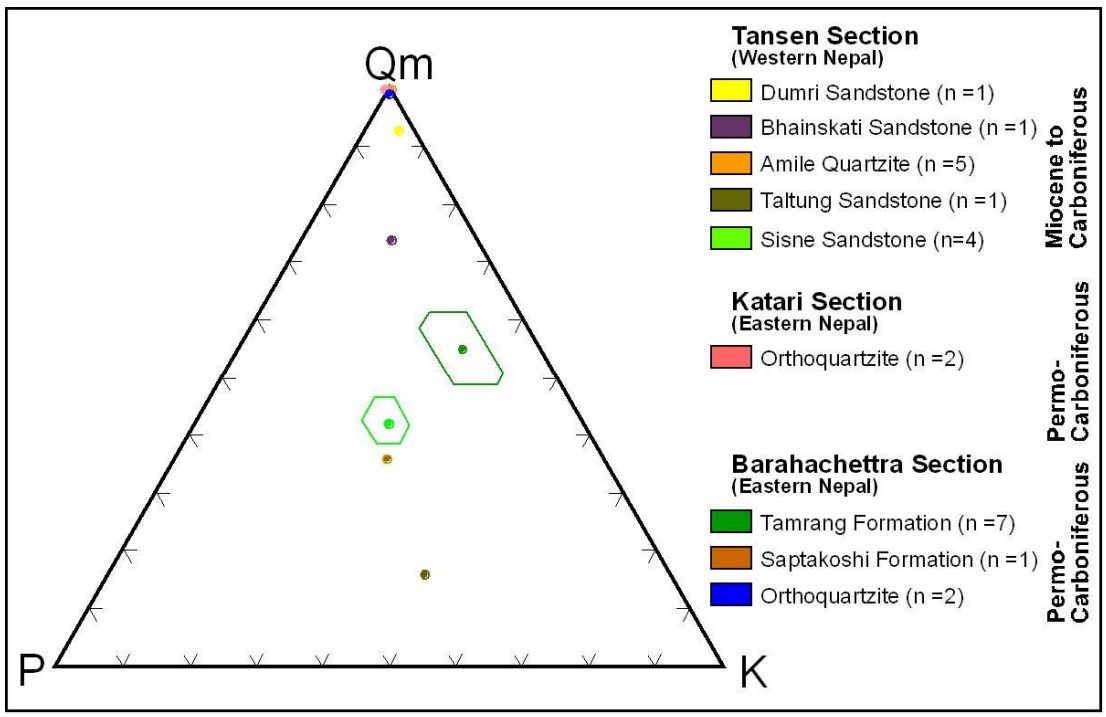

Figure 4.9 QmPK plot of the Gondwanan sandstones of Nepal showing mean and standard deviation polygons.

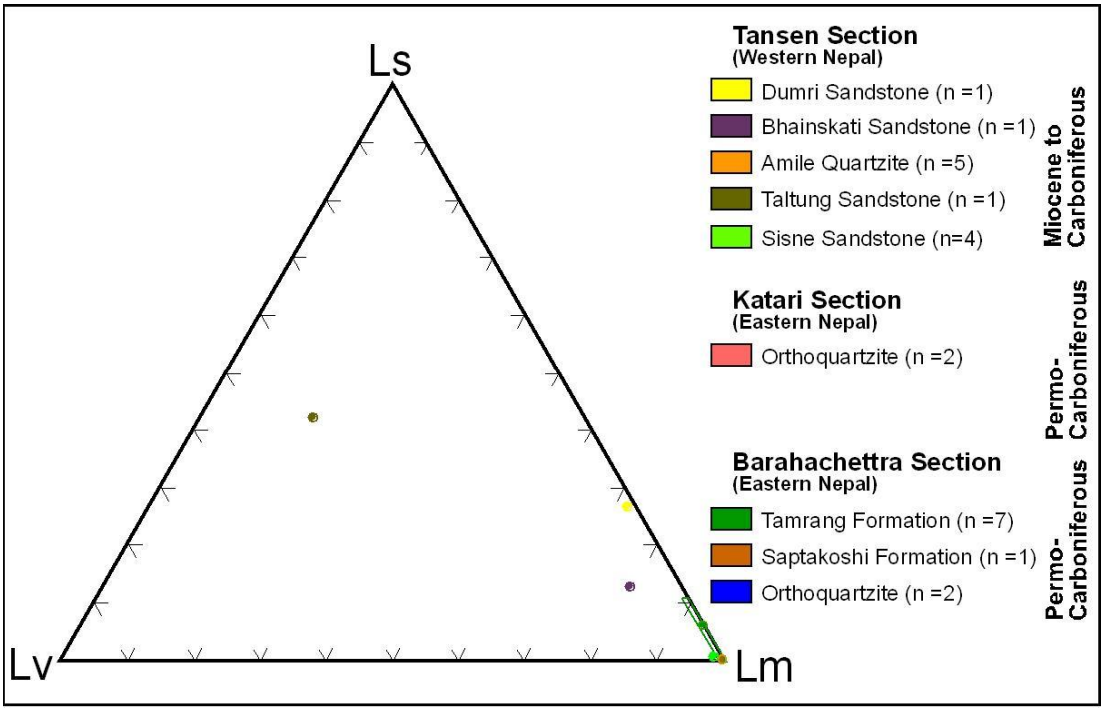

Figure 4.10 LsLvLm plot of the Gondwanan sandstones of Nepal showing mean and standard deviation polygons.

CHAPTER 5: HEAVY MINERAL ANALYSIS

5.1 INTRODUCTION

Detrital heavy minerals are powerful indicators of provenance. Analysis of heavy minerals from sediments can provide important information on provenance and help to discriminate distinct source rocks even within same tectonic unit (Morton, 1985; Najman and Garzanti, 2000; Garzanti et al., 2007). As wide ranges of heavy minerals are available in sandstones and the effects of sedimentation processes on heavy minerals have been comprehensively evaluated, high resolution provenance study is feasible with the analysis of heavy mineral assemblages (Uddin and Lundberg, 1998b; Morton and Hallsworth, 1999). Heavy minerals, which have a specific gravity of 2.9 or more, are usually present in sandstones in proportions of less than 1% (Tucker, 1988). More than 30 translucent heavy minerals are suggested as indicator of characteristics source terranes (Morton, 1985; Mange and Maurer, 1992).

Heavy mineral assemblages reflect the petrology of the source area, particularly in the case of proximal synorogenic sediments that have been transported relatively for short distances. However, various sedimentary processes operating from the source rock area to depositional basin can remarkably overprint the original assemblages of heavy minerals. These processes include weathering of the source rock, alluvial storage, mechanical breakdown and hydraulic processing during transport, and diagenesis during burial (Morton and Hallsworth, 1994; 1999). The stability of some key heavy minerals for major sedimentary processes is given in Table 5.1. Morton and Hallsworth (1999)

proposed that the effects of overprinting of these sedimentary processes can be overcome by relative abundances of minerals with similar hydraulic and diagenetic behaviors.

Table 5.1 Relative stability of heavy minerals for different sedimentary processes

Stability in weathering profiles (source rocks) (Grimm, 1973; Bateman & Catt, 1985; Dryden & Dryden, 1946) #	Mechanical stability during transport (Freise, 1931) #	Burial persistence North Sea (Morton. 1984, 1986)	Chemical weathering (Pettijohn, 1941)
Zircon, Rutile Tourmaline, Andalusite, Kyanite, Staurolite Epidote* Garnet Calcic Amphibole** Clinopyroxene Orthopyroxene Apatite	Tourmaline Corundum Chrome-spinel Spinel Rutile Staurolite Augite Topaz Garnet Epidote Apatite Zircon Kyanite Olivine Andalusite Diopside Monazite	Apatite, Monazite, Spinel, TiO_2 minerals, Tourmaline, Zircon Chloritoid Garnet Staurolete Kyanite Titanite Epidote Calcic Amphibole Andalusite, Silimanite Pyroxene Olivine	TiO_2 minerals Zircon Tourmaline Sillimanite Andalusite Kyanite Staurolite Topaz Titanite Monazite Garnet Epidote Calcic amphibole Orthopyroxene Clinopyroxene Olivine Apatite

[Stability of mineral increases towards the top part of the table; *Epidote has lower ranking than garnet and **Calcic Amphibole has lower ranking than clino- and ortho-pyroxene for eolian cover deposits in Bateman and Catt (1985)'s work; # doesn't include the opaque minerals]

Heavy mineral analysis has been used for in several provenance studies of peninsular India and also the adjoining Himalayan domain. The study of heavy mineral suites in the Barakar sandstone (Gondwanan sequence) of the Moher sub-basin in

peninsular India was done by Aslam et al. (1991). The method has been applied to paleo-tectonic and provenance studies of Himalayan foreland sequences (Chaudhri, 1972; Sinha and Sastri, 1973; Cerveny et al., 1989, Uddin and Lundberg, 1998a; Najman and Garzanti, 2000; Uddin et al., 2007) and on deep-sea cores from the Bengal fan (Yokoyama et al., 1990; Amano and Taira, 1992). These studies have been proved powerful in evaulating the nature of source rocks, in reconstructing the course of ancestral fluvial systems, and in establishing associations of source rocks to the unroofing of the Himalayas and Indo-Burman Ranges.

Further advances in heavy mineral analysis has led to the method of varietal studies that concentrates on relative abundances of minerals that are stable during diagenesis and have similar hydraulic behavior (Morton and Hallsworth, 1994). The hydraulic parameter is controlled by grain size, density, and shape. Morton and Hallsworth (1994) formulated several mineral ratios, pairs and indexes of heavy minerals comprising similar hydraulic behavior (e.g. index ATi with mineral pair apatite and tourmaline, GZi with mineral pair Garnet and Zircon, CZi with mineral pair chrome spinel and zircon). However, these methods are only applicable to the sedimentary rocks containing abundant heavy minerals.

In the absence of a full range of heavy minerals, study can be accomplished by determining the relative abundance of all important heavy mineral species preserved in each stratigraphic unit, recognizing dominant members of mineral groups, identifying the first key minerals indicative of certain levels of metamorphism, evaluating associations or

paragenesis of specific heavy minerals, and establishing index minerals from stratigraphic levels in selected sections (Rahman, 2008).

5.2 METHODS

Due to similar hydraulic behaviors, heavy minerals remain in certain grain-size fractions. Samples were disintegrated by drying in an oven and then sieving to extract 0-4 phi the size fractions. The samples were then treated with high-density liquids to separate the heavy minerals. As there is sharp difference in the density of heavy minerals with regular framework minerals, the heavy fraction gets settled first due to gravity. The liquid used for heavy mineral separation in this study was tetrabromoethane ($C_2B_2Br_4$, density 2.89-2.96 gm/cc). The samples were weighed and added to the heavy liquid in a separating funnel. The mixture was stirred three times to ensure that the grains were thoroughly wetted and not coagulated. As time passed, the heavy minerals settled down to the bottom of the funnel and the lighter fractions appeared floating above the heavy liquid at the top of the separating funnel. After 24 hours, the stopcock was opened slowly and the liquid bearing the heavy mineral fraction in the bottom part of the separating was allowed to flow slowly through a filter paper. The separated heavy fractions were washed carefully with acetone and dried in the open air and oven for 2 hours. The lighter fraction of the samples were also cleaned with acetone, dried, and stored. The heavy mineral fractions of samples were weighed and processed for magnetic separation. Magnetic separation of heavy minerals was carried out using a Frantz magnetometer at the Department of Geology and Geography at Auburn University. Four fractions of different magnetic susceptibility (Hess, 1966) were separated, including Group-1: Strongly

Magnetic (SM); Group-2: Moderately Magnetic (MM); Group-3: Weakly Magnetic (WM); and Group-4: Poorly Magnetic (PM). The separation of four groups of mineral was done by applying different slide slope angle and current values in the magnetic separator (Table 5.2).

Table 5.2 Four fractions of different magnetic susceptibility (Hess, 1966)

Side slope 15^o				Side slope 5^o	
Strongly magnetic	Moderately magnetic		Weakly magnetic	Poorly magnetic	
Hand magnet	0.4 Amps	0.8 Amps	1.2 Amps	1.2 Amps	
Magnetite Pyrrhotite Fe-oxides	Illmenite Garnet Olivine Chromite Chloritoid	Hornblende Hypersthene Augite Actinolite Staurolite Epidote Biotite Chlorite Tourmaline (dark)	Diopside Tremolite Enstatite Spinel Staurolite (light) Muscovite Zoisite Clinozoisite Tourmaline (light)	Sphene Leucozxene Apatite Andalusite Monazonite Xenotine	Zircon Rutile Anatase Brookite Pyrite Corundum Topaz Fluorite Kyanite Silimanite Anhydrite Beryl
Group 1	Group 2A	Group 2B	Group 3	Group 4	

Group-1 consists of strongly magnetic minerals including magnetite, pyrrhotite and Fe-oxides. However, this group was not separated using a hand magnet. Rather, it was separated along with Group 2A minerals including illmenite, garnet, olivine, chromite and chloritoid using a 15^o side slope and a 0.4-Amp current.

Group 2B minerals include of hornblende, hypersthene, augite, actinolite, staurolite, epidote, biotite, chlorite, and tourmaline. These were separated from weakly to poorly magnetic minerals using a 0.8-Amp current and a 15º side slope. Group 3

minerals, including diopside, tremolite, enstatite, spinel, staurolite (light), muscovite, zoisite, clinozoisite, and tourmaline (light), were separated from Group 4 using a 1.2-Amp current and a 15º side slope. The rest of the heavy minerals were classified as Group 4 (poorly magnetic) which was not separated further due to presence in small amount. This group includes slightly magnetic minerals, such as sphene, leucoxene, apatite, andalusite, monazite, and xenotine, and other non-magnetic minerals like zircon, rutile, pyrite, corundum, fluorite, kyanite, sillimanite and beryl. However, separation of heavy minerals belonging to all four groups was not achieved for each sample due to the absence or rarity of minerals from certain groups.

Separated heavy minerals were sent to Spectrum Laboratories in Vancouver, WA to prepare polished thin sections. Fourteen polished thin sections were prepared from fourteen samples. Each of the magnetically separated heavy mineral fractions were segregated in different areas (holes) of each thin section. Identification of minerals was carried out using a petrographic microscope and a modified Fleet method (Fleet, 1926). Numbers of grains from each holes were counted and then added together to calculate the percentage of different species of heavy minerals.

5.3 RESULTS

Heavy mineral assemblages of Gondwanan sandstones of Nepal are not very diverse. Only four to five minerals specimens dominate in all samples (Tables 5.3 and 5.4).

Heavy mineral suites in the Permo-Carboniferous Sisne sandstones (samples 16-3 and 16-5) differ markedly those of younger units (the Taltung and Amile formations of the Tansen Group). Highly stable minerals (ZTR) are present in very small numbers, and moderately stable garnets are abundant (Table 5.3) (Fig. 5.3). The abundance of opaque minerals is less than in overlying other units. A possible explanation for this major difference in heavy mineral assemblage is due to change of provenance in younger units. The garnets are irregular in shape and highly fractured (Fig. 5.3). Some of the grains also show corroded surfaces. These surface features suggest a burial dissolution for the Sisne heavy minerals letting only garnets to survive among all heavies contributed by source rocks.

The heavy mineral assemblage of Cretaceous-Jurassic Taltung sandstone (sample K-1) mostly consists of zircon, chrome-spinel, rutile, tourmaline, garnet, and dolomite as well as common opaque minerals (Table 5.3). Tourmaline grains are highly fractured and also show the effects of corrosion (Fig. 5.2). Chrome-spinel grains are in variable sizes and shapes. Garnets are rare and are irregular in shape. Abundant opaque grains present in this sample could have contributed from source rocks or formed as authigenic iron-oxide coating is the basin.

The Paleocene-Cretaceous Amile Formation of the Tansen Group in western Nepal is dominated by tourmaline, zircon and rutile, as well as opaque grains. Three samples from the Amile Formation were subjected to heavy mineral analysis (samples 15-6, 16-8, and 16-9) (Table 5.3).

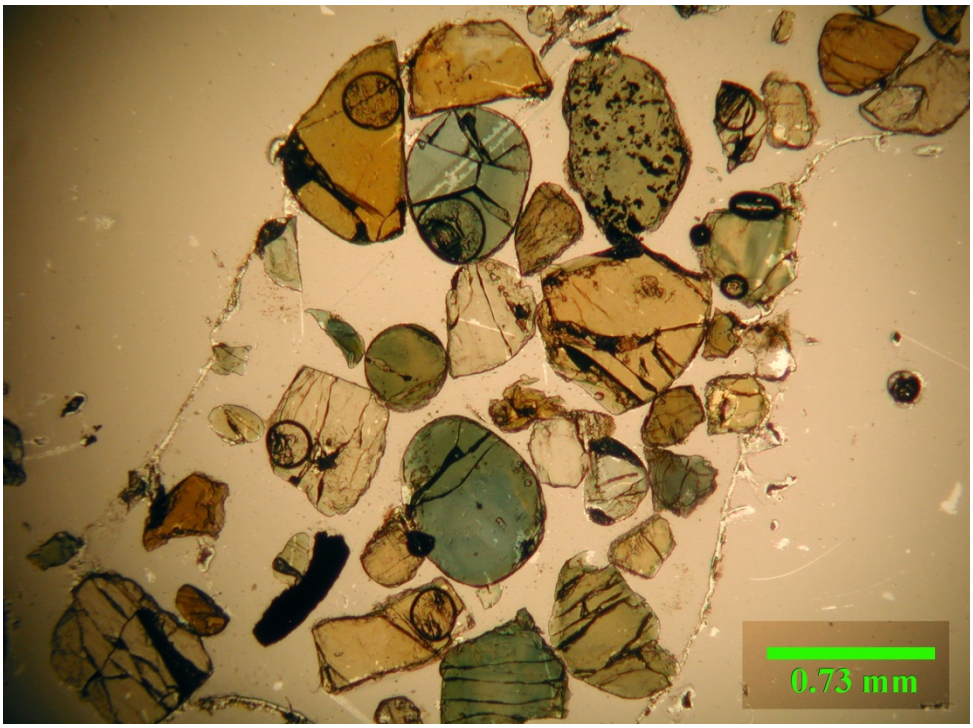

Figure 5.1 Representative photomicrograph of tourmalines in Amile sandstone (sample 15-6) of the Tansen Group, western Nepal.

Tourmaline grains are easy to identify with their strong pleochroism and low relief. Tourmalines from the Amile Formation are highly fractured (both primary and secondary fractures are present). The shape and size of the grains are variable (Fig. 5.1). Some of the grains are corroded. The zircon crystals are rounded and a little smaller than the tourmalines. The rutile grains are deep red and rounded. The presence of numerous

opaque minerals could have contributed from authigenic coating of iron oxides on mineral grains as well as a contribution from source rocks.

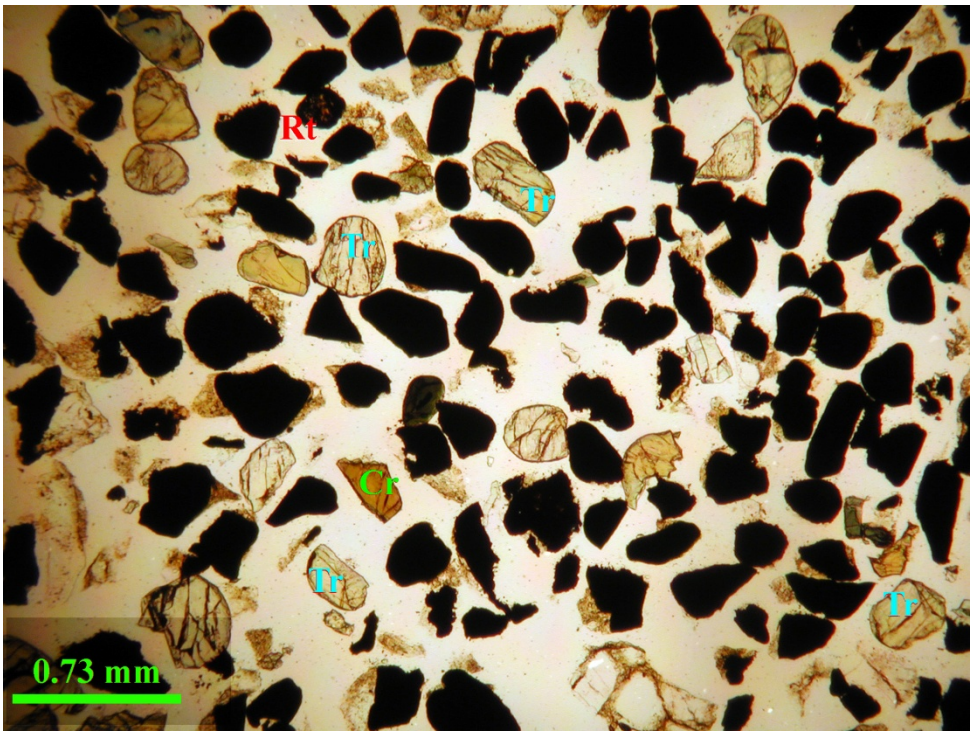

Figure 5.2 Representative photomicrograph of heavy mineral assemblage in the Taltung sandstone (sample K-1) of the Tansen Group, western Nepal (Cr- Chromium, Rt-Rutile, Tr-Tourmaline).

The Permo-Carboniferous Katari Group in eastern Nepal also shows variations in heavy mineral assemblage. Besides common heavy minerals present in other Gondwanan samples, this unit also contains biotite and chlorite/chloritoid (Table 5.4). The garnet grains are more irregular in shape than the zircons which are mostly rounded. As expected based on hydraulic equivalence, biotite and chlorite grains are larger than other types of heavy minerals (Morton and Hallsworth, 1999). However, the mica grains are deformed and folded (Figs. 5.4 and 5.5). This likely is related to some kind of

deformation in the source rocks rather than in the depositional basin as petrographic analyses of the thin section of this sample does not reflect post depositional deformation.

The Saptakoshi and Tamrang formations of the Barahachettra Group, another Permo-Carboniferous unit in eastern Nepal, show quite different heavy mineral assemblages. However, these assemblages are correlatable with assemblages of some units of the Tansen Group, albeit of different age.

The Tamrang sandstones (samples 22-6, 22-10, 23-4) from eastern Nepal are primarily dominated by highly stable minerals like zircon, tourmaline and rutile (Table 5.4) (Fig. 5.6) as well as opaque grains. However, the Tamrang Formation also contains common micas and a large number of unidentified heavy minerals.

The Saptakoshi sandstone (sample 23-5) contains few highly stable heavy minerals (i.e. zircon, rutile and tourmaline) but large numbers of less stable garnets (Table 5.4). This dominant assemblage of garnets in the Saptakoshi sandstone is similar to that of the Sisne sandstone of western Nepal. However, the sizes of garnets are smaller than that in the Sisne Formation. The Saptakoshi sandstones contain fewer opaque grains than the Sisne Formation.

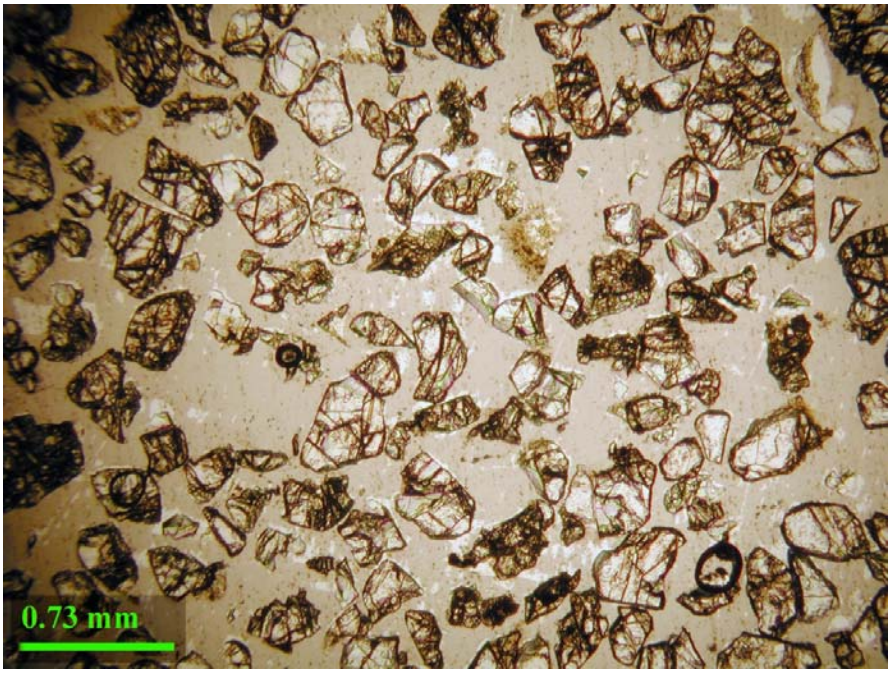

Figure 5.3 Representative photomicrograph of heavy mineral assemblage in the Sisne sandstone (sample 16-3) of the Tansen Group, western Nepal, showing abundance of garnets.

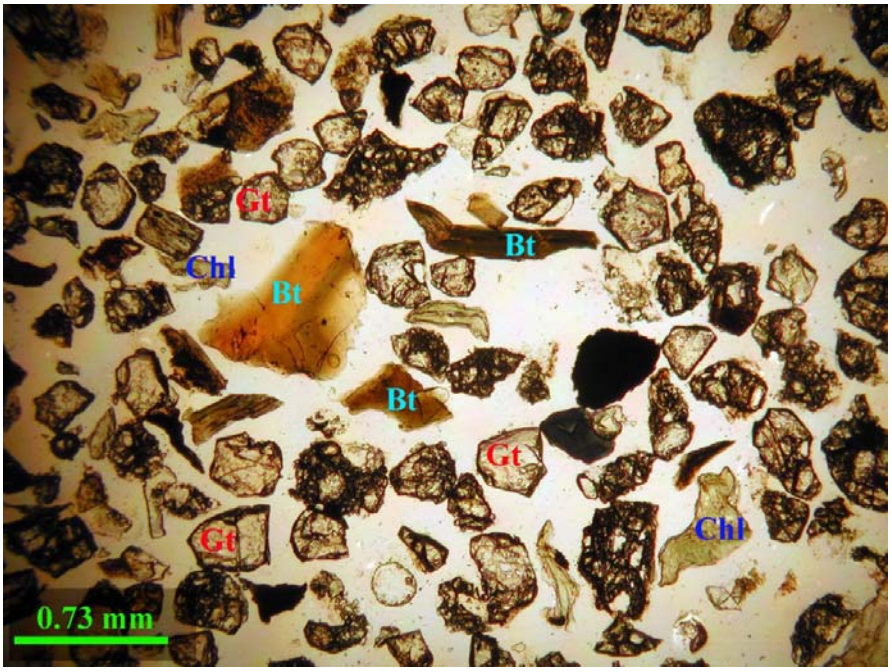

Figure 5.4 Representative photomicrograph of heavy mineral assemblage in the Permo-Carboniferous sandstone (sample 26-8) of the Katari Group, eastern Nepal. (Bt—Biotite; Chl- Chlorite; Gt—Garnet).

Table 5.3 Heavy mineral data in Gondwanan sandstones from western Nepal (Tansen Group).

Sample No	**16-9**		**16-8**		**15-6**	
Rock Unit	**Amile Formation**		**Amile Formation**		**Amile Formation**	
Age	**(Paleo-Cretaceous)**		**(Paleo-Cretaceous)**		**(Paleo-Cretaceous)**	
Heavy Minerals	No of Grains	Percentage	No of Grains	Percentage	No of Grains	Percentage
Zircon	22.00	6.73	11.00	5.02	7.00	4.05
Rutile	10.00	3.06	8.00	3.65	2.00	1.16
Tourmaline	97.00	29.66	55.00	25.11	53.00	30.64
Chrome-Spinel	0.00	0.00	0.00	0.00	0.00	0.00
Dolomite	0.00	0.00	0.00	0.00	0.00	0.00
Garnet	0.00	0.00	0.00	0.00	0.00	0.00
Biotite	0.00	0.00	0.00	0.00	0.00	0.00
Chlorite/Chloritoid	0.00	0.00	0.00	0.00	0.00	0.00
Opaque	186.00	56.88	136.00	62.10	103.00	59.54
Others	12.00	3.67	9.00	4.11	8.00	4.62
Total	**327.00**	**100.00**	**219.00**	**100.00**	**173.00**	**100.00**
ZTR		**39.45**		**33.79**		**35.84**

Sample No	**16-3**		**16-5**		**K-1**	
Rock Unit	**Sisne Formation**		**Sisne Formation**		**Taltung Formation**	
Age	**(Permo-Carboniferous)**		**(Permo-Carboniferous)**		**(Cretaceous-Jurassic)**	
Heavy Minerals	No of Grains	Percentage	No of Grains	Percentage	No of Grains	Percentage
Zircon	7.00	2.06	42.00	6.91	24.00	8.25
Rutile	5.00	1.47	16.00	2.63	32.00	11.00
Tourmaline	6.00	1.76	4.00	0.66	9.00	3.09
Chrome-Spinel		0.00		0.00	35.00	12.03
Dolomite		0.00		0.00	65.00	22.34
Garnet	280.00	82.35	480.00	78.95	17.00	5.84
Biotite		0.00		0.00		0.00
Chlorite/Chloritoid		0.00		0.00		0.00
Opaque	30.00	8.82	54.00	8.88	102.00	35.05
Others	12.00	3.53	12.00	1.97	7.00	2.41
Total	**340.00**	**100.00**	**608.00**	**100.00**	**291.00**	**100.00**
ZTR		**5.29**		**10.20**		**22.34**

Table 5.4 Heavy mineral distribution in Gondwanan sandstones from eastern Nepal (Barahachettra and Katari groups).

Sample No	**26-8**		**23-5**		**22-6**	
Rock Unit	**Katari Group**		**Saptakoshi Formation**		**Tamrang Formation**	
Age	**(Permo-Carboniferous)**		**(Permo-Carboniferous)**		**(Permo-Carboniferous)**	
Heavy Minerals	No of Grains	Percentage	No of Grains	Percentage	No of Grains	Percentage
Zircon	12.00	4.63	5.00	2.38	33.00	7.91
Rutile	12.00	4.63	2.00	0.95	43.00	10.31
Tourmaline	15.00	5.79	3.00	1.43	90.00	21.58
Chrome-Spinel		0.00		0.00		0.00
Dolomite		0.00		0.00		0.00
Garnet	123.00	47.49	182.00	86.67		0.00
Biotite	9.00	3.47		0.00		0.00
Chlorite/Chloritoid	17.00	6.56		0.00	55.00	13.19
Opaque	56.00	21.62	13.00	6.19	174.00	41.73
Others	15.00	5.79	5.00	2.38	22.00	5.28
Total	**259.00**	100.00	**210.00**	100.00	**417.00**	100.00
ZTR		**15.06**		**4.76**		**39.81**

Sample No	**22-10**		**23-4**	
Rock Unit	**Tamrang Formation**		**Tamrang Formation**	
Age	**(Permo-Carboniferous)**		**(Permo-Carboniferous)**	
Heavy Minerals	No of Grains	Percentage	No of Grains	Percentage
Zircon	25.00	7.00	18.00	9.63
Rutile	18.00	5.04	15.00	8.02
Tourmaline	99.00	27.73	34.00	18.18
Chrome-Spinel		0.00	2.00	1.07
Dolomite		0.00		0.00
Garnet		0.00		0.00
Biotite		0.00		0.00
Chlorite/Chloritoid	22.00	6.16	28.00	14.97
Opaque	180.00	50.42	72.00	38.50
Others	13.00	3.64	18.00	9.63
Total	**357.00**	100.00	**187.00**	100.00
ZTR		**39.78**		**35.83**

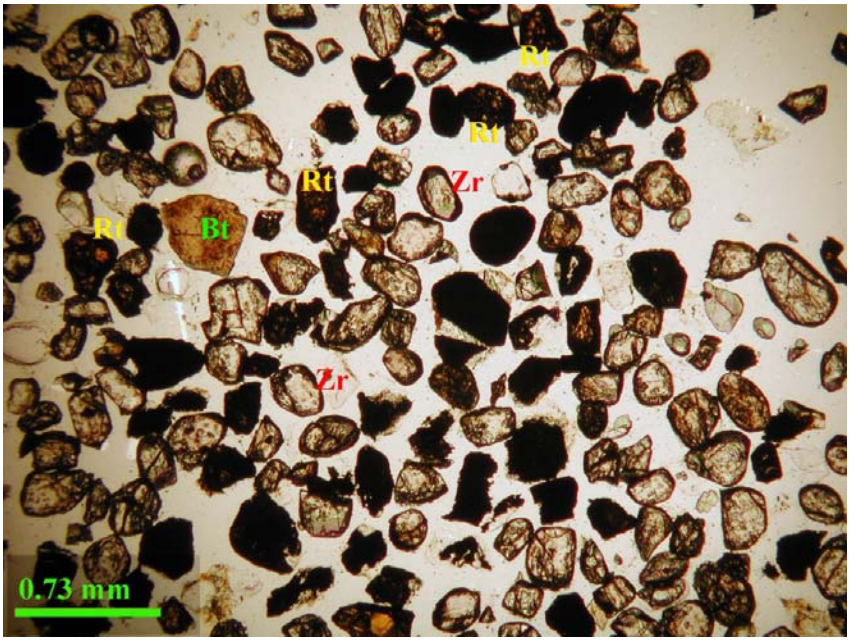

Figure 5.5 Representative photomicrograph of heavy mineral assemblage in the Permo-Carboniferous sandstone (sample 26-8) of the Katari Group, eastern Nepal (Bt-Biotite; Rt-Rutile; Zr-Zircon).

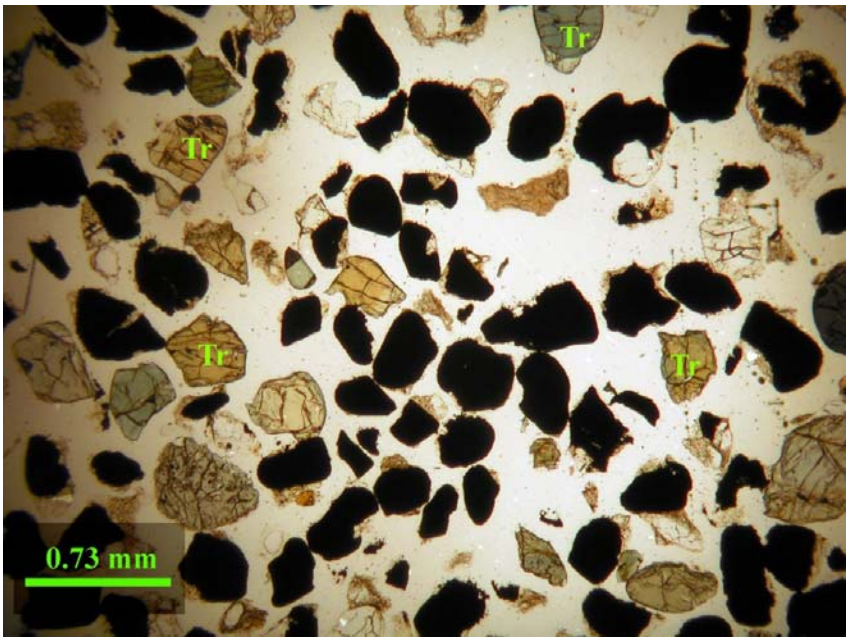

Figure 5.6 Representative photomicrograph of heavy mineral assemblage in the Permo-Carboniferous sandstone (sample 23-4) of the Barahachettra Group, eastern Nepal (Tr-Tourmaline).

5.3 PROVENANCE

The weight percentage of heavy minerals of the Gondwanan sandstones in eastern Nepal is less than that of western Nepal (Fig. 5.7). The presence of numerous faults in the eastern part could have played a significant role by allowing acid water to leach the heavy minerals (Morton and Hallsworth, 1999). Among individual units, the Taltung Formation (Cretaceous-Jurassic) of the Tansen Group contains the highest amount of heavy minerals, which may reflect sediment contribution from nearby lava flows (Sakai, 1983). The overall signature of heavy minerals in Gondwanan sequences of Nepal is the dominant contribution of garnet in Permo-Carboniferous units in western and eastern Nepal (Fig. 5.8). Assemblages dominated by highly stable minerals (zircon, rutile and tourmaline) characterize the Cretaceous-Paleocene Amile Formation of western Nepal (Tansen Group) and purported Permo-Carboniferous unit (Bashyal, 1979) of western Nepal (Fig. 5.9).

Presence of abundant chrome-spinel in the Jurassic-Cretaceous Taltung Formation of the western Nepal indicates a volcanic source. The puported Permo-Carboniferous Katari Group does not show similarities in heavy mineral contents with the Permo-Carboniferous units of Tansen and Barahachettra groups.

The garnet and tourmaline contents of Gondwanan units of Nepal show strong negative correlation (Fig. 5.10), which suggests a change in source rocks rather than some other control. Moreover, during the Permo-Carboniferous, India together with other masses of Gondwanaland, was situated in high southern latitudes (Veever and Tiwari, 1995). However, during Jurassic to Cretaceous deposition, India was already

positioned in an equatorial area, which resulted in intense weathering of source rocks and destruction of unstable heavy minerals. The possible provenance of garnet contributing sediments for the Gondwanans sequences of Nepal could be the Chotnagpur Gneissic terrain of peninsular India (Fig. 5.11). However, the Aravali-Delhi Supergroup and the Bundelkhand Gneiss could have also contributed garnets depending on the paleodirection of northerly flowing rivers from central India (e.g. Chambal, Betawa, and Son Rivers). The highly stable heavy minerals in Jurassic to Cretaceous units could have been supplied from Proterozoic sedimentary sequences of the Vindhyan Group.

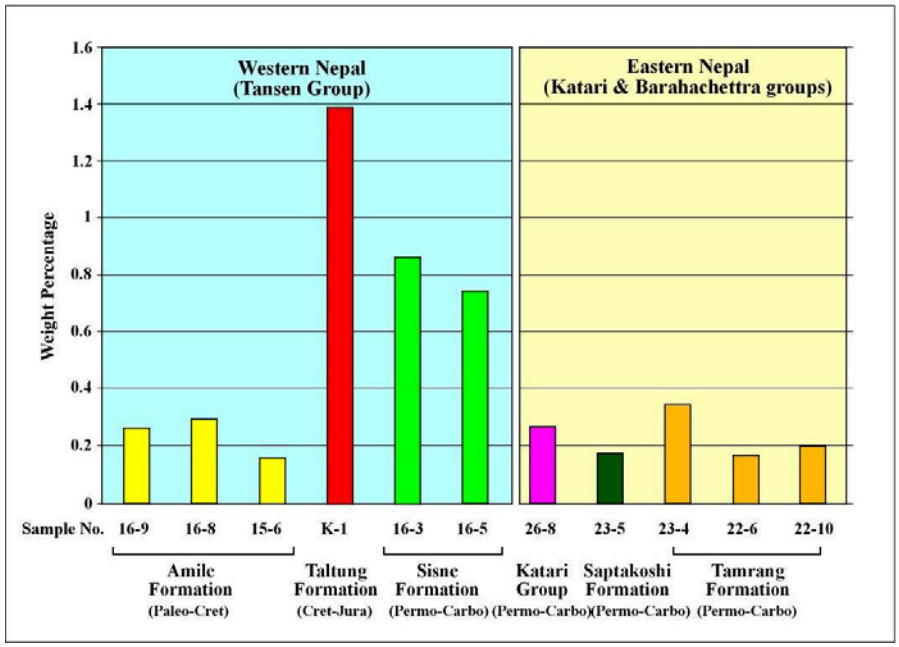

Figure 5.7 Distribution of heavy minerals among different units and sections of Gondwanan sandstones in Nepal.

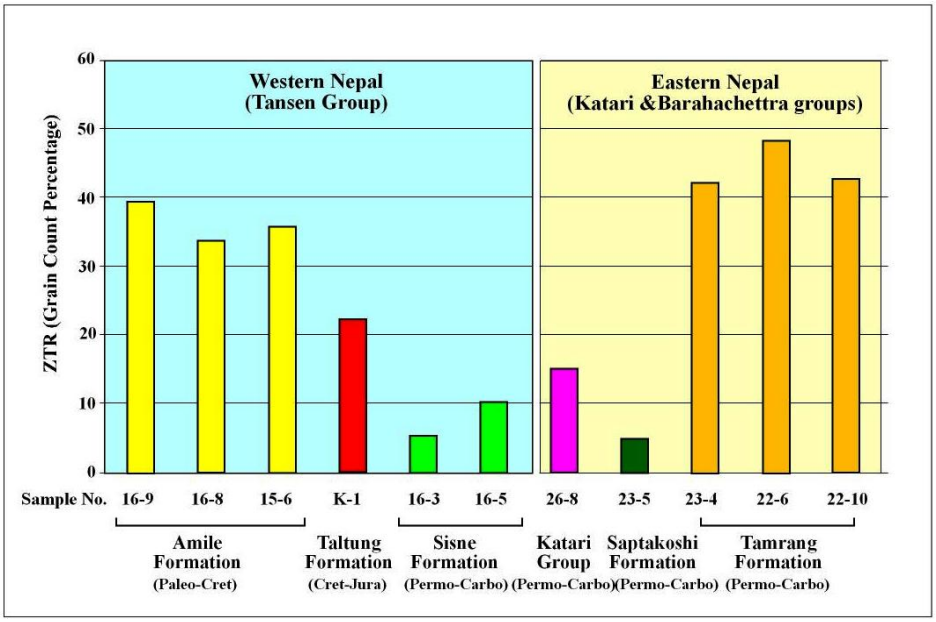

Figure 5.8 Distribution of highly stable heavy minerals (ZTR) among different units and sections of Gondwanan sandstones in Nepal.

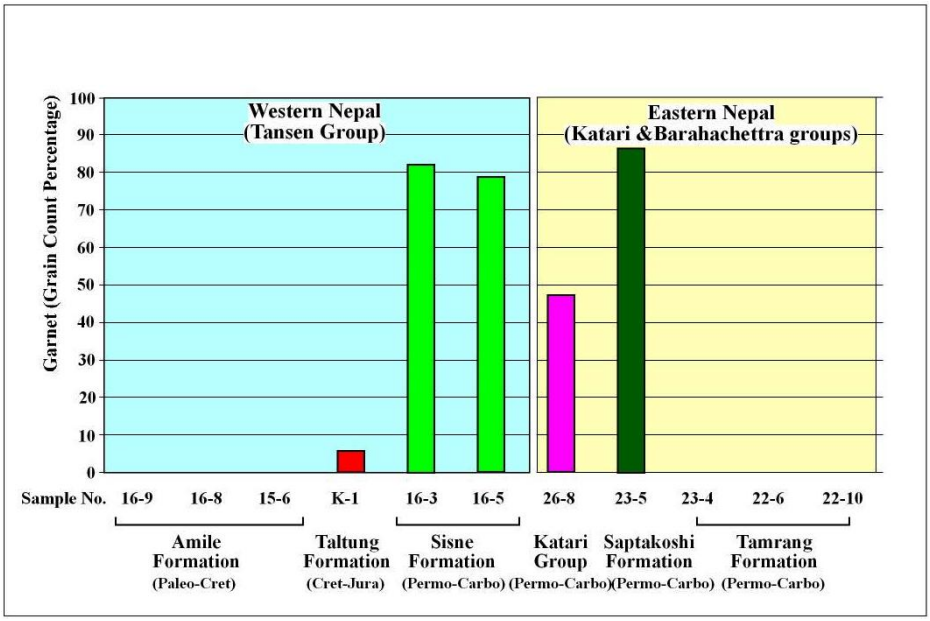

Figure 5.9 Distribution of garnets among different units and sections of Gondwanan sandstones in Nepal.

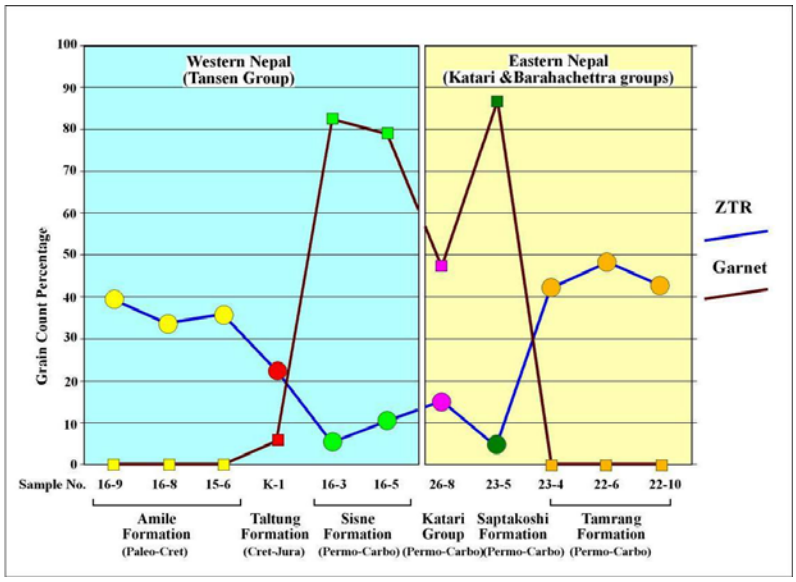

Figure 5.10 Variation in distribution of garnets and ZTR among different units and sections of Gondwanan sandstones in Nepal.

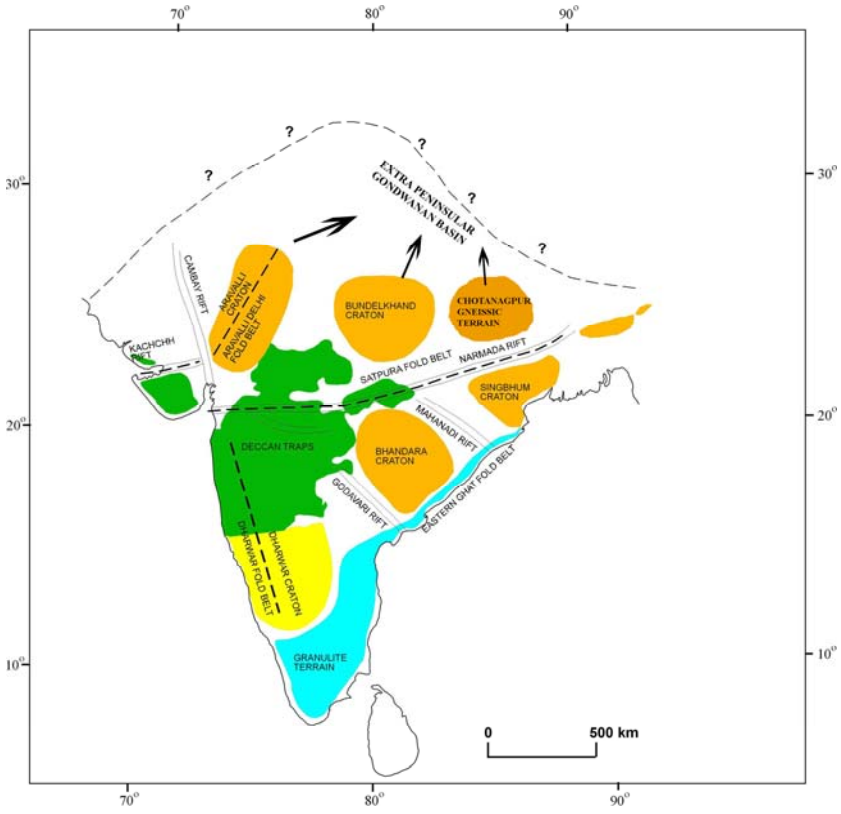

Figure 5.11 Possible source rock units for the Gondwanan sandstones of Nepal from cratonic India.

CHAPTER 6: MICROPROBE ANALYSIS

6.1 INTRODUCTION

Heavy mineral studies have been used as one of the most powerful tools in provenance analysis in the past and are gaining more recognition recently. Sandstones are easy to collect in the field and to process and analyze in the lab and hence are the materials utilized for heavy mineral analysis.

Mineral chemistry of some heavy minerals are very good indicators on discriminating source rock types. Chrome-spinel chemistry is useful in differentiating various types of mafic igneous rocks. The supply of sediment from different-grade metamrophic rocks can be tracked down with the help of garnet chemistry. Tourmaline chemistry is valuable in distinguishing types of plutonic source rocks.

Mineral chemistry analysis on some selected heavy minerals has been carried out with an objective to fingerprint provenance of Gondwanan sequences distributed in several patches along the Nepal Himalaya.

6.2 MINERAL CHEMISTRY

Three mineral groups were chosen for microprobe analysis: garnet, tourmaline, and chrome-spinel. Several workers have used these minerals to determine provenance of sediments (e.g., Kumar, 2004; Zahid; 2005; Rahman, 2008). The compositional variation of these mineral can be linked to different source rocks (Henry and Guidotti, 1985;

Morton, 1985; Henry and Dutrow, 1990; Morton and Taylor, 1991; Nanayama, 1997, Zhu et. al, 2004).

Garnet [$X_3Y_2(Si0_4)_3$], found commonly in metamorphic rocks and also in some igneous rocks, has proven to be a good indicator of pressure and temperature conditions during the formation of the source rock. The X-site is occupied by Fe^{2+}, Mg^{2+}, Ca^{2+} , and Mn^{2+}. As the metamorphic grade of the source rock will increases, the ratio of (Fe^{2+} + Mg^{2+})/(Ca^{2+} + Mn^{2+}) also increases (Sturt, 1962; Nandi, 1967). With an increase in metamorphic grade, pelitic schists will show an increase in Mg concentration with respect to Fe^{2+} (Spear, 1993). The Y-site is occupied by trivalent cations like Fe^{3+}, Cr^{3+} except Al^{3+} . The cations occupancy of this site can also be related to the type of source rock.

Compositional analysis of chrome-spinel has also been used by several workers for sediments provenance analysis. Chrome-spinel is a good indicator of provenance, particularly for discriminating different types of mafic and ultramafic rocks (Irvine, 1973, 1977; Dick and Bullen, 1984; Nixon et al., 1990). Chrome-spinel [AB_2O_4], found mostly in mafic igneous rocks, gives a good indication of source rocks based on variations of elements in cation sites. There are 4 oxygen ions and 3 cations in the unit cell (Brady and Perkins, 2009). The A-site is occupied by Fe^{2+}, Mg^{2+}, Ca^{2+} , Mn^{2+} and the B-site is occupied by Al^{3+}, Cr^{3+}, Ti^{4+}, Si^{4+}. Different end members can be calculated based on the occupancy of these two sites. In most cases, there will be presence of solid solutions rather than true end members (Deer et al., 1992).

Tourmaline generally has very complex compositional structure. The general structural formula of tourmaline is $XY_3Z_6(BO_3)Si_6O_{18}(OH)_4$. The X-site is usually occupied by Na^+, Ca^{2+}, the Y-site is by Mn^{2+}, Fe^{2+}, Al^{3+}, Li^{2+}, Mg^{2+}, and the Z-site by Al^{3+}, Cr^{3+}, Mn^{2+}or Mg^{2+} (Deer et. al, 1992). This mineralogical structure provides the opportunity for a wide range of cation substitutions during crystallization of tourmalines. Plots of tourmaline composition, Al-Fe(tot)-Mg and Ca-Fe(tot)-Mg, have been used for provenance analysis by many authors (e.g., Henry and Guidotti, 1985; Henry and Dutrow, 1990).

6.3 SAMPLE PREPARATION

Heavy minerals were separated from disintegrated samples using a heavy liquid. The separation process is described in the heavy mineral chapter (Chapter 5). Thin sections used for normal microscopic study of heavy mineral were also used for the microprobe analysis. The polished thin sections were carbon-coated to ensure proper conduction of the electron beam on the surface of the thin sections. Along with the desired samples, one standard sample was also coated to the same thickness. The carbon coating was carried out by carbon evaporation under vaccum, and the thickness of the carbon coat was monitered with the reference of its color on polished brass block. As the thickness of coat increases on the brass, its color will change from orange (150 Å) to indigo red (200 Å), then to blue (250 Å) and then to bluish green (300 Å).

6.4 THE ELECTRON MICROPROBE

An electron microprobe (EMP) is an analytical tool used for nondestructive micron-scale quantitative chemical analysis of small volumes of solid materials. It is also referred to as an electron probe microanalyser (EPMA) or electron micro probe analyser (EMPA).The working method of EMP is similar to the scanning electron microscope (SEM). The method utilizes characteristic x-rays excited by the bombardment on the surface of sample with an electron beam. When the electron beam hits on the surface of the sample it creates two different kinds of response. Some of the electrons of the incident beam will be scattered backward elastically multiple times carrying the energy between 0 and Eo (the incident beam energy). These back-scattered electrons carry information about the chemical composition of the sample. As the electron beam hits the sample, electron beam will loses its energy which will be received by the electrons in the shell of atoms of the sample. These electrons of the sample will be excited and jump from one shell to another shell throwing certain amount of energy. That energy transforms to x-rays that are very characteristic of the compositon of the sample. Secondary electrons from the sample are also mobilized by the beam through inelastic scattering. These have energies in the range of 0-50 eV (most probable energy 3-5 of eV). Different detector setups are required to detect these different types of electron signal.

The basic purposes of EPM are: (1) to get a complete quantitative chemical analysis of a small sample through x-ray emission spectral analysis without destroying the samples; and (2) to get high-resolution scanning electron and concentration maps (scanning x-ray). Among the scanning electron images, backscattered electron (BSE) will

show compositional contrast, while secondary electron (SE) will enhance surface and topographic features.

For this research, a JEOL JXA 8600 Superprobe was utilized at the Department of Geology, University of Georgia. The probe is automated by a Geller Micro analytical laboratory dQANT with the an accelerating voltage of 15 KV and a beam current of 15 nanno amps. Both natural and synthetic standards were used to calibrate the data.

Standard Intensity Calibration:

Before starting the actual microprobe analysis of samples, the standard x-ray intensities of the elements to be measured were obtained on appropriately chosen standards. These standards were also verified for the reproduction by analyzing secondary standards that were run as unknowns. The analytical environment (e.g., accelerating voltage, beam current, etc.) was remained fixed throughout the lab session.

The list of the standards used during this analysis is given in Table 6.1. Most of the standards came from C.M. Taylor Corporation. The USNM standards came from the National Museum of Natural History, a branch of the Smithsonian Institution. Standards from University of Oregon Microprobe Laboratory and an almandine standard obtained from the Harvard Mineral Museum were also used. Calbration for each analysis session was checked using the Kakanui Hornblende (USNM) and Pyrope # 39 (C.M. Taylor) standards.

Table 6.1 Electron microprobe standards used for this study

Electron Microprobe Standards			
Element	Standard	Source	Comment
Cr	Chromite#5	C M Taylor Corp	
Mn	Spessartine#4b	C M Taylor Corp	
TiO_2	Rutile	C M Taylor Corp	
Ca	Sphene#1A	C M Taylor Corp	
Fe	Hematite#2	C M Taylor Corp	Used for oxide (spinel) analysis
Fe	Syn. Fayalite Ol-11	Univ. of Oregon	Used for silicate analyses
Ni	Ni metal	C M Taylor Corp	
Si	Diopside 5A	C M Taylor Corp	Si standard for all phases except garnet
Mg	Olivine #1	C M Taylor Corp	
Al	Syn. Spinel	C M Taylor Corp	
K	Orthoclase MAD-10	C M Taylor Corp	
Na	Ameila Albite	USNM	This is ubiquitous Na Standard
Si	Almandine	Harvard Mineral Museum oxygen standard # 112140	Si standard for garnet analyses
F	Syn. Fluoro-Phlogopite	University of Oregon M-6	
Cl	Scapolite	USNM R 6600-1	

6.5 RESULTS

A total of 45 grains were analyzed under the supervision of Mr. Chris Fleisher. These included garnets, tourmalines, and chrome-spinels.

6.5.1 Garnet

Garnet grains are abundant in the Sisne Formation of the Tansen Group and also in the Barahachettra and Katari groups. However, garnets are rare to absent in younger units (Taltung and Amile formations) of the Tansen Group. Calculated endmembers and their variations of 20 garnet grains are plotted in figures 6.1 through 6.6. The end-member calculation was done for four endmembers-- almandine, pyrope, grossular and spessartine-- among which almandine is the dominant end-member. The average and maximum content of almandine in garnet grains is 65.49% and 81.88%, respectively. The average pyrope content is 14.44% with a maximum of 35.80%. Higher pyrope contents are found in the Taltung Formation of the Tansen Group. The average grossular content is 13.70% with a maximum of 32.83%. The average spessartine content is 6.35%. However, this average usually reflects high spessartine contents in just a few grains.

The (Sp+Gro)-Py-Alm plot (Fig. 6.1) shows that most of the garnets have high almandine content. Almost all of the grains from the Katari Group have very low pyrope content. Similary, the (Py+Alm)-Gro-Sp plot (Fig. 6.2) shows that most of the grains have high Py+Alm, particularly garnets from the Taltung Formation. Garnet grains from the Barahachettra Group show low spessartine contents of except one grain. The (Alm+Sp)-Py-Gro plot (Fig. 6.3) shows that all the garnets from the Katari Group fall in

field I with almandine and grossular and pyrope < 10%. Most of the garnets from the Barahachettra Group fall in field III with both pyrope and grossular >10%. The garnets from the Taltung Formation falls in field II with grossular <10%. The plot of Sp-Alm-Py (Fig. 6.4) shows that most of the garnet grains from all rock units fall in the amphobolite facies. Only one grain of the Sisne Formation falls in granulite facies. However, the grains from the Taltung Formation fall in the overlapping field between granulite facies and amphioblite facies.

The plot of grossular content (mol %) with the number of grains from each rock unit (Fig. 6.5) also shows that most of the grains fall in low- to medium-grade metamorphic pressure regimes. The only one grain from the Sisne Formation falls in eclogite facies. Garnet from the Taltung Formation reflects a low-grade metamorphic regime.

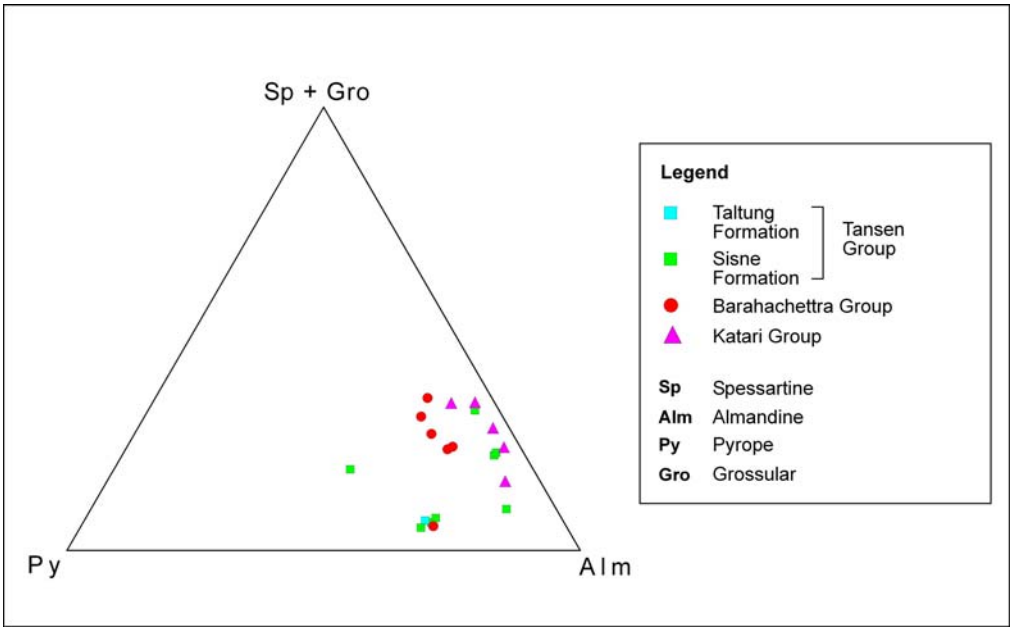

Figure 6.1 Chemical composition of garnets of Gondwanan sequences of Nepal (Tansen Group, western Nepal; Barahachettra and Katari groups in eastern Nepal) plotted on (Sp+Gro)-Py-Alm (adapted after Nanayama, 1997).

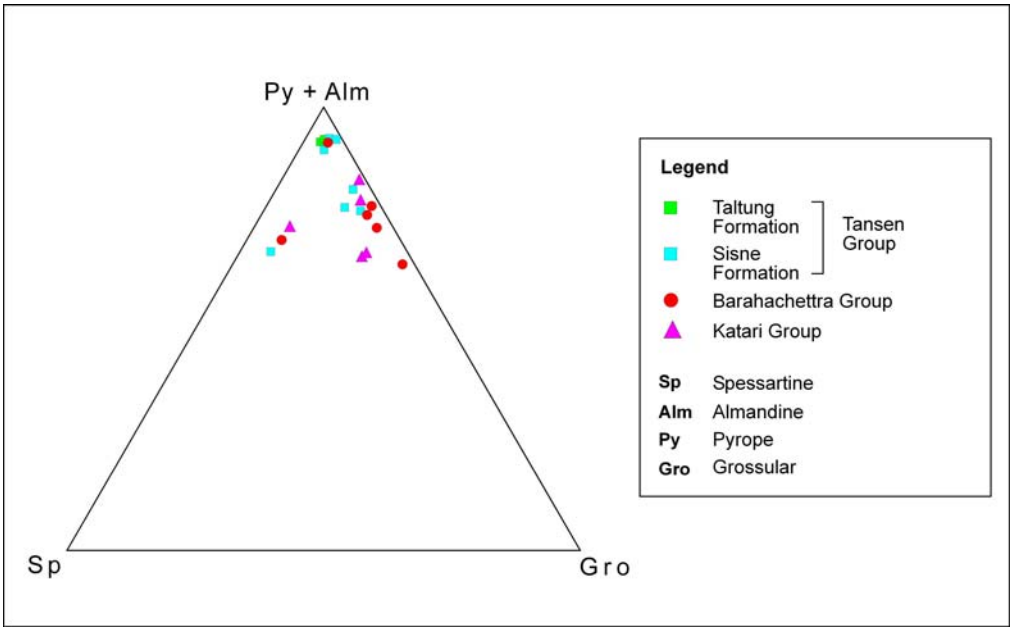

Figure 6.2 Chemical composition of garnets of Gondwanan sequences of Nepal (Tansen Group, western Nepal; Barahachettra and Katari groups in eastern Nepal) plotted on (Py+Alm)-Gro-Sp (adapted after Nanayama, 1997).

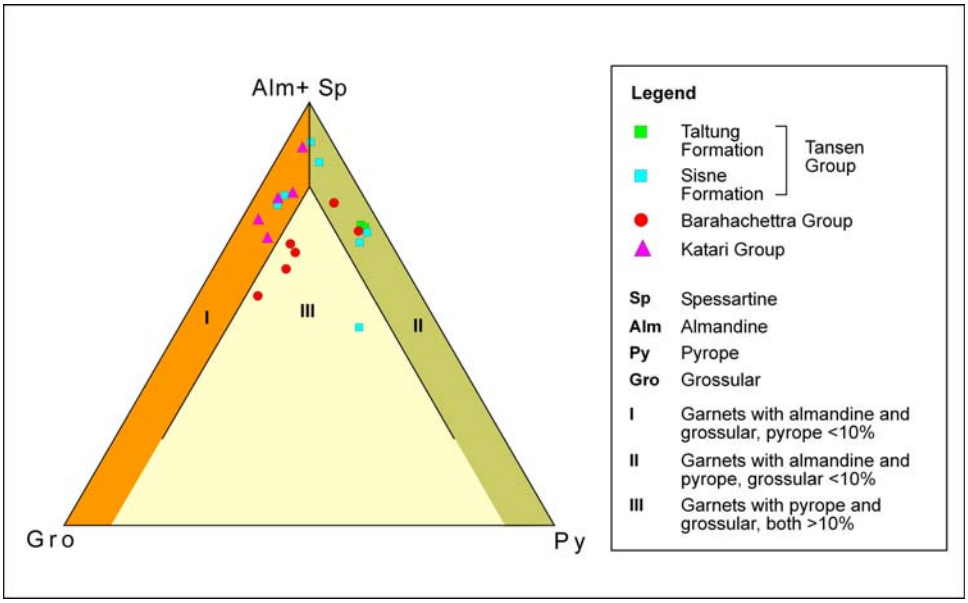

Figure 6.3 Chemical composition of garnets of Gondwanan sequences of Nepal (Tansen Group, western Nepal; Barahachettra and Katari groups in eastern Nepal) plotted on (Alm+Sp)-Py-Gro (adapter afted Nanayama, 1997).

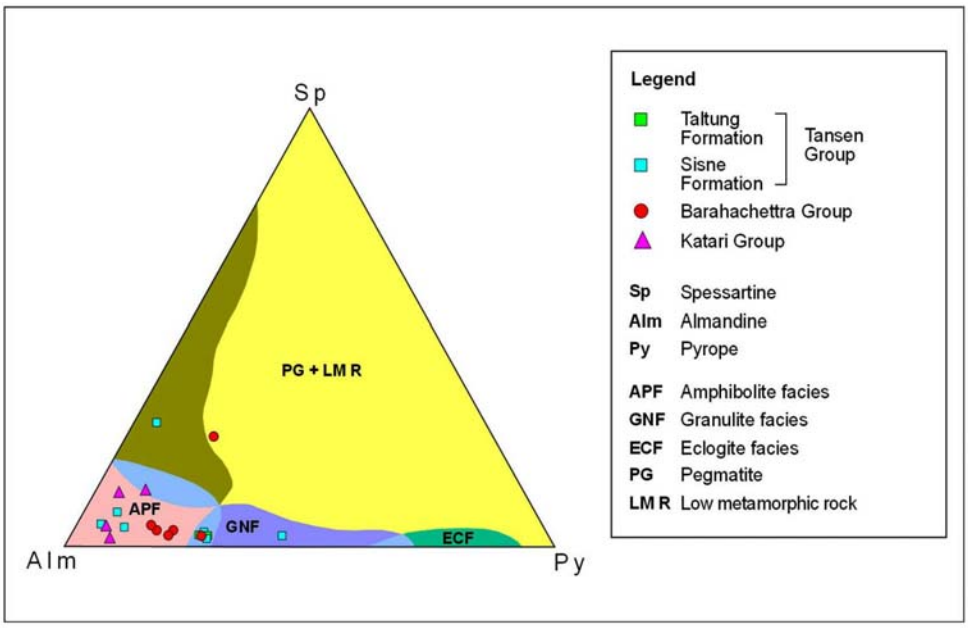

Figure 6.4 Chemical composition of garnets of Gondwanan sequences of Nepal (Tansen Group, western Nepal; Barahachettra and Katari groups in eastern Nepal) plotted on Alm-Py-Sp (adapted after Nanayama, 1997).

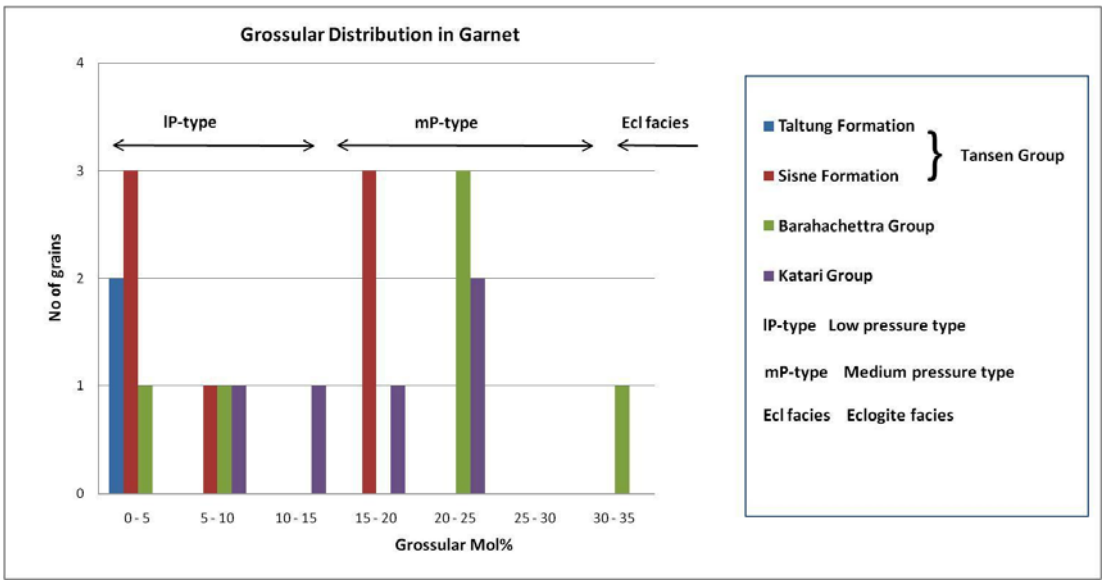

Figure 6.5 Grossular contents of garnets from Gondwanan sequences of Nepal (Tansen Group, western Nepal; Barahachettra and Katari groups in eastern Nepal) plotted on Alm-Py-Sp (adapted after Nanayama, 1997).

6.5.2 Tourmaline

Tourmaline has very complex structure and is commonly considered in terms of end-members. There is a complete solid solution between two end-member series: schorl-elbaite and schorl-dravite. However, there is a large miscibility gap between elbaite and dravite. Hence, tourmalines are usually described by their positions in the schorl-elbaite series or in the schorl-dravite series. Two different plot have been prepared using Al-$Al_{50}Fe_{50(tot)}$ -$Al_{50}Mg_{50}$ (Fig. 6.6) and Ca-Fe(tot)-Mg (Fig. 6.7). These plots Al-$Al_{50}Fe_{50(tot)}$ -$Al_{50}Mg_{50}$ show that all tourmaline grains from three different sections of Nepal (the Tansen, Barahachettra and Katari groups) fall between Li-poor granitiods and pegmatites and aluminous meta-pelites and meta-psammites.

On the Ca-Fe(tot)-Mg plot (Fig. 6.7), tourmalines from the Katari Group fall in three different fields: Li-rich granitoids pegmatites, Li-poor granitoids pegmatites, and Ca-poor metapelites, metapsammites. Samples from Barahachettra and Tansen groups have fallen only between the Li-poor granitoids pegmatites and Ca-poor metapelites, metapsammite fields. As the compositon of grains are fallen in different rock group types, there should be different sources of rocks for these units.

6.5.3 Chrome-spinel

Chrome-spinel was only found in the Taltung Formation of the Tansen Group. Five grains of chrome-spinel from this unit were analyzed. The average elemental percentage of chormium in these grains is 24.17%, with the maximum of 33.02%.

Various plots have been prepared from the compositional data of these chrome-spinel grains to judge the source rock of the sediment. A ternary plot of Al^{3+}-Cr^{3+}-Fe^{3+} suggests Alpine-type peridotite source rock (Fig 6.8). Alpine-type peridotites have compositions of > 95% harzburgite and originate as depleted residues of partial melting. The lower concentration of Fe^{3+} also supports this scenario.

The possibility that chrome-spinels from the Taltung Formation were derived from Alpine-type peridotite is also supported by a plot of Cr/(Cr+Al) with $Mg/(Mg+Fe^{2+})$ (Fig. 6.9). The low value of Cr# makes the grains fall in the Alpine-type peridotite field.

The plot of $Mg/(Mg+Fe^{3+})$ versus $Fe^{3+}/(Fe^{3+}+Al+Cr)$ (Fig. 6.10) also shows the Alpine-type peridotite as the possible source rock. However, the plots also overlap with

the field of stratiform complexes. Hence, derivation of these sediments from stratiform complex source terranes is also possible.

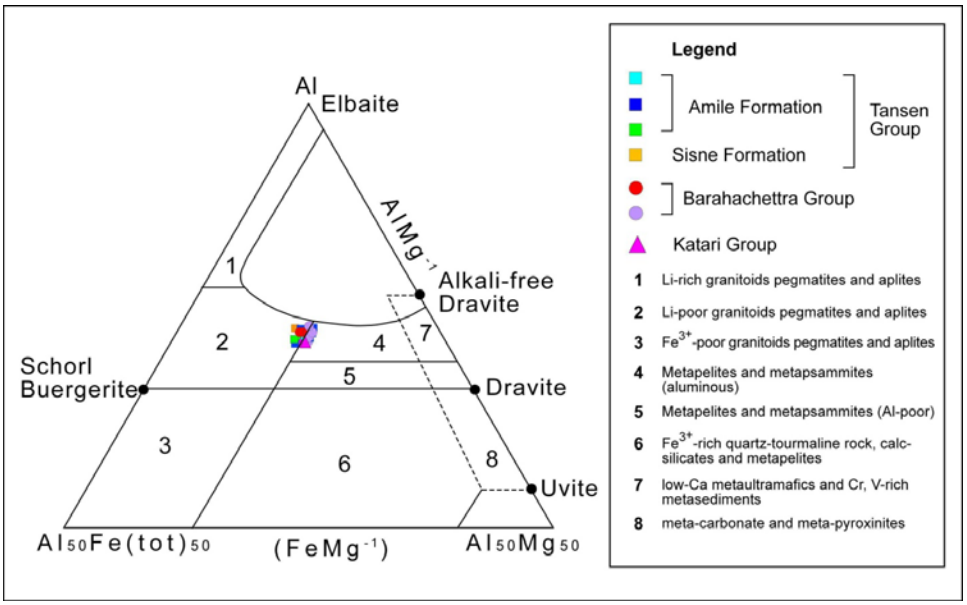

Figure 6.6 Al-Fe (tot)-Mg plot (in molecular proportion) for tourmalines from Gondwanan sequences of Nepal (Tansen Group, western Nepal; Barahachettra and Katari groups in eastern Nepal) plotted on Al-$Al_{50}Fe_{(tot)50}$-$Al_{50}Mg_{50}$ (adapted after Henry and Guidotti, 1985).

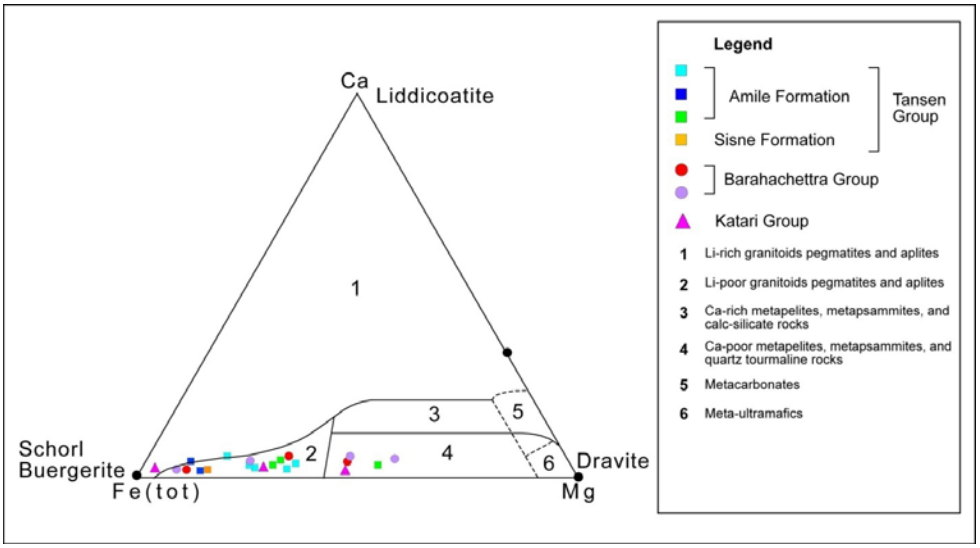

Figure 6.7 Ca-Fe(tot)-Mg plot (in molecular proportion) for tourmalines from Gondwanan sequences of Nepal (Tansen Group, western Nepal; Barahachettra and Katari groups in eastern Nepal) plotted on Ca-$Fe_{(tot)}$-Mg, (adapted after Henry and Guidotti, 1985).

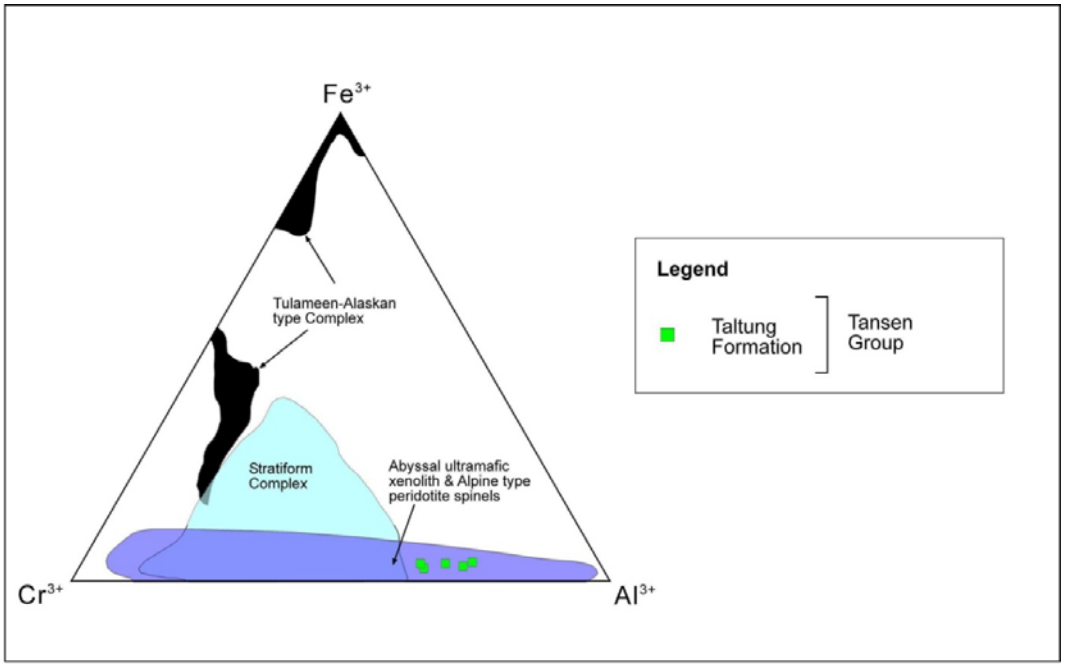

Figure 6.8 Ternary plot of major trivalent cations in chrome-spinels of the Taltung Formation of the Tansen Group (Gondwanan sequences) of the Nepal Himalaya with three major provenance fields (adapted after Nixon et al., 1990).

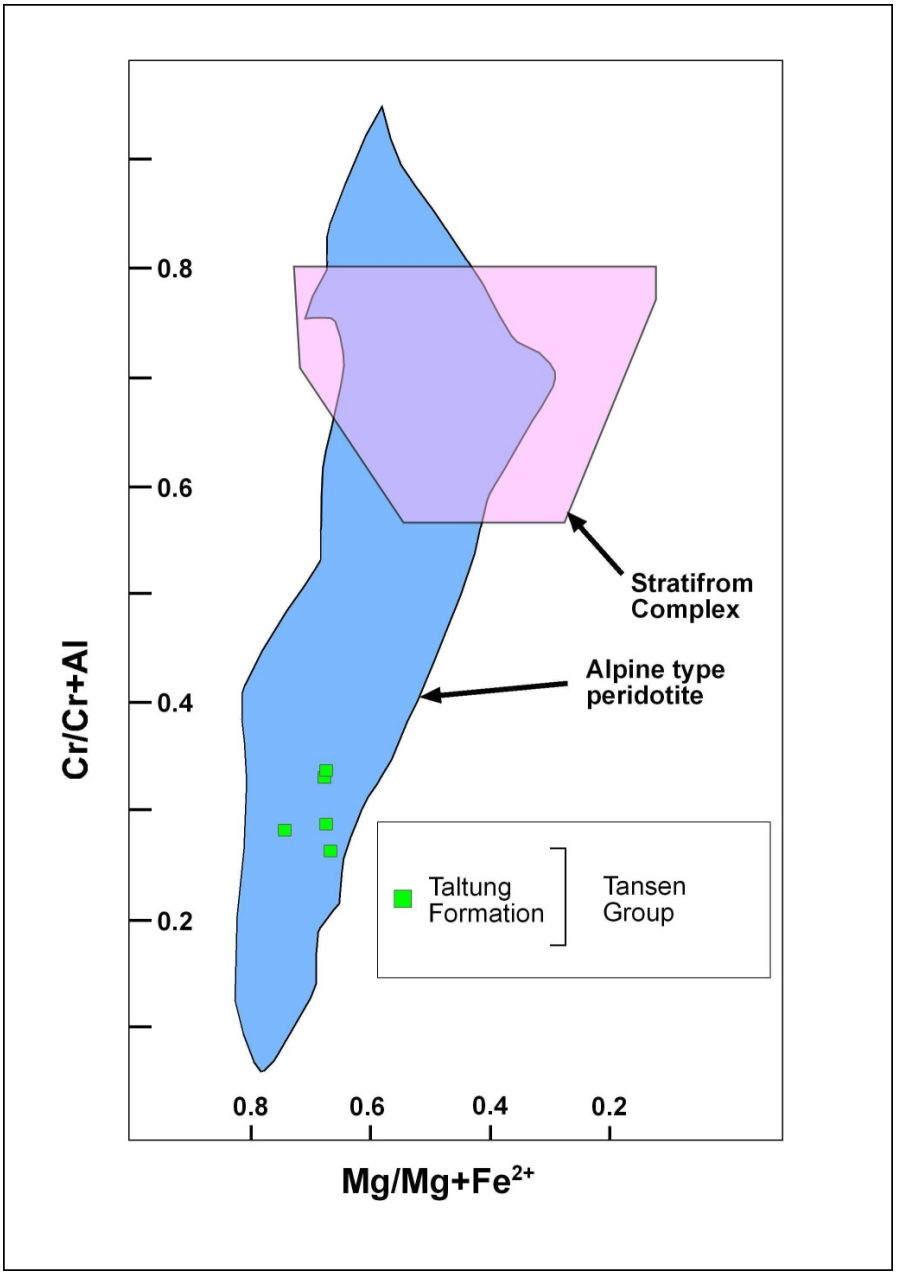

Figure 6.9 Plot of $Mg/(Mg+Fe^{2+})$ vs $Cr/(Cr+Al)$ for chrome-spinels of the Taltung Formation of the Tansen Group (Gondwanan sequences) of the Nepal Himalaya (adapted after Nixon et al., 1990).

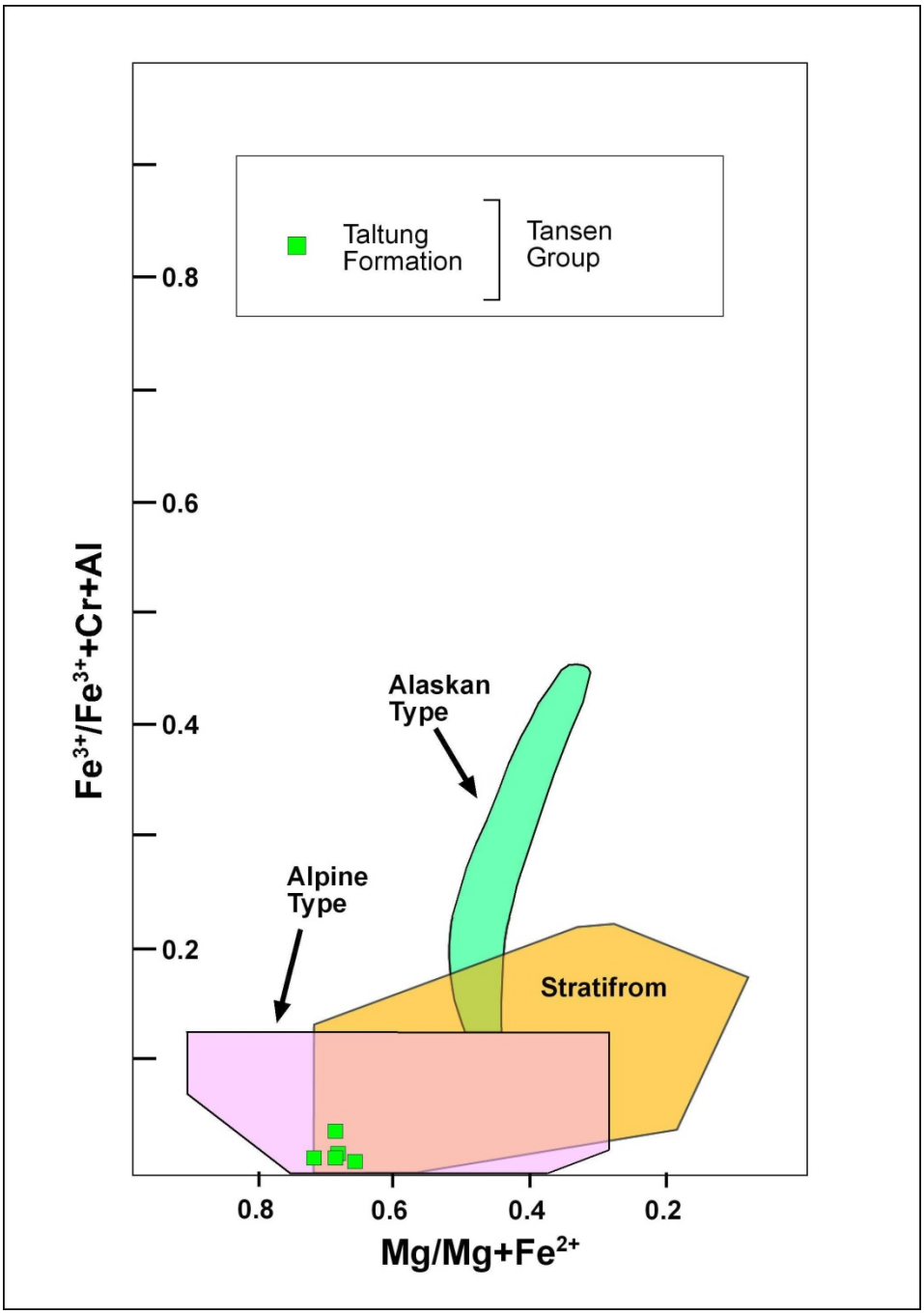

Figure 6.10 Plot of Mg/(Mg+Fe^{2+}) vs the ratio of trivalent cations Fe^{3+}/(Fe^{3+}+Cr+Al) for chrome-spinels of the Taltung Formation of the Tansen Group (Gondwanan sequences) of the Nepal Himalaya (adapted after Irvine, 1974). Note that all grains fall in the overlap between Alpine and stratifrom peridotite fields.

6.6 DISCUSSION

6.6.1 Garnets

Garnet composition of samples from different Gondwanan sequences in Nepal suggest different source terranes. The Katari Group, with low pyrope contents, belongs to the amphibolite regime, while the Taltung Formation, with low grossular and spessartine contents reflects low metamorphic grade (Figs 6.4 and 6.11). Most of the grains from the Barahachettra Group contain both grossular and pyrope (Fig. 6.3) but have low spessartine content. The most probable source of garnet could be the Bihar Mica Belt, the Ranchi Supracrustal Belt and the Munger Belt of Chotanagapur Gneissic Terrain. However, different igneous bodies, including the Malani Granite of the Delhi Supergroup and the Vindhyan System of peninsular India also could have supplied garnets to the Gondwanan basins of Nepal (Sakai, 1983).

6.6.2 Tourmaline

Microprobe data for tourmaline supports that the source rock for these tourmalines are Li-poor granitoids and aluminous meta-psammities and meta-pelites (Fig. 6.6). However, the plot of Ca, Fe(tot) and Mg, suggests different types of source rocks (Fig 6.7). The Amile Formation, which is basically rich in quartz arenite, shows a granitoid provenance, whereas other formations show a mixed provenance of granitioids and meta-psammites and meta-pelites. Hence, different granitic bodies of the Indian craton as well as pelites, from Vindhyan could have contributed tourmaline.

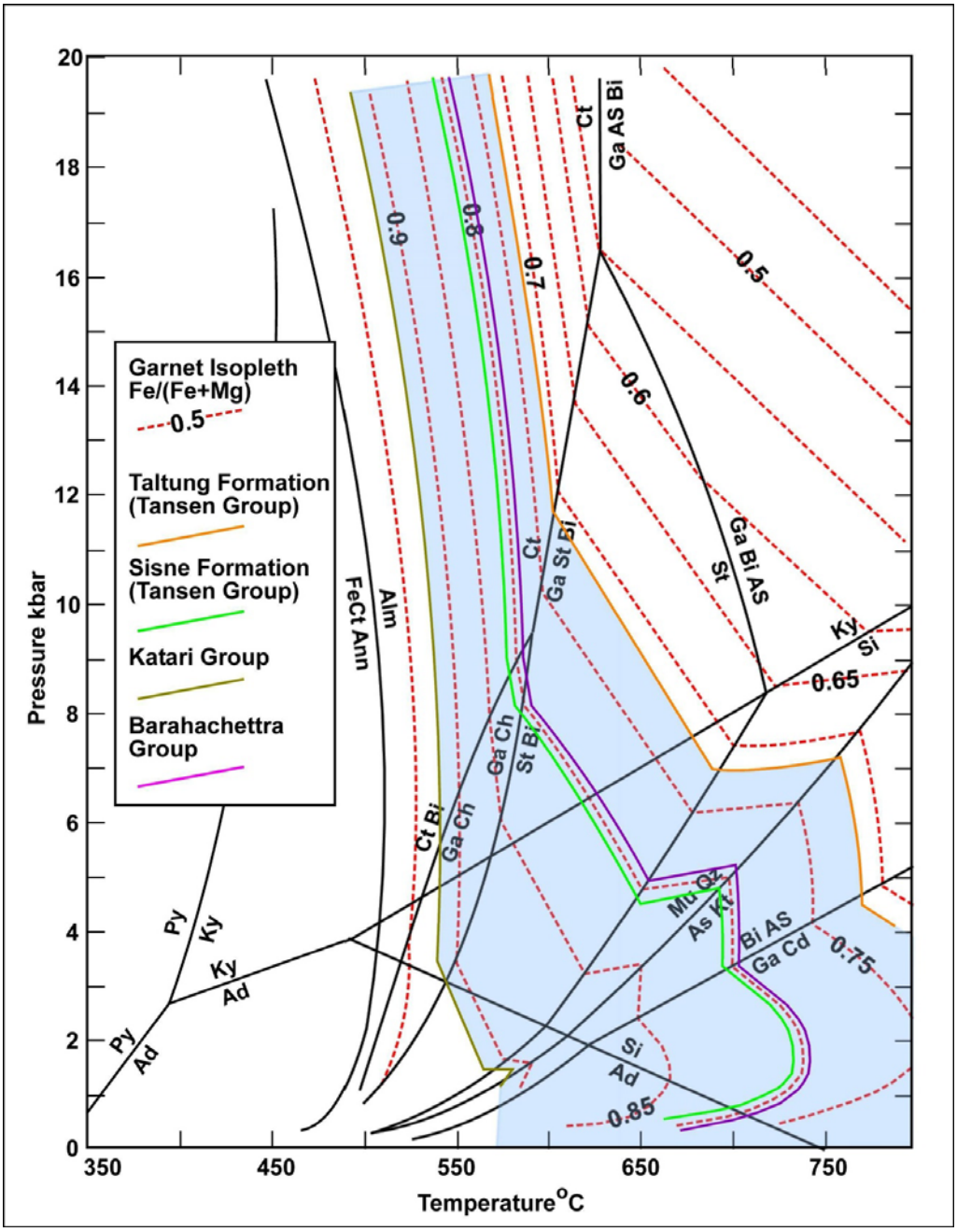

Figure 6.11 Petrographic grid for the KFMASH system contoured with isopleths of X_{Alm} in garnet (after Spear and Cheney, 1989). The isopleths are constructed assuming that garnet formed in equilibrium with biotite in a rock of pelitic bulk composition. The blue region shows the range of isopleth values for garnets from Gondwanan sequences of Nepal while solid color lines show the average of isopleth value for different rock units.

6.6.3 Chrome-spinel

The TiO_2% versus Cr# in chrome spinels shows that these grains were derived from mid-oceanic, island arc and alkaline basaltic sources (Fig. 6.11). However, as TiO_2 contents of these chrome-spinel grains are very low which is charecteristic of alkaline basalts, these chrome-spinel grains could have been contributed by the alkaline Aulis Basalt considered to be equivalent to the Rajmahal Traps (Sakai, 1983; Segev, 2002).

The Cr# value for the peridotites and basalts of mid-ocean ridges is less than 0.06 with Mg# between 0.55 -0. 85 (Dick and Bullen, 1984). This tectonic setting has been classified as Type I. Another type of tectonic setting that is also regarded as Type I setting is depleted marginal seafloor basalts which show slightly lower value for Mg# and narrower range of Cr# than mid-oceanic ridge basalts (MORB). The Cr# and Mg# of the Taltung Formation indicate mid oceanic ridge type basalts or peridotite as the source of chrome-spinels. The Cr# and Mg# for island arc basalts (Types III setting) are 0.6-0.9, and 0.4-0.69, respectively (Cookenboo et al., 1997). Ophiolites, which have compositions transitional between Type I and Type III are regarded as Type II settings (Dick and Bullen, 1984).

The high aluminium and high chromium contents of the Taltung Formation also suggest a mid-oceanic type of source rock.

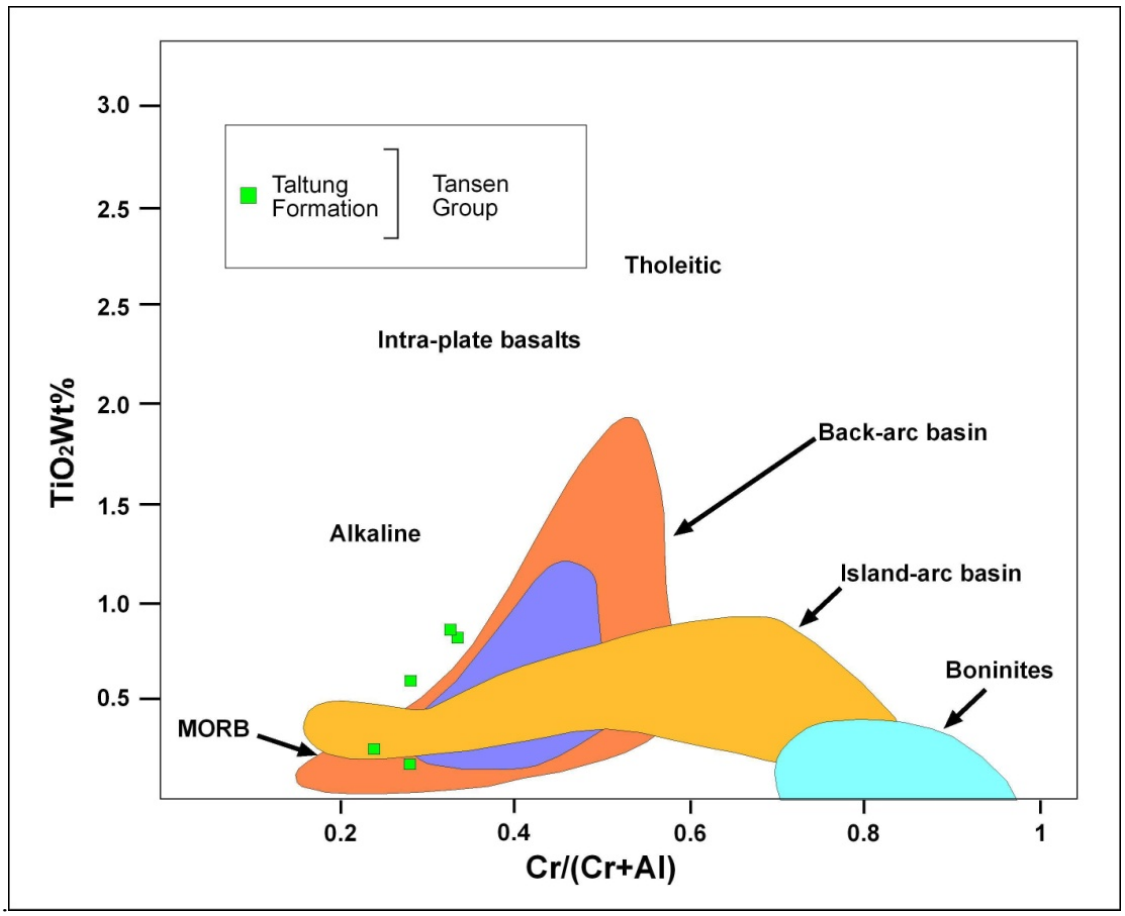

Figure 6.12 Plot of TiO_2 vs Cr# of Gondwanan sequences of Nepal (Tansen Group, western Nepal; Barahachettra and Katari groups in eastern Nepal) relative to spinels from various potential source rocks. MORB=Mid-oceanic ridge basalt (after Nanayama, 1992).

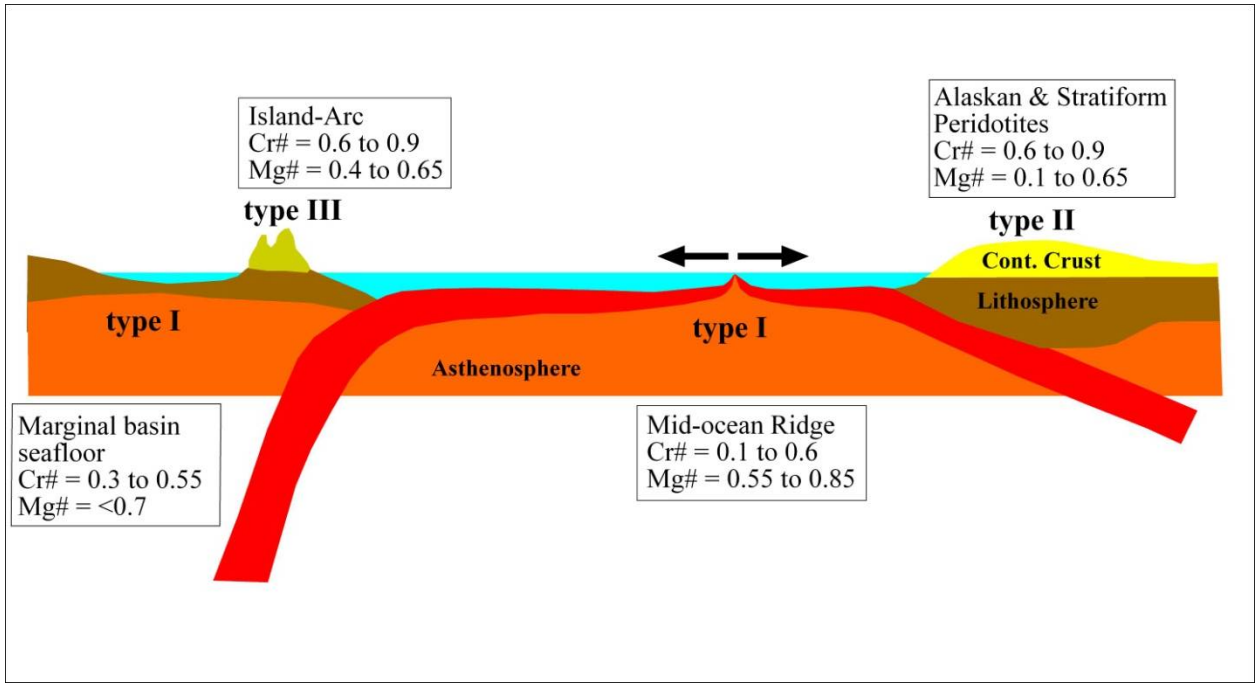

Figure 6.13 Schematic diagram showing spinel composition from different tectonic settings, including those of sea-floor and continental crust origins (modified from Cookenboo et al., 1997).

CHPATER 7: WHOLE ROCK CHEMISTY

7.1 INTRODUCTION

The whole rock chemistry of a sedimentary rock can provide an improved understanding of provenance of sediments and contemporaneous and subsequent sedimentary and weathering processes that impacted the sediments or the rock. Composition of sedimentary rock is primarily controlled by the composition of the source rocks and to some extent also by weathering and diagenetic processes (Dickinson, 1985; McLennan et al., 1993,).

It is necessary to understand the weathering process and climatic conditions during deposition of sedimentary rocks before making final interpretations on the source rock. The chemistry of sedimentary rocks is significantly influenced by weathering of the source rock and also post depositional diagenetic processes after the deposition of sediments (Nesbitt and Young, 1992). The 'Chemical Index of Alteration' (CIA) and ternary plot of Al_2O_3-(CaO+Na_2O)-K_2O are valuable tools to evaluate the degree of weathering and diagenetic processes. All chemical constituents present in a source rock do not behave in same way under a given weathering regime. When source rocks are exposed to weathering, they become depleted in oxides that are not resistant to weathering. Other more resistant oxides remain almost in the same amount that they were in parent rock. The proportions of some of the major oxides, such as SiO_2, Al_2O_3 and K_2O, have been found to be constant from source rock to the basin (Bhatia, 1983; Roser

and Korsch, 1988). Some trace elements (Zr, Th, Sc, Nb, Ga) and rare earth elements (REE) are generally remain constant from source rocks to the sediment because of their low solubility in water during weathering (McLennan et al. 1985; Bhatia and Crook, 1986). Relative concentration of resistant major oxides and trace elements present in sedimentary rocks are valuable indicators of source rocks.

One major limitation of using whole-rock chemistry alone is the inability to detect the mixing of different kinds of source rocks. Hence, chemical analyses should be supported by other methods of provenance study (e.g., traditional petrography, heavy mineral analysis, detrital geochronology, etc.). Representative sandstone samples have been subjected to whole-rock geochemical study to aid in the interpretation of paleotectonics and sediment provenance of Gondwanan sequences from Nepal.

7.2 METHODS

Nine representative sandstone samples were selected for the whole-rock geochemical analysis. The selected samples representing the Gondwanan sequence (Tansen Group) in the western part of Nepal include sample 16-1 from the Dumri Formation, sample 15-8 from the Bhainskati Formation, sample 15-5 from the Amile Formation, sample K-1 from the Taltung Formation, and sample 16-6 from the Sisne Formation. Samples from the eastern part of Nepal include samples 26-3 and 26-8 from the Katari Group, and sample 23-5 from the Tamrang Formation, and sample 22-9 from the Saptakoshi Formation of the Barahachhetra Group.

Selected samples were crushed in the rock-preparation lab of the Department of Geology and Geography, Auburn University. The size of the samples was further reduced with a mortar and pestle to the 200 mesh. Subsamples of ~10 gm from each sample were sent to ACME Laboratories Limited. Each sample was analyzed for 58 parameters including major oxides, minor elements, trace elements (rare earth and refractory elements), and precious and base metals. Major oxides, minor, rare earth and refractory elements were determined by 'Inductively Coupled Plasma' (ICP) mass spectrometry following lithium metaborate/tetraborate fusion and nitric acid digestion of 0.2-gm sub-samples. Precious and base metals were analyzed by ICP mass spectrometer after digesting separate 0.5-gm splits in Aqua Regia. Loss of ignition was calculated by weighing the difference after ignition at 1000^{o}C.

7.3 RESULTS

The results of geochemical analysis of 9 samples for 58 parameters including major oxides, minor elements, and trace elements are given in Table 7.1.

Table 7.1 Results of whole-rock chemical analysis of Gondwanan sandstones from Nepal

			S. No								
	Unit	MDL	16-1	15-8	15-5	K-1	16-6	23-5	22-9	26-3	26-8
SiO_2	%	0.01	70.09	85.01	89.79	35.4	70.19	70.98	76.99	95.8	85.19
Al_2O_3	%	0.01	8.09	5.64	4.38	14.48	10.37	8.52	5.03	2.14	5.61
Fe_2O_3	%	0.04	20.97	2.58	4.72	13.66	13.16	16.81	18.3	0.32	2.32
MgO	%	0.01	0.57	0.79	0.05	3.22	0.88	0.99	0.28	0.05	0.93
CaO	%	0.01	0.1	1.47	0.04	12.56	0.84	0.55	0.07	0.09	1.17
Na_2O	%	0.01	1.42	0.04	0.11	1.06	2.11	1.63	0.04	0.02	0.07
K_2O	%	0.01	1.53	1.36	0.08	2.1	2.82	2.07	0.73	0.03	1.21
TiO_2	%	0.01	0.69	0.47	0.35	2.38	0.33	0.21	0.51	0.08	0.41
P_2O_5	%	0.01	0.06	0.07	<0.01	0.77	0.08	0.07	0.03	0.01	0.07
MnO	%	0.01	0.13	0.04	0.02	0.44	0.1	0.09	0.07	<0.01	0.04
Cr_2O_3	%	0.002	0.008	0.003	0.006	0.118	0.007	0.007	0.01	0.002	0.004
Ni	PPM	20	57	<20	<20	282	30	29	42	<20	<20
Sc	PPM	1	6	5	4	27	8	4	5	1	5
LOI	%	-5.1	-3.9	2.4	0.4	13.3	-1.1	-2.1	-2.2	1.4	2.8
Ba	PPM	1	363	179	25	1352	604	357	148	358	247
Be	PPM	1	1	<1	<1	2	1	<1	1	<1	<1
Co	PPM	0.2	12	4.5	3	50.5	9.2	8.6	10.1	1.3	6.5
Cs	PPM	0.1	2.8	2.1	0.2	3.7	1.8	3.2	1.3	<0.1	1.8
Ga	PPM	0.5	10.8	6.6	6.7	16.3	12.1	10.1	8.5	3.2	7.7
Hf	PPM	0.1	11.4	9.3	3.5	8	7.2	5.7	6.9	0.7	7.2
Rb	PPM	0.1	69	55.4	3.3	74.8	96.9	76.9	36.7	1	45.1
Sn	PPM	1	6	3	2	4	4	4	5	<1	2
Sr	PPM	0.5	47.3	51.8	23.6	568	122.8	85.4	38.2	11.9	20.4
Ta	PPM	0.1	1.2	0.9	0.4	8	0.6	0.4	0.9	0.2	0.8
Th	PPM	0.2	18.9	13.2	3.7	27.4	6.5	4.5	10	2.1	12
U	PPM	0.1	3.2	2.2	1.6	5.1	1.2	1	2	0.8	2.4
V	PPM	8	35	28	43	217	43	26	30	14	28
W	PPM	0.5	2	1.5	<0.5	3.7	0.7	0.8	2.3	<0.5	1.5

Contd. (MDL = Minimum Detection Limit)

Table 7.1 Results of whole-rock chemical analysis of Gondwanan sandstones from Nepal

Contd.

			S. No								
	Unit	MDL	16-1	15-8	15-5	K-1	16-6	23-5	22-9	26-3	26-8
Zr	PPM	0.1	375.7	318.8	114.4	333.5	246.6	201.9	266	25.5	270.8
Y	PPM	0.1	36.6	25.2	6	28.7	19.1	13.7	14.8	3.1	20.3
La	PPM	0.1	48.8	40	20.4	142.4	22.3	14	33.6	7.3	30.7
Pr	PPM	0.02	12.25	9.61	3.68	26.33	5.2	3.53	8.4	1.98	7.54
Nd	PPM	0.3	46.2	35.8	11.4	90.2	19.4	13.6	30.1	7.3	27.1
Sm	PPM	0.05	8.45	6.26	1.78	12.09	3.24	2.48	4.85	1.29	5.17
Eu	PPM	0.02	1.4	1.03	0.3	3.18	0.82	0.7	0.86	0.28	0.89
Gd	PPM	0.05	7	5.19	1.32	9.02	2.94	2.32	3.59	1.01	4.38
Tb	PPM	0.01	1.08	0.76	0.19	1.12	0.52	0.39	0.49	0.17	0.66
Dy	PPM	0.05	6.27	4.38	1.12	5.76	3.15	2.33	2.6	0.71	3.84
Ho	PPM	0.02	1.21	0.86	0.2	1	0.67	0.46	0.51	0.14	0.72
Er	PPM	0.03	3.38	2.5	0.63	2.72	1.99	1.43	1.52	0.32	2.21
Tm	PPM	0.01	0.47	0.34	0.08	0.35	0.29	0.21	0.22	0.08	0.34
Yb	PPM	0.05	3.33	2.58	0.61	2.3	2.02	1.38	1.41	0.32	2.18
Lu	PPM	0.01	0.48	0.37	0.09	0.34	0.31	0.22	0.23	0.07	0.34
Mo	PPM	0.1	9.2	0.4	2.8	1.4	5.3	7.2	7.2	0.1	0.2
Cu	PPM	0.1	160.6	56.6	64.1	42.1	84.9	121.7	114.9	7	6.1
Pb	PPM	0.1	18.8	11.5	5.5	14.2	11.8	15	12.2	2.4	9.5
Zn	PPM	1	41	30	42	94	31	19	46	8	24
Ni	PPM	0.1	50.9	9.3	14.6	245.5	31.2	36.2	44.7	1.8	10.1
As	PPM	0.5	4	1.4	1.5	7.3	5	4.5	18.8	0.7	5
Cd	PPM	0.1	0.2	<0.1	<0.1	<0.1	<0.1	<0.1	<0.1	<0.1	0.1
Sb	PPM	0.1	0.9	0.2	0.3	0.3	0.6	0.9	1.2	0.1	0.2
Bi	PPM	0.1	0.3	0.1	<0.1	0.1	0.1	<0.1	0.3	<0.1	0.1
Ag	PPM	0.1	<0.1	<0.1	<0.1	<0.1	<0.1	<0.1	<0.1	<0.1	<0.1
Au	PPB	0.5	0.8	0.7	1	1.8	0.7	1	0.9	1.3	0.7
Hg	PPM	0.01	<0.01	<0.01	<0.01	0.03	<0.01	<0.01	0.03	<0.01	0.02
Tl	PPM	0.1	<0.1	<0.1	<0.1	<0.1	<0.1	<0.1	<0.1	<0.1	<0.1
Se	PPM	0.5	<0.5	<0.5	<0.5	<0.5	<0.5	<0.5	<0.5	<0.5	<0.5

(MDL = Minimum Detection Limit)

7.3.1 Major Elements

Major elements, which are generally measured in the form of oxides, are not generally considered as good source rock indicators. Some of the major oxides leach out during the weathering process. Additionally, diagenetic processes also contaminate and alter detrital grains. However, some of elements are immobile and remain in the sediment almost in the same amount as in the source rocks. Ratios of major oxides have been used as an indicator of provenance (Bock et al., 1998; Gotze, 1998, Rahman and Suzuki, 2007). Different discrimination functions have been developed by adding or subtracting the amount of major oxides that will be depleted or enriched in sediments during weathering to fabricate the proportions of major oxides similar to the parent rocks (Bhatia, 1983; Roser and Korsch, 1988). The effect of weathering and diagenetic processes on the concentration of major elements in sedimentary rocks has been clearly depicted in the chemical classification of the Gondwanan sandstones (Fig. 7.1).

The Amile sandstones, with its abundant well-rounded quartz grains are supposed to fall in the field of quartz arenite of figure 7.1. However, Al_2O_3 contents of the Amile sandstone are a little too high and the K_2O contents are somewhat too low to put this unit in the quartz arenite field. High iron oxide contents due to weathering, or presence of mica and other iron minerals made samples from the Dumri and Sisne formations, sample 23-5 from the Saptakoshi Formation, and sample 26-3 from the Katari Group to fall in the Fe-sandstone field.

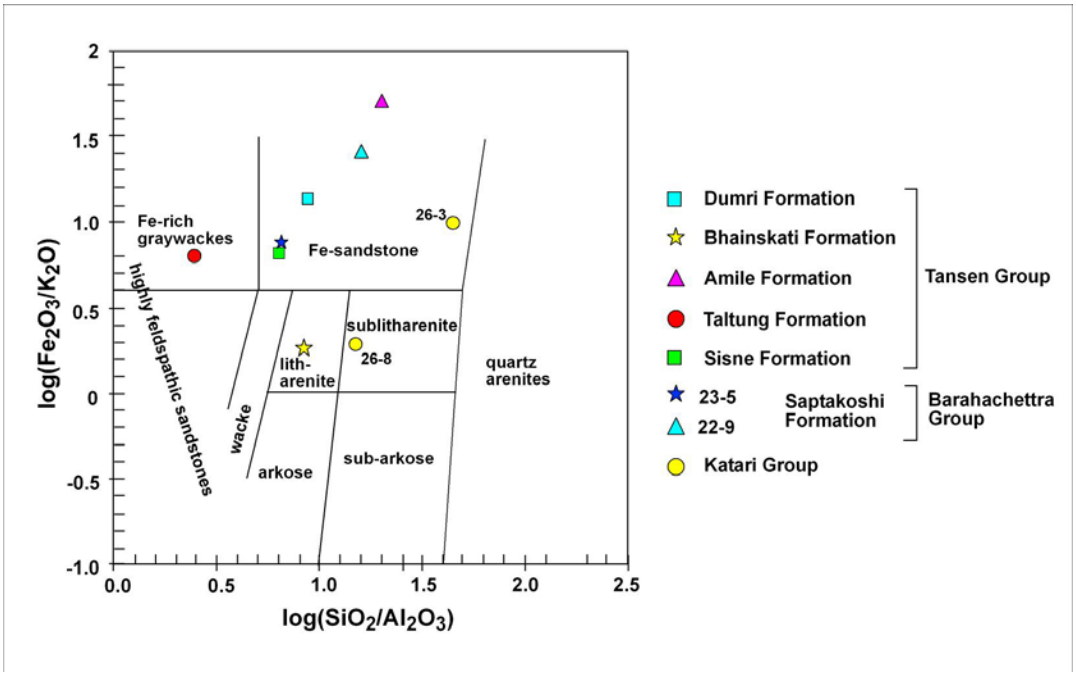

Figure 7.1 Chemical classification of Gondwanan sandstones of Nepal, classification fields are taken from Herron (1988).

Some major oxide ratios have been used to evaluate tectonic setting of source rocks. The Taltung sandstones (sample K-1) have $SiO_2/Al_2O_3 \leq 5$ (Table 7.2), which is typical for active margins. The remainder of the other samples, except for 26-3 from the Katari Group, has ratios between 5.2-28.2, which are typical for modern passive-margin settings (McLennan et al., 1990; Roser and Korsch, 1998). Sample 26-3 from the Katari Group has an anomalously high ratio of 44.

K_2O/Na_2O ratios for all samples, except those from the Amile sandstones, are higher than 1 which is expected for passive margin setting (McLennan et al., 1990). The lower values of Al_2O_3/TiO_2 in the Taltung sandstone reflect a mafic source rock signature (Sugitani et. al., 1996), while values for other samples indicate derivation from felsic terranes.

Table 7.2 Ratios of some major oxides of Gondwanan sandstones from Nepal.

	Rock Unit	Sample No	SiO_2/Al_2O_3	K_2O/Na_2O	Al_2O_3/TiO_2
Western Nepal	**Dumri Formation**	**16-1**	8.66	1.08	11.72
	Bhainskati Formation	**15-8**	15.07	34.00	12.00
	Amile Quartzite	**15-5**	20.50	0.73	12.51
	Taltung Formation	**K-1**	2.44	1.98	6.08
	Sisne Formation	**16-6**	6.77	1.34	31.42
Eastern Nepal	**Samptakoshi Formation**	**23-5**	8.33	1.27	40.57
	Saptakoshi Formation	**22-9**	15.31	18.25	9.86
	Katari Group	**26-3**	44.77	1.50	26.75
	Katari Group	**26-8**	15.19	17.29	13.68

Distribution of major elements in rock is usually related to the mineralogy of the rock. The distribution pattern of eight major element oxides in the Gondwanan sandstones of Nepal after normalizing the weight percentage of oxides with the values for Post-Archean Australian shales (PAAS) (Taylor and McLennan, 1985), is plotted in Figure 7.2. SiO_2 values in sandstone are expected to be little higher than for shale. Sample K-1 from the Taltung Formation, fall below the SiO_2 values of PAAS (62.4%). This sample contains higher amounts of Al_2O_3, Fe_2O_3, and CaO. CaO content could have elevated due to the presence of calcite cements in the rock. The SiO_2 and Al_2O_3 contents of the Bhainskati and Amile formations from the Tansen, the Saptakoshi Formation from the Barahachettra, and Katari group are typical of cratonic sandstones (SiO_2 ≥90%, Al_2O_3<5%), (Condie, 1993). With a slightly high aluminum content and a slightly low silica content, sample 23-5 from the Saptakoshi Formation, and samples from the Sisne and the Dumri sandstones fall between the graywacke and cratonic sandstones fields (Condie, 1993). With very low SiO_2 content and high Al_2O_3 content, the Taltung

sandstone falls in the oceanic island arc tectonic field (Bhatia, 1983). Usually, sandstones are more depleted in K_2O, Fe_2O, and TiO_2 than shales. The excessive iron oxide in the Dumri, Sisne, and Saptakoshi formations is related to daigenesis. However, the Taltung Formation not only contains high amount s of iron oxide, but also contains a range of Al_2O_3, Fe_2O_3 and TiO_2 values that are consistent with derivation from oceanic island arc settings. Na_2O content is higher in the Sisne sandstones in comparison to other units.

The Harker Variation diagram (Fig. 7.3) shows no correlation between SiO_2 and other oxides except for Al_2O_3. A negative correlation between SiO_2 with Al_2O_3 is due to sequestration of most of silica in quartz (Osman, 1996). The percentages of particular oxides in different samples do not change in accordance with SiO_2 percentage, indicating various source terranes for different Gondwanan sequences. Moreover, the Taltung sandstones show major shifts in composition from other analyzed samples, suggesting a significant difference in source rocks.

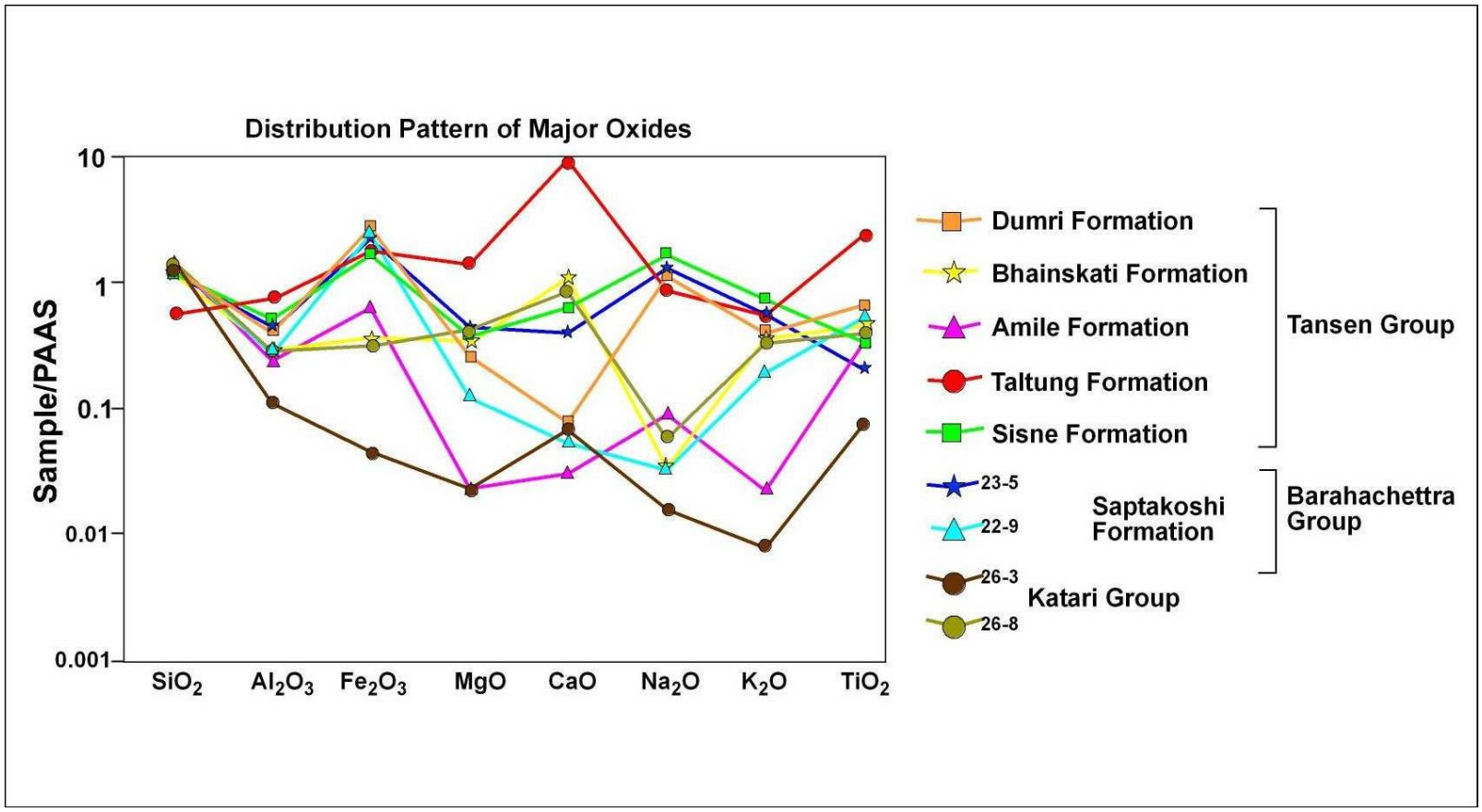

Figure 7.2 Distribution pattern of major element oxides in Gondwanan sandstone of Nepal. Data are normalized to Post Archean Australian Shale (PAAS) (Taylor and McLennan, 1995).

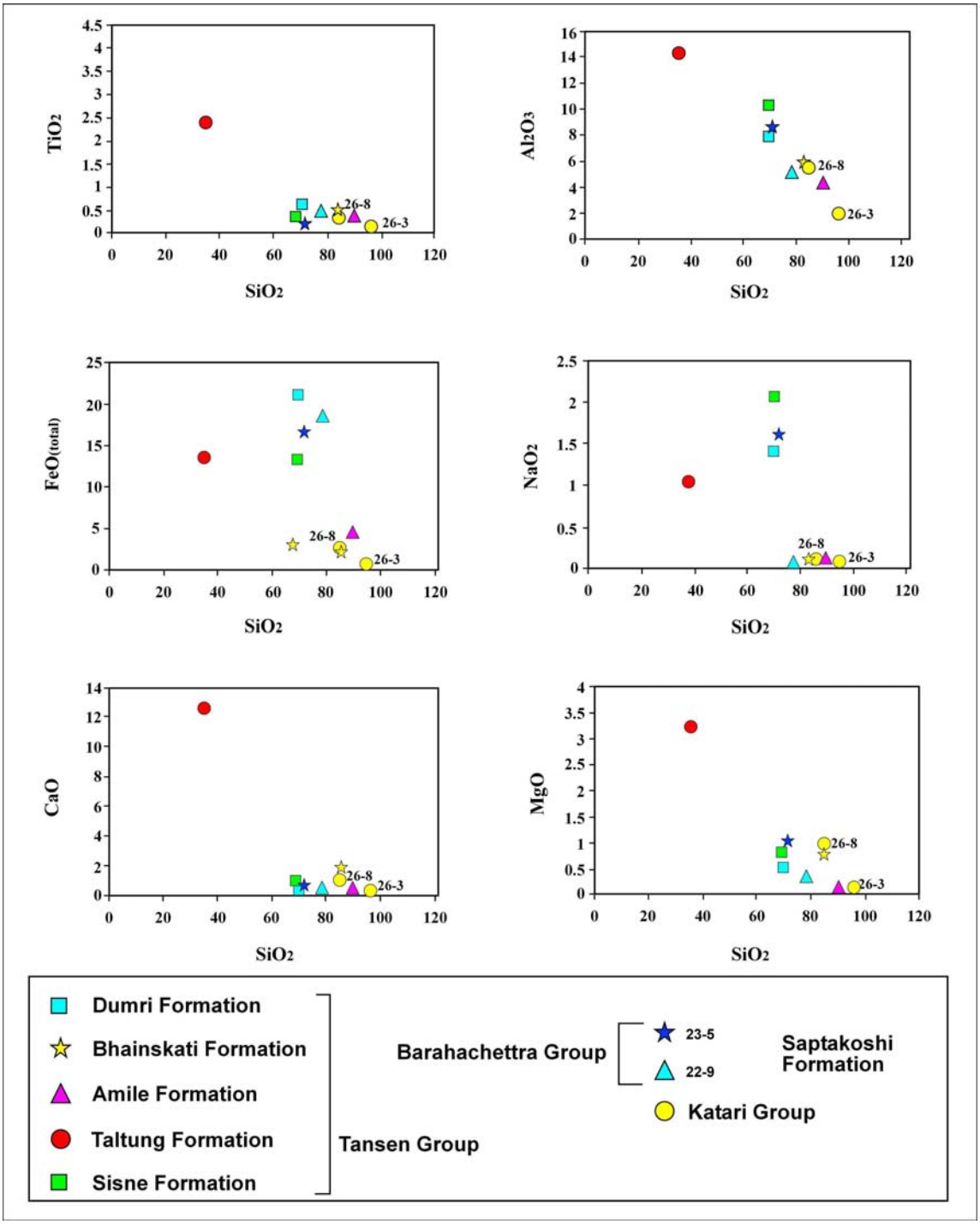

Figure 7.3 Distribution patterns of major element oxides in Gondwanan sandstone of Nepal.

7.3.2 Source Area Weathering and Diagenesis

The composition of sedimentary rocks can vary significantly based on the influence of the weathering through the whole sedimentary process starting with initial disintegration of the source rock to deposition in basin followed by diagenesis. The effect of weathering processes on sedimentary rocks can be measured quantitatively in terms of the molecular percentage of four major oxides (Nesbitt and Young, 1982). These percentages allow the determination of the chemical index of alteration (CIA), which is calculated as

$$CIA = 100 \text{ X } Al_2O_3/ (Al_2O_3+CaO^*+K_2O+Na_2O),$$

where CaO* is the amount of CaO in silicate minerals only. If CaO weight percent for an analysis appears greater than Na_2O weight percent then CaO* is fixed by taking value equal to Na_2O. A CIA value of 50 is considered for the fresh rocks whereas 100 is the value for extremely weathered rock which includes weathering of both the source rock and sedimentary deposit. In comparison to mudstones, sandstones generally show lower values for CIA (McLennan et al., 1990). CIA plots of the Gondwanan sandstones of Nepal show significant variations in CIA values (Fig. 7.4). Generally, the Amile Formation of the Tansen Group, the Saptakoshi Formation of Barahachettra Group, and the Katari Group (sample 26-3) show high values of CIA, which is consistent with their quartzose compositions. The ternary plot of Al_2O_3-($CaO+Na_2O$) + K_2O (Fig. 7.5) shows that most of the Gondwanan sandstone samples are following usual weathering trends. The sample from the Amile Formation and sample 26-3 from the Katari Group fall very close to Al_2O_3 corner, affirming the highest degree of weathering. The slight offset of the

Taltung Formation samples towards CaO-Na_2O can be attributed to contribution by of volcanic rock fragments.

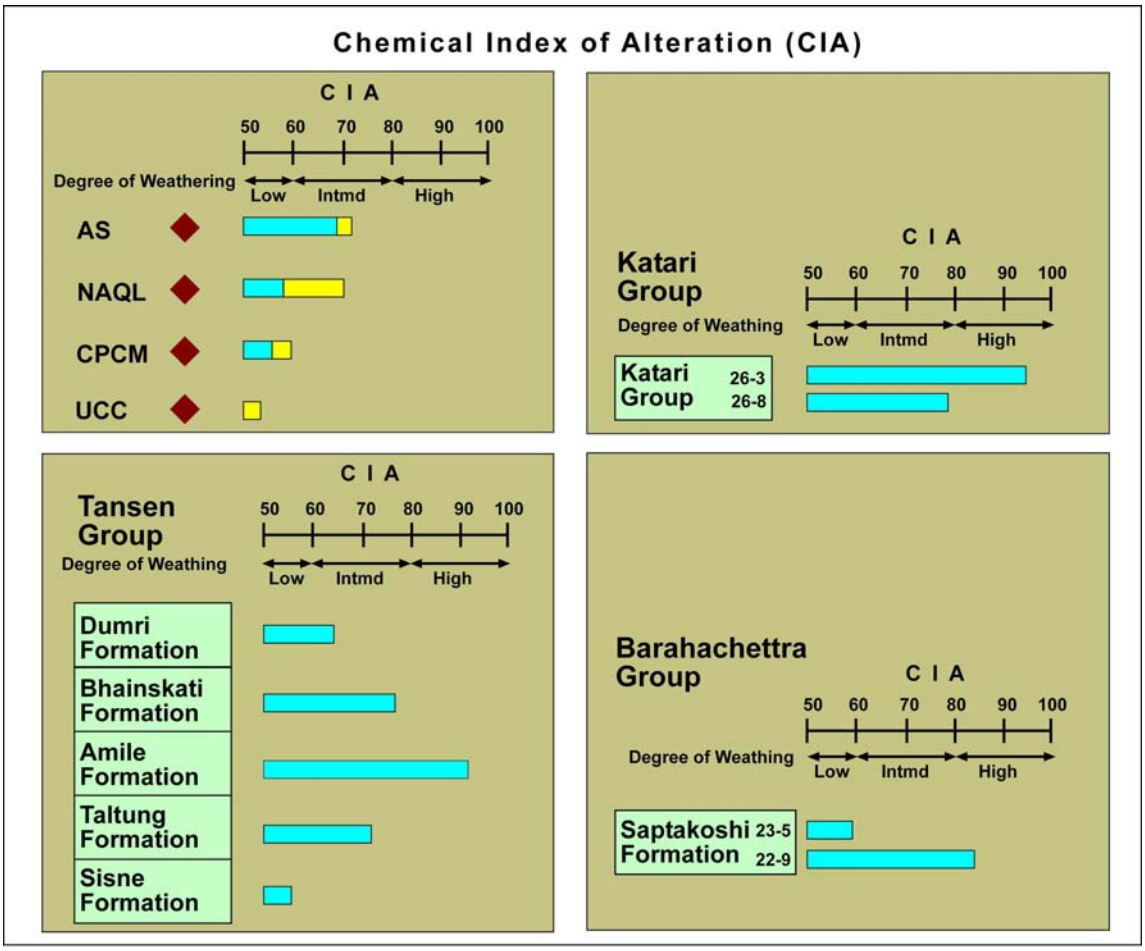

Figure 7.4 CIA values for the Gondwanan sandstones of Nepal. The reference values are given from average shale (AS), North America Quaternary loess (NAQL), Colorado Plateau crustal model (CPCM), and upper continental crust (UCC) (after Soreghan and Soreghan, 2007) where green bars represent the CIA value and yellow bars represent the ranges of maximum CIA values.

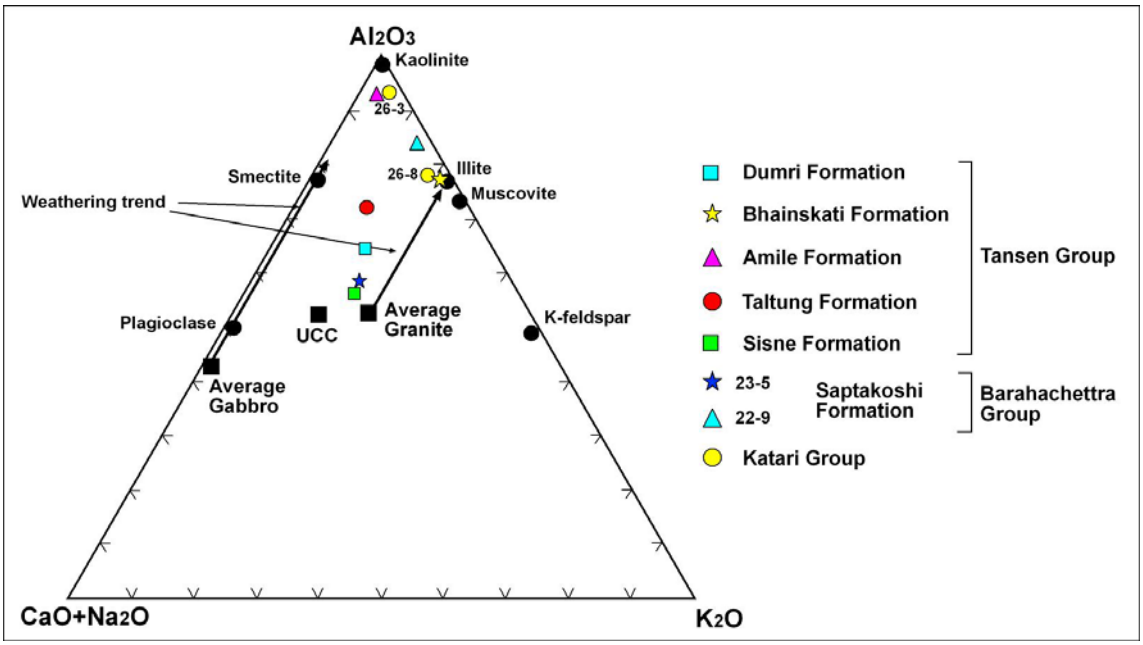

Figure 7.5 CIA plot of Gondwanan sandstones of Nepal (modified from Nesbit and Young, 1984, 1989; and Soreghan and Soreghan, 2007). The average composition of upper continental crust (UCC) is taken from Taylor and McLennan (1985)

7.4.4 Trace Elements

Trace element concentrations in sediments result from the competing influence of provenance, weathering, diagenesis, sediment sorting, and the aqueous geochemistry of the individual elements (Rollinson, 1993). The highest concentration of trace elements is found in clay-rich sediments rather than sand-sized sediments. However, several studies have been carried out on trace elements present in sand-sized sediments (Willan, 2003; Osae et al., 2006; Rahman and Suzuki, 2007).

Trace elements usually enter silicate structures replacing the major elements during fractional crystallization (Krauskopf and Bird, 1995). Large ion lithophile elements (LILE) like Rb, Cs, Ba, and Sr, usually replace K due to similarities in their ionic radii and are concentrated in rock in the late stages of crystallization. Transition trace elements (TTE), like Ni, Cr, Mn, V, and Ti, substitute for Fe and Mg during early stages of crystallization. High field strength elements (HFSE) including, Zr, Nb, Hf and Y, are partitioned into melts during crystallization and anatexis. Hence, they usually enter into felsic rocks rather than mafic rocks. Generally, compatible elements (TTE) are enriched in mafic rocks while incompatible elements (LILE, HFSE) are enriched in felsic rocks. Moreover, trace elements and rare earth elements (REE) remain essentially constant in abundance during weathering because of their low solubility in aqueous solutions at surface conditions (Taylor and McLennan, 1985).

The ratios of some trace elements in sedimentary samples have proven useful in tracing sediment provenance.

Table 7.3 Ratios of some trace elements in Gondwanan sandstones of Nepal. Reference values are taken from (a) Cullers et al. (1988) for ranges in sediments from felsic and mafic sources, and (b) McLennan (1981) for upper continental crust

Sample No	Eu/Eu*	La/Sc	Th/Sc	La/Co	Th/Co	Cr/Th
Western Nepal						
16-1 (Dumri Fm)	0.56	8.13	3.15	4.07	1.58	2.90
15-8 (Bhainskati Fm)	0.55	8.00	2.64	8.89	2.93	1.56
15-5 (Amile Fm)	0.60	5.10	0.93	6.80	1.23	11.10
K-1 (Taltung Fm)	0.93	5.27	1.01	2.82	0.54	29.48
16-6 (Sisne Fm)	0.81	2.79	0.81	2.42	0.71	7.37
Eastern Nepal						
23-5 (Saptakoshi Fm)	0.89	3.50	1.13	1.63	0.52	10.65
22-9 (Saptakoshi Fm)	0.63	6.72	2.00	3.33	0.99	6.84
26-3 (Katari Gp)	0.75	7.30	2.10	5.62	1.62	6.52
26-8 (Katari Gp)	0.57	6.14	2.40	4.72	1.85	2.28
Ranges in sediments from felsic sources (a)	0.40-0.94	2.50-16.3	0.84-20.5	1.80-13.8	0.04-3.25	4.00-15.00
Ranges in sediments from mafic sources (a)	0.71-0.95	0.43-0.86	0.05-0.22	0.14-0.38	0.04-1.40	25-100
Upper Continental Crust (b)	0.63	2.21	0.79	1.76	0.63	0.76

Most of the trace element ratios of trace elements support that all Gondwanan sandstones are supplied from mixed sources of felsic and mafic igneous rocks (Table 7.3). The Eu/Eu* ratio shows possible mafic source rock for the Taltung sandstone. La/Sc values for all samples support the supply from felsic igneous rocks. Th and Sc being incompatible and compatible respectively are used widely in provenance studies. The calculated ratio supports a mafic igneous source only for the Sisne Formation. La/Co ratios show that all the Gondwanan sandstones received sediment from felsic igneous sources, while Th/Co ratio indicates the possibility of mafic igneous source for the

Taltung and Sisne formations. Cr/Th ratio strongly supports a mafic source for the Taltung sandstone. The calculated Zr/Nb value of 1.95 indicates possible derivation from alkali-olivine basalt (Rollinson, 1993).

The distribution pattern (Fig. 7.6) of trace elements of the Gondwanan sandstones shows enrichment of some elements and depletion of others. The high value of Sr in the samples form the Taltung Formation correlates with Eu distribution (Fig. 7.7), which is probably due to high concentration of plagioclase. Also high Zr and Hf can be related with zircon content of this sample. Another major departure in the distribution pattern of trace elements is the high contents of Sr in many of samples. This also supports an alkaline source rock where Sr can replace K. The copper content of the Taltung sandstone is notably lower than other samples.

The distribution pattern of rare earth elements (REE), (Fig. 7.7) shows that sample K-1 from the Taltung Formation has high LREE (Light REE, La-Sm) than HREE (Heavy REE, Gd-Y). However, Eu value is significantly high in this sample. Generally, initial partial melting of mantle generates magma enriched in LREE (incompatible) and depleted in HREE (relatively compatible) (Rollinson, 1993). However, Eu is usually incorporated in Ca-plagioclase. Very high value of Eu and also LREE in any particular type of source rock is unusual and suggests for the mixing of source rocks or enrichment of plagioclase by sedimentary sorting (Nance and Taylor, 1977). In comparison to Archean basalts, post-Archean basalts are enriched in LREE (Condie, 1993). Hence, the REE pattern of the Taltung Formation can be explained by a post-Archean basalt source rock and sedimentary enrichment of plagioclase. Sample 26-3 from the Katari Formation

and the sample from the Amile Formation show relatively lower values of REE than PAAS which is expected for quartz-rich sandstones (McLennan, 1989). The Amile Formation is comparatively enriched LREE. Several samples, including samples from the Dumri, Bhainskati, Sisne, Saptakoshi formations and sample 26-8 from the Katari Group, show patterns similar to PAAS, although a few of them have slightly little lower values. This is typical for a provenance consisting of recycled sedimentary debris and/or older plutionic/metamorphic material with a relatively small volcanic component (Potter, 1978)

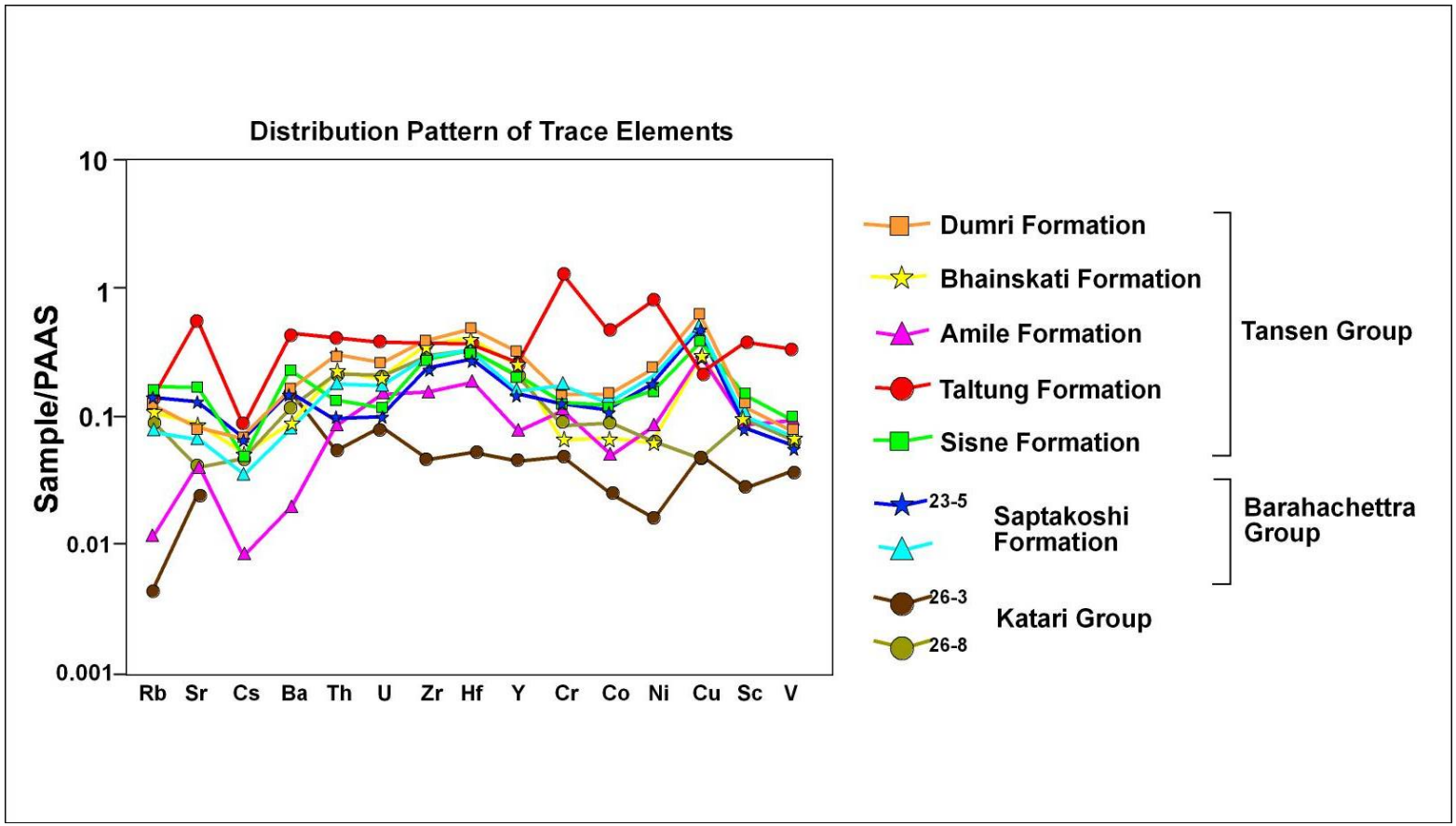

Figure 7.6 Distribution patterns of trace elements in Gondwanan sandstone of Nepal. Data are normalized to Post Archean Australian Shale (PAAS) (Taylor and McLennan, 1995).

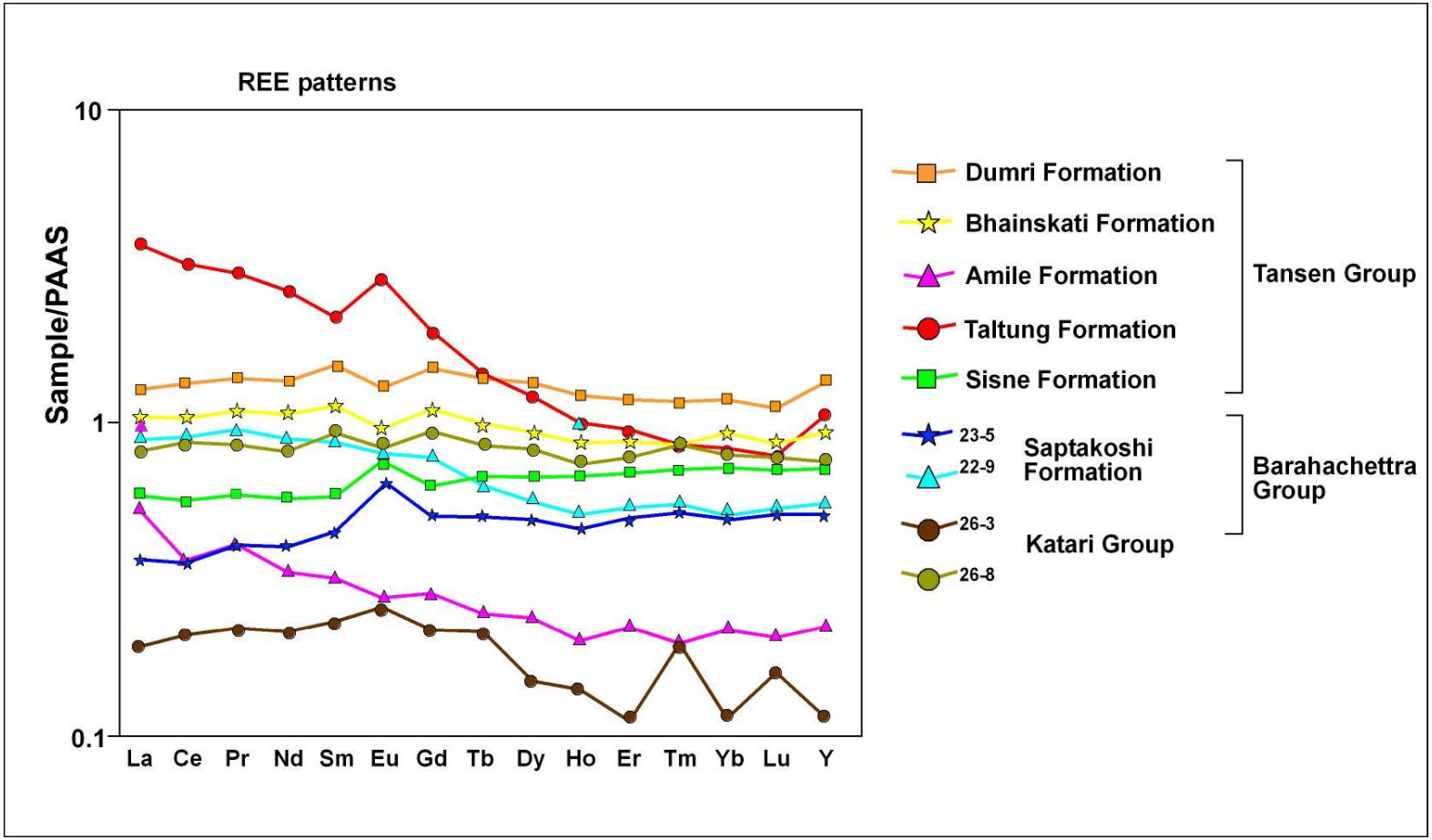

Figure 7.7 Distribution patterns of rare earth elements (REE) in Gondwanan sandstone of Nepal. Data are normalized to Post Archean Australian Shale (PAAS) (Taylor and McLennan, 1995).

The relationships among some major oxides and trace elements also have been used to trace source-rock types and tectonic setting. The immobile oxide TiO_2 and immobile trace element Zr have been used to infer the type of igneous source rock (Hayashi et al. 1997). The TiO_2-Zr plot (Fig. 7.8) shows that, except for the sample from the Taltung Formation, all units are derived from felsic igneous source rocks. Data for the Taltung Formation suggests derivation from an intermediate source rock.

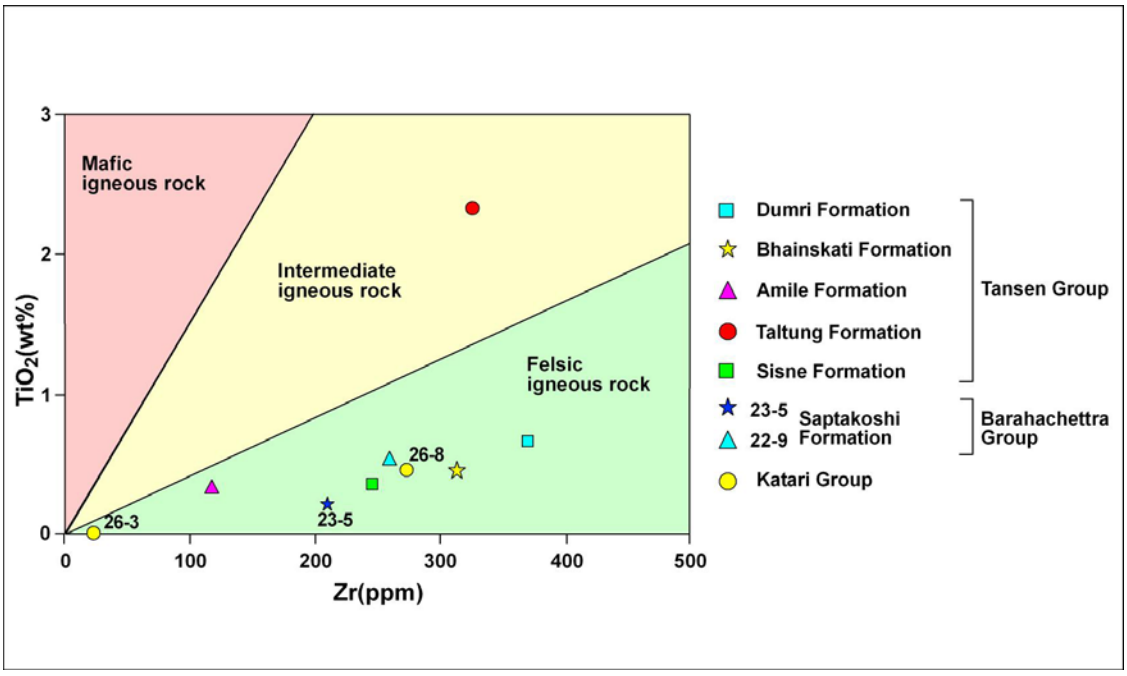

Figure 7.8 Plot of TiO_2 vs Zr content of the Gondwanan sandstones of Nepal. Fields for source rocks are drawn from Hayashi et al. (1997).

7.4.5 Tectonic Setting and Source Rocks

The K_2O/Na_2O-SiO_2 discrimination diagram of Roser and Korsh (1986) is plotted in figure 7.9. The plot suggests that Dumri sandstone of the Tansen Group fall in active margin setting. The sample K-1 of the Taltung Formation falls in the volcanic arc setting (Fig. 7.9). All other samples including Eocene Bhainskati sandstone fall in passive margin setting.

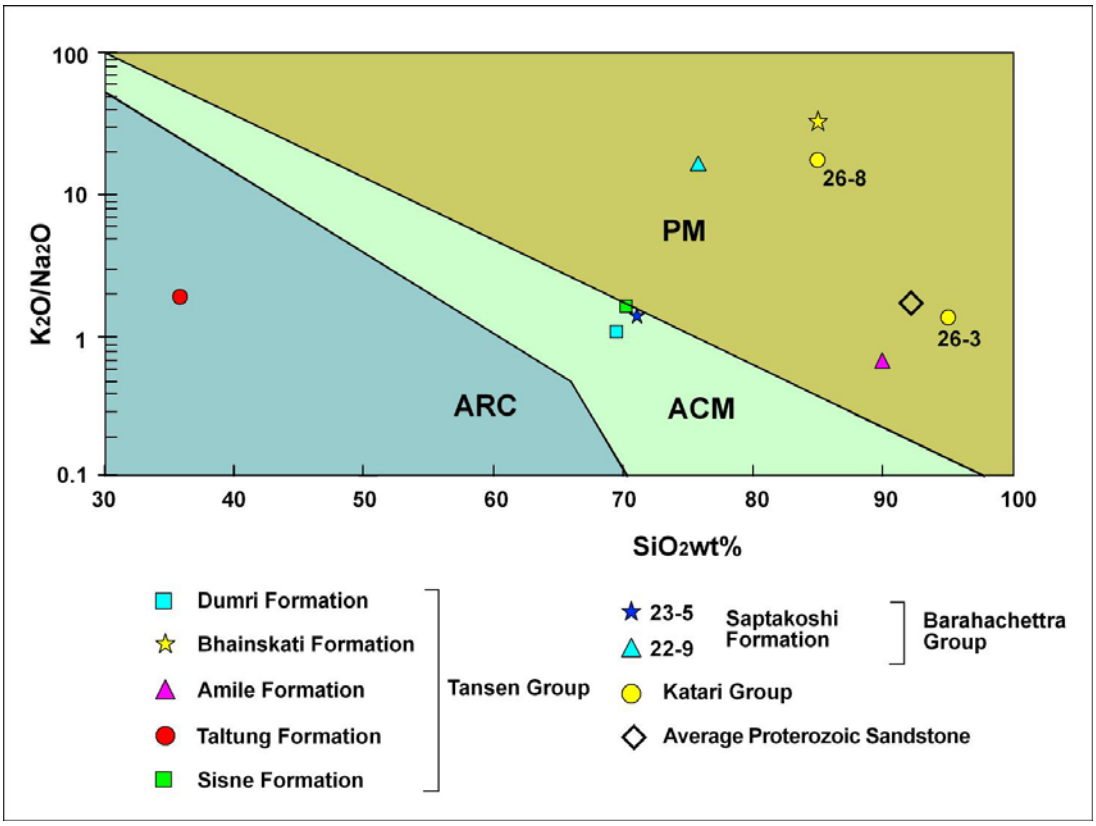

Figure 7.9 Tectonic discrimination diagram for Gondwanan sandstones of Nepal. Tectonic fields are from Roser and Korsh (1986). Tectonic setting: ARC = Volcanic Arc; ACM = Active Continental Margin; PM = Passive Margin.

The trace element plot of La-Th-Sc (Fig. 7-10, adopted from Bhatia and Crook, 1986) also shows that most of the samples fall in the passive and active continental margin fields. However, the Taltung Formation samples fall in the continental island arc field, and the Sisne Formation samples unexpectedly falls into continental island arc field.

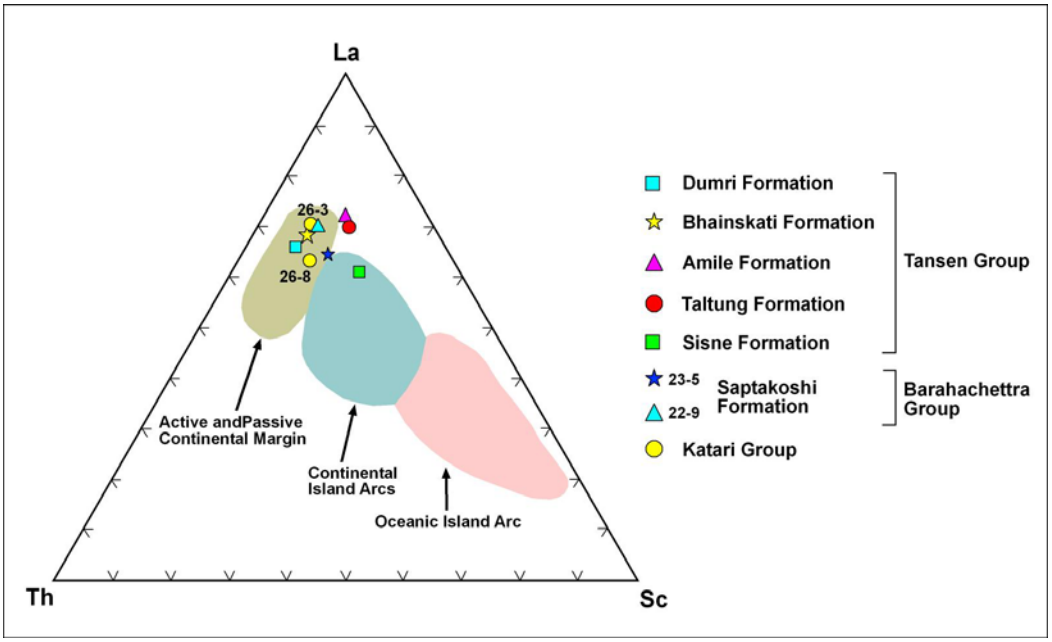

Figure 7.10 Plot of elemental percentage of La-Th-Sc of Gondwanan sandstones of Nepal. Fields of tectonic setting are drawn from Bhatia and Crook (1986).

CHAPTER 8

$^{40}Ar/^{39}Ar$ DETRITAL MUSCOVITE DATING

8.1 INTRODUCTION

Argon is a naturally occurring noble gas occupying 0.94% of the total atmospheric volume of the earth. The main isotopes of argon found in the earth are ^{40}Ar (99.6%), ^{36}Ar (0.34%), and ^{38}Ar (0.06%). Naturally occurring ^{40}K, with a half-life of 1.25×10^9 years, decays to stable ^{40}Ar (11.2%) by electron capture and positron emission, and also to stable ^{40}Ca (88.8%) via beta decay (Scherer, 2007). As ^{40}K in rock decays into ^{40}Ar through the time, the ratio of ^{40}Ar to its other isotopes will increase. The $^{40}Ar/^{36}Ar$ in the atmospheric air is 295.5, which is taken as reference to compare with $^{40}Ar/^{36}Ar$ in rock (McDougall and Harrison, 1999). ^{38}Ar forms by the radioactive decay of ^{38}Cl, ^{37}Ar formed from ^{40}Ca, and ^{36}Ar forms by the radioactive decay of ^{40}Ca (Dickin, 1995) (Fig. 8.1).

The $^{40}K/^{40}Ar$ method of dating is based on the decay of ^{40}K to ^{40}Ar with a half life of 1.25 Ga (McDougall and Harrison, 1999). This method was first applied by Wanke and Konig (1959). The $^{40}K/^{40}Ar$ dating method and the $^{40}Ar/^{39}Ar$ method differ. In $^{40}K/^{40}Ar$ method, K is determined by independent analysis, while in the $^{40}Ar/^{39}Ar$ dating method, ^{40}Ar and ^{39}Ar, produced by neutron irradiation of sample, are measured

simultaneously. The abundance of ^{39}Ar in the irradiated sample is a measure of the K content of that sample. The nuclear reaction that takes place during the irradiation is

$$^{39}_{19}\text{K (n, p) } ^{39}_{18}\text{Ar}$$

where n denotes neutron capture and p proton emission (Faure, 1986).

In addition to ^{39}Ar several other beneficial and undesirable isotopes are produced during irradiation in nuclear reactors. The effects of these interference reactions are corrected by using laboratory salt and glasses (Scherer, 2007). Table 8.1 shows the isotopes produced during the irradiation process.

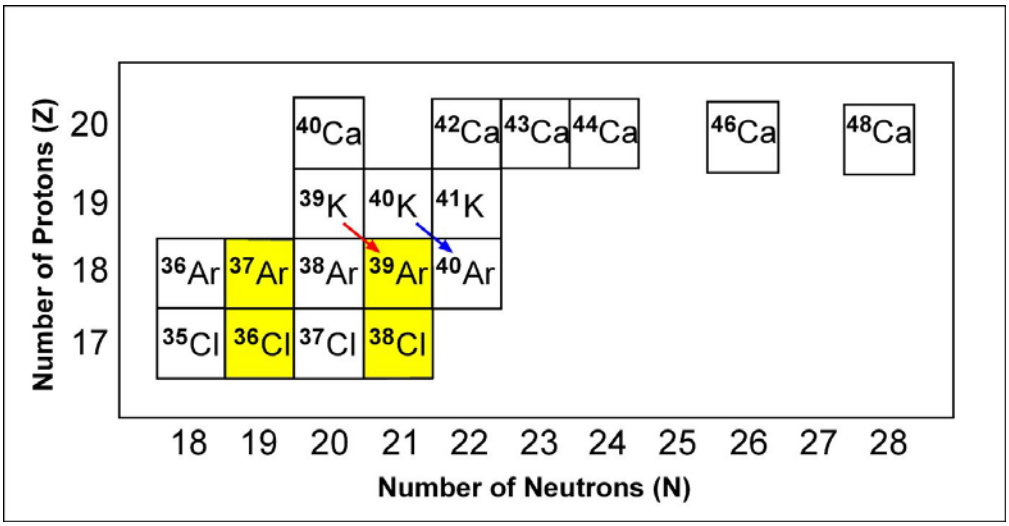

Figure 8.1 Some stable and radioactive isotopes related to $^{40}Ar/^{39}Ar$ dating method. The isotopes in yellow box are unstable isotopes. The blue arrow shows the natural decay reaction of $^{40}K \rightarrow ^{40}Ar$. The red arrow shows the $^{39}K\ (n,p)^{39}Ar_K$ reaction during irradiation.

Table 8.1 Isotopes produced during the irradiation process of muscovite.

Argon Produced	Calcium	Potassium	Argon	Chlorine
^{36}Ar	^{40}Ca			
^{37}Ar	^{40}Ca	^{39}K	^{36}Ar	
^{38}Ar	^{42}Ca	^{39}K ^{40}K	^{40}Ar	^{37}Cl
^{39}Ar	^{42}Ca ^{43}Ca	^{39}K ^{40}K	^{38}Ar ^{40}Ar	
^{40}Ar	^{43}Ca ^{44}Ca	^{40}K ^{41}K		

Beneficial reactions		Insignificant reactions		Undesirable reactions	

The age equation for $^{40}Ar/^{39}Ar$ dating (e.g., McDougall and Harrison, 1999) is as follows:

$$t = (1/\lambda)\ln(^{40}Ar^*/^{39}Ar_K(J)+1),$$

where λ is the decay constant for $^{40}K \rightarrow ^{40}Ar$, which is 5.543×10^{-10}/year. $^{40}Ar^*$ is the ^{40}Ar formed due to radioactive decay in the phase of interest. $^{39}Ar_K$ is the ^{39}Ar formed artificially by bombardment with fast, high-energy neutrons in a nuclear reactor during the irradiation process (Merrihue and Turner, 1966; McDougall and Harrison, 1999) and is used as a proxy for measurement of the parent potassium. The parameter J reflects the neutron flux (fluence) in the reactor and is determined from a standard sample (monitor) with a known age that is irradiated at the same time as the sample of interest (Scherer, 2007).

The $^{40}Ar/^{39}Ar$ method is equally applicable for igneous, metamorphic, and sedimentary systems. However, for intrusive igneous rocks, the $^{40}Ar/^{39}Ar$ method does

not provide the date of intrusion; rather, it will provide the age when the K-bearing mineral cooled through its closing temperature. The closing temperature varies among minerals. For example, it is approximately 300^{o}C for biotite, 400^{o}C for muscovite and 550^{o}C for hornblende. An igneous rock containing all three of these minerals will have three different ages for three separate cooling temperatures and will not give the true age of intrusion. However, it is helpful to know the thermal history of the rock. In the case of metamorphic rocks, minerals crystallized through their cooling temperatures during any metamorphic event will record the age of that metamorphic event. The $^{40}Ar/^{39}Ar$ dating method has been widely used also in the field of sedimentary research, with muscovite being the primary mineral for the analysis. When muscovite grains are transported from a source rock unit to a sedimentary basin, the $^{40}Ar/^{39}Ar$ dates of these grains can provide a measure of the time of cooling of its source through the closure temperature interval (typically 300-400°C; Hames and Bowring, 1994), with the consideration that no additional ^{40}Ar is added or lost during the transportation and deposition (Hodges et al. 2005).

Detrital minerals usually will show a range of ages related to different sediment source terranes. The stronger relative probability of a particular age suggests greater contribution of detritus from the source rock having that age. The age of the sediment source rock and the depositional age of the sample represent the maximum time gap that is required for sediment transport. To the extent that rapid transport is related to high relief in the source region, this phenomenon may indicate that a well-developed

Himalayan orogenic 'front' existed, and uplifted and unroofing ages may come closer to the depositional age of the clastic wedge (Hodges et al., 2005).

The northern passive margin of India has evolved through different tectonic settings through geological time and has contributed sediment to its northern margin in the Tethys Sea. After the collision with the Tibetian block, the depositional environments changed from marine to continental accompanied by a change in drainage patterns. Previous workers have used $^{40}Ar/^{39}Ar$ method for age-dating sediments accumulated in the Tethys Sea and attempted to identify their provenance (e.g., Gizbert et al., 2008).

8.2 METHODOLOGY

Muscovite crystals from four sandstone samples from three different Gondwanan sections of Nepal were selected for analysis. Two samples, sample 15-8 from the Bhainskati Formation and sample 16-3 from the Sisne Formation of the Tansen Group, were selected from western Nepal. The other two samples, sample 22-8 from the Tamrang Formation of the Barahachettra Group and sample 26-8 from the Katari Group, are from eastern Nepal.

Samples were prepared in the Himalayan Research Laboratory at Auburn University. Sandstone samples were crushed and sieved to extract grains in 0-4 phi size range. Afterwards, samples were processed for heavy mineral separation using a heavy liquid (tetrabromoethane). Lighter fractions of the samples were collected after washing carefully with acetone. From each sample, approximately 100 muscovite grains were separated using binocular microscope and packed into an irradiation disc. The samples

were sent to the McMaster University Research Reactor in Hamilton, Ontario, Canada for irradiation produce to ^{39}Ar from ^{39}K.

The Gondwanan sandstones of Nepal were analyzed at the Auburn Noble Isotope Mass Analysis Laboratory (ANIMAL) at Auburn University. ANIMAL is equipped with a low-volume, high-sensitivity, 10-cm radius sector mass spectrometer and automated sample extraction system (based on CO_2 laser) for analysis of single crystals (Uddin et al., 2007). Analyses are typically made using a filament current of 2.240 Amp, and potentials for the source and multiplier of 2000 V and –1300 V, respectively. The high sensitivity and low blank of the instrument permits measurement of 10^{-14} mole samples to within 0.2% precision. The GA-1550 biotite (9.879 Ma; Renne et al., 1998) was used as a flux monitor for this study.

Twenty-five irradiated muscovite grains from each sample were placed in a copper holding disc and analyzed by fusing single muscovite crystals with a CO_2 laser. Data were reduced using Isoplot 3 (Ludwig, 2003). All samples were corrected for atmospheric argon contamination and inferring nuclear reactions. Mass fractionation was evaluated by measuring multiple air aliquots daily and procedural blanks were measured after every sample analyses.

8.3 $^{40}Ar/^{39}Ar$ RESULTS

The distribution of age populations provided by the $^{40}Ar/^{39}Ar$ method for each sample is plotted in relative probability plots (Figs. 8.2 through 8.5). The data used for these plots are given in Appendix E. All samples show polymodal distributions of

muscovite age. However, some samples show fewer modes than others. Sample 15-8 from the Eocene Bhainskati Formation of the Tansen Group shows several modes in age distribution. Significant age distributions are found approximately at 50 Ma, 140 Ma, 300 Ma, 800 Ma and 900 Ma (Fig. 8.2). These multiple age distributions and wide range of age indicate contribution of muscovites from multiple source terranes. Sample 16-3 from the Permo-Carboniferous Sisne Formation of the Tansen Group also shows multiple age distributions with signification age distributions at 30 Ma, 135 Ma, 300 Ma, 500 Ma, 800 Ma, 1300 Ma and 1700 Ma (Fig. 8.3). Unlike other samples, sample 26-8 from the Katari Group shows only three modes in age distributions: 18 Ma, 24 Ma, and 290 Ma (Fig. 8.4). Sample 22-8 from the Permo-Carboniferous Saptakoshi Formation of the Barahachettra shows a wide range of age distribution modes at 20 Ma, 32 Ma, 220 Ma, 290 Ma, 580 Ma, 790 Ma, 900 Ma, 1050 Ma and 1180 Ma (Fig. 8.5)

The results for the sample from the Eocene Bhainskati Formation are consistent with the stratigraphic age assignment to this unit. The Cenozoic ages of other samples in this study, however, are dramatically younger than the Permo-Carboniferous stratigraphic ages assigned to them. The ages of ca. 18-30 Ma determined for them, in contrast, are suggestive of Himalayan orogenesis.

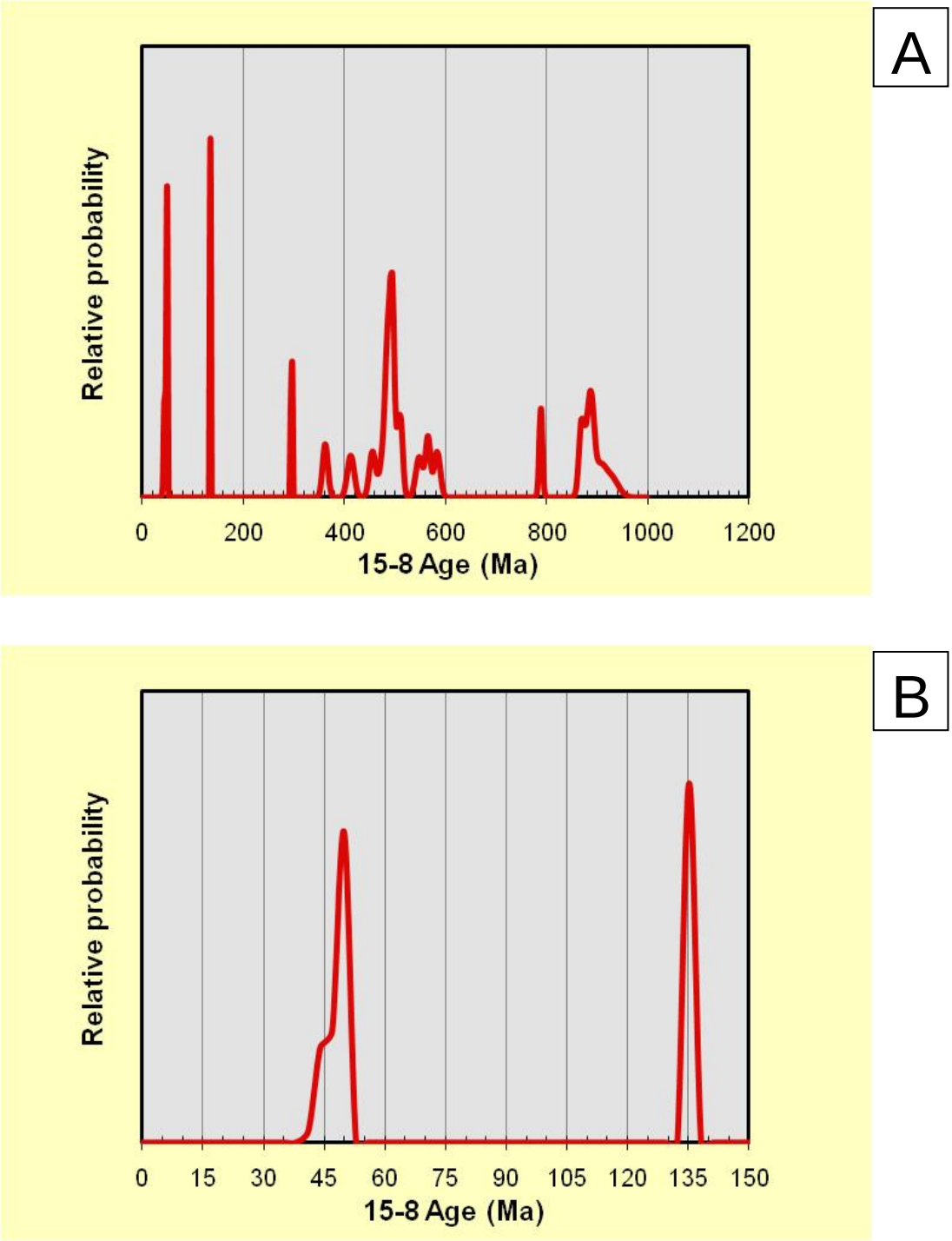

Figure 8.2 Probability plot for $^{40}Ar/^{39}Ar$ of single muscovite crystals from the Eocene Bhainskati Formation (sample 15-8) (A) all data (B) ages less than 150 Ma of the Tansen Group, western Nepal.

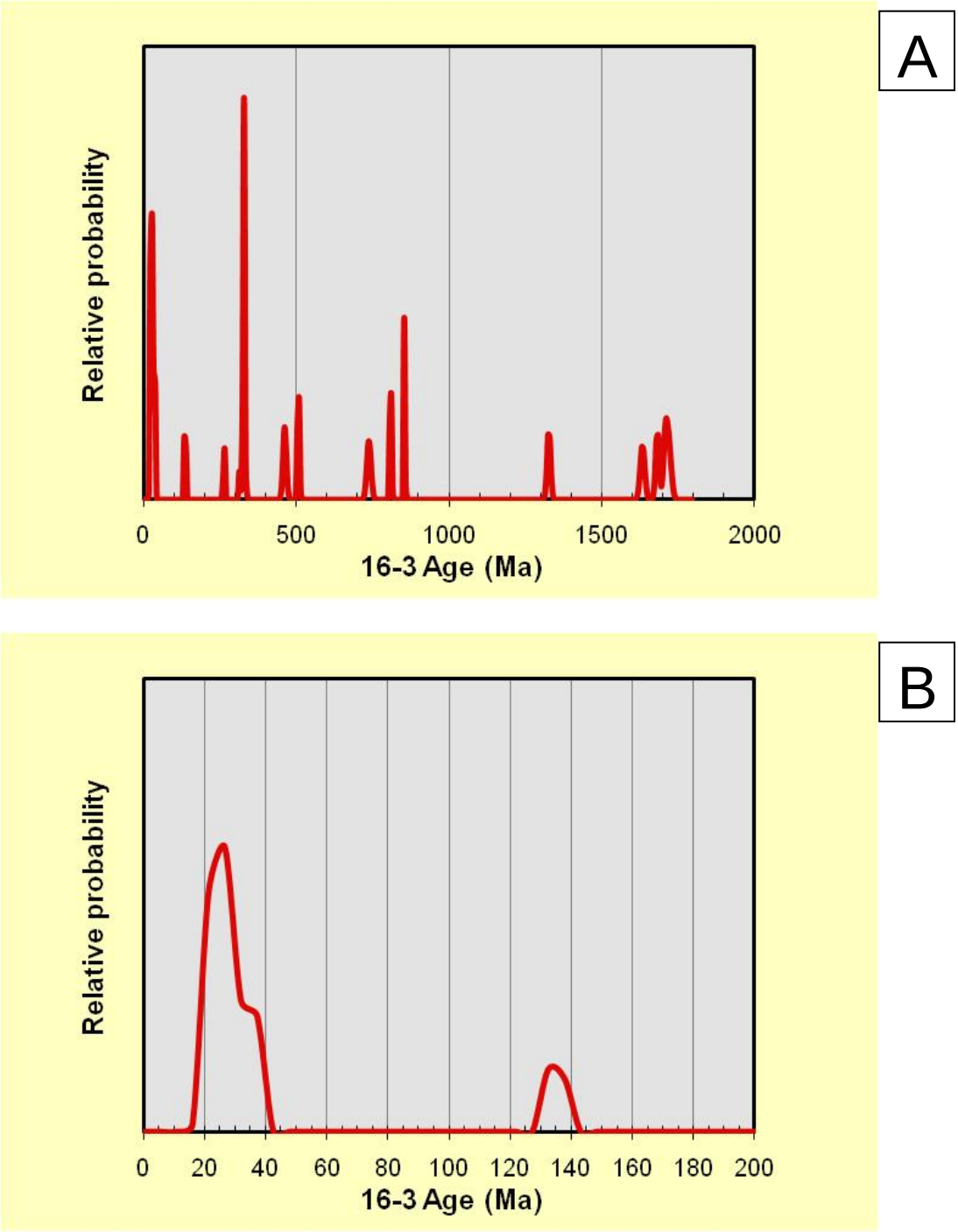

Figure 8.3 Probability plot for $^{40}Ar/^{39}Ar$ of single muscovite crystals from the Permo-Carboniferous Sisne Formation (sample 16-3) (A) all data (B) ages less than 200 Ma, of the Tansen Group, western Nepal.

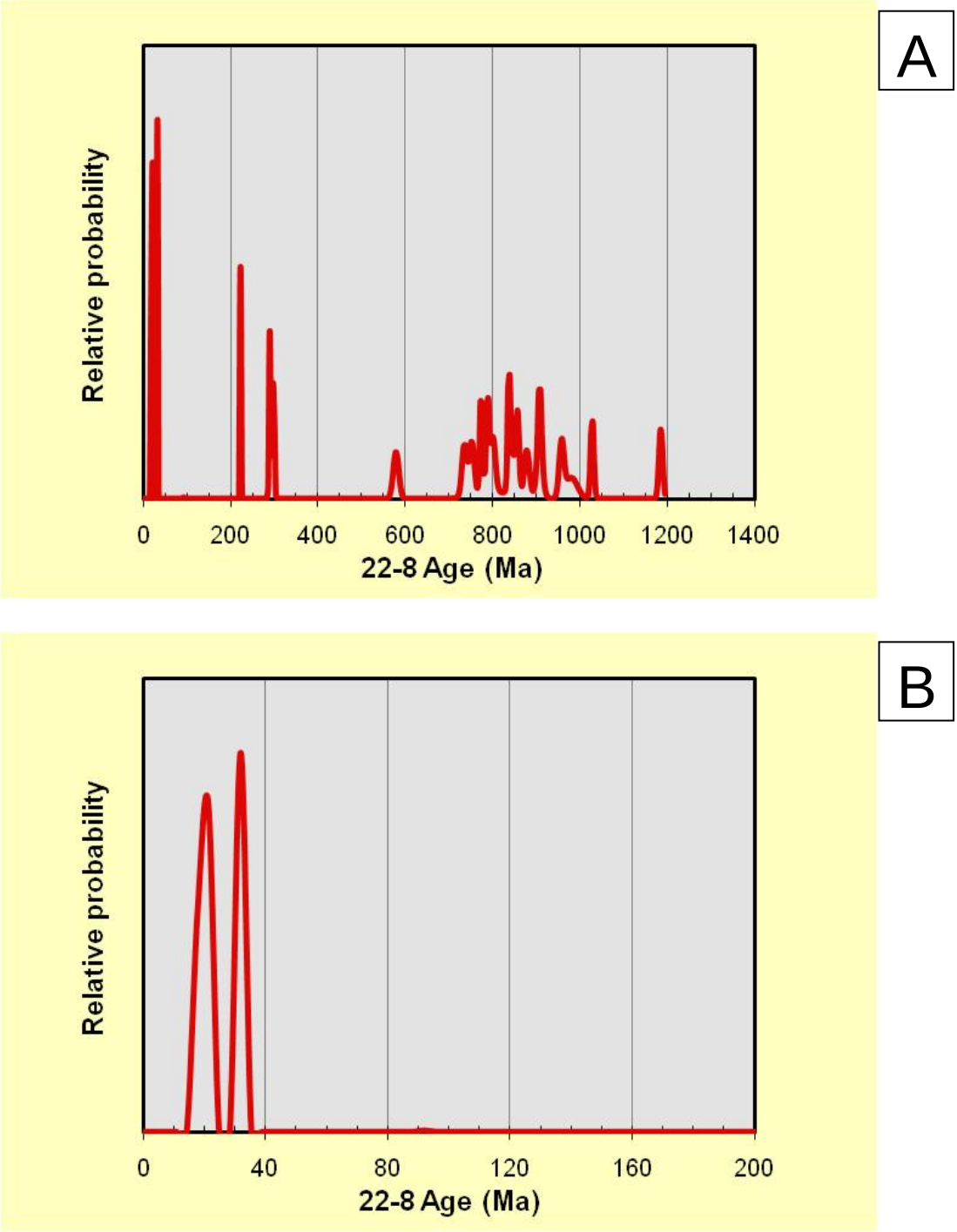

Figure 8.4 Probability plot for $^{40}Ar/^{39}Ar$ of single muscovite crystals from the Permo-Carboniferous Saptakoshi Formation (sample 22-8) (A) all data (B) ages less than 200 Ma of the Tansen Group, eastern Nepal.

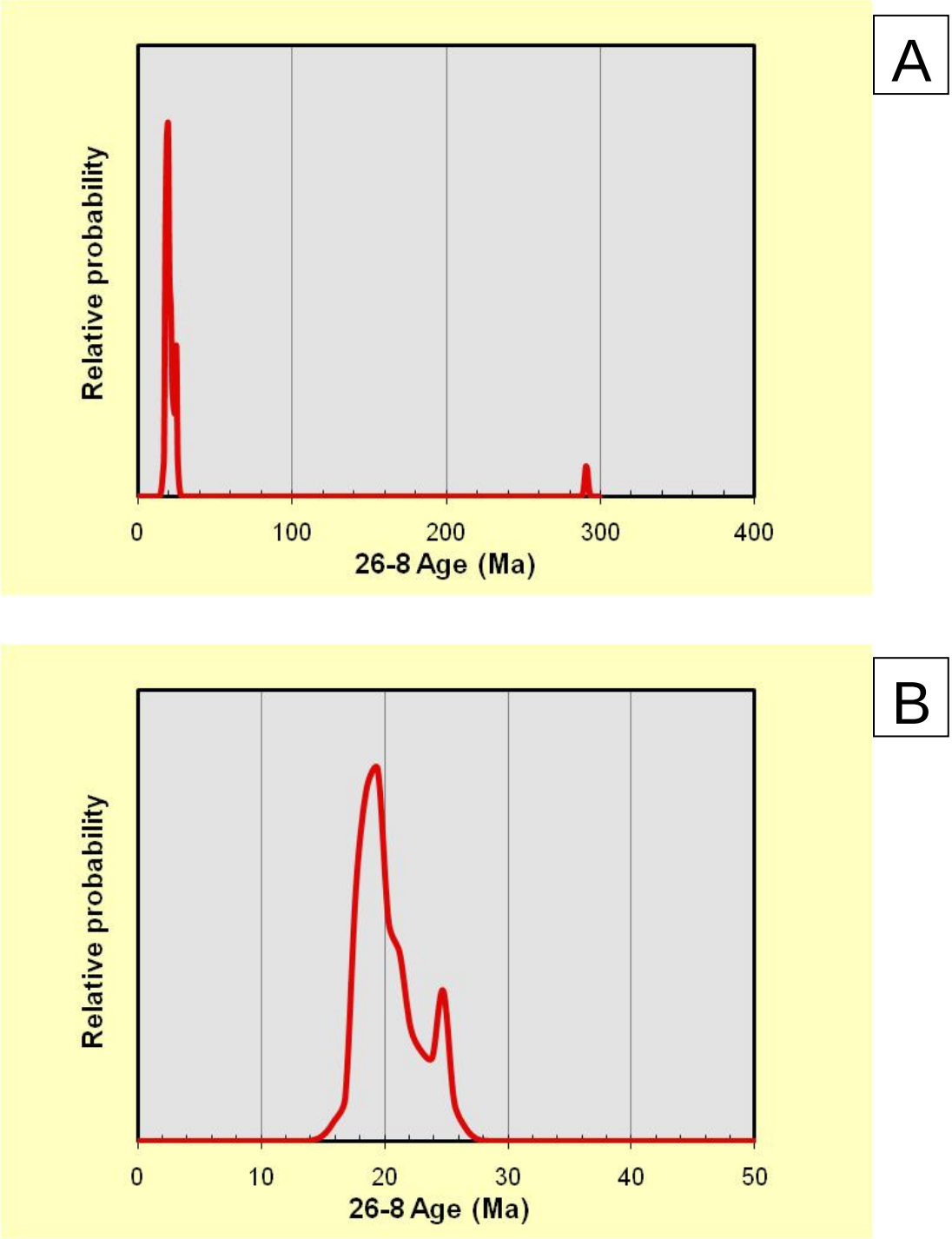

Figure 8.5 Probability plot for $^{40}Ar/^{39}Ar$ of single muscovite crystals from the Permo-Carboniferous Katari Group (sample 26-8) (A) all data (B) ages less than 50 Ma, eastern Nepal.

The fact that some detrital muscovite ages from the Sisne and Saptakoshi formations as determined in this study appear younger than expected o the basis of stratigraphic age assignment could be explained in several ways. Possible causes of the age discrepancy are raised and discussed below:

1. Laboratory error in the measurement, including incorrect J-value, or mass spectrometer parameters (ratio measurement, etc.).

Laboratory analytical errors listed in the appendices (Appendix –F) represent the precision of argon isotopic measurements for the individual muscovite crystals, and generally result in an uncertainty of about 1% in the single-crystal ages. The J-values were constrained by placing monitor minerals in close proximity to the samples of this study and are reproducible to within 0.5%. Combining all sources of laboratory and monitor mineral uncertainty a resulting accuracy for the ages determined would be within 2% (or, about 200,000 years for the Miocene ages determined in this study). Thus, it is certain that laboratory errors cannot be responsible for producing the Miocene ages in samples of this study.

2. Sample misidentification, and mislabeling, or contamination in the field or in the laboratory.

Samples 15-8, 16-3, and 22-8 contain muscovite with ages of calculated 500-1700 Ma that are compatible with Gondwanan source terranes in the Indian craton, and ages less than ~ 17 Ma are not found in these samples or in sample 26-8. In contrast, muscovite samples collected and processed for laboratory analysis in the same general

time frame as samples of the present study are from the Bengal Basin (with typical muscovite ages of 14-20 Ma, and a large proportion of micas that are 15-16 Ma) and the Appalachians (with ages of 300-450 Ma). Considerable care was taken in handling samples, both in the field and laboratory, and sample contamination is very unlikely to be a cause of the ages that are younger than stratigraphic assignment. Furthermore, the modes of 19-22 Ma (see samples 26-8, 22-8, and 16-3), and the pre-500 Ma ages, are not compatible with other laboratory samples. Therefore, there is no basis to infer sample mishandling or laboratory contamination could be responsible for the Miocene ages determined for these presumably pre-Cretaceous stratigraphic units.

3. Incorrect assessment of geology including (3a) stratigraphy and (3b) tectonics of the study area.

3a. Wide-ranging and polymodal age distributions for the Bhainskati Formation (sample 15-8) of the Tansen Group was expected. Post-Gondwanan fossils like *Nummulites beaumonti* d'ARCHAIC and HEIME, and *Assilina papillata* NUTTLE are reported from the Eocene Bhainskati Formation (Sakai, 1983). The Bhainskati Formation is considered as the record of sediment source switching from Indian craton to the Himalayan orogenic belt (Najman, 2003).

The depositional age of the Sisne Formation has been suggested to be Permo-Carboniferous based on discovery of *Fenestella, Polypora* and *Acanthocladia* from the Tansen area (Sakai, 1983). Sakai (1983) has suggested that this formation was supplied sediment from cratonic India. However, muscovite dating of sample 16-3 from the Sisne Formation unexpectedly yields few much younger age of 30 Ma and other expected older

ages correlatable to Indian source rocks. Notably, the Sisne Formation is overlain by the Taltung Formation. The latter unit contains basalt flows considered to be equivalent of Rajmahal Traps (Sakai, 1983). The age of the Rajmahal Traps is considered to be 118 Ma (Kent et al., 2002). Thus, the Permo-Carboniferous ages inferred for regional Gondwanan sequences in the Tansen area seem well supported.

The age distribution of sample 22-8 from the Saptakoshi Formation of the Barahachettra Group poses a similar problem. The Gondwanan plant fossils, *Schizoneura gondwanesis* FEISTM of Permian age, have been reported from the black slate of the Barahachettra Group (Bashyal, 1980). However, occurrence of plant fossils in that area has not been reported afterwards. The quartzite unit of the Saptakoshi Formation, which also includes fossiliferous slate, has been kept below the diamictic beds and above Precambrian basement rock (Bashyal, 1980, Dhital 1992). Everywhere else, diamictite beds are reported above Precambrian basement in the Gondwanan sequences. Moreover, the contact between the quartzite beds and Precambrian basement rocks is not an unconformity but a normal fault. So, all these controversies make the stratigraphy of the Barahachettra difficult to understand. The younger muscovite ages for sample 22-8 (~17 Ma) would be compatible with the Miocene Dumri Formation. However, the latter is a litharenite and is lithologically very different than the Barahachettra quartzite unit. Sample 26-8 of Katari Group poses similar problem. Muscovite grains from this sample are not giving significant older age modes representing source rocks from the India except one 290 Ma. The major age modes occur at 18 and 24 Ma (Fig. 8.5).

3b. The major tectonic structure of the Himalayan orogenic belt is Main Central Thrust (MCT) (Fig. 2.1) which was activated during 25~20 Ma and reactivated during ~10 Ma (Le Fort, 1996). Another major thrust is Main Boundary Thrust (MBT) which became activated ~3 Ma and move the Lesser Himalayan rocks above the Siwaliks. However, there are several small scale thrusts between MCT and MBT and the area of this study, particularly in the eastern part. MCT itself is an issue of major debate in Himalayan geology. Several believe that the MCT is a zone rather than single plane. The Barahachettra and Katari groups include several small scale thrusts and some of the samples in the present study show post-depositional deformational features.

4. Thermal resetting of muscovite grains

A closure temperature of 350-400 °C has been commonly suggested for muscovite (e.g., Hames and Bowring, 1994; McDougall and Harrison, 1999). In metamorphic rocks, early-formed muscovite has been shown to be resistant to argon loss during overprinting metamorphism (to temperatures of at least 425°C; Hames and Cheney, 1997). There are also many examples of detrital muscovite that was not completely reset during low grade metamorphism of slates (Dallmeyer and Takasu, 1992). The muscovite grains analyzed during this study shows their detrital characteristics with well rounded shape and average diameter of grains ~0.3 - 0.5 mm (see representative photographs in Appendix – G). So there is no possibility to get young ages by analyzing the diagenetically formed sericitic muscovite in low temperature due to activities of the Main Central Thrust (MCT). Quartz textures in the sandstones of this study, including sample 26-8, include undulose extinction, sutured grain boundaries, and

polycrystalline grains. Such intercrystalline strain textures and disequilibrium grain boundaries would presumably anneal if sandstone were heated to ~ 300 °C or higher for a geologically significant length of time. MCT, which could be the only possible deformational agent, was suggested to be active around 24 Ma (Le Fort, 1996) that may not provide sufficient heat and time period of high temperature for resetting of muscovite. In metamorphic rocks younger ages of muscovite has been recorded from the overgrown muscovite due to polymetamorphism rather than the lattice diffusion due to temperature increase (Hames and Cheney, 1997). But none of these Gondwanan samples show any attribute of metamorphism. The loss of argon along deformed edges and cracks of muscovite has been also reported. However, the relationship of detrital muscovite behavior to that of metamorphic muscovite is unclear. The older, Precambrian ages determined in this are compatible with Gondwanan sources and do not seem 'reset' by younger events. Thus, on the basis of preserved detrital mineral texture (e.g., quartz undulose extinction) and previous studies of muscovite, it is not easy to explain younger ages by thermal resetting.

8.4 PROVENANCE INTERPRETATION

The older muscovite age mode for the Gondwanan sandstone samples can be correlated with the ages of possible source rocks in Pennisular India, primarily the Aravalli-Delhi Supergroup, the Malani Igneous Suite, the Bundelkhand Massif, and the Chotnagpur Gneissic Terrain (Fig. 8.8). In addition to these igneous and metamorphic units; the Vindhyan Supergroup, equivalent to the Lesser Himalaya, also may have been a major contributor of sediments for the Gondwanan sequences of Nepal (Sakai, 1983).

Chaudhary et al. (1984) have identified five broad periods of acid magmatism in the Delhi Supergroup, including 1700-1500 Ma which gave rise to Erinpura Granite, and 870-750 Ma, which related with the Malani Igneous Suites. These ages were obtained from Rb-Sr geochronology. Another possible source of older muscovites could be the Pilbara craton of Western Australia, where alkaline intrusive rocks have been dated at 1,724 Ma using $^{40}Ar/^{39}Ar$ analyses (Matchan, 2008).

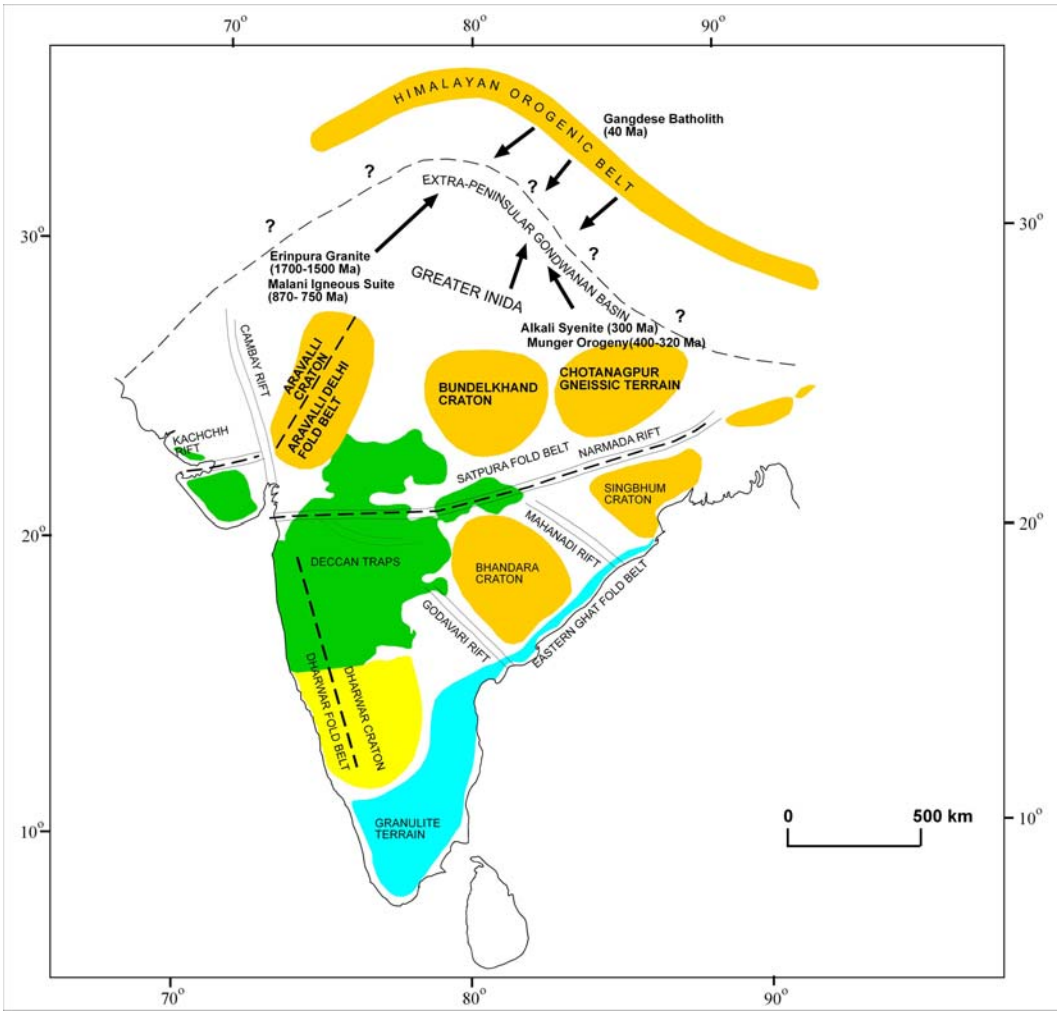

Figure 8.8 Possible source rock with the age given by the detrital muscovite analyzed.

CHAPTER 9: DISCUSSION

9.1 SYNTHESIS

Permo-Carboniferous Gondwanan sequences of the Nepal Himalaya are mostly continental deposits developed along a passive-margin setting. However, sequences also include some marine beds and have been influenced by at least one event of rifting. The setting gradually changed to a foreland basin when the Indian plate collided with the Tibetan plate. Post-Gondwanan sequences preserve the history of this collision. The research carried on the petrography; heavy minerals, whole-rock geochemistry, mineral chemistry, and detrital muscovite dating of sandstones has generated two important types of information regarding the provenance and the correlation of the Gondwanan sequences in different sections of Nepal Himalaya.

9.2 SANDSTONE PETROGRAPHY AND STRATIGRAPHY

The Tansen Group, the type section of the Gondwanan sequence and post-Gondwanan sequences, shows very sharp compositional variation between different time-stratigraphic units. The Permo-Carboniferous Sisne Formation contains abundant feldspars in sandstones that are interbedded with daimictitic beds (Sakai, 1983). Another important character of the Sisne sandstones is common garnets. Clasts of the diamicite are believed to have come from the Malani Granite and other associated rock units, including the Vindhyan Group (Sakai, 1983). The depositional environment can be

inferred to be glacial with intervals of glacio-fluvial deposits. The Chotanagpur Gneissic terrain of peninsular India could have been the main source for providing garnets. The 300 Ma alkaline syenite intrusive rocks in the Chotanagapur Terrain (Mahadevan, 2000) may have been a source for the feldspars in the Sisne Formation (Fig. 4.1A).

A major shift is observed in the depositional environment of Jurassic- Cretaceous Taltung Formation. The fluvial depositional basin was not only receiving detritus from the southern highland in India but also accumulating volcanic rock fragments from the rift volcanics, which are believed to be contemporary with the Rajmahal Basalt (Sakai, 1983). Diagenetic replacement of quartz and feldspars by calcite is very strong in the Taltung Formation (Fig. 4.1B). The Late Cretaceous-Paleocene Amile Formation is shallow-marine deposit that is dominated by mature quartz (Figure 4.2 A). Besides quartz arenite, the sequence contains shale and limestone, which likely reflect sea-level changes rather than shifts in source terranes.

The Eocene Bhainskati Formation contains abundant lithic fragments (Fig. 4.2B). The Bhainskati Formation has been suggested to receive sediments from both the Himalayan orogenic belts and as well as the Indian craton (DeCelles, 1998). The lower Miocene Dumri Formation is considered to be a foreland deposit. It is distinguished from other units based on low abundance of feldspar contents (DeCelles, 1998).

The Permo-Carboniferous Gondwanan sequence of the Katari area in the eastern Nepal has not been studied well (Dhital, 2006). Petrographic study of the carbonaceous quartzite from the Katari area shows mature quartz grains cemented by calcite. The quartzites are deformed but the degree of deformation is variable. From perspective of

petrology only, the quartzite beds of the Katari section can be correlated with the Amile Formation of western Nepal.

Dhital (1992) revised the stratigraphy of the Barahachettra area of eastern Nepal. The Saptakoshi Formation of the Barahachettra Group consists of diamictite, quarzites, and volcanic materials. Quartzites are carbonaceous and interbedded with gray shale. Petrographic studies of quartzites show that these are pure quartz arenites with mature quartz grains. However, the quartz grains are deformed in many instances. The petrography of these quartzites as well as the alternation with the gray shale strongly suggests correlation with the Amile Formation of the Tansen Group (western Nepal). The sandstone beds, interbedded in diamictites, contain abundant plagioclase and garnet (Fig. 4.4 A), which suggests that the Saptakoshi Formation may be correlated with the Sisne sandstones.

The Tamrang sandstone contains of angular to subrounded grains of quartz, feldspar, and metamorphic rock fragments. Abundant mica is present. The matrix consists of calcite and clay. This formation was earlier proposed to be Cretaceous-Paleocene by Dhital (1992). However, based on high percentages of metamorphic fragments; it could be correlated with the Bhainskati Formation of western Nepal.

The occurrence of quartzite beds below the diamictite in the Saptakoshi Formation which is below the diamictite makes the finding of the Gondwanan fossils in these beds suspicious. Elsewhere, in peninsular India and in extra-peninsular basins, Gondwanan sequences always begin with a diamictite directly above the Precambrian basement which is not consistent in the Barahachettra Group (Sakai, 1983; Dhital, 1992,

Veevers, 1995, Dhital, 2006). The fossils reported from the Barahachettra Group have been never reported in that area by other workers after their first discovery by Bashyal (1980, 1981). The unconformity considered contact between the quartzites of the Saptakoshi Formation and the underlying Precambrian basement is actually a normal fault.

Based on a recent communication with Dr. Meghraj Dhital, a leading expert in Gondwana sequences of Nepal, a new stratigraphic framework for eastern Nepal is proposed (Table 9.1) (Fig. 1).

Table 9.1 Proposed Stratigraphy of Gondwanan and post- Gondwanan sequences in the Barahachettra area (eastern Nepal) and its correlation with Gondwanan sequences in other parts of Nepal.

Age	**Tansen Group**	**Katari Group**	**Barahachettra Group**
Early Miocene	Dumri Formation	Yellow Sandstone	-
Eocene	Bhainskati Formation	disconformity	Tamrang Formation
Paleocen-L. Cretaceous	Amile Formation	Carbonaceous Quartzite	Saptakoshi Formation
Cretaceous-Jurassic	Taltung Formation	Volcanics	Volcanic Tuffs
Permo-Carboniferous	Sisne Formation	Diamictite	Kokaha Diamictite

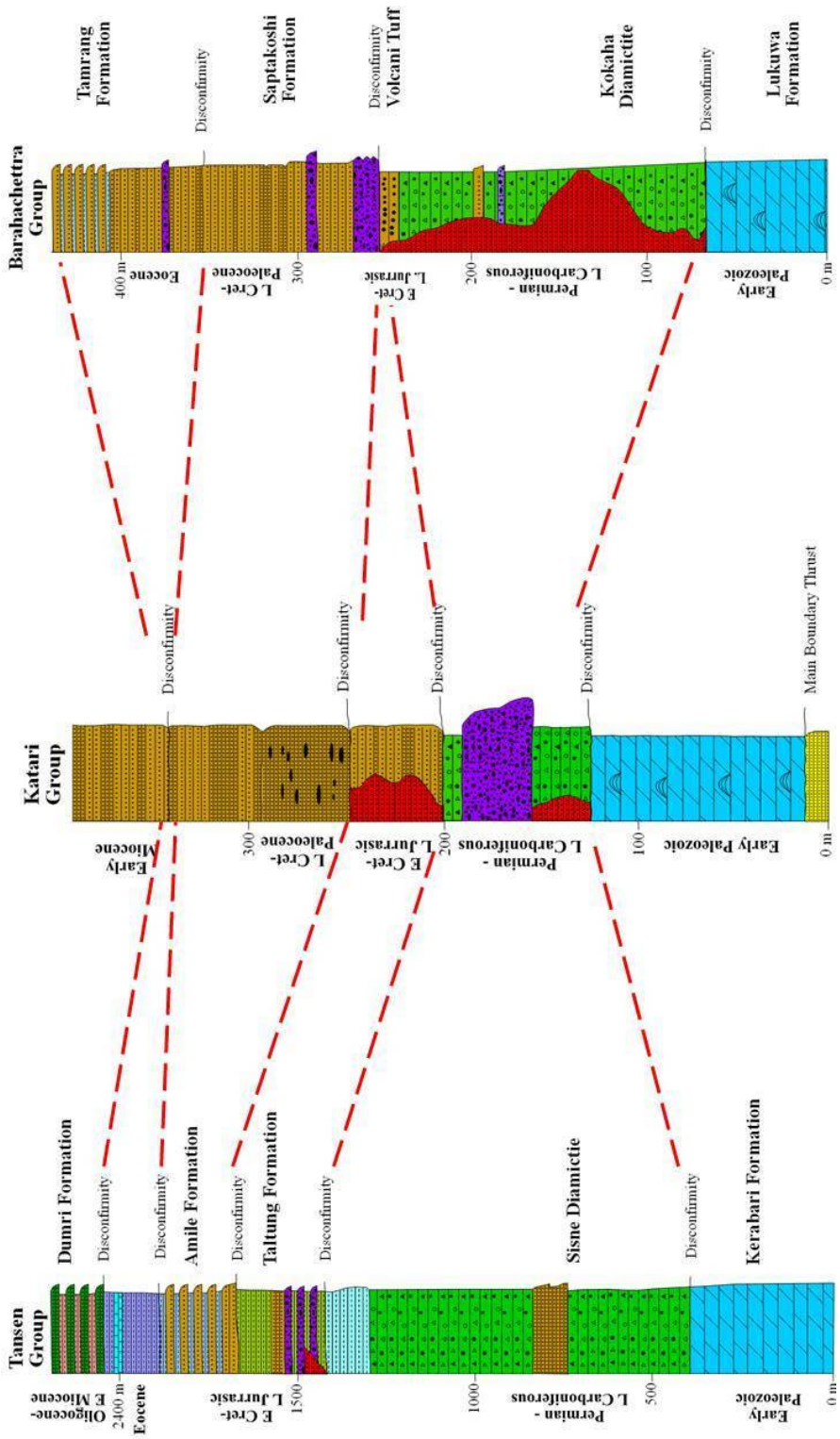

Figure 9.1 Correlation of stratigraphy of Gondwanan sequences in western part of Nepal and proposed stratigraphy of eastern Nepal

9.3 HEAVY MINERAL STUDY

Heavy minerals in Gondwanan sandstones are dominated by two assemblages; garnet rich and ZTR (zircon, tourmaline, and rutile) rich. The Sisne and Kokaha (Saptakoshi Formation of Dhital, 1992) sandstones contain abundant garnet grains, which not only require garnet-rich source rocks as well as preservation of those grains. Subordinate amounts of ZTR are also present in the samples where garnet dominates. In contrast, the samples that are rich in ZTR contain few garnets, reflecting their relatively low preservation potential. The Amile Formation does not contain unstable minerals. The Taltung Formation consists of high number of garnets as well as ZTR. The Tamrang Formation of the Barahachettra contains abundant micas. The probable provenance for the garnets could be the Bihar Mica Belt and the Munger Belt of the Chotanagpur Gneissic terrain of eastern peninsular India. The recycled Vindhyan systems, the Aravalli Belt and the Bundhelkhand Granite could be potential sources of the ZTR grains.

9.4 MICROPROBE ANALYSIS

Garnets

Garnets are found mostly in the Sisne and Taltung formations in the western part of Nepal, and the Saptakoshi Formation and Katari Group in the eastern part of Nepal. The garnets are mostly almandine rich. Pyrope is significantly high in garnet from the Taltung Formation. Grossular content is high for some samples from the Saptakoshi Formation. As most of the garnet grains are rich in almandine, these grains were derived

from a low-grade metamorphic source rocks. The high pyrope contents in the Taltung Formation may reflect high grade metamorphic source rock.

Tourmaline

On the Ca-Fe(tot)-Mg plot, the Katari Group tourmaline show high variations reflecting three different source rock types: Li-rich granitoid pegmatites, Li-poor granitoid pegmatites, and Ca-poor metapelites, metapsammites. Tourmaline from the Barahachettra (the Tamrang Formation) and Tansen group fall in within the Li-poor granitoid pegmatites and Ca-poor metapelites, and metapsammite fields.

Chrome Spinel

Chrome spinels are not very common in the Gondwanan sequence of the Nepal Himalaya. Chrome-spinel was found only in the Taltung sandstones. These chrome spinels contain high aluminum and high chromium, suggesting a source from an Alpine-type peridotite. Low percentages of TiO_2 contents suggest that alkaline basalts were the source of volcanic clasts.

9.5 GEOCHEMICAL ANALYSIS

The Taltung Formation differs geochemically from other samples, which could be due to sediment supply from the volcanic source rocks. Various ratios of major oxides and trace elements like Al_2O_3/TiO_2, TiO_2/Zr also show that Taltung Formation is derived from igneous sources. The Harker plot does not show any evolutionary trends. Hence, the rock units supplying sediments to the Gondwanan basins likely were not genetically related.

Discrimination analysis of the tectonic setting diagrams (Figs. 7. 9 and 7.10) show that the Taltung Formation belongs to arc or rift zones, the Dumri and the Bhainskati formations deposited in active continental margins, and other formations deposited passive margin setting. Basaltic materials commonly have lower HREE, but if the basalt is alkaline, HREE can be significantly high and contain high Eu value. The REE pattern of the Taltung Formation is similar to the Bengal Trap alkali basalts (Fig. 9.2) (Baksi, 1995).

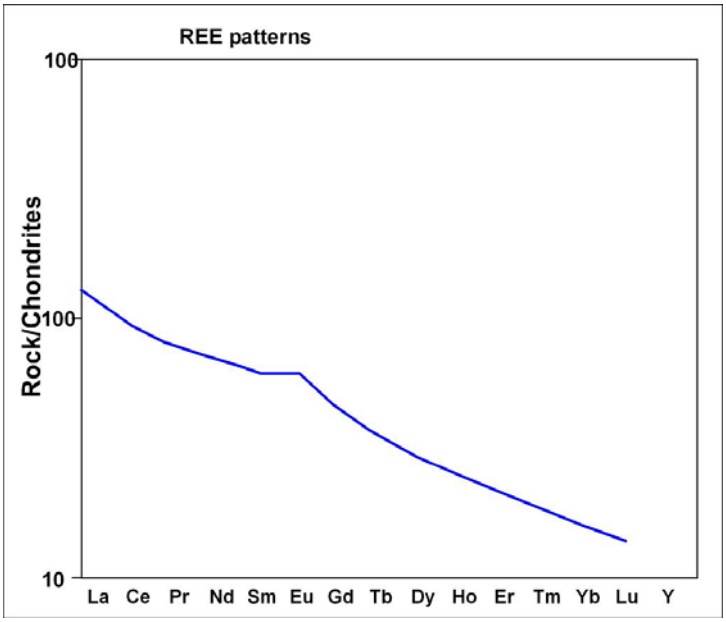

Figure 9.2 Chondrite normalized REE pattern of Bengal Trap Basalt (from Baksi, 1995).

9.6 $^{40}Ar/^{39}Ar$ MUSCOVITE GEOCHRONOLOGY

The $^{40}Ar/^{39}Ar$ muscovite dating of the Gondwanan sandstones carried for this study has provided two types of ages. The older ages (>40 Ma) provide cooling ages of muscovite crystals from igneous intrusions or metamorphic events that took place in the Indian craton. Hence, this gives the approximate ages of source rocks. In contrast,

younger ages (<24 Ma) given by muscovites could have one of the reasons including misunderstanding of stratigraphy or loss of argon from the detrital muscovites. Several older ages of detrital muscovite grains from the Gondwanan sandstone samples may be related with the cooling ages of the Malani igneous suites (870-750 Ma), the Erinpura granite (1700 – 1500 Ma), the Munger orogeny (400 – 320 Ma) and or alkali syenite intrusions (300 Ma) in the Chotanagpur Terrain (Fig. 9.3).

The 40 Ma age found from muscovite grains in the Eocene Bhainskati Formation (sample 15-8) indicates the source rocks from the Himalayan orogenic belt and other older ages going up to 900 Ma indicates source rocks from Indian craton as well. 40 Ma could refers to the cooling ages may also be related to the Gangdese batholith (Copeland et al., 1995).

9.7 PALEOTECTONIC SETTING

During the Permo-Carboniferous, West Gondwanaland had already separated from East Gonwananland. India together with East Gonwanaland was in the southern hemisphere around 60^{o} S (Fig. 9.4A). Due to initial stretching along a major lineament, the half graben basins were created in peninsular India. At the same time, towards the northern margin of India, glacial diamictite and glacio-fluvial deposits were being deposited.

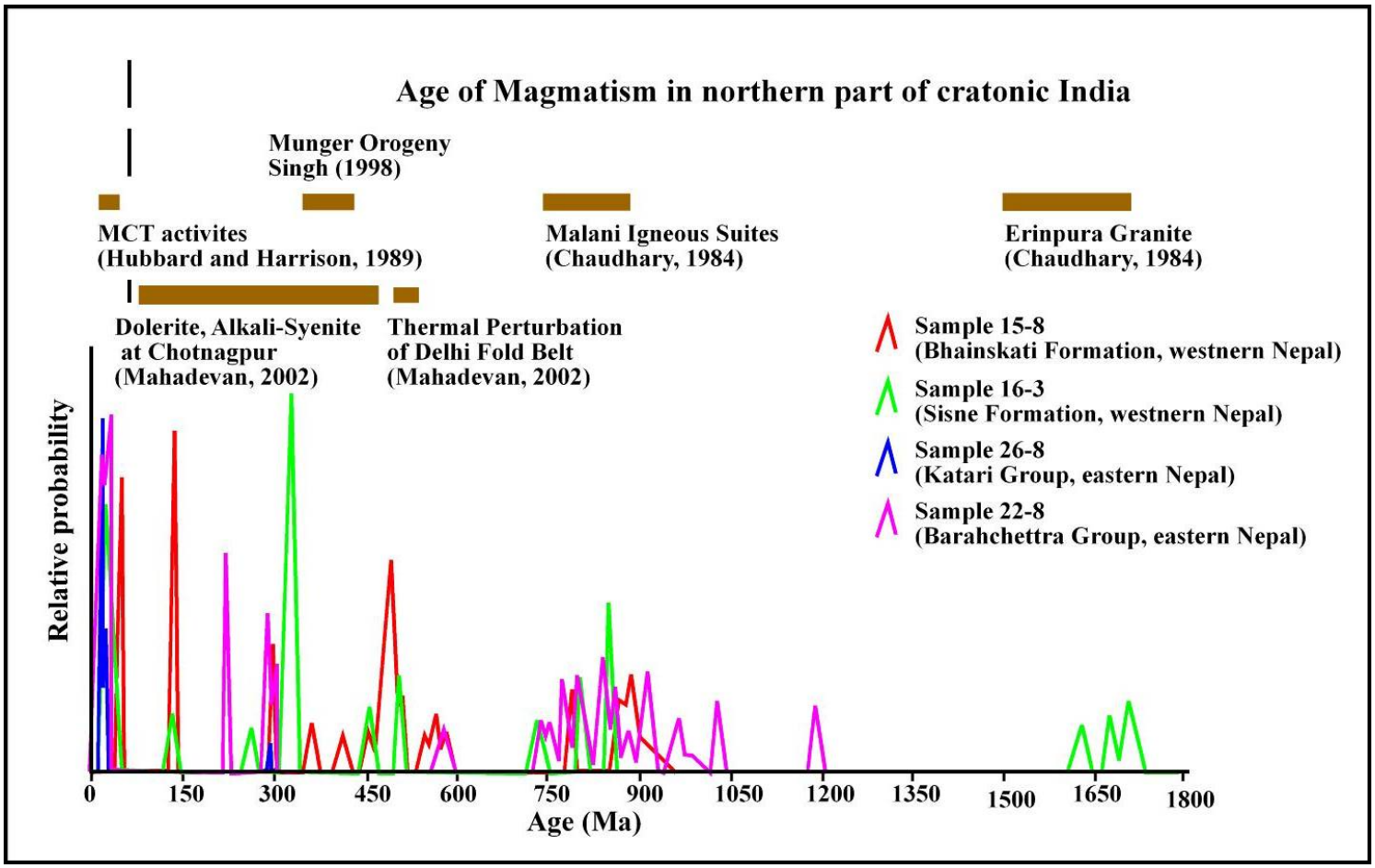

Figure 9.3 $^{40}Ar/^{39}Ar$ cooling ages of single grain muscovite from the Gondwanan sandstone of Nepal. The thick horizontal bars represent published geochronological data for potential source rocks in peninsular India and Himalayas.

During the Cretaceous, Gondwanaland was positioned around 30^{o}S latitude and deposition was in fluvial environments. As Australia rifted from India toward east, several hot spots formed in India (Fig. 9.4 B), including the well-known Rajmahal Trap. Further west, more volcanic activities were taking place, including the eruption of the Aulis Trap, which contributed volcanic clasts to the Taltung Formation.

Due to global fall of sea level during the Late Cretaceous-Paleocene, sediments eroding from the central region of India had to cover a longer distance. Moreover, as the Indian continent was already in a temperate zone at that time, weathering was extreme resulting in deposition of the Amile Formation (Fig. 9.4 C).

The collision between India and Tibet occurred by the Eocene. However, there was still a shallow sea at the backbulge of the foreland basin (DeCelles, 1998). Sediment derived from the Himalayan belt as well as from the Indian craton towards the south were deposited in these shallow sea (Fig. 9.4 D).

The India-Tibet collision was complete by the early Miocene, resulting in the complete retreat of the sea. A thick pile of sediment resulting from the rapid unroofing of the Himalayan belt was deposited in the forebulge of the foreland (Fig. 9.4 E).

Figure 9.4 Paleotectonic setting of India from Permo-Carboniferous to Miocene during deposition of Gondwanan and post-Gondwanan sequences (modified after Sakai, 1989; Veevers and Tiwari, 1995; DeCelles et al., 1998) (1= Delhi-Aravalli Supergroup, 2= Bundelkhand Granite, 3= Chotanagapur Gneissic Terrain).

9.8 CONCLUSIONS

Based on the results of Analysis done for this research following conclusions can been drawn:

1. Gondwanan and post-Gondwanan sequences were deposited along the northern passive margin of India from Late Carboniferous to Early Miocene.
2. In the Barahachettra area, quartzites of the Saptakoshi Formation are not Permo-Carboniferous in age. These quartzites are equivalent to the Paleocene-late Cretaceous Amile Formation of western Nepal. The contact between quartzites of the Saptakoshi Formation and underlying Precambrian basement is a fault, not an unconformity.
3. The carbonaceous quartzite beds of the Katari area also do not belong to the Permo-Carboniferous age. Rather, based on sandstone petrography, whole-rock geochemistry, heavy mineral analysis and mineral chemistry of this unit suggest that they are equivalent to the Amile Formation of western Nepal.
4. The Tamrang Formation, which contains high percentage of the lithic fragments, could be equivalent to the Eocene Bhainskati Formation of western Nepal.
5. The older detrital muscovite ages are sensibly correlated to the source rocks in the Aravali-Delhi Supergroup, Bundelkhand Granite, and Chotanagpur Gneissic Terrain. Source rocks from the Himalayan orogenic belts have been inferred for the ~40 Ma ages from the Eocene Bhainskati Formation. However, the younger muscovites ages (< 30 Ma) are difficult to explain given our present

understanding and the argon-retention characteristics of muscovite along with the regional stratigraphic and tectonic constraints for the study area.

6. Further sampling from the study area is suggested to address the problem related with younger ages. Dating of basalt flow units from all three units may give a better control on stratigraphy. The fossil study on the Cretaceous-Paleocene units will be also helpful to clarify the stratigraphy.

REFERENCES

Amatya, K.M., and Jnawali, B.M., 1994, Geological map of Nepal: Department of Mines and Geology, Nepal, Scale 1:1000000, 1 sheet

Acharya, S.K., 2000, Coal and lignite resources of India: an overview: Geological Society of India, Banglore, 50 p.

Amano, K., and Taira, A., 1992, Two-phase uplift of Higher Himalayas since 17 Ma: Geology, v. 20, p. 391-394.

Auden, J. B., 1935, Traverses in the Himalaya, Record of Geological Survey of India, v. 69, p. 123–169.

Aslam, M., Arora, M., and Tewari, R.C., 1991, Heavy mineral suite in the Barakar sandstone of Moher sub-basin, Singrauli coalfield, central India: Journal of the Geological Society of India, v. 29, p. 66-75.

Baksi, A.K., 1995, Petrogenesis and timing of volcanism in the Rajmahal flood basalt province, north eastern India: Chemical Geology, v. 121, p 73-90

Azmi, R.J., and Pancholi, V.P., 1983, Early Cambrian (Tommotian) conodonts and other shelly microfauna from the Upper Krol of Mussoorie Syncline, Garhwal Lesser Himalaya, with remarks on the Precambrian-Cambrian boundary: Himalayan Geology, v. 11, p. 360-372.

Bateman, R.M., and Catt, J.A., 1985, Modification of heavy mineral assemblages in English coversands by acid pedochemical weathering: Catena, v. 12, p. 1-21.

Bashyal, R.P., 1980, Phosphatic rocks of Barakhsetra Formation: 3rd International field workshop and seminar, Khubsugul, Ulan-bator, p. 1-9.

Bashyal, R.P., 1979, The Gondwana type of formation with phosphatic rocks in southeastern Nepal: Report Published by Department of Mines and Geology, p. 4-18.

Bhatia, M., 1983, Plate tectonics and geochemical composition of sandstones: Journal of Geology, v. 91, p. 611-627.

Bhatia, M. R., and Crook, K. A. W., 1986, Trace element chracteristics of graywacke and tectonic setting discrimination of sedimentary basins: Contributions to Mineralogy and Petrology, v. 92, p. 181-193.

Bock, Barbara, McLennan, S.M., and Hanson, G.N., 1998, Geochemistry and provenance of the Middle Ordovician Austin Glen Member (Normanskill Formation) and the Taconian Orogeny in New England: Sedimentology, v. 45, p. 635-655.

Brookfield, M.E., 1993, The Himalayan passive margin from Precambrian to Cretaceous times: Sedimentary Geology, v. 84, p. 1-35.

Catuneanu, O., Wopfner, H., Eriksson, P.G., Carincross, B., Rubidge, B.S., Smith, R.M.H., and Hancox, P.J., The Karoo basins of south-central Africa: Journal of African Earth Sciences, v. 43, p. 211-253.

Clark, M.K., and Bilham, R., 2009, Miocene rise of Shilong Plateau and the beginning of the end for the Eastern Himalaya: Earth and Planetary Science Letters, v. 269**,** p. 337-351.

Cookenboo, H.O., Bustin, R.M., and Wilks, K.R., 1997, Detrital chromian spinel compositions used to reconstruct the tectonic setting of provenance: Implications for orogeny in the Canadian Cordillera: Journal of Sedimentary Research, v. 67, p 116-123.

Condie, K. C., 1993, Chemical composition and evolution of the upper continental crust: Contrasting results from surface samples and shale: Chemical Geology, v. 104, p. 1-37.

Cerveny, P.F., 1986, Uplift and Erosion of the Himalaya over the past 18 Million years: Evidence from Fission Track Dating of Detrital Zircons and Heavy Mineral Analysis, unpublished MS thesis, Dartmouth College, 198 p.

Cerveny, P.F., Johnson, N.M., Tahirkheli, R.A.K., and Bonis, N.R., 1989, Tectonic and geomorphic implications of Siwalik Group heavy minerals, Tectonics of western Himalayas: Geological Society of America Special Paper, v. 232, p. 129-136.

Chaudhary, A.K., Gopalan, K., and Sastry, C.A., 1984, Present status of the geochronology of the Precambrian rocks of Rajasthan: Tectonophysics, v. 105, pp. 131-140.

Chaudhri, R.S., 1972, Heavy minerals from Siwalik formations of the northwestern Himalayas: Sedimentary Geology, v. 8, p. 77-82.

Copeland, P., Harrison, T.M., Yun, P., Kidd, W.S.F., Roden, M., and Yuquan, Z., 1995, Thermal evolution of the Gangdese batholith, southern Tibet: A history of episodic unroofing: Tectonics, v.14, p.223-236.

Cullers, R.L., Basu, A., and Suttner, L.J., 1988, Geochemical signature of provenance in sand-size material in soils and stream sediments near the Tobacco Root Batholith, Montana, U.S.A: Chemical Geology, v. 70, p. 335-348.

Dallmeyer, R.D., and A. Takasu., 1992, $^{40}Ar/^{39}Ar$ ages of detrital muscovite and whole-rock slate/phyllite, Narragansett Basin, RI-MA, USA: implications for rejuvenation during very low-grade metamorphism: Contributions to Minearlogy and Petrology, v. 110, p. 515-527.

Decelles, P.G., Gehrels, G.E., Quade, J., and Ojha, T., 1998, Eocene-early Miocene foreland basin development and the history of Himalayan thrusting, western and central Nepal: Tectonics, v.17, p. 741-765.

Decelles, P.G., Gehrels, G.E., Najman, Y., Martin, A.J., Carter, A., Garzanti., E., 2004, Detrital geochronology and geochemistry of Cretaceous-Early Miocene strata of Nepal: implications for timing and diachroneity of initial Himalayan orogenesis: Earth and Planetary Science Letters, v. 277, p. 313-330.

Deer, W.A., Howie, R.A., and Zussman, J., 1992, An introduction to the rock-forming minerals: Longman Scientific Technical, Harlow, United Kingdom, 696 p.

Dhital, M.R., and Kizaki, K., 1987, Lithology and Stratigraphy of The Northern Dang, Lesser Himalaya: Bulletin of College Sciences, University of Ryukus, v. 45, p. 183-244.

Dhital, M. R., 1992, Lithostratigraphic comparison of three diamictite successions of Nepal Lesser Himalaya: Journal of Nepal Geological Society, v. 8, p. 43–54.

Dhital, M.R., *unpublished*, The study of Gondwana type of rock in eastern Nepal Lesser Himalaya, (report submitted to Nepal Academy of Science and Technology), 38 p.

Dickin, A.P., 1995, Radiogenic Isotope Geology: New York, Cambridge Press, 452 p.

Dickinson, W.R., 1970, Interpreting detrital modes of greywacke and arkose: Journal of Sedimentary Petrology, v. 40, p. 695-707.

Dickinson, W.R., and Suczek, C., 1979, Plate Tectonics and Sandstone compositions: American Association of Petroleum Geologists Bulletin, v. 63, p. 2164-2182.

Dickinson, W.R., 1985, Interpreting provenance relations from detrital modes of sandstones, in Zuffa, G.G., ed., Reading Provenance from Arenites: Dordecht, The Netherlands, Riedel, p. 333-361.

Dick, H.J.B., and Bullen, T., 1984, Chromian spinel as a petrogenetic indicator in abyssal and alpine-type peridotites and spatially associated lavas: Contributions to Mineralogy and Petrology, v. 86, p. 54-76.

Dorsey, R. J., 1988, Provenance evolution and unroofing history of a modern arc-continent collision: Evidence from petrography of Plio-Pleistocene sandstones, eastern Taiwan: Journal of Sedimentary Petrology, v. 58, p. 208-218.

Dryden, A.L., and Dryden, C., 1946, Comparative rates of weathering of some common heavy minerals: Journal of Sedimentary Petrology, v. 16, p 91-96.

Dutta, P., 2002, Gondwana lithostratigraphy of Peninsular India: Gondwana Research (Gondwana Newsletter Sec), v. 5, p. 540-553.

Dutta, P.K., and Ghosh, S.K., 1993, The century old problem of the Pali–Parsora –Tiki stratigraphy and its bearing on the Gondwana classification of Peninsular India. Journal Geological Society of India, v. 42, p. 17–31.

Faure, G., 1986, Principles of Isotope Geology, second edition: New York, John Wiley and Sons, 589 p.

Fleet, W.F., 1926, Petrological notes on the Old Red Sandstones of the West Midlands: Geological Magazine, v. 63, p. 505-516.

Frakes, L.A., Kemp, E.M., and Crowell, J.C., 1975, Late Paleozoic Glaciation: Part VI, Asia, Geological Society of America Bulletin, v. 86, p. 454-464

Freise, F.W., 1931, Untersuchung von Mineralen auf Ab-nutzbarkeit bei Verfrachtung im Wasser: Tschermaks Mineralogy of Petrology, v. 41, p. 1-7

Friedenreich, O.R., Slind, O.L., Pradhan, U. M.S. and Shrestha, R.B., 1994, Petroleum Geology of Nepal; Canadian Journal of Exploration Geophysics, v. 30, p. 103-114.

Gansser, A., 1983, The morphogenic phase of mountain building, *in* Hsu, K.J., eds., Mountain building processes: Academic Press, London, p. 221-28.

Garzanti, E., Vezzoli, G., Ando, S., Lave, J., Attal, M., France-Lanord, C., and DeCelles, P., 2007, Quantifying sand provenance and erosion (Marsyandi River, Nepal Himalaya): Earth and Planetary Science Letters, v. 258, p. 500-515.

Gizbert,, C.S., Burchfiel, B.C., Li, Z., and Chen, Z., Early Tertiary Gonjo basin, eastern Tibet: Sedimentary and structural record of the early history of India-Asia collision: Geosphere, v. 4, p. 713-735

Graham, S.A., Ingersoll, R.V., and Dickinson, W.R., 1976, Common provenance for lithic grains in Carboniferous sandstones from Ouachita Mountains and Black Warrior Basin: Journal of Sedimentary Petrology, v. 46, p. 620-632.

Gray, D.R., Foster, D.A., Meert, J.G., Goscombe, B.D., Armstrong, R.,Truow, R.A.J., and Passchier, C.W., (in press), A Damaran perspective on the assembly of southwestern Gondwana: Geological Society of London, special publication,

Grimm, W.D., 1973, Stepwise heavy mineral weathering in the resiudal quartz gravel, Bavarian Molasse (Germany): Contribution to Sedimentology, v. 1, p 103-125

Gotze, J., 1998, Geochemistry and provenance of the Altendorf feldspathic sandstone in the Middle Bunter of the Thuringian basin (Germany): Chemical Geology, v. 150, p. 43-61.

Hames, W.E., and Bowring, S.A., 1994, An empirical evaluation of the argon diffusion geometry in muscovite: Earth and Planetary Science Letters, v. 124, p. 161-167

Hames, W.E., and Cheney, J.T., 1997, On the loss of 40Ar* from muscovite during polymetamorphism*: Geochimica et Cosmochemica Acta, v. 61, p. 3863-3872

Hayashi, K. I., H.Fujisawa, Holland, H. D., and H.Ohmoto, 1997b, Geochemistry of 1.9 Ga sedimentary rocks from northeastern Labrador, Canada: Geochimica et Cosmochimica Acta, v. 61, p. 4115–4137.

Henry, D.J., and Dutrow, B.L., 1992, Tourmaline as a low grade clastic metasedimentary rock: an example of the petrogenetic potential of tourmaline: Contributions to Mineralogy and Petrology, v. 112, p. 203-218.

Henry, D.J., and Guidotti, C.V., 1985, Tourmaline as a petrogenetic indicator mineral: an example from the staurolite grade metapelites of NW Maine: American Mineralogists, v. 70, p. 1-15.

Hess, H.H., 1966, Notes on operation of Frantz isodynamic magnetic separator, Princeton University: User manual guide, 6 p.

Hodges, K.V., Rhul, K.W., Wobus, C.W., and Pringle, M.S., 2005, $^{40}Ar/^{39}Ar$ thermochronology of the detrital minerals, *in* Thermochronology, Reviews in Mineralogy and Geochemistry, Reiners, P.W., and Ehlers, T.A., eds., Mineralogical Society of America, Washington, D.C., v. 58, p. 235-257.

Hossain, H.M.Z., Islam, M.S.U., Ahmed, S.S., and Hossain, I., 2002, Analysis of sedimentary facies and depositional environemnts of the Permian Gondwana sequence in borehole GDH-45, Khalaspir Basin, Bangladesh: Geosciences Journal, v. 6, n. 3, p. 227-236

Hubbard, M., and Harrison, T.M., $^{40}Ar/^{39}Ar$ Age Constraints on the Deformation and metamorphism in the Main Central Thurst zone: Tectonics, v. 8, p 865-880

Ingersoll, R.V., Bullard, T.F., Ford, R.L., Grimm, J.P., Pickle, J.D., and Sares, S.W., 1984, The effect of grain size on detrital modes: A test of the Gazzi-Dickinson point-counting method: Journal of Sedimentary Petrology, v. 54, p. 103-116.

Ingersoll, R.V., and Suczek, C.A., 1979, Petrology and provenance of Neogene sand from Nicobar and Bengal Fans, DSDP sites 211 and 218: Journal of Sedimentary Research, v. 49, p. 1217-1228.

Ingersoll, R.V., Graham, S.A., and Dickinson, W.R., 1995, Remnant ocean basins, in Busby, C.J., and Ingersoll, R.V., eds., Tectonics of sedimentary basins: Blackwell Science, Cambridge, p. 363-391.

Irvine, T.N., 1974, Petrology of the Duke Island ultramafic complex, southern Alaska: Geological Society of America Bulletin, v. 138, p. 240.

Irvine, T.N., 1977, Origin of chromite layers in the Muskox Intrusion and other stratiform intrusions; a new interpretation: Geology, v. 5, p. 273-277.

Jain, S.P., and Kanwar, R.C., 1970, Himalayan ridge in the light of the theory of continental drift: Nature, v. 227, p. 829

Johnsson, M.J., 1993, The system controlling the composition of clastic sediments, *in* Johnsson, M.J. and Basu, A., eds., Processes controlling the composition of clastic sediments: Geological Society of America Special Paper 284, p. 1-19.

Kayastha, N.B., 1992, Stratigraphy of the lower Tertiary rocks of Nepal Himalaya: Journal of Nepal Geological Society, v. 8, p. 21-30

Kent, R.W, Pringle, M.S., Muller, R.D., Saunders, S.D. , Ghose, N.C., $^{40}Ar/^{39}Ar$ Geochronology of the Rajmahal Basalts, India, and their Relationship to the Kerguelen Plateau: Journal of Petrology, v. 43, p. 1141-1153

Khan, A.A., Sattar, G.S., Rahman, T., 1994, Tectogenesis of the Gondwana rifted basins of Bangladesh in the so-called Garo-Rajmahal gap and their pre-drift regional tectonic correlation: Ninth International Gondwana Symposium, p 647-655.

Krauskopf, K. B., and D. K. Bird, 1995, Introduction to geochemistry: McGraw-Hill, New York, 647 p

Kumar, P., 2004, Provenance history of Cenozoic sediments near Digboi-Margherita area, eastern syntaxis of the Himalayas, Assam, northeast India [M.S. Thesis]: Auburn University, Auburn, Alabama, 131 p.

Kumar, R., 1998, Fundamental of historical geology and stratigraphy of India, New Age International Publishers, p. 176-188

Le Fort, P., 1996, Evolution of the Himalaya, *in* Yin, A., and Harrison, M., eds., The tectonic evolution of Asia: New York, Cambridge University Press, World and Regional Geology Series, p. 95-109.

Ludwig, K.R., 2003, User's manual for Isoplot, v. 3.0, a geochronological toolkit for Microsoft Excel: Berkeley Geochronological Center, Special Publication no. 4.

Mahadevan, T.M., 2002, Geology of Bihar and Jharkhand: Geological Society of India, Bangalore, 563 p.

Mange, M. A., and Maurer, H. F. W., 1992, Heavy minerals in color.: London, Chapman & Hall, London, 147 p.

Matchan, E., 2008, The age, geochemisty and petrogenesis of an unusual alkaline intrusion in the western Pilbara craton, Western Australia: 9th International Kimberlinte Conference Extended Abstract

McDougall, I., and Harrison, M.T., 1999, Geochronology and thermochronology by the $^{40}Ar/^{39}Ar$ method: New York, Oxford University Press, 269 p.

McLennan, S.M., Taylor, S.R., McCulloch, M.T., Maynard, J.B., 1990, Geochemical and Nd-Sr isotopic composition of deep-sea turbidites: Crustal evolution and plate tectonic associations, Geochemica et Cosmochemica Acta, v. 54. p. 2015-2050.

McLennan, S. M., Hemming, S., McDaniel, D. K., and Hanson, G. N., 1993, Geochemical approaches to sedimentation, provenance and tectonics. i*n* Johnson, M. J., Basu, A., eds, processes controlling the composition of the clastic sedimemts: Geological Society of America., Boulder, Colorado, Special Paper, v. 284, p. 21-40.

Medlicott, H. B., 1864, On the geological structure and relations of the southern portion of the Himalayan ranges between the rivers Ganges and the Ravee: Memoire of Geological Survey of India, v. 3, p. 1–212.

Merrihue, C., and Turner, G., 1966, Potassium-argon dating by activation with fast neutrons: Journal of Geophysical Research, v. 71, p. 2852-2856.

Morton, A.C., 1984, Stability of detrital heavy minerals in Tertiary sandstones of the North Sea Basin: Clay Mineralogy, v. 19, p 287-308.

Morton, A.C., 1985, Heavy minerals in provenance studies, in Zuffa, G.G., eds., Provenance of Arenites: Boston, D. Reidel Publishing Company, p. 249-277.

Morton, A.C., 1986, Dissolution of apatite in North Sea Jurassic sandstone: implications for the gengeration of secondary porosity: Clay Mineralogy, v. 21, p 711-733.

Morton, A. C., and Hallsworth, C., 1994, Identifying provenance-specific features of detrital heavy mineral assemblages in sandstones: Sedimentary Geology, v. 90, p. 241-256.

Morton, A.C., and Hallsworth, C.R., 1999, Processes controlling the composition of heavy mineral assemblages in sandstones: Sedimentary Geology, v. 124, p. 3-30..

Morton, A.C., and Taylor, P.N., 1991, Geochemical and isotopic constraints on the nature and age of basement rocks from Rockall Bank, NE Atlantic: Journal of the Geological Society, London, v. 148, p. 630-634.

Najman, Y., and Garzanti, E., 2000, Reconstructing early Himalayan tectonic evolution and paleogeography from Tertiary foreland basin sedimentary rocks, northern India: Geological Society of America Bulletin, v. 112, p. 435-449.

Najman, Y., Carter, A., Oliver, G., Garzanti, E., 2005, Provenance of Eocene foreland basin sediments, Nepal: Constraints to the timing and diachroneity of early Himalayan orogenesis: Geology, v. 33, p. 309-312.

Najman, Y., 2005, The detrital record of orogenesis: A review of approaches and techniques used in the Himalayan sedimentary basins: Earth Science Reviews, v. 74, p. 1-72.

Nanayama, F., 1997, An electron microprobe study of the Amazon Fan: Proceedings of the Ocean Drilling Program, Scientific Results, v. 155, p. 147-168.

Nance, W.B., and Taylor, S.R., 1977, Rare earth element patterns and crustal evolution-II Archean sedimentary rocks from Kalgoorlie, Australia: Geochemicia et Cosmochimica Acta, v. 41. p 225-231.

Nandi, K., 1967, Garnets as indices of progressive regional metamorphism: Mineralogical Magazine, v. 36, p. 89-93.

Naqvi, S.M., 2005, Geology and Evolution of the Indian Plate: Capital Publishing Company, 450 p.

Nesbitt, H.W., and Young, G.M., 1984, Prediction of some weathering trends of plutonic and volcanic rocks based on thermodynamic and kinetic considerations: Geochimcia Cosmochimcia Acta, v. 48, p.1523–1548.

Nixon, G.T., Cabri, L.J., and Laflamme, J.H.G., 1990, Platinum-group-element mineralization in lode and placer deposits associated with the Tulameen alaskantype complex, British Columbia: The Canadian Mineralogist, v. 28, p. 503-535.

Osae, S., Asiedu, D.K., Yakubo, B.B., Koeberl, C., and Dampare, S.B., 2005, Provenance and tectonic setting of Late Proterozoic Buem sandstones of southeastern Ghana:

Evidence from geochemistry and detrital modes: Journal of African Earth Sciences, v. 44, p. 85-96.

Pettijohn, F.J., 1941, Persistence of heavy minerals and geologic age: Journal of Geology, v. 49, p 610-625.

Pilgrim, G.E., West, W.D., 1928, The structure and correlation of the Simla rocks: Memoire of the Geological Survey of India 53, 140 p.

Potter, P.E., 1978, Petrology and Chemistry of Modern Big River Sands: Journal of Geology, v. 86, p. 423-449.

Le Fort, P., 1996, Evolution of Himalaya, in Yin, A., and Harrison, M., eds., Tectonic Evolution of Asia: World and regional geology series, Cambridge University Press, p. 95-107.

Rahman, M. J. J., and Suzuki, S., 2007, Geochemistry of sandstones from the Miocene Surma Group, Bengal Basin, Bangladesh: Implications for Provenance, tectonic setting and weathering: Geochemical Journal, v. 41, p. 415-428

Rahman, M.W., 2008, Sedimentation and tectonic evolution of Cenozoic sequence from Bengal and Assam foreland basin, Eastern Himalayas [Unpublished M.S. Thesis]: Auburn, Auburn University, 180 p.

Renne, P.R., Swisher, C.C., Deino, A.L., Karner, D.B., Owens, T.L., and DePaolo, D.J.,

1998, Intercalibration of standards, absolute ages, and uncertainties in $^{40}Ar/^{39}Ar$ dating: Chemical Geology, v. 145, p. 117-152.

Rollinson, 1993, Using geochemical data: evaluation, presentation, interpretation: Longman Scientific and Technical and J. Wiley & Sons, 352 p.

Roser, B. P., and Korsch, R. J., 1988, Provenance signatures of sandstone-mudstone suites determined using discriminant function analysis of major-element data Chemical Geology, v. 67, p. 119-139.

Sakai, H., 1983, Geology of the Tansen Group of the Lesser Himalaya in Nepal: Memoirs of the Faculty Science, Kyushu University, Series D, v. XXV (1), p. 27-74.

Sakai, H., 1989, Rifting of the Gondwanaland and uplifting of the Himalayas recorded in Mesozoic and Tertiary fluvial in the Nepal Himalayas in Taira, A. and Masuda, F., eds., Sedimentary Faceis in the Active Plate Margin, p. 723-732.

Sakai, H., 1999, Inverted metamorphism in the Pre-Siwalik foreland basin sediments beneath the crystalline nappe, western Nepal Himalaya: Journal of Asian Earth Sciences, v. 17, p. 727-739.

Scherer, A., 2007, $^{40}Ar/^{39}Ar$ dating and errors, www.geoberg.de, (June, 2009)

Segev, A., 2002, Flood basalts, continental breakup and the dispersal of Gondwana: evidence for periodic migration of upwelling mantle flows (plumes): EGU Stephen Mueller Special Publication Series, v. 2, p. 171-191.

Selley, R.C., 1998, Elements of Petroleum Geology: 2nd edition, Academic Press, London, 470 p.

Sharma, T., Kansakar, D.R., Kizaki, K., 1984, Geology and tectonics of the region between Kali Gandaki and Bheri rivers in central west Nepal: Bulletin of the College of Science University of the Ryukyus, v. 38, p. 57-102.

Shrestha, S.B., Shrestha, J.N., Sharma, S.R., 1987, Geological map of mid-western Nepal (scale: 1250,000): Department of Mines and Geology, Kathmandu.

Singh, S.P., 1998, Precambrian stratrigraphy of Bihar-An overview *in* The Indian Precambrian. Paliwal, B.S., eds., Scientific Publication of India, p. 376-408

Sinha, R.N., and Sastri, V.V., 1973, Correlation of the Tertiary geosynclinal sediments of the Surma Valley, Assam, and Tripura state (India): Sedimentary Geology, v. 10, p. 107-134.

Spear, F.S. and Cheney, J.T., 1989, A petrogenetic grid for pelitic schists in the system SiO2 - Al2O3 - FeO - MgO - K2O - H2O: Contributions to Mineralogy and Petrology, v. 101, p. 149-164.

Soreghan, M. J., and Soreghan, G. S. L., 2007, Whole-rock geochmistry of upper Paleozoic loessite, western Pangaea: Implication for paleo-atmospheric circulation: Earth and Planetary Science Letters, v. 255, p. 117-132.

Strut, B.A., 1962, The composition of garnets from pelitic schists in relation to the grade of regional metamorphism: Journal of Petrology, v. 3, p. 181-191.

Sugitani, K., Yamashita, F., Nagako, T., Yamamota, K., Minami, M., Mimura, K., and Suzuki, K., 2006, Geochemistry and sedimentary petrology of Archean clastic sedimentary rocks at Mt. Goldsworthy, Pilbara Craton, Western Australia: Evidence for the early evolution of continental crust and hydrothermal alteration: Precambrian Research, v. 147, p. 124-147

Suttner, L.J., 1974, Sedimentary petrologic provinces: An evaluation, *in* Ross, C.A., eds., Paleogeographic Provinces and Provincialtiy, Society of Economic Paleontologists and Mineralogists, special publication, v. 21, p. 75-84.

Taylor, S. R., and McLennan, S. M., 1985, The continental crust: Its composition and evolution: Oxford, Blackwell Scientific Publication, 312 p.

Tucker, M., 1988, Techniques in Sedimentology: Blackwell Scientific Publications, London, 395 p.

Uddin, A., Hames, W.E., Rahman, M.W., and Zahid, K.M., 2007, Rapid middle Miocene denudation of the eastern Himalayas: Laser $^{40}Ar/^{39}Ar$ age constraints on Miocene sequences from the Bengal basin: Geological Society of America, Abstracts with Programs, v. 39, p. 592.

Uddin, A., and N., Lundberg, 1998, Cenozoic history of the Himalayan-Bengal system: Sand composition in the Bengal basin, Bangladesh: Geological Society of America Bulletin, v. 110, p. 497-511.

Upreti, B.N., 1999, An overview of the stratigraphy and tectonics of the Nepal Himalaya: Journal of Asian Earth Sciences, v. 17, p. 577-606.

Vail, P.R., Mitchum, R.M. and Thompson, S., 1977, Seismic stratigraphy and global changes of sea-level, Part 4: Global cycles of relative changes of sea-level: American Association of Petroleum Geologists Memoir, v. 26, p. 83-97.

Valdiya, K.S., 1997, Himalaya, the Northern Frontier of East Gondwanaland: Gondwana Research, v. 1, no, 1, p. 3-9.

Veevers, J.J., and Tiwari, R.C., 1995, Gondwana Master Basin of peninsular India between Tethys and the interior of the Gondwanaland province of Pangea: Memoir of Geological Society of America, v. 187, 71 p.

Veevers, J.J., 2006, Updated Gondwana (Permian-Cretaceous) earth history of Australia: Gondwana Research, v. 9, p. 231-260.

Velbel, M.A., 1985, Mineralogically mature sandstone in accretional prisms: Journal of Sedimentary Petrology, v. 55, p. 685-690.

Wadia, D.N., 1919, Geology of India, 3rd edition, Macmillan and Co Ltd., London, 536 p.

Wanke, H., and Konig, H., 1959, Eine neue Methode zur Kalium-Argon-Altersbestimmung und ihre Anwendung auf Steinmeteorite: Z. Naturforschung, v. 14a, p. 860 – 866.

Willan, R.C.R., 2003, Provenance of Triassiac-Cretaceous sandstones in the Antartic peninsula: implications for terrance models during Gondwana breakup: Journal of Sedimentary Research, v. 73, p. 1062-1077

Yokoyama, K., Taira, A., and Saito, Y., 1990, Mineralogy of silts from the Bengal Fan: Proceedings of Ocean Drilling Programs, Scientific Results, v. 116, p. 59-73.

Zahid, K.M., 2005, Provenance and basin tectonics of Oligocene-Miocene sequences of the Bengal Basin, Bangladesh [M.S. Thesis]: Auburn University, Auburn, Alabama, 142 p.

Zhu, B., Delano, J.W., and Kidd, S.F.W., 2005, Magmatic compositions and source terranes estimated from melt inclusions in detrital Cr-rich spinels: An example

from mid-Cretaceous sandstones in the eastern Tethys Himalaya: Earth and Planetary Science Letters, v. 233, p. 295-309.

APPENDIX A: Micropobe Analysis Data of Tourmaline from the Gonwanan sequences of the Nepal Himalaya (Tansen, western Nepal)

Sample No.	15-6 trm 1	15-6 trm 2	15-6 trm 3	16-5 trm 1	16-8 trm 1	16-8 trm 2	16-8 trm 3	16-8 trm 4	16-8 trm 5	16-9 trm 1	16-9 trm 2	Standard1
SiO_2	35.98	35.76	35.97	34.51	34.69	35.31	35.25	34.94	35.05	35.19	34.22	39.73
TiO_2	0.58	0.54	0.84	0.36	0.69	0.27	0.68	0.77	0.83	0.65	0.89	4.90
Al_2O_3	34.42	34.73	33.74	34.89	29.61	33.69	33.95	33.67	34.27	33.61	32.94	14.64
MgO	3.06	2.60	5.28	1.19	2.07	2.41	3.36	3.24	2.40	1.28	1.03	12.90
FeO	11.81	10.73	7.90	13.40	16.27	12.07	10.97	11.03	11.82	14.86	15.74	10.99
CaO	0.56	0.25	0.51	0.18	0.67	0.33	0.59	0.31	0.35	0.16	0.49	10.63
MnO	0.10	0.30	0.00	0.09	0.13	0.07	0.04	0.04	0.11	0.12	0.04	0.04
K_20	0.06	0.03	0.03	0.08	0.05	0.04	0.04	0.06	0.01	0.01	0.06	2.32
Na_2O	1.51	1.59	1.64	1.65	1.91	1.54	1.73	1.83	1.92	2.05	2.10	2.30
Cr_2O_3	0.04	0.01	0.00	0.06	0.01	0.00	0.00	0.00	0.09	0.00	0.01	0.00
Total	86.94	86.53	85.92	86.85	86.11	85.75	86.74	85.92	86.92	88.12	88.08	98.55
End Member Calcualtion												
Ca	3.97	2.01	3.61	1.45	4.11	2.52	4.28	2.34	2.69	1.17	3.42	
Mg	30.34	29.57	52.41	13.48	17.71	25.60	33.80	33.56	25.88	13.19	10.06	
Fe (tot)	65.69	68.42	43.99	85.08	78.18	71.89	61.91	64.10	71.43	85.64	86.52	
Total	100.00	100.00	100.00	100.00	100.00	100.00	100.00	100.00	100.00	100.00	100.00	
Al	45.91	46.36	45.83	46.34	44.66	46.03	45.93	45.93	46.15	45.85	45.68	
Al50Fe(tot)50	28.55	28.26	26.72	29.49	31.04	28.87	28.23	28.31	28.72	30.12	30.58	
Al50Mg50	25.54	25.38	27.45	24.17	24.30	25.10	25.84	25.76	25.12	24.03	23.74	
Total	100.00	100.00	100.00	100.00	100.00	100.00	100.00	100.00	100.00	100.00	100.00	

APPENDIX B: Micropobe Analysis Data of Tourmaline from the Gonwanan sequences of the Nepal Himalaya (Katari and Brahachettra groups, eastern Nepal)

Sample No.	22-10 trm 1	22-10 trm 2	22-10 trm 3	23-4 trm 1	23-4 trm 2	23-4 trm 3	23-4 trm 4	23-4 trm 5	26-8 trm 1	26-8 trm 2	26-8 trm 3	Standard
SiO_2	34.90	36.12	34.98	35.98	35.21	35.98	35.25	34.73	36.20	34.13	35.82	39.73
TiO_2	0.92	0.11	0.74	0.65	0.82	0.51	0.31	0.10	0.19	0.28	0.16	4.90
Al_2O_3	35.01	34.56	34.84	33.45	31.88	31.12	34.22	34.03	36.23	32.86	35.67	14.64
MgO	4.58	0.99	3.12	4.12	6.45	5.46	2.12	0.70	2.57	0.12	2.47	12.90
FeO	8.95	13.32	11.30	9.60	8.17	10.25	11.87	14.26	11.05	16.69	11.28	10.99
CaO	0.61	0.03	0.53	0.13	0.60	0.69	0.22	0.19	0.15	0.14	0.08	10.63
MnO	0.05	0.00	0.07	0.02	0.07	0.05	0.16	0.10	0.00	0.15	0.16	0.04
K_20	0.04	0.00	0.01	0.04	0.00	0.04	0.02	0.03	0.02	0.09	0.02	2.32
Na_2O	1.74	1.27	1.61	1.93	2.21	1.98	1.61	1.63	1.35	1.92	1.34	2.30
Cr_2O_3	0.00	0.00	0.02	0.05	0.01	0.06	0.00	0.00	0.00	0.10	0.02	0.00
Total	86.81	86.41	87.22	85.97	85.44	86.16	85.78	85.76	87.77	86.65	87.03	98.55
End Member Calcualtion												
Ca	4.36	0.26	3.86	0.95	3.74	4.23	1.75	1.50	1.21	1.08	0.61	
Mg	45.62	11.68	31.71	42.93	56.28	46.65	23.75	7.95	28.94	1.28	27.87	
Fe (tot)	50.02	88.06	64.43	56.12	39.99	49.12	74.49	90.55	69.85	97.64	71.52	
Total	100.00	100.00	100.00	100.00	100.00	100.00	100.00	100.00	100.00	100.00	100.00	
Al	46.01	46.41	46.05	45.88	45.07	44.89	46.25	46.26	46.45	45.82	46.38	
Al50Fe(tot)50	27.18	29.55	28.32	27.61	26.63	27.69	28.81	30.01	28.25	31.17	28.40	
Al50Mg50	26.81	24.04	25.63	26.51	28.30	27.42	24.94	23.73	25.31	23.02	25.22	
Total	100.00	100.00	100.00	100.00	100.00	100.00	100.00	100.00	100.00	100.00	100.00	

APPENDIX C: Micropobe Analysis Data of Garnet from the Gonwanan sequences of the Nepal Himalaya (Tansen, western Nepal)

Sample No.	K-1 Gt1	K-1 Gt2	16-3 Gt1	16-3 Gt2	16-3 Gt3	16-5 Gt1	16-5 Gt2	16-5 Gt3	16-5 Gt4	Standard
SiO_2	36.45	37.13	37.77	36.85	36.89	36.01	36.57	36.28	38.61	38.58
TiO_2	0.28	0.24	0.01	0.02	0.00	0.04	0.00	0.02	0.00	0.1168
Al_2O_3	21.56	21.84	21.93	20.75	21.89	21.04	21.39	20.98	22.87	22.73
MgO	6.45	6.73	7.27	1.54	7.31	1.01	2.37	1.06	9.72	10.4
FeO	31.90	30.61	31.64	32.70	31.78	28.31	37.12	32.96	22.07	21.08
CaO	1.33	1.01	1.19	5.54	2.25	1.58	1.66	6.83	6.24	7.45
MnO	1.14	1.02	0.95	2.75	0.33	11.78	1.84	1.44	0.99	0.6193
Cr_2O_3	0.02	0.05	0.00	0.03	0.08	0.10	0.00	0.01	0.00	0
Total	99.14	98.63	100.77	100.19	100.53	99.88	100.96	99.57	100.51	100.97
End Members										
Pyrope	24.85	26.70	27.52	6.04	27.13	4.10	9.31	4.18	35.80	
Almandine	68.95	68.13	67.18	72.15	66.17	64.23	81.89	73.16	45.60	
Grossular	3.69	2.88	3.25	15.66	6.00	4.60	4.68	19.42	16.52	
Spessartine	2.50	2.29	2.05	6.14	0.70	27.07	4.12	3.23	2.07	
Total	100.00	100.00	100.00	100.00	100.00	100.00	100.00	100.00	100.00	

APPENDIX D: Micropobe Analysis Data of Garnet from the Gonwanan sequences of the Nepal Himalaya (Katari and Brahachettra groups, eastern Nepal)

Sample No.	23-5 Gt2	23-5 Gt3	23-5 Gt4	23-5 Gt5	23-5 Gt6	26-8 Gt1	26-8 Gt2	26-8 Gt3	26-8 Gt4	26-8 Gt5	23-5 Gt1
SiO_2	37.79	34.84	36.44	35.55	36.75	37.15	35.76	36.37	36.57	35.93	37.48
TiO_2	0.04	0.11	0.00	0.12	0.07	0.04	0.07	0.08	0.04	0.08	0.05
Al_2O_3	20.95	22.14	21.79	21.25	21.87	21.87	21.62	21.20	21.56	21.01	21.76
MgO	3.76	4.20	3.88	3.31	6.57	1.97	0.98	1.18	1.81	0.93	2.94
FeO	26.75	24.05	27.00	29.10	32.03	27.06	28.77	32.96	35.84	30.83	24.87
CaO	6.83	2.50	8.76	7.30	1.64	8.91	8.61	6.59	5.03	2.13	11.94
MnO	0.84	10.21	1.18	1.36	0.93	4.18	3.88	1.27	0.12	9.18	1.16
Cr_2O_3	0.00	0.09	0.11	0.00	0.03	0.05	0.00	0.02	0.03	0.16	0.00
Total	96.96	98.14	99.15	97.99	99.90	101.23	99.69	99.68	101.00	100.24	100.22
End Members											
Pyrope	15.57	16.61	14.93	12.90	25.03	7.59	3.84	4.71	7.09	3.71	11.26
Almandine	62.13	53.35	58.28	63.64	68.46	58.55	63.26	73.57	78.53	69.28	53.38
Grossular	20.32	7.10	24.22	20.45	4.48	24.70	24.26	18.85	14.12	6.12	32.83
Spessartine	1.98	22.94	2.57	3.00	2.02	9.16	8.64	2.88	0.27	20.89	2.53
Total	100.00	100.00	100.00	100.00	100.00	100.00	100.00	100.00	100.00	100.00	100.00

APPENDIX E: Micropobe Analysis Data of Chrome-spinel from the Gonwanan sequences of the Nepal Himalaya (Tansen Group, western Nepal)

Sample No.	K-1 CrSp1	K-1 CrSp2	K-1 CrSp3	K-1 CrSp4	K-1 CrSp5	Standard
SiO_2	0.11	0.20	0.15	0.15	0.14	0.00
TiO_2	0.80	0.21	0.29	0.89	0.68	0.11
Al_2O_3	36.95	40.10	42.72	35.55	41.89	23.65
MgO	17.76	18.74	17.66	18.01	17.31	16.08
FeO	15.99	13.57	16.29	17.04	16.78	12.65
CaO	0.03	0.01	0.03	0.04	0.04	0.01
MnO	0.16	0.21	0.16	0.18	0.23	0.17
Cr_2O_3	28.15	24.39	21.09	27.74	23.08	46.47
NiO	0.21	0.20	0.20	0.14	0.02	0.14
Total	100.16	97.63	98.59	99.73	100.17	99.28
End Member Calculation						
Al3+	64.32	69.12	72.99	63.09	71.27	
Cr3+	32.87	28.20	24.17	33.03	26.34	
Fe3+	2.80	2.68	2.83	3.88	2.39	
Total	100.00	100.00	100.00	100.00	100.00	

Fe3+/Fe3++Cr+Al	0.03	0.03	0.03	0.04	0.02
Mg#(Mg/Mg+Fe2+)	0.70	0.75	0.69	0.70	0.68
Cr#(Cr/Cr+Al)	0.34	0.29	0.25	0.34	0.27
TiO2 (wt%)	0.80	0.21	0.29	0.89	0.68

APPENDIX F: $^{40}Ar/^{39}Ar$ GEOCHRONOLOGY

Sample Name:	Raju Situala
Date Run:	4/3/09
Irradiation Packages:	AU-12, 13
Date of Irradiation:	1/30/2009
Monitor Age	9.879E+07
Air $^{40}Ar/^{36}Ar$:	293.0 + 1.5

Single crystal, total fusion analyses of muscovite crystals, obtained with automated laser extraction in the ANIMAL facility.
Data are in Moles; samples generally run with a sensitivity of 5.1x10-15 moles/volt
Data are corrected for interfering nuclear reactions and blanks.
Errors are the standard deviation in precision, obtained by regression or averaging of measurements (8 cycles).

APPENDIX F (1): $^{40}Ar/^{39}Ar$ Age data of detrital muscovite from the Katari Group (eastern Nepal, sample 26-8; Permo-Carboniferous)

n	40Ar(*+atm)			39ArK			38Ar(atm+Cl)			37ArCa			36Ar(atm)			%Rad	R	Age (Ma)			%-sd
11	2.9983E-15	+	1.2E-17	2.898E-15	+	6.31E-18	5.5E-18	+	1.11E-19	2.6E-18	+	6.5E-19	6.2E-19	+	1.4E-19	93.9%	0.9717	24.7	+	0.4	2%
12	1.3742E-15	+	1E-17	1.553E-15	+	5.61E-18	2.8E-18	+	7.97E-20	-1.9E-19	+	8.3E-19	4.3E-19	+	1.4E-19	90.7%	0.8026	20.4	+	0.7	3%
13	3.2175E-15	+	1.4E-17	4.056E-15	+	1.36E-17	7.5E-18	+	1.44E-19	3.3E-18	+	6.8E-19	5.1E-19	+	1.3E-19	95.3%	0.7563	19.2	+	0.3	1%
14	1.3373E-15	+	1E-17	1.119E-15	+	4.32E-18	1.8E-18	+	4.75E-20	-5.9E-19	+	5.1E-19	1.6E-18	+	1.2E-19	65.0%	0.7773	19.8	+	0.9	4%
15	8.9989E-16	+	1E-17	7.975E-16	+	3.28E-18	1.4E-18	+	5.33E-20	3.8E-18	+	1.3E-18	8.4E-19	+	1.5E-19	72.3%	0.8158	20.7	+	1.5	7%
16	2.0129E-15	+	9.4E-18	2.088E-15	+	9.31E-18	4.4E-18	+	8.7E-20	9.3E-19	+	9.5E-19	5.5E-19	+	1.1E-19	91.9%	0.8859	22.5	+	0.4	2%
17	1.486E-14	+	1.6E-17	1.212E-15	+	3.88E-18	2.2E-18	+	3.42E-20	9.3E-19	+	3.3E-19	1.9E-19	+	3.8E-20	99.6%	12.2172	290.6	+	1.0	0%
18	2.2236E-15	+	9.6E-18	2.836E-15	+	5.82E-18	6.6E-18	+	1.6E-19	2.5E-18	+	5.5E-19	8.5E-19	+	1.1E-19	88.6%	0.6949	17.7	+	0.3	2%
19	3.5085E-15	+	6.3E-18	4.670E-15	+	1.38E-17	7.4E-18	+	1.43E-19	3.9E-18	+	9.8E-19	5.8E-19	+	1.1E-19	95.1%	0.7148	18.2	+	0.2	1%
20	1.4732E-15	+	8.3E-18	1.524E-15	+	6.91E-18	3.2E-18	+	5.37E-20	4.4E-18	+	1.1E-18	1.1E-18	+	1.2E-19	77.3%	0.7474	19.0	+	0.6	3%
21	7.3014E-16	+	3.9E-18	8.25E-16	+	2.74E-18	1.4E-18	+	4.55E-20	2.1E-18	+	4.9E-19	2.6E-19	+	4.8E-20	89.5%	0.7923	20.3	+	0.5	2%
23	8.0824E-16	+	3.4E-18	1.057E-15	+	4.96E-18	4.1E-18	+	2.46E-19	2.1E-18	+	7.5E-19	1.1E-19	+	4.5E-20	95.8%	0.7322	18.8	+	0.3	2%
24	6.9889E-16	+	1.5E-18	9.637E-16	+	2.87E-18	1.7E-18	+	4.24E-20	-6E-19	+	4.6E-19	-3.6E-20	+	-5E-20	101.5%	0.7362	18.9	+	0.4	2%
25	4.4652E-16	+	4.7E-18	5.955E-16	+	2.74E-18	1.6E-19	+	2.01E-20	-1.7E-18	+	9.1E-19	6.7E-20	+	5.2E-20	95.6%	0.7167	18.4	+	0.7	4%
26	3.3196E-16	+	2E-18	4.194E-16	+	1.64E-18	1E-18	+	4.71E-20	-8.9E-19	+	4.3E-19	-2.3E-20	+	-4E-20	102.1%	0.8081	20.7	+	0.8	4%
27	3.511E-16	+	5.1E-18	4.472E-16	+	4.68E-18	8.5E-20	+	8.42E-21	-8.5E-19	+	6.4E-19	-1.4E-19	+	-8E-20	112.0%	0.8796	22.6	+	1.4	6%
28	1.1392E-15	+	2.3E-18	1.042E-15	+	2.9E-18	2.6E-18	+	5.12E-20	2.9E-19	+	4.9E-19	1.2E-18	+	6.1E-20	68.3%	0.7464	19.2	+	0.5	2%
30	5.2395E-16	+	4.7E-18	5.584E-16	+	5.32E-18	8.9E-19	+	3.76E-20	-1.3E-18	+	4.1E-19	2.2E-21	+	4.4E-20	99.9%	0.9372	24.0	+	0.7	3%
31	9.4041E-16	+	3.2E-18	1.214E-15	+	4.06E-18	2.1E-18	+	4.22E-20	1.4E-18	+	4E-19	3.1E-19	+	4E-20	90.3%	0.6996	18.0	+	0.3	1%
32	3.032E-16	+	2.6E-18	4.023E-16	+	1.92E-18	1.2E-18	+	3.66E-20	9.8E-19	+	3.7E-19	5.6E-20	+	4E-20	94.5%	0.7124	18.3	+	0.8	4%
33	7.7194E-16	+	3.5E-18	9.039E-16	+	4.72E-18	1.6E-18	+	5.77E-20	4.9E-19	+	4.8E-19	5.7E-20	+	3.7E-20	97.8%	0.8353	21.4	+	0.3	2%
34	8.4182E-16	+	1.7E-17	8.385E-16	+	2.01E-17	1.1E-18	+	3.25E-20	9E-19	+	3.3E-19	6.1E-20	+	5.8E-20	97.9%	0.9826	25.2	+	1.0	4%
35	3.0781E-16	+	2.2E-18	3.288E-16	+	1.05E-18	7.5E-19	+	3.26E-20	9E-20	+	3.4E-19	3.1E-19	+	4.4E-20	70.1%	0.6564	16.9	+	1.0	6%

APPENDIX F (2): $^{40}Ar/^{39}Ar$ Age data of the detrital muscovite form the Barahachettra Group (eastern Nepal, sample 22-8, Permo-Carboniferous)

51	2.7939E-13	+	4.5E-16	6.005E-15	+	2.31E-17	1.7E-17	+	1.08E-19	4.3E-17	+	1.8E-18	5.9E-18	+	2.1E-19	99.4%	46.2327	908.9	+	3.8	0.4%
52	5.2428E-14	+	5.7E-17	5.616E-15	+	2E-17	1.3E-17	+	1.55E-19	7.2E-18	+	7.5E-19	2.1E-18	+	1.4E-19	98.8%	9.2251	221.6	+	0.9	0.4%
53	3.754E-16	+	2.3E-18	3.412E-16	+	2.5E-18	9E-19	+	2.44E-20	4.5E-19	+	2.3E-19	3E-19	+	3.5E-20	76.4%	0.8405	21.6	+	0.8	3.8%
54	3.1709E-14	+	7E-17	7.991E-16	+	5.18E-18	2.1E-18	+	7.69E-20	1.3E-18	+	4.4E-19	5.5E-19	+	9.4E-20	99.5%	39.4806	801.5	+	5.6	0.7%
55	1.5678E-15	+	4.9E-18	1.067E-15	+	7.9E-18	4.1E-18	+	2.28E-19	-6.3E-19	+	4.9E-19	8E-19	+	1E-19	84.9%	1.2483	31.6	+	0.8	2.4%
56	6.8798E-14	+	3.8E-17	1.278E-15	+	4.38E-18	4E-18	+	1.16E-19	3.7E-18	+	3.1E-19	2.8E-19	+	3.6E-20	99.9%	53.7632	1029.3	+	3.6	0.3%
57	5.8735E-15	+	9.1E-18	1.537E-15	+	2.99E-18	3.3E-18	+	6.26E-20	1.1E-18	+	6.9E-19	3.6E-19	+	8.5E-20	98.2%	3.7512	93.4	+	0.5	0.5%
58	3.665E-15	+	7.1E-18	2.881E-16	+	1.89E-18	5.5E-19	+	1.76E-20	1.7E-19	+	2.8E-19	1.8E-19	+	2.5E-20	98.6%	12.5422	297.7	+	2.1	0.7%
59	1.3314E-14	+	1.2E-17	1.082E-15	+	6.18E-18	3.6E-18	+	1.04E-19	2.2E-18	+	2.8E-19	4.6E-19	+	3.7E-20	99.0%	12.1800	289.8	+	1.7	0.6%
60	1.0247E-14	+	2.3E-17	2.818E-16	+	1.96E-18	5.6E-19	+	1.79E-20	3.3E-19	+	3E-19	1.6E-19	+	2.9E-20	99.5%	36.1982	752.9	+	5.6	0.7%
61	1.1048E-14	+	1.1E-17	2.61E-16	+	2.08E-18	3.8E-19	+	2.9E-20	1.1E-19	+	3.7E-19	4.8E-19	+	4.6E-20	98.7%	41.7783	845.4	+	7.0	0.8%
62	4.6771E-14	+	3.7E-17	1.243E-15	+	4.19E-18	3.9E-18	+	7.99E-20	4.8E-18	+	6.5E-19	5.5E-19	+	6E-20	99.7%	37.4848	774.6	+	2.7	0.3%
63	2.6937E-14	+	2E-17	5.833E-16	+	4.55E-18	2.1E-18	+	6.93E-20	4E-18	+	6.2E-19	8.1E-19	+	5.5E-20	99.1%	45.7698	908.7	+	7.2	0.8%
64	6.4939E-14	+	3E-16	1.28E-15	+	1.71E-17	4.1E-18	+	8.55E-20	5.7E-18	+	7.7E-19	9.7E-19	+	2.3E-19	99.6%	50.5106	981.2	+	14.0	1.4%
65	7.4333E-14	+	2.8E-16	1.691E-15	+	9.79E-18	3.8E-18	+	6.34E-20	1.1E-17	+	5.8E-19	4E-19	+	5.5E-20	99.8%	43.8922	879.2	+	6.1	0.7%
66	3.1208E-14	+	6.2E-17	7.521E-16	+	1.83E-18	2.4E-18	+	4.59E-20	4.4E-18	+	4.9E-19	4E-19	+	5.6E-20	99.6%	41.3403	838.3	+	2.7	0.3%
67	5.2662E-16	+	3.4E-18	1.372E-17	+	4.17E-19	-1E-19	+	-5.54E-19	3.7E-20	+	3.3E-19	-6.8E-21	+	-5E-20	100.4%	38.5234	792.0	+	31.9	4.0%
68	3.1468E-14	+	3.6E-17	4.789E-16	+	1.56E-18	2.3E-18	+	6.9E-20	7.5E-18	+	6.3E-19	1.1E-18	+	6.6E-20	99.0%	65.0374	1186.7	+	4.2	0.4%
69	3.1042E-16	+	3.4E-18	2.436E-16	+	2.3E-18	9.1E-19	+	3.84E-20	2.9E-18	+	2.5E-19	4.6E-19	+	2.9E-20	56.2%	0.7161	18.4	+	1.0	5.6%
70	4.2647E-14	+	2.4E-17	8.639E-16	+	4.81E-18	4E-18	+	1.49E-19	8.3E-18	+	8.5E-19	9.4E-19	+	7.4E-20	99.3%	49.0422	959.0	+	5.4	0.6%
71	4.6713E-14	+	3.9E-17	1.079E-15	+	4.5E-18	3.3E-18	+	8.94E-20	5.2E-18	+	6.3E-19	2.6E-18	+	7.2E-20	98.4%	42.5710	858.1	+	3.7	0.4%
72	6.3681E-14	+	3.8E-17	1.658E-15	+	6.92E-18	4.2E-18	+	6.25E-20	5.7E-18	+	5E-19	2.4E-19	+	5.2E-20	99.9%	38.3750	789.5	+	3.3	0.4%
73	3.5047E-14	+	4.6E-17	9.924E-16	+	7.34E-18	3.2E-18	+	9.59E-20	5.1E-18	+	4.5E-19	3.5E-19	+	1.3E-19	99.7%	35.2096	736.0	+	5.6	0.8%
74	1.2338E-14	+	4.8E-17	4.602E-16	+	4.38E-18	1.9E-18	+	1.19E-19	4.7E-18	+	5.2E-19	5.5E-19	+	1.3E-19	98.7%	26.4552	579.1	+	6.3	1.1%

APPENDIX F (3): $^{40}Ar/^{39}Ar$ Age data of detrital muscovite from the Tansen Group (western Nepal, sample 16-3, Permo-Carboniferous)

76	4.8053E-15	+	6.1E-18	3.444E-16	+	4.13E-18	-1E-20	+	-1.34E-21	4.7E-18	+	6.6E-19	5.7E-20	+	8.4E-20	99.7%	13.9051	327.3	+	4.3	1.3%
77	4.0994E-16	+	4E-18	4.896E-16	+	2.85E-18	6.9E-19	+	5.08E-20	7.3E-19	+	6.7E-19	1.2E-19	+	8E-20	91.4%	0.7657	19.7	+	1.3	6.4%
78	2.9399E-15	+	1.3E-17	5.36E-16	+	3.58E-18	1.3E-18	+	7.62E-20	9.5E-19	+	6E-19	1E-19	+	7.8E-20	99.0%	5.4279	134.9	+	1.5	1.1%
79	9.1023E-15	+	1.7E-17	2.587E-16	+	2.21E-18	9.8E-19	+	9.8E-20	2.2E-20	+	7.3E-19	-6.8E-20	+	-8E-20	100.2%	35.2580	736.8	+	6.7	0.9%
80	6.7013E-16	+	3.7E-18	8.825E-16	+	4.01E-18	2.2E-18	+	1.08E-19	2.7E-18	+	7.1E-19	1.3E-19	+	8.8E-20	94.3%	0.7164	18.4	+	0.8	4.2%
81	5.109E-16	+	3.9E-18	3.765E-16	+	2.51E-18	3.8E-19	+	2.56E-20	-1E-19	+	6.3E-19	-1.7E-20	+	-9E-20	101.0%	1.3702	35.0	+	1.8	5.1%
82	3.447E-15	+	9E-18	1.689E-16	+	1.4E-18	-2E-20	+	-3.88E-21	1.2E-18	+	5.6E-19	3.5E-20	+	9.1E-20	99.7%	20.3522	461.0	+	5.4	1.2%
83	2.0933E-14	+	2.9E-17	9.185E-16	+	5.41E-18	1.9E-18	+	6.89E-20	1.9E-18	+	5.4E-19	4.7E-19	+	1E-19	99.3%	22.6374	506.2	+	3.2	0.6%
84	3.5185E-14	+	3.5E-17	3.145E-16	+	1.38E-18	3.9E-19	+	4.16E-20	1.2E-18	+	5.4E-19	5.1E-19	+	1E-19	99.6%	111.3972	1719.5	+	7.9	0.5%
85	9.8256E-17	+	8.2E-19	9.895E-17	+	5.46E-19	1.6E-19	+	2.09E-20	-2.3E-19	+	2.3E-19	5.6E-21	+	3.4E-20	98.3%	0.9762	25.0	+	2.6	10.4%
86	8.9053E-14	+	9.3E-17	1.164E-15	+	4.69E-18	4.6E-18	+	1.46E-19	1.3E-17	+	6.4E-19	2.5E-18	+	8.1E-20	99.2%	75.8617	1325.9	+	5.6	0.4%
87	1.3632E-15	+	4.4E-18	1.481E-15	+	2.1E-18	3.3E-18	+	3.75E-20	-7.3E-19	+	6.3E-19	3.1E-19	+	4.5E-20	93.3%	0.8590	22.0	+	0.2	1.1%
88	9.2332E-16	+	3.1E-18	8.69E-16	+	3.19E-18	1.9E-18	+	2.91E-20	-2E-19	+	4.4E-19	4.6E-19	+	4.4E-20	85.2%	0.9056	23.2	+	0.4	1.7%
89	2.5189E-14	+	2.1E-17	5.947E-16	+	1.04E-18	1E-18	+	3.28E-20	-5.6E-19	+	4.5E-19	1.4E-19	+	4.5E-20	99.8%	42.2863	853.5	+	1.7	0.2%
90	7.8196E-16	+	5E-18	5.74E-16	+	3.74E-18	1.2E-18	+	2.59E-20	5.3E-18	+	6.6E-19	3.4E-19	+	4.8E-20	87.1%	1.1866	30.4	+	0.7	2.4%
91	9.9713E-14	+	8E-17	9.254E-16	+	3.05E-18	3.2E-18	+	7.42E-20	6E-18	+	5.2E-19	4.5E-19	+	5.7E-20	99.9%	107.6054	1681.3	+	5.7	0.3%
92	1.0431E-14	+	6.6E-18	7.741E-16	+	2.04E-18	1.5E-18	+	4E-20	2.1E-17	+	4.5E-19	4.2E-19	+	5E-20	98.8%	13.3165	314.6	+	1.0	0.3%
93	2.6471E-16	+	6E-18	2.674E-16	+	1.34E-18	6.4E-19	+	3.04E-20	-1.4E-19	+	3.2E-19	5.4E-21	+	7.4E-20	99.4%	0.9840	25.2	+	2.2	8.6%
94	1.7893E-14	+	3E-17	1.275E-15	+	4.88E-18	2.5E-18	+	4.7E-20	1.8E-17	+	3.5E-19	7E-19	+	4.9E-20	98.8%	13.8769	326.7	+	1.4	0.4%
95	2.4941E-14	+	2.2E-17	2.248E-16	+	8.26E-19	1.5E-18	+	1.27E-19	5.8E-19	+	2.6E-19	5.5E-19	+	3.9E-20	99.4%	110.2149	1707.7	+	6.5	0.4%
96	8.8812E-14	+	5.3E-17	8.599E-16	+	3.76E-18	2.4E-18	+	5.91E-20	5.5E-18	+	4.8E-19	1.2E-18	+	7.2E-20	99.6%	102.8641	1632.5	+	7.3	0.4%
97	1.1838E-15	+	2.8E-18	9.55E-16	+	2.34E-18	1.9E-18	+	3.18E-20	6.2E-19	+	5.3E-19	1.1E-18	+	6.2E-20	73.4%	0.9093	23.3	+	0.5	2.1%
98	4.7833E-15	+	1.1E-17	3.343E-16	+	1.69E-18	9.9E-19	+	3.07E-20	3.7E-18	+	3.7E-19	4.8E-19	+	4.2E-20	97.0%	13.8845	326.9	+	2.1	0.6%
99	7.0591E-15	+	8.9E-18	6.278E-16	+	2.6E-18	1.5E-18	+	3.15E-20	2E-17	+	6.2E-19	6.5E-19	+	4.6E-20	97.3%	10.9373	262.3	+	1.3	0.5%
100	8.4636E-14	+	4.8E-17	2.131E-15	+	7.73E-18	5.9E-18	+	8.14E-20	6.1E-18	+	5.7E-19	1.6E-18	+	7.5E-20	99.4%	39.4861	807.9	+	3.0	0.4%

APPENDIX F (4): $^{40}Ar/^{39}Ar$ Age data of detrital muscovite from the Tansen Group (western Nepal, sample 15-8, Eocene)`

1	6.7706E-15	+	7.9E-18	6.16E-17	+	4.48E-19	6.3E-19	+	7.37E-20	8E-19	+	3.8E-19	7.7E-20	+	4.2E-20	100%	109.5987	492.7	+	3.8	0.76%
2	6.3919E-15	+	1.2E-17	1.02E-16	+	3.96E-19	6E-19	+	4.93E-20	-4.8E-19	+	5E-19	2.4E-19	+	4.5E-20	99%	62.1894	295.8	+	1.4	0.49%
3	2.89E-15	+	3.2E-18	2.75E-17	+	3.8E-19	3.4E-19	+	7.52E-20	-1.6E-18	+	3.5E-19	-5.2E-20	+	-4E-20	101%	105.4777	476.4	+	6.8	1.42%
4	3.5787E-15	+	4.3E-18	3.15E-17	+	2.52E-19	3.9E-19	+	8.79E-20	-1.1E-18	+	3.2E-19	-7.2E-20	+	-4E-20	101%	114.3535	511.3	+	4.4	0.86%
5	2.4316E-14	+	3.7E-17	1.27E-16	+	4.55E-19	1.3E-18	+	8.37E-20	3.7E-18	+	5.5E-19	1.8E-19	+	5E-20	100%	191.0953	787.7	+	3.1	0.40%
6	9.3613E-15	+	1.9E-17	4.00E-17	+	5.99E-19	4.5E-19	+	3.27E-20	4.8E-19	+	6.5E-19	-4.9E-20	+	-5E-20	100%	234.2799	926.5	+	14.0	1.52%
7	9.2501E-15	+	9.4E-18	8.60E-17	+	8E-19	4.2E-19	+	2.43E-20	-4.7E-20	+	3.5E-19	1E-19	+	4.2E-20	100%	107.2100	483.2	+	4.6	0.95%
8	4.9712E-15	+	9.2E-18	2.25E-17	+	2.54E-19	3.1E-19	+	4.49E-20	6.5E-19	+	5.7E-19	1.3E-19	+	3.6E-20	99%	219.5829	880.4	+	10.3	1.17%
9	1.4737E-14	+	1.3E-17	6.62E-17	+	4.07E-19	5E-19	+	2.64E-20	9.3E-19	+	5.4E-19	1.7E-19	+	4.3E-20	100%	221.8770	887.7	+	5.6	0.63%
10	5.9933E-15	+	9E-18	4.31E-17	+	4.18E-19	6E-19	+	4.67E-20	9.7E-19	+	4.7E-19	8.8E-19	+	4.1E-20	96%	133.1298	582.9	+	6.1	1.05%
11	1.5281E-14	+	1.8E-17	6.71E-17	+	7.86E-19	3.2E-19	+	2.54E-20	-2.9E-19	+	4.6E-19	1.4E-19	+	4.3E-20	100%	227.1964	904.4	+	10.7	1.18%
12	8.4694E-15	+	1E-17	6.58E-17	+	5.37E-19	3.7E-19	+	3.19E-20	-9.8E-19	+	4E-19	9.6E-20	+	4.1E-20	100%	128.3320	564.9	+	4.7	0.84%
13	1.9595E-15	+	2.3E-18	2.50E-17	+	3.21E-19	2.3E-19	+	3.48E-20	-5.6E-19	+	3.9E-19	7.9E-20	+	4.1E-20	99%	77.5755	362.1	+	5.3	1.45%
14	9.5745E-15	+	9.6E-18	8.65E-17	+	5.43E-19	2.2E-19	+	1.75E-20	1.7E-19	+	4.4E-19	6.9E-20	+	4.1E-20	100%	110.4149	495.9	+	3.2	0.65%
15	2.3154E-15	+	2.2E-18	2.12E-17	+	1.68E-19	1.6E-19	+	3.06E-20	-6.6E-19	+	5.4E-19	4.6E-20	+	3.8E-20	99%	108.5661	488.6	+	4.6	0.94%
16	3.7531E-15	+	6E-18	3.39E-17	+	3.12E-19	3.9E-19	+	9.76E-20	-4.3E-19	+	5.6E-19	2.4E-19	+	6.8E-20	98%	108.5554	488.5	+	5.4	1.10%
17	1.1116E-14	+	6.7E-18	5.15E-17	+	2.82E-19	2.3E-19	+	2.6E-20	-6.6E-19	+	3.4E-19	6E-20	+	4.1E-20	100%	215.5280	867.5	+	4.9	0.56%
18	2.8996E-16	+	3E-18	3.10E-17	+	2.97E-19	5.7E-20	+	1.03E-20	8.6E-19	+	4.7E-19	3.8E-20	+	4.1E-20	96%	8.9806	45.8	+	2.1	4.64%
19	1.7357E-15	+	3.5E-18	1.76E-17	+	2.29E-19	2E-19	+	3.92E-20	9E-19	+	3.9E-19	5.4E-19	+	3.8E-20	91%	89.6522	412.4	+	6.7	1.62%
20	3.6205E-15	+	6.5E-18	3.22E-17	+	3.51E-19	1.9E-19	+	3.32E-20	1.1E-19	+	5E-19	1.8E-20	+	3.6E-20	100%	112.1908	502.8	+	5.8	1.15%
21	1.0792E-15	+	4E-18	1.07E-16	+	3.63E-19	3.2E-19	+	3.08E-20	1.6E-18	+	5.2E-19	1.4E-19	+	4.3E-20	96%	9.6949	49.4	+	0.7	1.33%
22	6.9677E-15	+	7.6E-18	2.54E-16	+	6.7E-19	7.4E-19	+	2.34E-20	9.8E-19	+	4.7E-19	1.2E-19	+	3.7E-20	100%	27.2805	135.8	+	0.4	0.33%
23	7.6207E-15	+	1.1E-17	6.12E-17	+	7.6E-19	5.1E-19	+	2.85E-20	6.3E-19	+	3.9E-19	1.3E-19	+	3.8E-20	99%	123.8114	547.7	+	6.9	1.26%
24	2.4564E-15	+	2.6E-18	2.39E-17	+	2.85E-19	2.3E-19	+	3.46E-20	2.1E-18	+	4.8E-19	2E-19	+	4.4E-20	98%	100.2078	455.3	+	6.1	1.34%
25	2.522E-14	+	2E-17	1.14E-16	+	1.01E-18	1.7E-18	+	1.9E-19	6.5E-18	+	5E-19	5.5E-19	+	6.4E-20	99%	219.8737	881.4	+	7.9	0.90%

APPENDIX G: Photographs of detrital muscovite grains analyzed for argon dating.

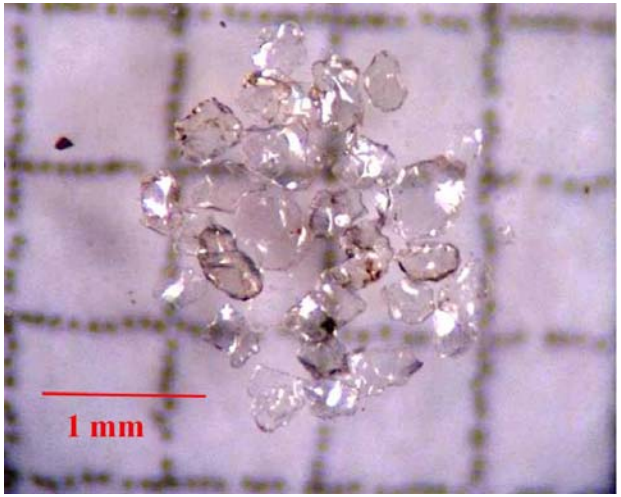

Sample 26-8 (Katari Group, eastern Nepal)

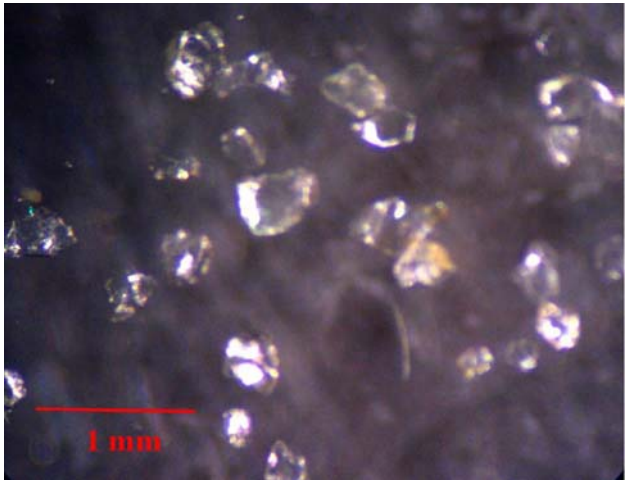

Sample 16-3 (Sisne Formation, western Nepal)

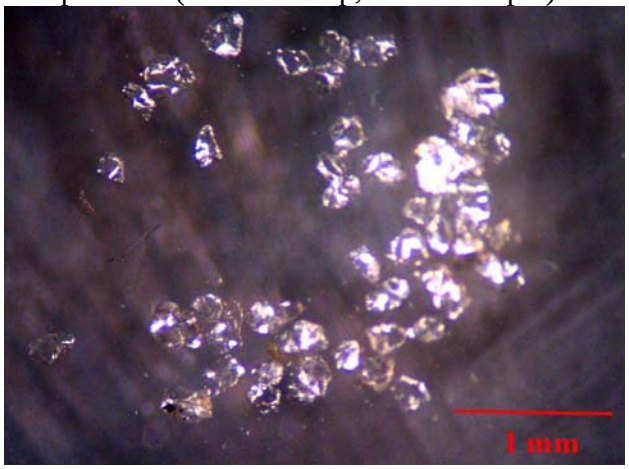

Sample 15-8 (Bhainskati Formation, western Nepal)